

STRUCTURAL CONDITION DOCUMENTATION AND
STRUCTURAL CAPACITY EVALUATION
OF THE
BATTELLE MEMORIAL INSTITUTE COLUMBUS LABORATORIES
WEST JEFFERSON SITE
FOR
EARTHQUAKE AND FLOOD

TASK II -- STRUCTURAL CAPACITY EVALUATION

prepared for
Nuclear Test Engineering Division
LAWRENCE LIVERMORE LABORATORY
Livermore, California

January 1979

EDAC

ENGINEERING DECISION ANALYSIS COMPANY, INC.

480 CALIFORNIA AVE., SUITE 301

2400 MICHELSON DRIVE

BURNITZSTRASSE 34

PALO ALTO, CALIF 94306

IRVINE, CALIF 92715

6 FRANKFURT 70, W. GERMANY

7911200

1363 002

~~7911200~~

596

TABLE OF CONTENTS

<u>Section</u>		<u>Page</u>
	LIST OF TABLES	iii
	LIST OF FIGURES	iv
	SYNOPSIS - TASK II	vii
1	INTRODUCTION	1-1
2	FACILITY AND SITE DESCRIPTION	2-1
	2.1 General Facility Layout	2-1
	2.2 Critical Facility Areas	2-3
	2.3 Site Seismicity	2-4
3	EVALUATION OF STRUCTURAL BEHAVIOR	3-1
	3.1 JN-1B Structural Systems	3-1
	3.2 JN-1B Structural Analysis Procedures	3-4
	3.2.1 JN-1B Modelling Considerations	3-4
	3.2.2 Inelastic Behavior	3-6
	3.2.3 JN-1B Seismic Capacity Evaluations	3-7
	3.3 JN-1B Structural Models and Results	3-11
	3.4 JN-4 Structural Systems	3-17
	3.5 JN-4 Structural Analysis Procedures	3-19
	3.5.1 JN-4 Modelling Considerations	3-19
	3.5.2 JN-4 Inelastic Behavior	3-22
	3.6 JN-4 Structural Models and Results	3-24
	3.6.1 JN-4 Elastic Analysis	3-24
	3.6.2 Modified Elastic Analysis of the JN-4 Facility	3-26
	3.6.3 Dynamic Response of Unreinforced Masonry Walls	3-28
	3.6.4 Ultimate Collapse Capacity of the JN-4 Structure	3-30

TABLE OF CONTENTS

(continued)

<u>Section</u>		<u>Page</u>
4	EVALUATION OF CRITICAL EQUIPMENT	4-1
	4.1 JN-1B Critical Equipment Considered	4-1
	4.2 JN-1B Equipment Analysis Procedures	4-3
	4.2.1 JN-1B Equipment Response	4-3
	4.2.2 JN-1B Equipment Object Impact	4-4
	4.3 JN-1B Equipment Analysis Results	4-5
	4.4 JN-4 Critical Equipment Considered	4-8
	4.5 JN-4 Equipment Analysis Procedures	4-10
	4.5.1 JN-4 Equipment Response	4-10
	4.5.2 JN-4 Equipment Object Impact	4-11
	4.6 JN-4 Equipment Analysis Results	4-12
5	SUMMARY OF RESULTS AND STRUCTURAL DAMAGE SCENARIO	5-1

REFERENCES

APPENDICES

- A Uncertainty Bound Analysis Procedure
- B Determination of Channel Slab Slippage During JN-4 Rigid Body Rocking
- C Selected Data and Details from the Task I Report
- D Verification of Approximate Analysis Method for Wall/Roof Systems

1368 004

LIST OF TABLES

<u>Table</u>	<u>Title</u>	<u>Page</u>
3-1	System Ductility Factors and Damping Ratios for the JN-1B Analysis	3-34
3-2	Summary of Seismic Capacities Affecting JN-1B Confinement Barriers	3-35
3-3	JN-1B Truss Model Boundary Element Properties . .	3-36
3-4	JN-1B Truss Model Node Masses	3-37
3-5	JN-1B Truss Model Beam Properties	3-38
3-6	JN-1B Roof Truss Diagonal Member Forces (SRSS)	3-39
3-7	JN-1B Roof Truss Boundary Element Forces (SRSS)	3-40
3-8	Modified JN-4 Elastic Model Frequencies	3-41
3-9	Summary of JN-4 Wall Cracking Levels	3-42
3-10	Seismic Collapse Capacities of JN-4 Walls for Out-of-Plane Ground Motion	3-43
3-11	Summary of JN-4 System Seismic Capacities	3-44
5-1	Summary of Critical Seismic Capacities	5-5

LIST OF FIGURES

<u>Figure</u>	<u>Title</u>	<u>Page</u>
2-1	JN-1B High Energy Cell Facility Floor Plan	2-7
2-2	JN-4 Plutonium Laboratory Floor Plan	2-8
2-3	Exhaust System of JN-1B High Energy Cell	2-9
2-4	JN-4 Plutonium Laboratory Glove Box Arrangement	2-10
2-5	JN-4 Plutonium Laboratory Ventilation System . . .	2-11
2-6	Return Periods for Seismic Acceleration at the BMI West Jefferson Facility (From Ref. 5) . . .	2-12
3-1	JN-1B Longitudinal Section of High Energy Cell (HEC)	3-45
3-2	Transverse Section of High Energy Cell	3-46
3-3	JN-1B Roof Truss	3-47
3-4	JN-1B North Wall Braced Frame	3-48
3-5	JN-1B South Wall Braced Frame	3-49
3-6	JN-1B West Wall Braced Frame	3-50
3-7	JN-1B Cross Bracing for Crane Framing at Line 13	3-51
3-8	JN-1B Diagonal Bracing Along Column Line Q	3-52
3-9	JN-1B Mezzanine Floor Framing	3-53
3-10	Typical JN-1B Bolted Connection of the Roof Truss	3-54
3-11	Median Alluvium Response Spectra (Ref. 7)	3-55
3-12	Finite Element Model of the High Energy Cell . . .	3-56
3-13	Dynamic Response Analysis Results of the HEC	3-57
3-14	Mathematical Model of the JN-1B Roof Truss	3-58
3-15	First Mode of the JN-1B Structure (Plan)	3-59

1363 006

LIST OF FIGURES

(continued)

<u>Figure</u>	<u>Title</u>	<u>Page</u>
3-15a	First Mode of the JN-1B Structure with Buckled North Frame Cross Brace Frame (Plan)	3-60
3-16	Second Mode of the JN-1B Structure (Plan)	3-61
3-16a	Second Mode of the JN-1B Structure with Buckled North Frame Cross Brace (Plan)	3-62
3-17	Third Mode of the JN-1B Structure (Plan)	3-63
3-17a	Third Mode of the JN-1B Structure with Buckled North Frame Cross Brace (Plan)	3-64
3-18	JN-4 South Exterior Masonry Wall - Finite Element Model	3-65
3-19	JN-4 Roof Finite Element Model	3-66
3-20	Typical Rigid Body Wall System	3-67
3-21	Force-Deflection Relations for Typical Rigid Body System	3-68
3-22	Wall/Roof System Models	3-69
3-23	Structural Steel Framing for the JN-4 Facility	3-70
3-24	Fundamental Mode of the JN-4 Facility	3-71
3-25	Modified Elastic Model-Mode Shapes	3-72
3-26	Modified Elastic Model-Mode Shapes	3-73
3-27	Rigid Body Wall Rocking Failure Mode Assuming Rigid Roof Framing	3-74
3-28	Rigid Body Wall Rocking with Flexible Roof Beam Interference Considered	3-74
3-29	Rigid Body Rocking of the JN-4 Facility for N-S Excitation	3-75
3-30	Rigid Body Rocking of the JN-4 Facility for E-W Excitation	3-76

1363 007

LIST OF FIGURES

(continued)

<u>Figure</u>	<u>Title</u>	<u>Page</u>
3-31	Plan of the JN-4 Main Laboratory	3-77
3-32	Elevation of a Typical Exterior Column, Lintel, and Wall Pier System	3-78
3-33	Rigid Body Rocking Model at Clerestory Drop Along Column Line 4	3-79
4-1	JN-1B Final Filter Unit Assembly	4-16
4-2	Glove Box 20 Configuration	4-17
4-3	Glove Box 20 (Larger)	4-18
4-4	Glove Box Stand Anchor Bracket	4-19
4-5	Typical Box-Mounted Exhaust Filter	4-20
4-6	JN-4 Filter at Floor	4-21
4-7	JN-4 Filter Above Ceiling	4-22
4-8	Exhaust System - Glove Box 20 and 37 Area	4-23

1363 008

POOR ORIGINAL

SYNOPSIS - TASK II

This report presents the results of the Task II -- Structural Capacity Evaluation of the Battelle Memorial Institute (BMI) Columbus Laboratories, located at West Jefferson, Ohio. The purpose of the Task II effort was to evaluate the structural capacity of those building structures and critical equipment components which could potentially release hazardous chemicals into the environment from the BMI facility as a result of damage or failure during an earthquake or flood. This report summarizes the structural capacities of critical building and equipment systems as subjected to earthquake-induced ground shaking. A second volume will report capacities to resist flood-induced loadings when such loadings are determined for the BMI site by other NRC consultants.

The Task II effort was devoted to the JN-1B Hot Cell Facility and the JN-4 Plutonium Laboratory. The primary items of concern for the release of hazardous chemicals from the JN-1B facility were the High Energy Cell (HEC) and its filter and exhaust system. Within the JN-4 Plutonium Laboratory, attention was centered on several key glove boxes which contain Uranium/Plutonium in dispensible forms together with the glove box filters and building exhaust system. The loss of primary confinement due to collapse or overturning of the HEC or from rupture of a glove box, either from direct glove box failure or from damage caused by interaction with adjacent structures was identified as the ultimate mode of release resulting from extreme earthquake hazard. The

structural capacity of the building structures and associated equipment systems as related to the ultimate modes of release are addressed in this report. Operational and functional aspects of the facility were not considered.

The JN-1B Hot Cell Laboratory was built in 1971 as an expansion immediately adjacent to the JN-1A Laboratory. The structure consists of a single-story high-roof braced frame steel structure which houses the High Energy Cell and its ancillary equipment. The main portion of the building is 86 feet by 74 feet in plan dimension and approximately 62 feet high. With the exception of the East wall which is a curtain wall adjacent to the JN-1A structure, the exterior walls are constructed of free-standing unreinforced concrete block with brick veneer from ground level to 10 feet above grade. The walls above 10 feet are constructed of double-layered metal wall panels attached to the steel framing.

The High Energy Cell is constructed of poured-in-place concrete walls and ceiling with steel liners on all walls. Wall thicknesses are from 4 to 6 feet at floor level to approximately 16 feet elevation and 3 to 5 feet thick up to the roof. The roof is 4 foot thick concrete. The interior dimensions of the cell are 9 by 38 feet in plan and 25 feet high.

The JN-4 Plutonium Laboratory is a U-shaped structure with legs of unequal length and width and completely different methods of construction. However, no hazardous chemicals are contained in the older portion of the structure, and with the exception of some light sheet metal flashing, the structures are separated by a 6-1/4 inch gap. The investigation was therefore concentrated on the main laboratory part of the structure. This portion is constructed of

POOR ORIGINAL

unreinforced masonry block and block/brick walls on a concrete slab with a 16 foot high roof of 6 inch by 24 inch by approximately 12 foot long concrete channel slabs resting on steel roof beams. A drop ceiling is installed at the 12-foot level to provide a crawl space for the building ventilation and exhaust systems.

The lateral force resistance of the HEC is provided by the thick concrete shear wall box system tied together by the 4 foot thick reinforced concrete roof slab. The HEC is rectangular in plan with a length to width ratio of 2.5 to 1 so that its resistance to overturning in the E-W direction (long axis) is significantly greater than for N-S excitation. Because of the large mass and stiffness of the HEC and the weak coupling through the mezzanine and crane framing, the HEC will behave virtually independently of the main steel building frame.

The lateral force resisting system of the JN-1B steel frame building is a box system comprised of vertical braced frames tied together by a roof system consisting of a roof truss and steel deck. The east wall is a curtain wall which does not extend to ground and is not tied to the JN-1A structure. Consequently it acts as a deep flange to provide roof stiffening but does not act as a shear wall. The structure responds as an open section and all lateral loads must be reacted by the other braced frames.

In the main laboratory section of the JN-4 facility, lateral force is resisted by a steel column/unreinforced masonry wall system supporting the roof. Inertial roof loads are transmitted to the exterior walls at the steel column locations where the flexible columns bear against the masonry blocks. At very low levels of response, sufficient friction between the roof

POOR ORIGINAL

channels and beams exists to provide diaphragm action of the roof. After the channels begin to slip, forces are developed in the individual channel slabs which oppose rotation and provide restraint against deformations of the roof system relative to the shear walls.

Finite element models were developed in order to determine equivalent stiffness characteristics of the major structural systems and subsystems for use in the dynamic response calculations. These same models were utilized in determining the component stress levels resulting from given levels of ground motion. The dynamic models were suitably modified or replaced with more representative models as the levels of ground motion were increased and significant nonlinear response occurs. Uplift of the HEC footing was calculated to begin for rocking about the major axis at a median ground acceleration of 0.23g. Overturning of the cell about the same axis is not anticipated until acceleration levels of over 3g are reached. Collapse of the JN-1B steel frame structure was calculated to occur at a median ground acceleration of 0.3g in the N-S direction. Although this will not cause sufficient damage to cause rupture of the HEC, it will result in loss of the exhaust fan system. This will result in loss of the pressure difference across the cell boundary and allow some unfiltered access to the cell. Also, at ground acceleration levels of approximately 0.3g to 0.4g, some shield plugs may be shaken out of the HEC, further increasing the unfiltered leak path area to atmosphere.

The critical equipment items which form the primary confinement barrier in the JN-4 Plutonium Laboratory also exhibit higher capacities than the building structures. In general, they will only be affected by total facility collapse or by large

relative displacements between the floor and the roof which occur just prior to collapse. Median ground acceleration levels of 0.23g in the N-S direction or 0.17g in the E-W direction were calculated to result in collapse of the main laboratory roof/wall system.

Thus, for the purposes of the natural hazard study, potential release of hazardous chemicals from any of the BMI facilities would not be expected to occur until a ground motion acceleration level of 0.17g with an associated return period of greater than 2,000 years is reached. Based upon the statistical uncertainty bound analyses, the estimated standard deviation lower and upper bound seismic capacities are 0.11g and 0.26g respectively.

POOR ORIGINAL

1363 013

1. INTRODUCTION

POOR ORIGINAL

This report presents the results of the structural evaluation of the structures and equipment of the West Jefferson Site of Battelle Memorial Institute Columbus Laboratories (BMI) which contain hazardous materials. The report is submitted in accordance with Contract No. 5453703, dated 2 May 1977, between Lawrence Livermore Laboratory (LLL) of the University of California and Engineering Decision Analysis Company, Inc. (EDAC). The Task II Structural Evaluation and prior Task I Condition Documentation by EDAC (as defined in the referenced contract) are part of an overall natural hazards evaluation (Reference 1) performed by a group of consultants expert in the various hazard fields. The study is sponsored and directed by the Fuel Reprocessing and Recycle Branch of the United States Nuclear Regulatory Commission (USNRC). The natural hazards study includes evaluation of several facilities at different locations within the United States. EDAC is responsible for the structural evaluation of these facilities for both earthquake and flood induced loadings.

Battelle-Columbus maintains and operates the Battelle Memorial Institute Columbus Laboratories (BMI) West Jefferson site. The site is located in West Jefferson, Ohio, approximately 17 miles west of Columbus, Ohio. The site consists of the Engineering Area and the Nuclear Sciences Area located on a 1,000 acre tract. In accordance with the general guidelines given in Reference 1, only the Nuclear Sciences Area is of concern in this study. The JN-1 Hc Cell Laboratory facility is equipped for postirradiation examination

of reactor materials and components up to and including light water reactor fuel assemblies. The JN-4 Plutonium Laboratory is equipped for research and development related to plutonium bearing materials. For the purposes of this study only the JN-1B and JN-4 structures and equipment were considered (Reference 2).

The structural evaluation effort was divided into two phases or tasks. The Task I effort encompassed the documentation of the present condition of the BMI facility including a review of drawings and specifications related to the structures and critical equipment. The Task I report (Reference 4) identified the critical locations within the facility, presented details of the critical process equipment and the structural systems which are able to carry seismic loads, and described the analysis procedures which would be subsequently used in the Task II seismic capacity evaluation of the BMI facility. In addition to providing a data base for structural evaluations by EDAC, the Task I condition documentation was intended to provide structural data for the extreme wind load evaluation by other consultants.

The Task II effort encompasses the analysis of the building structures and all critical equipment in order to establish the ground motion acceleration which could cause the structure or critical component to collapse or to result in loss of confinement of hazardous chemicals. This report describes the results of the Task II analyses which are presented in the following sections:

- Section 2. Facility and Site Description
- Section 3. Evaluation of Structural Behavior
- Section 4. Evaluation of Critical Equipment
- Section 5. Structural Damage Scenario

1363 015

Section 2 presents a brief discussion of the BMI facility layout, its critical areas and general structural descriptions, together with a brief discussion of the general seismicity of the region. Section 3 presents the seismic capacity evaluation of the building structures including a description of the structural systems, a discussion of the analysis procedures used in the seismic evaluation, and a description of each of the structural behavior models together with the analysis results pertaining to the collapse or confinement breach of the building structures. Similarly, Section 4 presents the evaluation of the critical equipment items, again describing the analysis procedures and the results. Section 5 summarizes the capacity evaluation of the BMI facility by means of the presentation of a seismic damage scenario which describes the potential damage to the facility at various levels of seismically induced ground motion acceleration.

1363 016

2. FACILITY AND SITE DESCRIPTION

This section of the report presents a brief discussion of the structural information pertinent to the Task II seismic capacity evaluation of the Task II seismic capacity evaluation of the BMI facility. A general structural description of the BMI buildings of interest together with an identification of the critical areas and a discussion of the site seismicity is contained herein. The JN-1 Hot Cell Facility and the JN-4 Plutonium Laboratory were both constructed in several phases over periods of several years. In several instances the type of construction varies significantly and, in most instances, essentially no structural ties exist between portions of the structures constructed at different times. Consequently, during an earthquake the individual parts of these structures will tend to behave independently.

2.1 GENERAL FACILITY LAYOUT

The JN-1B Hot Cell Laboratory was built in 1971 to expand and complement the capability of JN-1A Laboratory. This addition, which is adjacent to the west wall of JN-1A, consists of a main one-story high-roof steel frame structure which houses the High Energy Cell (HEC) with its ancillary functions (e.g., transfer pool, service area, etc.) and a low roof pool mechanical equipment room located at the north-east corner of the main building. The general layout of the building is shown in Figure 2-1. The main portion of the building, which is 86 feet by 74 feet in plan dimension and approximately 62 feet high, is constructed of a three-dimensional steel frame with a steel roof deck and double-layered metal exterior

walls with several inches of insulation. From ground level up to 10 feet above grade, the exterior walls are constructed of 12 inch thick unreinforced concrete block walls with brick veneer masonry. An 8-inch concrete floor slab is poured on grade.

The High Energy Cell (HEC) housed in JN-1B is constructed of poured-in-place concrete walls and ceiling with steel liners on all walls. The interior dimensions of the HEC are 38 feet long by 9 feet wide by 25 feet high. The HEC is connected to a fuel handling and examination pool (20 x 20 x 45 feet deep) via a transfer canal. A mezzanine area used as a HEC mechanical equipment room is located between the south wall of the JN-1B building and the south wall of HEC at 18 feet 8 inches above the ground level. A 50-ton bridge crane which can travel the full length of JN-1B is used to handle casks and the solid steel door of the HEC.

The JN-4 Plutonium Laboratory building is essentially a U-shaped structure with legs of unequal length and widths as shown in Figure 2-2. The outside dimensions of the main laboratory and office (including the old laboratory) are approximately 113' - 4" by 105' - 10". This building was built in three separate segments (Figure 2-2) and the construction features are quite varying. The earlier two segments that were built in 1960 and 1964 are constructed of double-layered metal walls with several inches of insulation and a metal roof. The newer segment of the facility, built in 1967, is constructed of masonry block and block/brick walls on a concrete slab with a 16-foot-high roof of 6" by 24" concrete channels. A drop ceiling is installed at the 12-foot level providing a 4-foot space for ventilation duct and utility services.

1363 018

2.2 CRITICAL FACILITY AREAS

For purposes of the overall natural hazards study, critical areas are those locations in which hazardous chemicals are processed or stored in a dispersible form. Release of these chemicals to the outside is possible should the confinement barriers be breached. In these areas release may be postulated as a result of given natural events (e.g., earthquakes, tornados, etc.). Similarly, critical equipment is equipment which is used to process materials (i.e., hazardous chemicals in dispersible form) and whose structure serves as a primary confinement barrier. The area of primary concern is the High Energy Cell (HEC) with additional attention given to features whose failure may cause loss of containment of hazardous chemicals (i.e., viewing windows, HEPA filters, and exhaust system etc.). A plan view of the HEC with connecting pool and cask wash-down area is given in Figure 2-1. The JN-1B building has its own ventilation system which is designed so that all the air in the building is exhausted through the High Energy Cell. Conditioned outside air is supplied to each area by two air conditioning units in the HEC mechanical equipment room. All the air is exhausted through 3 sets of primary high efficiency filters recessed into the rear wall of the HEC and 3 sets of final high efficiency filters located outside the cell on the mezzanine. Eight-inch diameter exhaust pipes connecting the primary and final filters are embedded in the cell wall and ceiling. A section through the cell depicting the exhaust system is shown in Figure 2-3. The High Energy Cell provides the primary confinement barrier for hazardous chemicals in the JN-1B facility while the building exterior walls and roof provide the final barrier.

The JN-4 Plutonium Laboratory consists of separate glove box areas for hazardous chemicals in conjunction with areas for support activities. The areas of principal concern are glove boxes 20 and 37 which contain Plutonium/Uranium in dispersible forms. Other features whose failure may increase the hazard potential have been identified in Reference 3 as: windows, final HEPA filters, the natural gas line in the service room, hydraulic fluid reservoirs in the main lab, and IA-gas cylinders.

The glove box arrangement is shown in Figure 2-4, and the building ventilation system is shown schematically in Figure 2-5. Filtered conditioned air is supplied to each room by diffusers near the ceiling. Air is exhausted from the rooms through HEPA filters in metal frames with their faces set a few inches from the floor. Ducting and final HEPA filters are located in the 4 foot crawl space in the main laboratory which is the area of concern. Most of the glove boxes used in the facility are "inerted" (nitrogen atmosphere) with single-pass inert gas supplied. Gas is exhausted from the glove boxes through at least a single stage of high filtration in an 8" diameter metal canister and then piped into the exhaust piping.

The confinement barriers for the main lab portion of the JN-4 building consist of the process glove boxes as primary confinement barriers, the building walls and roof as final barriers, and the non-load bearing concrete block walls and drop ceiling act as secondary barriers within the building envelope.

2.3 SITE SEISMICITY

The BMI site is located approximately 17 miles west of Columbus, Ohio. The Nuclear Sciences Area is situated north of the Battelle Lake at an elevation approximately 910 feet above sea level. The site may be generally described as underlain by glacial

till with bedrock reported at a depth of approximately 100 feet. A limited soils and foundation investigation (Reference 6) was conducted for the Hot Cell Pool location of building JN-1B. Three test borings ranging in depth from 50 to 100 feet were taken, and although these were limited to the vicinity of the Hot Cell Pool, they are considered to be representative of the soil conditions for other structures within the Nuclear Sciences Area.

The value of the soil shear modulus, G , was previously computed (Reference 4) as 9000 psi which included the effects of increased strain levels during seismic motion. For a soil density of 130 lb/cu.ft., the corresponding shear wave velocity is 570 ft/sec. for the moist silty clay encountered in the BMI Nuclear Sciences Area. For the BMI site, the ground-water table was reported to be at approximately 40 feet below ground surface at the Hot Cell Laboratory location (References 5 and 6). Seepage was encountered in the test borings in a thin discontinuous layer of fine to medium sand of limited volume. Liquefaction requires a combination of saturation and cohesionless soils which have the ability to compact into a more dense condition. Due to the very limited amounts of saturated sands encountered in comparison with clayey silts, the possibility of liquefaction at the BMI site is considered remote.

A seismic risk analysis of the BMI site was conducted by other consultants (Reference 5) in order to define the ground motions which the facility could be expected to encounter. The analysis included a review of the historical data and included earthquakes up to 600 km from the site in conjunction with an appropriate attenuation relationship. The results indicate the site is in a region of low to moderate seismic activity. Based on a

1363 021

probabilistic approach (Reference 5), earthquakes with peak seismic ground acceleration levels within the range of approximately 3 to 5% g may be expected every 100 years and approximately 8 to 14% g every 1000 years. The best estimate curve together with bounding curves corresponding approximately equal to one standard deviation for return period accelerations is shown in Figure 2-6 (reproduced from Reference 5). Data were not available on which to base return periods for peak ground horizontal acceleration levels in excess of 0.14g. Thus, throughout this report where the seismic capacity of structures or equipment exceeds 0.14g, the return period can only be determined as greater than 2000 years.

1363 022

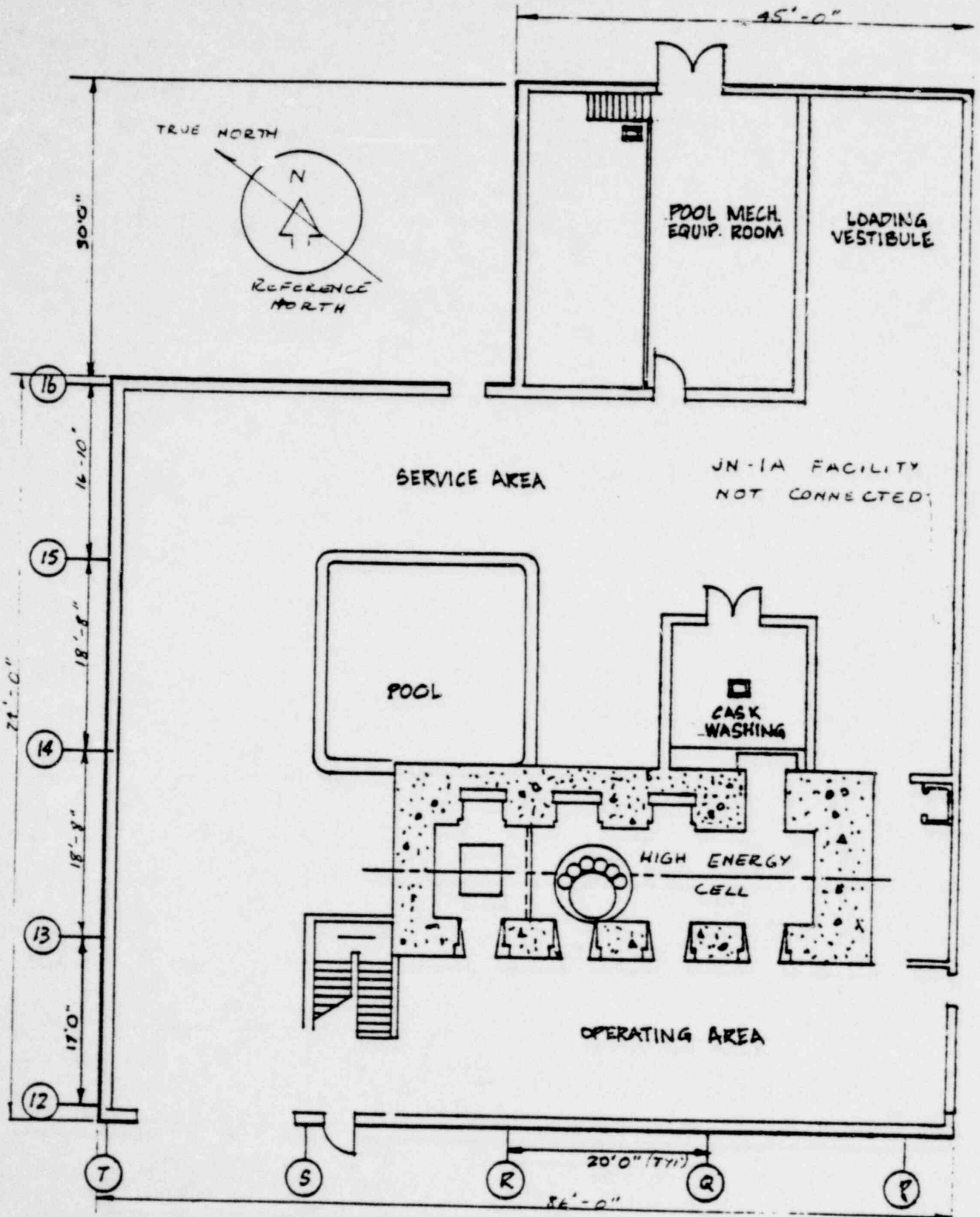






FIGURE 2-1. JN-1B HIGH ENERGY CELL FACILITY FLOOR PLAN

-  INITIAL SECTION (1960)
-  FIRST ADDITION (1964)
-  SECOND ADDITION (1967)
-  FINAL OFFICE ADDITION (1968)

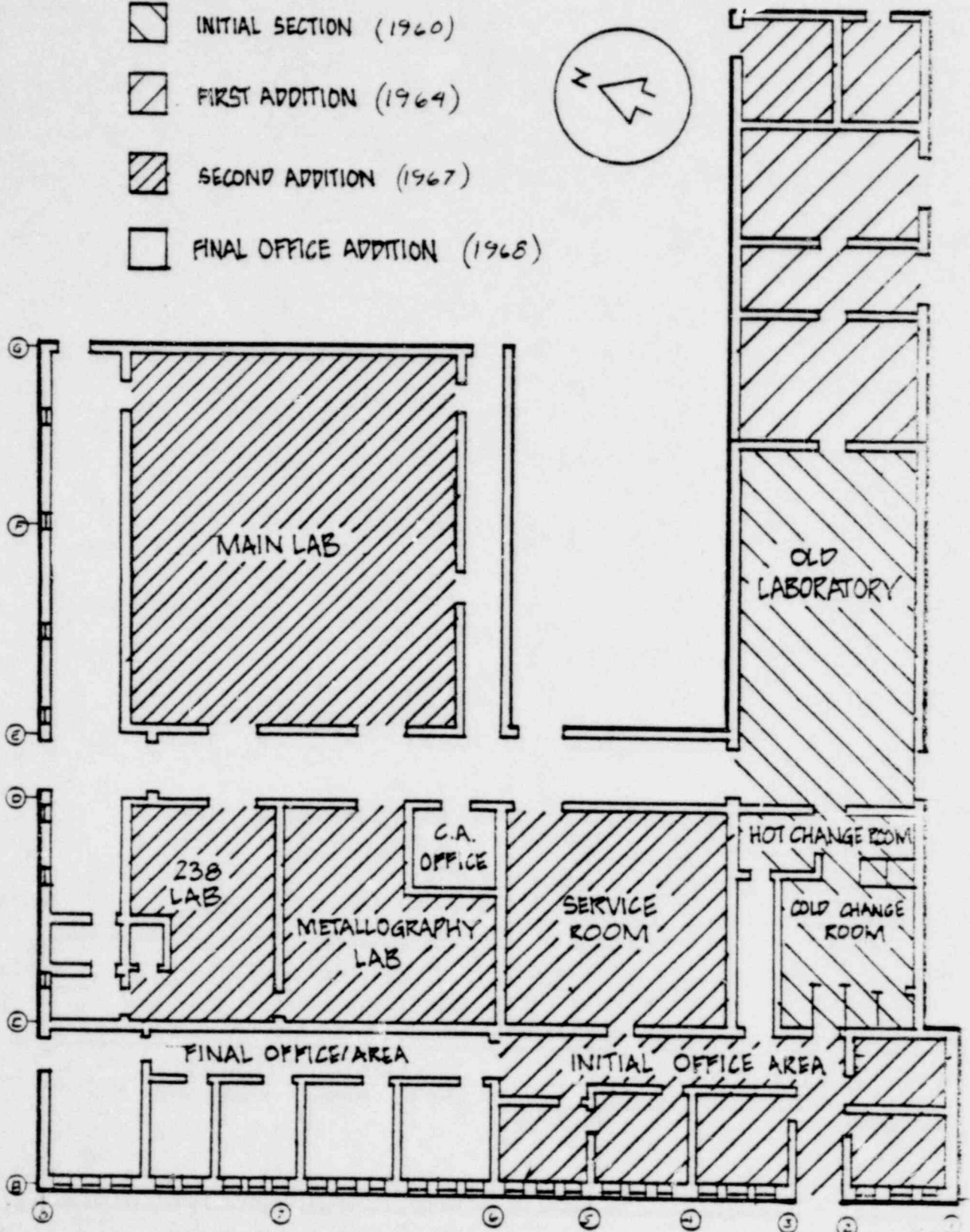
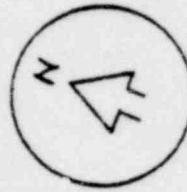


FIGURE 2-2. JN-4 PLUTONIUM LABORATORY FLOOR PLAN

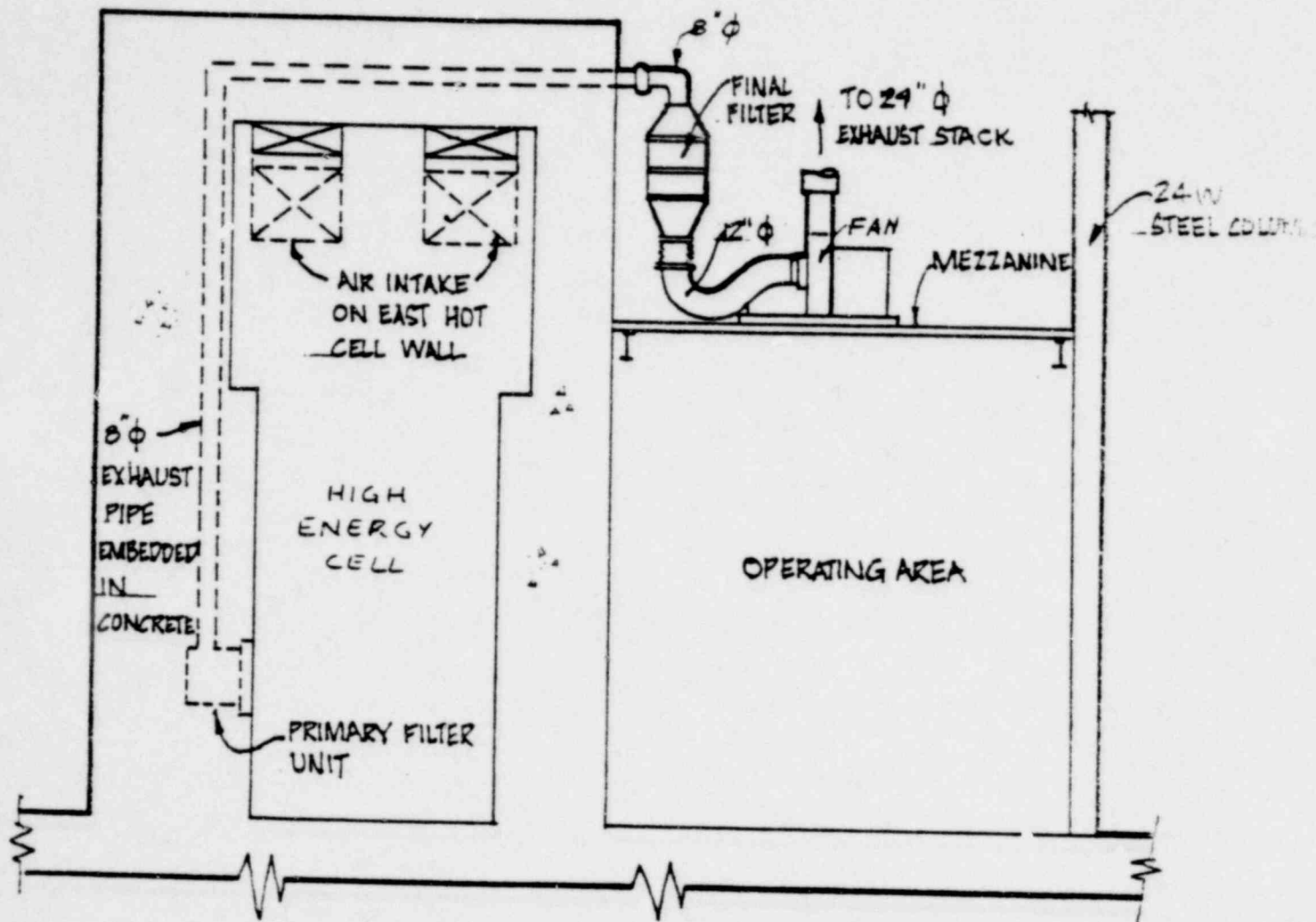
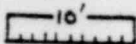


FIGURE 2-3. EXHAUST SYSTEM OF JN-1B HIGH ENERGY CELL

POOR ORIGINAL

- FLOOR EXHAUST FILTER
- A- POWER SUPPLY CONSOLE
- B- OPEN FRONT HOOD
- C- CONSOLE
- D- GAS RECIRCULATION UNITS
- E- HOT PRESS



▨ - CRITICAL GLOVE BOXES

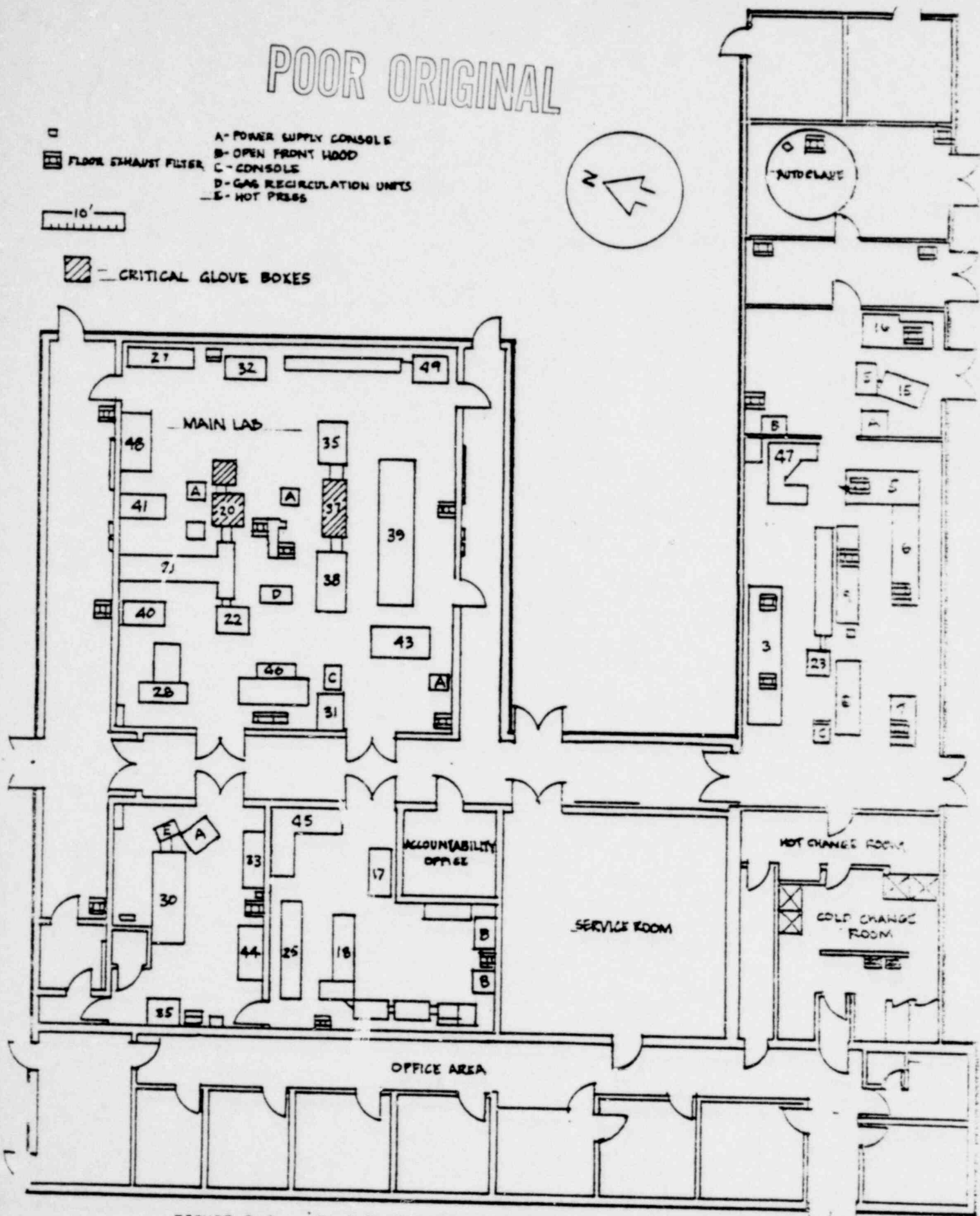
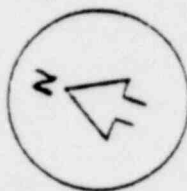


FIGURE 2-4. JN-4 PLUTONIUM LABORATORY GLOVE BOX ARRANGEMENT

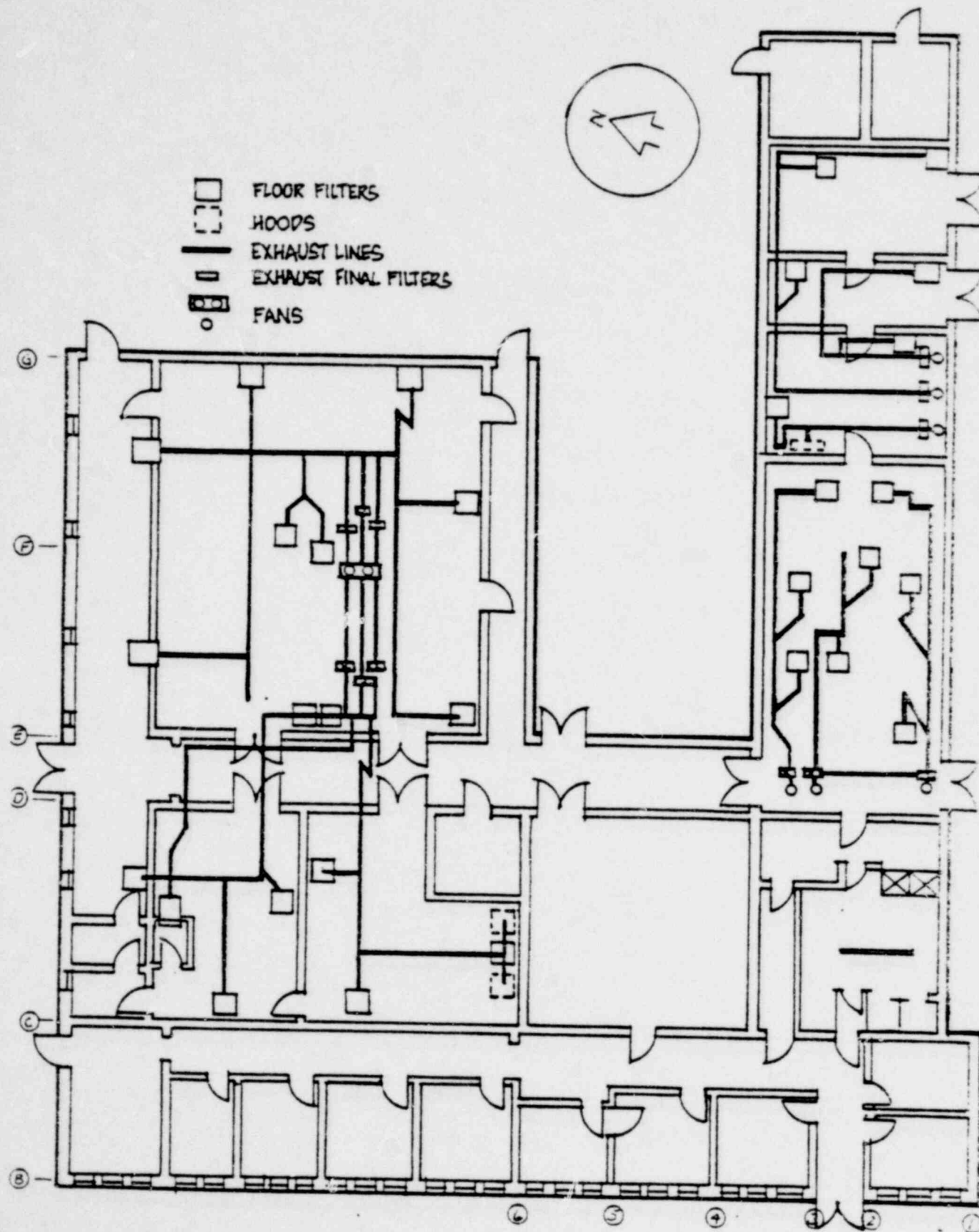


FIGURE 2-5. JN-4 PLUTONIUM LABORATORY VENTILATION SYSTEM

POOR ORIGINAL

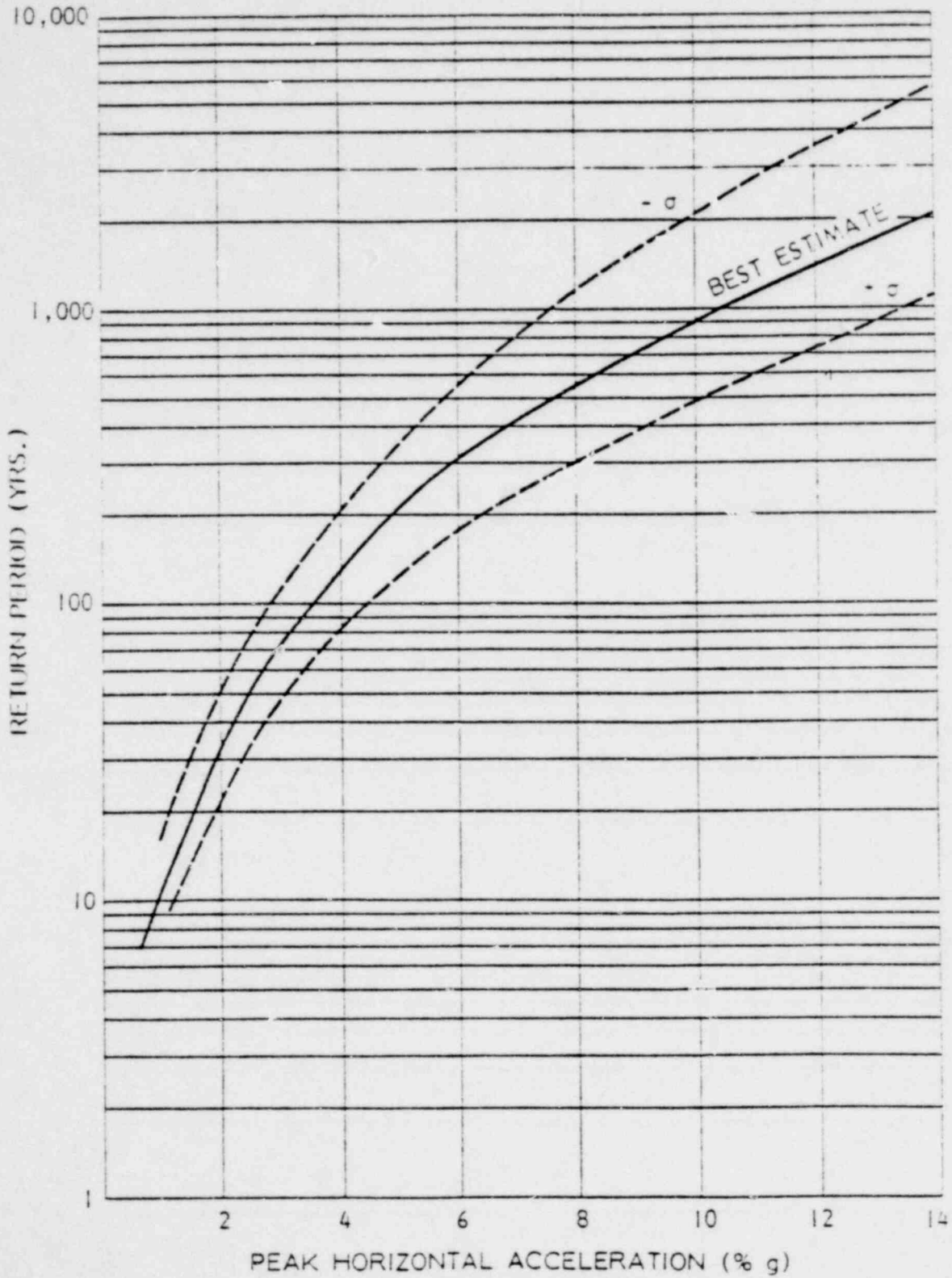


FIGURE 2-6. RETURN PERIODS FOR SEISMIC ACCELERATION AT THE BMI WEST JEFFERSON FACILITY (FROM REFERENCE 5)

3. EVALUATION OF STRUCTURAL BEHAVIOR.

This section of the report presents a discussion of the analysis of the BMI building structures including an identification of the lateral force resisting systems and the analysis procedures used in the evaluation. Information concerning the key structural details is given more extensively in the Task I Report (Reference 4). A discussion of the modeling considerations and a short description of the structural models utilized for analysis together with the analysis results are represented in this section.

3.1 JN-1B STRUCTURAL SYSTEMS

The principal area of concern in the JN-1B building is the response of the High Energy Cell (HEC) which forms the primary confinement barrier for the hazardous chemicals. The lateral seismic force resistance of the HEC is provided by the thick reinforced concrete shear wall box system tied together by a 4-foot-thick reinforced concrete cell roof slab. The HEC is rectangular in plan with a length-to-width ratio of 2.5 to 1. A vertical cross section through the cell is shown in Figure 2-1. Longitudinal and transverse sections are shown in Figures 3-1 and 3-2 respectively.

Deviations from structural symmetry are due to differences in wall thickness and the amount of high density concrete in each wall. The HEC may be considered to resist seismic forces by two independent systems; one for each major building direction, north-south and east-west. However, it is observed from the geometric layout that the north-south system of the HEC will be the

lowest capacity system. Because of the large mass and stiffness of the HEC and the weak coupling through the mezzanine and crane framing, the HEC will behave virtually independently of the main steel building frame. The HEC structure was modelled as a lumped-mass system supported by equivalent soil springs. The necessary soil properties required for calculation of soil compliance due to the HEC wall footing reactions were discussed in the Task I Report (Reference 4). The analysis of the nonlinear motion of HEC due to footing uplift was treated by means of the reserve energy method which is discussed in detail in Section 3.5.2.

The lateral seismic force resisting system of the JN-1B steel frame building may be described as a box system which consists of vertical braced frames with attached metal panels tied together by the roof system. The roof system consists of a 1-1/2 inch steel deck and a roof truss. The roof and wall panel inertia forces are transferred to the braced frames through diaphragm action of the roof system. The schematic drawings of the roof truss and vertical braced frames are shown in Figures 3-3 through 3-8. The east wall was designed and constructed so that the wall framing is hung from the roof with no structural ties to the JN-1A west wall. Thus, the east wall acts only as a deep flange for the roof and all lateral loads must be resisted by the other vertical braced frames. The metal wall panels were found to be incapable of resisting lateral inertia force transferred from the roof due to the fact that the metal panel joint lips at the vertical panel joints are too flexible to transfer any significant shear loads. Details of the metal wall panels were discussed in the Task I report. A sketch of the panels and their attachment is contained in Appendix C.

The in-plane wall seismic shear forces are transferred to grade through the spread footings and through the building floor slab. The 8-inch concrete floor slab is positively connected to the masonry wall foundation through steel dowels. The in-plane seismic overturning forces are transferred to the footings as axial forces through the steel column base connections.

The mezzanine is framed to the HEC and the south wall of JN-7B building as shown in Figure 3-9. The mezzanine floor slab is a 4-inch concrete slab poured on top of the 1-1/2 inch metal decking to form a composite section. The floor slab is classified as a "rigid" diaphragm based on Reference 8. However, due to the lack of vertical shear resisting elements the mezzanine will move in phase with the HEC under seismic ground motion. The mezzanine inertia force is transferred through the two 12W45 floor beams into the HEC.

Both tributary gravity roof loads and vertical seismic forces are transferred directly to the columns by roof girders (33W118) which span 71'-2" in the north-south direction. The exterior unreinforced masonry walls act independently of the rest of the building. The masonry walls are isolated from the structural steel frame because the void space between the masonry and steel is filled with plastic foam.

Due to the unsymmetric distribution of braced frame stiffnesses and heavy concentrated mass of the crane, there is a significant amount of eccentricity of the lateral inertia force with respect to the center of rigidity of the system. In order to

1363 031

account for this torsional effect, the response due to ground motion accelerations in both major building directions was determined in assessing the element capacities of the lateral force resisting system as discussed in the following section.

3.2 JN-1B STRUCTURAL ANALYSIS PROCEDURES

A general discussion of the analytical approach used in the Task II analyses of the High Energy Cell and the building structure follows. The procedure relating to the determination of the uncertainty bounds is presented in Appendix A and is discussed more extensively since it was not included in the Task I Report.

3.2.1 JN-1B Modelling Considerations

The development of a mathematical model which represents the physical behavior of a structure subjected to earthquake ground motion requires the idealization of the effective structural behavior of an assemblage of structural components and the appropriate lumping of distributed structure mass (weight). As previously discussed, the HEC structural system is essentially a shear wall box system tied together by a rigid concrete roof slab. Thus the HEC was modelled as a lumped-mass system supported by equivalent soil springs. In view of the very thick cell walls and length-to-width ratio of the HEC, the sectional properties of this shear wall box system were calculated based on elementary beam theory without considering the shear lag effect. The equivalent lumped-mass model was formed by considering the tributary mass of all four walls and other tributary masses where applicable.

1363 032

POOR ORIGINAL

For a structure which is as massive and rigid as the HEC, the foundation soil compliance can influence the overall dynamic response. The procedure used in this analysis was to include equivalent soil springs at the cell footing to account for the effect of soil compliance. The stiffnesses of the equivalent soil springs were estimated using relationships such as presented in Reference 9 for rectangular footings resting on the soil surface. The soil springs are based on the approximate elastic properties of the supporting soil developed in Task I. The effects of footing embedment (References 10 and 11) were included in the compliance estimate.

The JN-1B steel frame is also a box system which consists of vertical braced frames tied together by a roof system. The roof system consists of 1-1/2-inch deep steel decking supported by open web steel joists and roof beams and a roof truss which is located approximately 16" below the steel decking. The roof truss is an assemblage of roof girders, roof beams and steel angle cross bracings. To realistically model the behavior of the steel decking, a fairly detailed finite element analysis would be needed to model the nonisotropic properties of the decking and the behavior at and near the connections. However, preliminary calculations indicated that the roof truss by itself is stiff enough and has adequate capacity to provide the required diaphragm action so that an elaborate analysis of the roof decking was not warranted. The structural steel framing was modelled by a lumped-mass, two-dimensional finite element model representing the roof truss with springs attached at the boundary to represent the vertical braced systems. In general, the diagonal bracing members of the roof truss and the vertical braced frames are single structural steel angles which have very low compressive capacity. Thus, only

1363 033

diagonal braces in tension are considered effective in transferring inertia forces at the seismic response levels of interest. To reflect this behavior, only half of the actual axial area was used for the diagonal members in the mathematical model and the resulting forces modified accordingly. The lumped masses which were assigned to the model node points were formed by considering the tributary gravity roof weight and wall weight. The 50 ton crane was assumed to be located at the position where it would cause the most severe torsion on the roof truss.

Due to the different load paths for the crane mass in the two principal directions, the inertias representing the crane occur at different locations in the mathematical model. This occurs due to the two-dimensional representation of the structure which did not allow a detailed representation of the crane support system. The vertical response of the roof girders subjected to vertical ground motion accelerations at their supports was analyzed assuming a simple beam dynamic model.

3.2.2 Inelastic Behavior

In order to determine the seismic ground accelerations which characterize failure or collapse, behavior in the inelastic range must be considered. The nonlinear response of braced frame systems is generally relatively small compared with moment resisting structural systems due to fewer energy absorption and ductility mechanisms. Sources of nonlinear response prior to collapse of such systems come from yielding of steel members and from working or tearing of connections. Where significant steel yielding is involved prior to collapse, energy absorption is enhanced. For the JN-1B building, elastic buckling of diagonal members and local failure of connections govern the failure of the system with corresponding relatively low ductility.

The modal spectral method of dynamic analysis is appropriate for determination of response of the JN-1B building as represented by lumped-mass models. A system such as described, with hysteretic behavior and geometrically no particular weak point (i.e., a relatively uniform system), is well suited to analysis by the approximate nonlinear spectral-method (References 12 and 17). In this method, the elastic response spectra which define seismic input (and are used to calculate elastic system response) are modified to account for hysteretic energy absorption in the nonlinear system. The nonlinear analysis procedure is the same as for an elastic spectral analysis except for the utilization of the reduced or nonlinear spectra. The hysteretic energy absorption capacity is measured by the ductility factor which is the ratio of the maximum response deflection of a single-degree-of-freedom structure to its yield point deflection. The procedure for altering elastic response spectra to account for nonlinear behavior may be found in References 15 and 17. The spectral acceleration reduction factor, R , is a function of the system ductility factor, μ , within each spectral region. The factor R is taken as unity for the ground acceleration portion of the response spectrum, $1/\sqrt{2\mu-1}$ for the amplified acceleration spectral region, and $1/\mu$ for the spectral velocity and spectral displacement regions.

A number of references are available to assist in judging appropriate damping and ductility levels to represent response at the point of incipient collapse in the nonlinear analysis. In particular, References 18 and 19 report values of ductility and damping for various systems which may be used as guideline values. On the basis of values found in these references together with an

POOR ORIGINAL

1363 035

POOR ORIGINAL

evaluation of the connection details, upper and lower bound (one standard deviation) and median values for ductility and damping were selected. The ductility factors were determined based on whether the braced frame system is ductile or nonductile. A ductile braced frame is defined as one in which the ultimate strength of the joint (either welded or bolted) is at least 1.3 times the yield strength of the member being connected. Using this definition together with a detailed examination of the connections of all the diagonal members in the JN-1B structural system indicated the system would be classed as nonductile. A typical bolted connection detail of the roof truss diagonal bracing is shown in Figure 3-10. Based on values reported in Reference 18 for similar structures, median ductility factors as well as upper and lower one standard deviation bounds were selected. These values appear in Table 3-1. Table 3-1 also provides ductility factors which are appropriate for the independent analysis of the roof girder vertical response. The rigid body analysis of the HEC and the nonload-bearing masonry was based on the reserve energy method so no determination of the ductility factors of these systems was necessary. However, Table 3-1 includes the median as well as upper and lower bound damping values used for these systems in addition to those for the JN-1B frame and roof girders. The selection of the damping factors involved a comparison of the JN-1B building with similar structures for which referenced values are tabulated (Reference 19).

The definition of the seismic ground motion input for the site is provided (Reference 5) by elastic response spectra. The horizontal and vertical spectra to be used in the analysis are based upon the median data for an alluvium site resulting from the earthquake ground motion study presented in Reference 7. The resulting analysis response spectra, normalized to 1.0g peak

1363 036

horizontal ground motion, for ductility ratios of 1.0 (elastic) and 2.5 are shown in Figure 3-11. Also included in Figure 3-11 are the elastic horizontal response spectrum for 10 percent damping and vertical response spectrum, normalized to 2/3g peak ground motion, for a ductility factor of 6.5.

3.2.3 JN-1B Seismic Capacity Evaluations

Given a capacity criteria in terms of internal stress or deflection for a selected key structural element or connection, a capacity force resultant F_C , was directly obtainable using relations of engineering mechanics. For most of the details and elements investigated for structural capacity, the seismic response to ground motion was obtained from the overall dynamic analysis of the building. The forces within key elements (or connections) due to ground acceleration of 1.0g were obtained from the modal spectral analysis of the building models using the appropriate spectrum (median) given in Figure 3-11 for damping, β , and ductility factor, μ . The modal components of force within an element, $F_{m,1g}$, were combined using the square-root-sum-of-squares (SRSS) procedure to obtain an estimate of the element median resultant force due to dynamic response:

$$F_{SRSS,1g} = \sqrt{\sum_m (F_{m,1g})^2} \quad (3-1)$$

The ground acceleration capacity, A_g , for the element or connection under consideration, is then given by:

$$A_g = F_C / F_{SRSS,1g} \quad (3-2)$$

As discussed previously, there is a significant amount of torsional response of the JN-1B building due to the eccentricity of the lateral inertia forces with respect to the center of rigidity. Thus, the effects of response in both major horizontal directions were included in the analysis and the assessment of the structural element capacity. To reflect the fact that concurrent ground excitations in the two major horizontal directions are not necessarily of the same magnitude, and that the response maxima do not normally occur simultaneously, the element force resultant corresponding to 100 percent of the motion in one direction was combined with 40 percent of the resultants due to response in the other orthogonal direction by addition of the absolute values (Reference 19). On the basis that 40 percent of 2/3 of the horizontal accelerations (0.2 to 0.3g) is an order of magnitude less than the static 1g vertical forces, it is judged that the effect of concurrent vertical ground motions on these structural systems will be small and generally they were not included in the analysis.

The determination of the ultimate element or connection capacity, F_c , was generally based upon the ultimate stress distribution for the given material in the mode of element response considered. The determination of the structural material properties for the structural elements of the JN-1B Hot Cell Laboratory was part of the Task I effort. The estimated upper bound, median, and lower bound values of the material strength are tabulated in Reference 4 (see also Appendix C).

The determination of the soil capacity against shear failure under the HEC wall footing or each individual spread footing

1368 038

was based on ultimate soil pressure which was determined by multiplying the allowable soil pressure by a safety factor. Based on the soil report (Reference 6), the allowable design soil pressure at the JN-1B site was 4000 psf with a factor of safety of at least 3 against shearing failure. Thus the ultimate soil pressure is estimated to be 12,000 psf.

The ultimate strength capacities of the structural steel elements and connections were calculated using the requirements of Reference 20 and the general recommendations and guidelines given in Reference 21. The capacity of the column anchor bolts in combined tension and shear was estimated using the classical elliptical interaction curve (Reference 21). The ultimate static pull-out and shear criteria, including proximity and free-edge effects, for concrete inserts was based upon relationships and test data presented in References 23-24. The dynamic (seismic) ultimate capacities for concrete inserts were taken as 80 percent of the single cycle static ultimate value. Tests have indicated that no significant degradation in strength occurs under cyclic loadings below 80 percent of the static ultimate but that degradation and failure are rapid for loadings above the 80 percent level (References 25-27). Combined pullout and shear capacity of inserts was estimated using the ultimate strength interaction relation given in Reference 24.

3.3 JN-1B STRUCTURAL MODELS AND RESULTS

This section contains a summary of the mathematical model properties and the results obtained in the analysis of the High Energy Cell and the JN-1B steel frame structure. The results are summarized in terms of ground motion acceleration levels which would cause collapse of an individual detail or system mode collapse.

1363 039

These results are presented in Table 3-2. For lower levels of collapse response and particularly for the controlling collapse models, median as well as one standard deviation upper and lower bounds are given. For details which have significantly greater capacity, only the median values are given. Ground acceleration capacities are given to several significant figures in order to indicate the likely range of failure. It should not be implied that the analysis justifies accuracy to this level. Additional details of the analysis are contained in Appendix B.

The mathematical model used to evaluate the dynamic response of the HEC in the weak axis (N-S) is shown in Figure 3-12 with the equivalent soil springs attached at the base to account for the effect of soil compliance. The formulation of the equivalent soil springs was discussed in Section 3.2.1 of this report. The model was formulated employing the EDAC/MSAP computer code which is a version of the general structural analysis computer program SAP IV (Reference 28). The numerical values assigned to the element properties and lumped masses for the mathematical model are also given in Figure 3-12.

The dominant principal mode shapes for the N-S response obtained from a modal analysis of the HEC model are shown in Figure 3-13 together with the natural frequencies. It is observed that the first two significant modes are basically rigid body rocking of the HEC. Also shown in Figure 3-13 are the SRSS element forces obtained from a response spectrum analysis using the ground spectrum given in Figure 3-11 ($\mu = 1.0$, $P = 10\%$). Based on the nominal shear strength of the reinforced concrete, the shear capacity of the HEC was found to be 0.74g. A linear soil pressure distribution was assumed in the HEC uplift analysis. Although this is inexact, it

does not introduce an appreciable error in the overturning moment calculation which is the principal concern. Using the median overturning moment (SRSS) obtained from a dynamic response spectrum analysis of the lumped-mass cell model and the restoring moment due to the gravity weight of the cell, the median initiation of uplift ground acceleration capacity, A_g , was found to be 0.23g. At this level the HEC will respond essentially as a rigid body, even after initiation of uplift. Uplift is defined as the point at which initial separation of an edge of the footing from the soil occurs and not when the entire footing is pivoting about a corner.

As discussed in Task I report, the reserve energy method was also utilized in the HEC rigid body rocking analysis in order to evaluate the ground acceleration capacity for the eventual overturning of the HEC. This capacity was found to be 4.2g. Even the initiation of uplift (0.23g) is significantly above the range of ground accelerations where valid data exists upon which to determine the return period. Therefore, with such a high approximate capacity for overturning it was judged that a time history dynamic analysis of the HEC including the effect of uplift was unnecessary.

The dynamic model used to evaluate the response of the JN-1B building for seismic ground motions is shown in Figure 3-14. The finite element mathematical model was formulated employing the EDAC/MSAP computer code. The three-dimensional elastic beam elements and boundary spring elements were utilized to construct the model with the necessary kinematic constraints to achieve the element stiffnesses desired. As discussed previously, the model is a two-dimensional representation of the roof truss with boundary spring elements representing the vertical braced frames. The stiffnesses of the vertical braced frames were calculated based on

1363 041

static analyses assuming that only those diagonal bracings in tension are effective in transferring shear force. In view of the connection details, the columns of these braced frames were assumed pinned at the base. The effective stiffnesses of the braced frames along column lines Q and 13 of the crane framing were calculated to account for the force transfer from the roof truss to the crane framing. Table 3-3 summarizes the stiffnesses of all braced frames. As noted previously, the modeling of the mass distribution of the 50 ton crane mass in the roof truss is dependent on the direction of the roof truss response. Assuming the crane is parked at the east end of the building as shown in Figure 3-14, for response in the N-S direction, more than half of the total crane inertia loading is transferred to the roof truss through the 12W27 horizontal strut at the crane level and the main building column along line P. This mass distribution is reflected by the two heavy Y-direction nodal masses at node 5 and node 25 as shown in Table 3-4. The rest of the crane mass inertia in the Y-direction is resisted by the braced system (12W40 diagonal strut) along line Q. For roof response in the E-W direction, the crane mass along column 16 is transferred to the roof truss through the cross bracings of the north wall framing as reflected by the heavy X-direction lumped masses at node 1 and node 3 in Table 3-4. The crane mass inertia along column line 13 is then resisted directly by the cross braced system of the crane framing. The material property and section properties of the beam elements are summarized in Table 3-5.

The dominant mode shapes obtained from the modal analysis of JN-1B building frame for ground motion levels less than 0.11g are shown in Figures 3-15 through 3-17. The first three modes, which have more than 95 percent of the mass participating, were included in the dynamic response spectrum analysis. An elastic response

1363 042

spectrum analysis was first conducted in order to evaluate the yielding of the structural bolts at the connections and the elastic buckling of the diagonal bracing members. It was found that at some of the highly stressed connections the bolts begin to yield at a ground acceleration of 0.08g. The double angle tension/compression diagonal member of the north wall braced frame (Figure 3-4) was also calculated to buckle at a relatively low ground acceleration (0.11g). The north frame is assumed to lose its lateral force resisting capacity as soon as this diagonal member buckles. Thus, the inelastic response spectrum analysis of the JN-1B building frame was performed with any remaining stiffness of the north wall braced frame neglected. The mode shapes of the first three significant modes for the JN-1B structure with buckled north frame cross brace are shown in Figures 3-15(a) through 3-17(a). The SRSS element forces obtained from inelastic dynamic analyses for a) 1.0g N-S and concurrent 0.4g E-W ground motions and b) 1.0g E-W and concurrent 0.4g N-S ground motions are summarized in Tables 3-6 and 3-7.

The most critical structural elements and details evaluated for the inelastic behavior of the JN-1B building are the connections of the diagonal bracings of the roof truss and the remaining vertical braced frames, the compressive capacity of the braced frame member, and the capacity of the main building columns and the column anchor bolts.

Using the median element forces (SRSS) obtained from the dynamic response spectrum analysis of the finite element model and the median element capacities, the median ground acceleration capacities, A_g , were computed as indicated by Equation 3-2. Additional inertia forces of the part of the crane mass which is

resisted directly by the crane framing were evaluated and included in assessing the ground acceleration capacity of the crane framing. Table 3-2 presents the ground acceleration determined for each of the elements or connections with major damage potential considered for the JN-1B structural system.

The critical detail of the mezzanine framing in transferring the mezzanine inertia force to the HEC is the one-inch diameter concrete inserts which connect the two 12W45 floor beams to the HEC south wall. The detail of this connection is shown in Figure 3-9. The spectral acceleration of the mezzanine due to the seismic ground motions was determined based on the ground response spectrum and the dynamic properties of the HEC. The ground acceleration capacity of this connection was found to be 1.90g which is greatly in excess of any anticipated ground motion acceleration levels for the site.

Some ground acceleration capacities for other system considerations (vertical roof girder response and rigid body rocking of the HEC and unreinforced masonry walls) are also tabulated for comparison. The lower and upper bounds of the ground acceleration capacities were determined as described in Appendix A. For details with collapse capacities significantly greater than the controlling capacity, only median values are given.

The lowest collapse capacity of the JN-1B building system (0.30g) is associated with the shear failure of the bolts at the connection of the roof truss diagonal bracing. The loss of the diaphragm action of the roof truss due to this connection failure is postulated to then lead to the total collapse of the JN-1B building. Again, this acceleration level is considerably above the predictable return period acceleration levels.

1363 044

3.4 JN-4 STRUCTURAL SYSTEMS

The JN-4 Plutonium Laboratory is an unsymmetric, U-shaped building constructed in several phases with different methods of construction. A floor plan is shown in Figure 2-2. Although they are nominally part of the same building, the initial (Old Lab) and final office addition portions of the structure were not analyzed. No critical facilities are located within these parts of the structure and they will tend to respond independently to seismic excitation due to lack of structural ties and a 6-1/4 inch gap between the Old Lab and the main lab portion of the structure. In the main laboratory, lateral force is resisted by a steel column/unreinforced masonry wall system supporting the roof. The roof system is fabricated from 6-inch deep by 24-inch wide precast concrete channel sections which span between the roof beams. A 1-1/2 inch rigid insulation and built-up roof is supported by the channels. Inertial roof loads are transmitted to the exterior walls at the steel column connections and to the exterior masonry walls by means of the columns bearing against the masonry blocks. The exterior masonry walls thus act as shear walls preventing large deformations of the adjacent steel frame. The shear walls of concern are the north, south, east, and west exterior walls of the Main Lab and north-south wall between the original office and service room and Old Lab portions of the structure. The interior masonry walls do not support any roof structure but are locally grouted to the joists. Grout was considered to be ineffective in transmitting shear due to the observed presence of cracks between the grout and beams.

The ability of the masonry to act as shear walls is significantly degraded by the numerous floor to ceiling windows in the north and south exterior walls. Also, the ability of the south wall between the service room and the original structure (Old Lab)

1363 045

to transmit shear is quite limited. This occurs because the load path for the horizontal inertia roof load which must be transferred to the wall through a precast concrete slab is limited by the friction between the lower steel beam and the slab. The vertical roof load is carried by the steel columns, however, so that the normal (vertical) load and hence the friction capacity to transmit shear is quite low.

The channel slabs resting on top of the steel beams will act as a diaphragm transmitting the lateral inertia loads to the exterior shear walls for low levels of response. Due to the fact that the structure is unsymmetric, the center of mass and the center of rigidity are not coincidental. Therefore, the torsional effects due to earthquake loads must be considered at levels for which the diaphragm action exists.

The vertical force resisting system consists of the precast concrete roof channels supported by unbraced 8 to 21-inch deep rolled steel beams. Lightweight square steel columns embedded in the masonry walls support the roof system. The exterior columns are field welded to the continuous 3/8-inch steel plate which rests on the concrete grade beams. Window and door openings are spanned by 8 x 8 inch precast concrete lintels.

Inelastic behavior of the structure begins upon the cessation of diaphragm action of the channel slabs and significant cracking of the masonry occurs. At this point, the structural resistance of the building may be examined in two independent orthogonal directions since the torsional coupling becomes of negligible importance. At these levels of response, the structural

1363 046

elements which resist the inelastic behavior of the JN-4 facility, (rigid body rocking of the walls and roof) are the couple action of the channel slabs on the steel beams, the interference of the exterior masonry walls with steel beams, and the in-plane shear resistance of the unreinforced masonry walls. These systems will be discussed more extensively in Section 3.8 and in Appendix B.

3.5 JN-4 STRUCTURAL ANALYSIS PROCEDURES

This section contains the modeling techniques and assumptions used in the analysis of the JN-4 Plutonium Laboratory. Significant differences in the approach are evident between the linear models valid for low levels of seismic response compared to the models used for increased levels where collapse of the structure is imminent. The procedure for determining the uncertainty bounds is presented in Appendix A.

3.5.1 JN-4 Modelling Considerations

In creating a mathematical model of a structure such as the JN-4 Plutonium Laboratory for various levels of earthquake response, idealization of the various structural elements need to be made. Judicious choice of mathematical models which will accurately represent the dynamic response of the physical structure is necessary. These are in addition to the normal requirements of mass and stiffness considerations required in order to calculate the correct response of the structures for various levels of ground excitation.

In modeling the JN-4 facility for low levels of ground excitation, consideration of the steel framing interacting with the unreinforced masonry walls in order to develop an elastic model representing the complete structure composed of the Main Lab,

1363 047

initial office building, etc., was required. Finite element models were created for the north wall, the east wall, and south wall of the laboratory portion of the JN-4 building. These models considered soil compliance, footing flexibility, and masonry wall stiffness. A typical finite element model used for the south wall is shown in Figure 3-18. Soil compliance was evaluated through the use of the soil properties presented in the Task I report. Discrete soil springs were used to represent the support of the surrounding soil in both the vertical and horizontal directions. The soil spring constants were evaluated using relationships presented in Reference 9. Soil springs were calculated for a rectangular footing resting on top of the soil surface. These values were then modified to account for the effects of footing embedment (References 10 and 11). It should be noted that the soil springs were included in the models in order to assess the effect of soil compliance on wall stress distribution and not to model soil-structure interaction effects which are considered negligible for this type of structure.

The soil springs were used in conjunction with plane stress membrane elements and beam elements in order to accurately determine the equivalent stiffnesses of the various walls. The footing was modeled as a continuous beam supported at discrete points by boundary elements (soil spring). Steel columns and surrounding masonry comprising the individual columns were represented by beam elements. A transformed section was used to account for differences in the material properties of the steel and masonry. The unreinforced masonry walls were represented by plane stress membrane elements. The finite element models were analyzed using a static analysis with the EDAC/MSAP computer program.

POOR ORIGINAL

The static analysis calculated an equivalent in-plane shear stiffness for the wall. Displacements and rotations were distinctly different from the corresponding values computed for a uniform shear wall. However, the finite element model results for the east wall, which is a homogenous unreinforced masonry wall, may be closely approximated by hand calculations. Therefore the elastic shear stiffnesses of the other homogeneous walls in the JN-4 facility were evaluated using simple hand calculations.

In creating an overall elastic dynamic model of the JN-4 facility, a two-dimensional model was used as shown in Figure 3-19. The shear springs attached to the model account for the in-plane stiffness of walls along the various column lines. The shear spring stiffnesses were evaluated from the results of the finite element models of the north, south, and east walls, and from hand calculations of other critical walls. For low levels of response where the roof channel friction forces are sufficient to provide diaphragm action, the channel slabs were modeled as plane stress membrane elements attached to the structural steel roof framing system.

The distribution of mass was accounted for in two manners in the JN-4 facility. Distributed mass was used in conjunction with the plane stress membrane elements. Additional discrete tributary lumped masses were used at appropriate nodes to account for interaction of the shear walls with the roof framing system.

1363 049

POOR ORIGINAL

3.5.2 JN-4 Inelastic Behavior

In order to accurately determine the collapse capacity of a building of this type under earthquake loading, behavior of the structure in the inelastic range must be considered. The approach taken in analyzing the JN-4 facility was to use the Reserve Energy (RE) Method in conjunction with rigid body rocking of the roof framing system and the unreinforced masonry walls.

The RE method is relatively simple to use and has been shown to give good results for rigid body wall systems (Reference 29). The rigid body behavior to be analyzed is illustrated in Figure 3-20 for a simple wall/roof system and involves pivoting (rotating) of the wall about a small segment (effectively a corner) at the edge of the wall base. This rotation occurs under the action of the horizontal inertial forces due to ground shaking. The inertial forces may be represented by a force F , concentrated at the roof line. This is appropriate for analysis as a large share of inertia is generally contributed by the roof. As the wall moves through the displacement δ , measured at the roof line, the stabilizing weight of the roof and wall becomes less effective until at δ_{RB} the restoring moment is zero. This deflection, δ_{RB} , is taken to be the collapse displacement for purposes of the evaluation analysis, and it occurs when the lateral force resistance capacity becomes essentially zero. At the beginning of rigid body resistance (with $\delta = 0$) the maximum inertial force capacity F_{RB} , maintains equilibrium with the restoring force of the wall and roof weight, considering pivoting about the edge of the base. The force-deflection diagram shown in Figure 3-21 depicts the behavior of a typical wall through the first cycle of motion as it cracks through, and then responds as a rigid body with the effective

1363 050

POOR ORIGINAL

degrading stiffness from F_{RB} at $\delta = 0$ to $F = 0$ at δ_{RB} . After through-wall cracking at low shaking levels, the force-deflection diagram for subsequent cycles of shaking is essentially that shown by the dashed line in the nonlinear diagram of Figure 3-21. It is noted that the maximum force level prior to cracking is approximately equal to F_{RB} as indicated by the dashed and solid diagrams. Thus the two diagrams are essentially colinear and K and K_2 both have equal values.

The RE method consists of analyzing an equivalent elastic system by the modal spectral method of analysis. The equivalency is maintained by equal energy capacity of the nonlinear system and its equivalent elastic system. This equivalence is obtained as shown in Figure 3-21 by comparing the non-linear and linear diagrams. Failure of the linear system thus occurs at the force F_{RB} and deflection δ_{RB} which corresponds to the force and deflection capacity of the nonlinear wall/roof system. The energy equivalence is shown in Figure 3-22 together with the equivalent linear and nonlinear models. A time history response analysis was conducted in conjunction with the evaluation of another facility in this study (Reference 29) on a similar unreinforced masonry wall and the results were favorably compared with those obtained from the RE method. The results of this comparison are contained in Appendix D.

Response spectrum analysis techniques are used in conjunction with the Reserve Energy Method. The WASH 1255 median response spectrum for alluvium soil conditions (Reference 7) with 10% damping and a ductility ratio equal to 1.0 was deemed appropriate for use in the inelastic analysis. The damping in the masonry wall is the result of cracking and crushing of the mortar

1363 051

under the concrete blocks during rigid body rocking. Damping of the roof system results from the sliding of the concrete channel slabs relative to the steel beam as well as yielding at the framing connections.

3.6 JN-4 STRUCTURAL MODELS AND RESULTS

Due to the fact that the JN-4 facility is an unsymmetric structure, torsional effects on the building are important for low levels of earthquake response. Therefore the initial section, 3.6.1, will consider a completely elastic structure with concurrent loadings in two orthogonal directions. Subsequent sections will examine the building under higher ground accelerations. An elastic model with a released roof diaphragm and rigid body rocking models were used to determine structural system capacities as appropriate for increasing ground motion input levels.

3.6.1 JN-4 ELASTIC ANALYSIS

The dynamic model used to evaluate the initial elastic response of the JN-4 facility is shown in Figure 3-19. The two-dimensional model contained boundary elements, (shear springs), beam elements, and plane stress membrane elements. The shear springs represented the in-plane stiffness of the unreinforced masonry wall. These springs accounted for wall flexibility, soil compliance, and the footing stiffness.

The finite element beam members represented the beams in the roof framing system. End conditions of the beams were evaluated as fixed or pinned as required by the structural steel drawings of the JN-4 facility. The plane stress membrane elements attempted to account for the couple action of the channel slabs interacting with the steel framing. This couple action is more fully explained in Appendix B.

The main purpose of the elastic model was to investigate the degree of dynamic coupling between the Main Laboratory Building and the Initial Office Area (Figure 2-2) and determine the onset of masonry cracking and other nonlinear response and the locations where these effects would occur. The Old Lab and Final Office Areas were not considered in the dynamic model because of absence of structural ties with the Main Laboratory Building as previously discussed.

Figure 3-23 is an isometric sketch of the structural steel layout in the JN-4 Facility. The portion of the sketch labeled building interface required some additional consideration in developing a two-dimensional model of the facility. To account for the flexural stiffness of the columns extending above the office area, artificial beam elements were included in the two-dimensional model. The axial stiffness and shear stiffness of these elements accounted for the out-of-plane and the in-plane bending of the columns, respectively. These beam elements are numbered 77, 81, 88 in View A of Figure 3-19.

The elastic dynamic analysis used the median horizontal response spectrum for alluvium soils (Reference 7) with $\beta = 7\%$ and $\mu = 1.0$ (Figure 3-11). The analysis was run on the EDAC/MSAP computer program.

The results of the elastic dynamic analysis showed that the Main Laboratory and the Initial Office Area essentially are uncoupled. The first six modes investigated had almost 100% of the structural mass participating in both the X and Y directions. The fundamental mode shape is shown in Figure 3-24. The Main Laboratory portion of the facility responds in the N-S direction while the Office Area is unaffected, even though the interface wall is loaded in the in-plane direction.

1363 053

The Main Laboratory Building responded within a range of frequencies from 10-23 hertz. In order to account for torsional effects, the hypothesized earthquake loading was applied to the building concurrently in two orthogonal directions. The major acceleration component was designated $1.0 A_g$ with the minor acceleration component assumed as $0.4 A_g$. Initial failure of the diaphragm action of the roof channels slabs occurred at $A_{gm} = 0.03g$ for E-W direction excitation along the channel slab-beam interface atop the wall between the Old Lab and the service room (Location I in Figure 3-19). For principal excitation in the N-S direction the corresponding median ground acceleration is $0.076g$ with initial slipping occurring along the east wall.

3.6.2 Modified Elastic Analysis of the JN-4 Facility

The loss of the diaphragm action of the channel slabs was accounted for by some basic modification in the two-dimensional computer model. The modified elastic model deleted all the plane stress membrane elements and lumped all the roof mass at discrete nodes. This model was then used to investigate the dynamic characteristics of the structure at ground motion accelerations above the 0.03 to $0.08g$ levels, but below the collapse levels where very large deformations result. The analysis results show a large frequency shift will result due to the release of the roof diaphragm. The structure now responds in two basically independent fashions. The roof framing with the lumped masses due to uniform roof weight was found to respond at frequencies in the range of 1 hertz. The wall masses located along column lines represented by the shear springs were found to respond at much higher frequencies.

1363 054

Figures 3-25 and 3-26 show the mode shapes of the major framing systems for the modified two-dimensional model. Table 3-8 lists the frequencies of these modes.

For ground acceleration levels above the accelerations which cause loss of roof diaphragm action but below the point where significant rigid body out-of-plane rocking of the masonry walls occurs, the response is characterized by in-plane motion of the various roof bays. The channel slabs contribute virtually no restraint for these modes with the only restraint resulting from bending about the weak axis of the roof beams. Since the out-of-plane motion of the walls is not sufficient to result in arching of the masonry between the roof beams and foundation and since the grout was assumed incapable of transmitting out-of-plane shear, no restraint results from out-of-plane loading of the walls.

A response spectrum analysis was run with the modified elastic model in order to calculate forces on the shear walls due to the dynamic response of the roof. The range of ground motion levels for which this model is applicable varies with the direction of motion and the location within the structure. For E-W input, hinging of the steel columns at the base occurs in the range of 0.04g along column line 7 while slipping of the 2-foot wide concrete slab adjacent to the corridor between the service room and the Old Lab along column line 4 results at approximately 0.08g. For N-S excitation hinging of the columns along column line F occurs in the range of 0.09g. Portions of the solution to the modified elastic two-dimensional model were combined with the rigid body rocking analysis in order to calculate shear forces on various structural elements.

1363 055

3.6.3 Dynamic Response of Unreinforced Masonry Walls

The cracking capacity and the collapse capacity of the unreinforced masonry walls were investigated for several modes of collapse. The cracking capacity of the walls at the base was defined as the dynamic load required in order to create a condition of zero strength under one edge of the wall for the exterior walls. This assumes there is no tensile bond strength between the steel base plate and the masonry wall. The interior walls crack when the dynamic tensile stress equals the tensile strength of the grout. Table 3-9 identifies four different wall cracking capacities.

The two capacities listed as most probable for cracking to occur are the ones in which the walls act as a free-standing cantilever. The second set of capacities were developed on the hypothesis that the steel roof beams interface with the walls to such an extent that the tops of the walls are restrained. In this mode, in order for the walls to form significant cracks, a second crack must occur close to the mid-height of the wall (Figure 3-27). Since cracks are known to exist in the grout between the top of the wall and the bottom flange of the beam, significant rocking of the walls must occur before interference can occur.

The collapse capacities of both the interior and exterior walls were also investigated for a number of different failure modes. Table 3-10 identifies three basic failure modes with their respective collapse capacities.

The first failure mode for both the interior and exterior walls considered the walls acting as a free-standing rigid body cantilevers rocking about their own base (Figure 3-20). For this case, the walls were assumed to be totally independent of the roof

1363 056

girders which implies no out-of-plane shear is transmitted through the grout between the top of the wall and the bottom of the beam flange. Collapse was calculated to occur at a median ground capacity, A_g , of 0.18g for exterior walls and 0.14g for interior walls. Interior walls which do not have the benefit of roof beam support are expected to collapse at this ground acceleration.

The second type of failure mode considered interference between the roof beam and the wall during rigid body rocking. The roof beam was modeled as a spring supported roller which provided a normal force to the wall for all wall configurations during rigid body rocking (Figure 3-28). This model accounts for some interference between the wall and beam such as would result due to closure of cracks in the grout due to rigid body rotation of the wall about a lower corner. The flexibility of the beam is considered in this model and a low coefficient of friction between the wall and beam is assumed as should be appropriate as the result of the pulverizing of some of the grout. This model provides intermediate levels of collapse between those resulting from a free-standing cantilever exterior wall and one which is restrained at the top by a pinned connection and hence cause cracking and subsequent buckling at some mid-height elevation. This failure mode was considered to be the most likely with median ground motion collapse levels calculated at 0.18g for E-W excitation and slightly lower at 0.178g for N-S excitation. The Reserve Energy Method was also used in conjunction with this model. Although the maximum displacements and the effective masses for this case are substantially different from the free-standing wall model, the resulting ground acceleration capacities for failure were almost the same (Table 3-10). The reason for the similarity of the answers is

because that although the second failure mode is stiffer due to the restraining influence of the beam, the additional mass from the beam acting with the wall negates any large shift in frequencies that normally would occur. The slight difference in ground acceleration capacity for the two orthogonal directions is due to the different wall configurations considered.

The third type of failure mode considered assumed that the roof provided so much restraint that the walls had to fail in the knee action mode shown in Figure 3-27. This is unlikely to occur except possibly close to the intersection of the shear walls since the walls and roof framing must act integrally as a unit at all times.

3.6.4 Ultimate Collapse Capacity of the JN-4 Structure

Three basic failure modes were found to be critical when examining the collapse of the Main Laboratory portion of the JN-4 facility. Figures 3-29 and 3-30 show the basic rigid body rocking failure modes which were considered. At ground motion levels approaching the collapse levels of the structure, rigid body rocking of the JN-4 facility in the E-W direction along column line 7 occurs because of the low lateral resistance of this column line in comparison with the other column lines. A plan view of the structural steel columns and important masonry walls along column lines 6, 7, and 8 is shown in Figure 3-31. Column line 7 has almost no restraint in the way of masonry shear walls for rigid body rocking of the roof in a westerly direction. Although stronger than column line 7, column lines 6 and 8 also have shear capacities below that of uniform homogeneous shear walls due to the numerous floor to roof windows. Examination of the detail of a typical column (Figure 3-32) shows that each 4 x 4 inch steel column is surrounded by a small masonry pier. In between this small pier and the adjacent

masonry wall is a 3/16-inch plate glass window. However, Figure 3-32 shows the 8 x 8 inch precast concrete lintel which is capable of transferring in-plane loads from the steel column to the adjacent masonry wall. In considering the strength of this detail, consideration was given to the bearing stresses occurring at both the steel-lintel interface and the lintel-masonry block interface. The shear stress in the masonry walls was investigated along with the possibility of the whole masonry wall sliding along the steel base plate. All shear walls were examined for both lateral loads due to rigid body rocking and the simultaneous nearly elastic response of the structure forming the adjacent stronger bays.

As previously discussed, a significant restraint effect results due to the couples formed in the individual roof channels at significant response levels. These couples develop through friction between the roof beams and the channels. Appendix B describes the development and magnitude of these restraint forces when the ground motion is assumed parallel to the direction of rigid body rocking response of the bay. Also described is an approximate method of accounting for simultaneous horizontal input components. The reduction in capacity as a result of a simultaneous ground acceleration equal to 0.4 times the principal horizontal input was computed on the basis of a typical critical slab and results in a decrease in capacity of approximately 16 percent when compared to only a single input component.

The median ground motion collapse capacity of the structure with maximum response along column line 7 was calculated to correspond to a ground motion input of 0.17g. The resulting maximum rigid body displacement at the roof elevation is 7.3 inches.

1363 059

Another critical section of the building considered for E-W excitation was the rigid body rocking of the bay between column lines 4 and 6. This portion of the building was determined in the Task I report to contain a natural gas line. The model used in evaluating the rigid body rocking capacity is shown in Figure 3-33. The same figure shows the brick and block wall which ties the separate stories together. Therefore a displacement, δ , of the lower story will create a displacement of the same magnitude at the roof line of the upper story. For this model, the restraint of the structure due to the 2-foot-wide channel slab roof was again evaluated in considering the rigid body rocking. The median ground motion collapse capacity of the structure was determined to be 0.26g at a maximum displacement of 9.8 inches.

The other major rigid body rocking motion that occurs in the N-S direction in the JN-4 structure is along column line F (Figure 3-29). This motion again occurs because of the relatively low lateral resistance of the steel frame along column line F (Figure 3-31) in comparison to the adjacent column lines Ea and G which act as shear walls. The restraint provided by the couple action of the channel slabs is different for rigid body rocking of the structure in this direction. This is because the forces created by the channel slabs are dependent on the orientation of the slabs on top of the steel framing. Appendix B contains a more detailed explanation of the channel slab-steel frame interaction forces developed during rigid body rocking in the N-S direction.

The collapse of the structure for rigid body rocking along column F was calculated to occur at a median ground acceleration of 0.23g with a maximum rigid body displacement of 9.6 in. Thus, the

first part of the JN-4 structure to collapse is the Main Laboratory. This is calculated to occur at median ground acceleration levels of approximately 0.17g for E-W excitation or 0.23g for N-S excitation. The initial mode of failure for both these directions is rigid body rocking out-of-plane of the outside walls as shown in Figures 3-29 and 3-30. At least initially after this type of collapse, some portions of the shear walls could remain standing as well as other portions of the structure such as the service room and initial office portions of the structure. Total collapse, however, is expected at median ground excitation levels of approximately 0.26g. A summary of the important seismic capacities of the JN-4 structure together with their upper and lower bounds appears in Table 3-11.

1363 061

TABLE 3-1

SYSTEM DUCTILITY FACTORS AND DAMPING RATIOS
FOR THE JN-1B ANALYSIS

Key Element	Ductility Factor, μ			Damping, β (%)		
	Lower Bound	Median Value	Upper Bound	Lower Bound	Median Value	Upper Bound
Braced Frame System	1.5	2.5	4	10	15	22
Roof Girder Vertical Response	2.5	6.5	10	3.5	5	7
High Energy Cell	—	1.0	—	7	10	14
Masonry Wall Rigid Body Rocking	—	1.0	—	7	10	14

1363 062

TABLE 3-2. SUMMARY OF CAPACITIES AFFECTING JN-1B CONFINEMENT BARRIERS

Structural Element Description	Structural Response Description	Structural Damage	Ground Acceleration Capacity, A_g (g)		
			Lower	Median	Upper
Bolted Connection of the Diagonal Members of the Roof Truss	Elastic Response to Concurrent N-S and 0.4 E-W Ground Motions	Yielding of the A307 Bolts	0.06	0.09	0.11
Bolted Connection of the Diagonal Members of the Roof Truss	Roof Response to Concurrent N-S and 0.4 E-W Ground Motions	Shear Failure of 2-A307 Bolts; Loss of Roof Diaphragm Action	0.17	0.30	0.54
Bolted Connection of the Diagonal Member of the South Wall Braced Frame	Shear Response to Concurrent N-S and 0.4 E-W Ground Motions	Shear Failure of 2-A307 Bolts	—	0.27	—
C8x11.5 x L2-1/2 x 2-1/2 x 1/4 Horizontal Strut of the South Wall Braced Frame	Inertia Force Due to Response to Concurrent N-S and 0.4 E-W Ground Motions	Compressive Capacity Being Exceeded	—	2.4	—
Anchor Bolts of the Main Column of the South Wall Braced Frame	Tension and Shear Force Due to Concurrent N-S and 0.4 E-W Ground Motions	Failure of Anchor Bolts Subject to Tensile and Shear Forces	—	2.4	—
Spread Footing of the Main Column of the South Wall Braced Frame	Overturning Response to Concurrent N-S and 0.4 E-W Ground Motions	Uplift of the Footing	—	1.1	—
Main Column of the South Wall Braced System	Overturning Response to Concurrent N-S and 0.4 E-W Ground Motions	Compressive Capacity Being Exceeded	—	1.7	—
Soil Pressure Under Spread Column Footing of the South Wall	Overturning Response to Concurrent N-S and 0.4 E-W Ground Motions	Shearing Failure of the Soil Under the Footing	—	1.6	—
Bolted Connection of the Diagonal Member of the North Wall Braced Frame	Elastic Response to Concurrent E-W and 0.4 N-S Ground Motions	Yielding of the A307 Bolts	0.06	0.08	0.11
1-JL 5x3-1/2 x 5/16 Diagonal Member of the North Wall Braced Frame	Elastic Response to Concurrent E-W and 0.4 N-S Ground Motions	Elastic Buckling; North Wall Loses its Capacity to Resist Lateral Force	0.08	0.11	0.15
Bolted Connection of the Diagonal Member of the West Wall Braced Frame	Shear Response to Concurrent N-S and 0.4 E-W Ground Motions	Shear Failure of 3-A307 Bolts	—	0.58	—
Bolted Connection of the Diagonal Bracings of the Braced Crane Frame Along Column Line 13	Roof Inertia to Concurrent E-W and 0.4 N-S Ground Motion Plus Crane Inertia Force Due to E-W Ground Motions	Shear Failure of A-307 Bolts	—	0.60	—
Anchor Bolts of the Crane Column Along Column Line 13	Tension and Shear Force Due to Concurrent E-W and 0.4 N-S Ground Motion Plus Crane Inertia Force Due to E-W Ground Motion	Failure of Anchor Bolts Subject to Tensile and Shear Forces	—	0.60	—
Column of the Crane Braced Frame Along Column Line 13	Overturning Response to Concurrent E-W and 0.4 N-S Ground Motions	Compressive Capacity of the Column Being Exceeded	—	1.6	—
12W40 Diagonal Strut of the Braced Crane Frame Along Column Line 11	Roof Inertia Force Due to Concurrent N-S and 0.4 E-W Ground Motions Plus Crane Inertia Force Due to N-S Ground Motions	Compressive Capacity of the Diagonal Strut Being Exceeded	—	0.54	—
24W68 Main Building Column of the Braced Crane Frame Along Column Line 2	Column is Subjected to Bending and Axial Force from Roof Inertia Force Due to Concurrent N-S and 0.4 E-W Ground Motions Plus Crane Inertia Force Due to N-S Ground Motions	Ultimate Capacity of this Beam-Column Being Exceeded	—	0.55	—
13W11H Roof Girder of the Steel Frame	Vertical Response Considered as Independent System ($\mu = 6.5$)	Yield Hinge at Center Span; Collapse Mechanism	—	4.0	—
High Energy Cell (HEC)	Overturning Response to N-S Ground Motions	Overturn of the HEC Based on Reserve Energy Method	—	4.0	—
High Energy Cell (HEC)	Overturning Response to N-S Ground Motions	Initiation of Uplift	0.18	0.23	0.31
Masonry Wall	Elastic Response to Out-of-Plane Ground Motions	Cracking at the Wall Base	0.06	0.08	0.10
Masonry walls	Out-of-Plane Response to N-S Ground Motions Considered as an Independent System	Collapse of the wall Based on Reserve Energy Method	0.18	0.27	0.40
Connection of 12W45 Mezzanine Floor Beam to HEC	Response to Concurrent E-W and 0.4 N-S Ground Motions	Failure of Concrete Inserts Under Tensile and Shear Force	—	1.4	—

TABLE 3-3. JN-1B TRUSS MODEL BOUNDARY ELEMENT PROPERTIES

Element No.	Description	Stiffness (lb/in)
1	North Wall Braced Frame	29500
2	Crane Braced Frame Along Line 13	11000
3	South Wall Braced Frame	18500
4	West Wall Braced Frame	20800
5	Crane Braced Frame Along Line Q	14650

1363 064

TABLE 3-4 JN-1B TRUSS MODEL NODE MASSES

Node No.	X-Mass (lb-sec ² /in)	Y-Mass (lb-sec ² /in)
1	140.68	11.28
2	16.45	16.45
3	145.85	16.45
4	16.45	16.45
5	13.05	139.86
6	16.14	16.14
7	19.39	19.39
8	19.39	19.39
9	19.39	19.39
10	16.81	16.81
11	16.97	16.97
12	20.39	20.39
13	20.39	20.39
14	20.39	20.39
15	17.68	17.68
16	16.21	16.21
17	21.16	21.16
18	22.84	22.84
19	22.84	22.84
20	18.57	18.57
21	11.36	11.36
22	16.55	16.55
23	16.55	16.55
24	16.55	16.55
25	13.13	139.94

1363 065

TABLE 3-5. JN-1B MODEL BEAM PROPERTIES

Beam Description	Material No.	Area (in ²)	Moment of Inertia (in ⁴)	Beam No.
L4 x 3 x 1/4	1	0.845*	2.77	6, 7, 8, 9, 10, 11, 12, 13, 27, 28, 38, 39, 49, 50
14W22	1	6.490	7.00	18, 19, 20, 21, 29, 30, 31, 32, 40, 41, 42, 43
14W30	1	8.830	19.50	1, 2, 3, 4, 5, 22, 33, 44, 51, 52, 53, 54
33W118	1	34.800	187.00	14, 15, 16, 17, 23, 24, 25, 26, 34, 35, 36, 37, 45, 47, 48

* Half of the Axial Area

Material No.	Material	E (psi)	v
1	A36 Structural Steel	29×10^6	0.3

3-38

1363 066

TABLE 3-6. JN-1B ROOF TRUSS DIAGONAL MEMBER FORCES (SRSS)

<u>Beam Element No.</u>	<u>1.0g N-S + Concurrent 0.4g E-W (Lbs)</u>	<u>1.0g E-W + Concurrent 0.4g N-S (Lbs)</u>
6	60160	59680
7	95480	85400
8	45880	50440
9	69360	60840
10	58960	57960
11	95000	85040
12	48280	52240
13	70680	62040
27	42040	42520
28	43240	43000
38	58920	57000
39	57440	55400
49	31384	27220
50	31280	26960

1363 067

POOR ORIGINAL

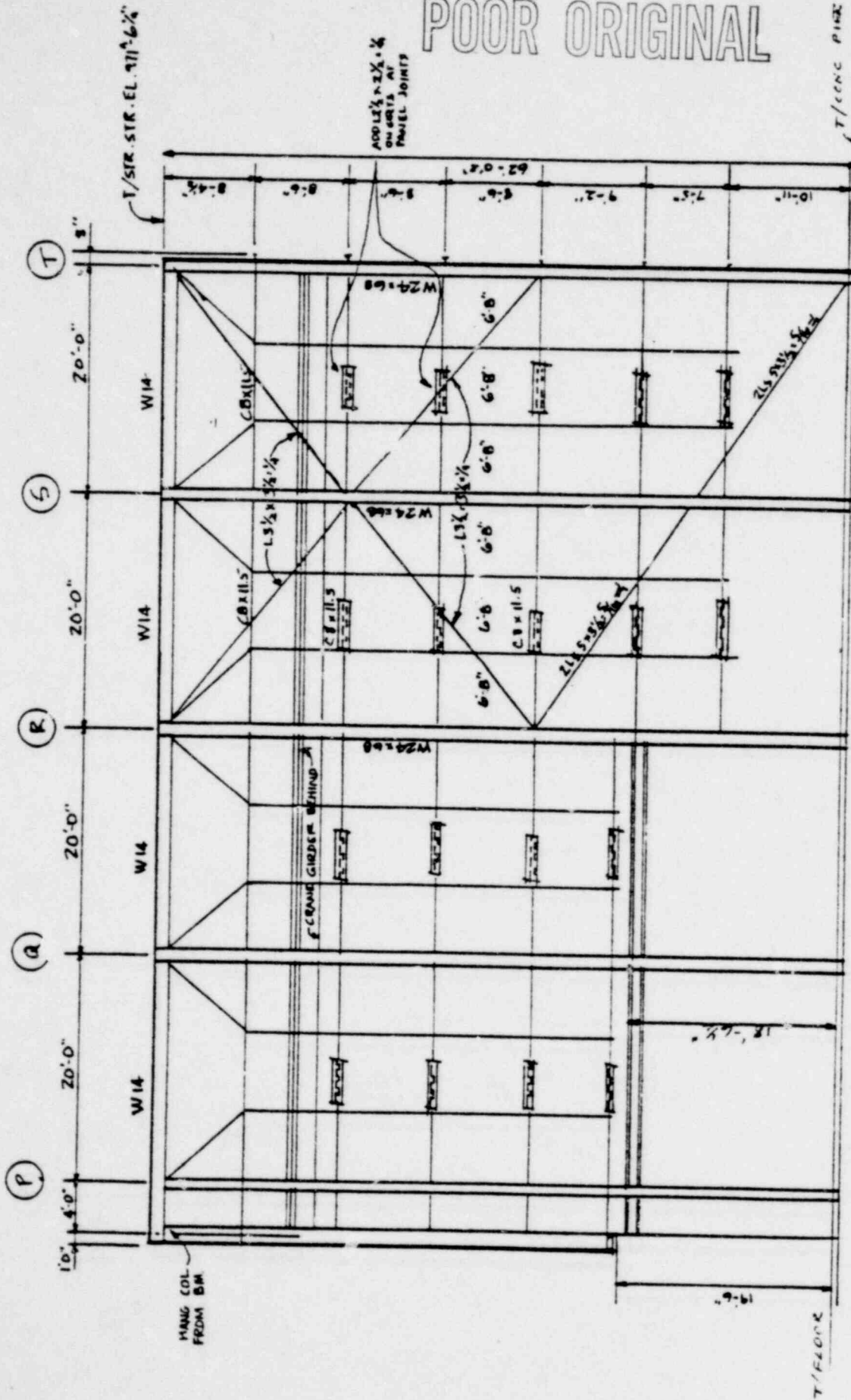
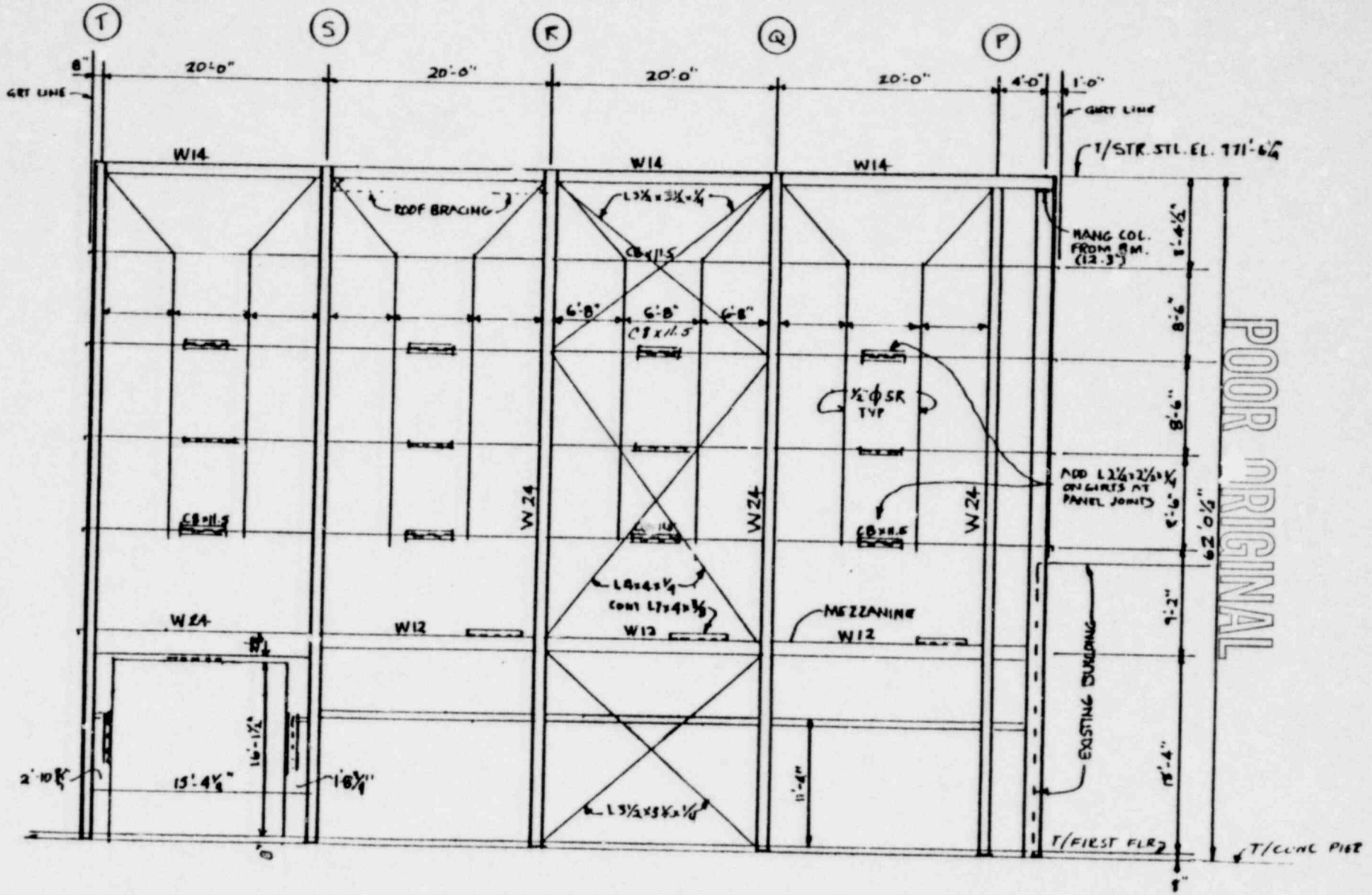


FIGURE 3-4. JN-1B NORTH WALL BRACED FRAME



POOR ORIGINAL

FIGURE 3-5. JN-1B SOUTH WALL BRACED FRAME

3-49

1363 069

POOR ORIGINAL

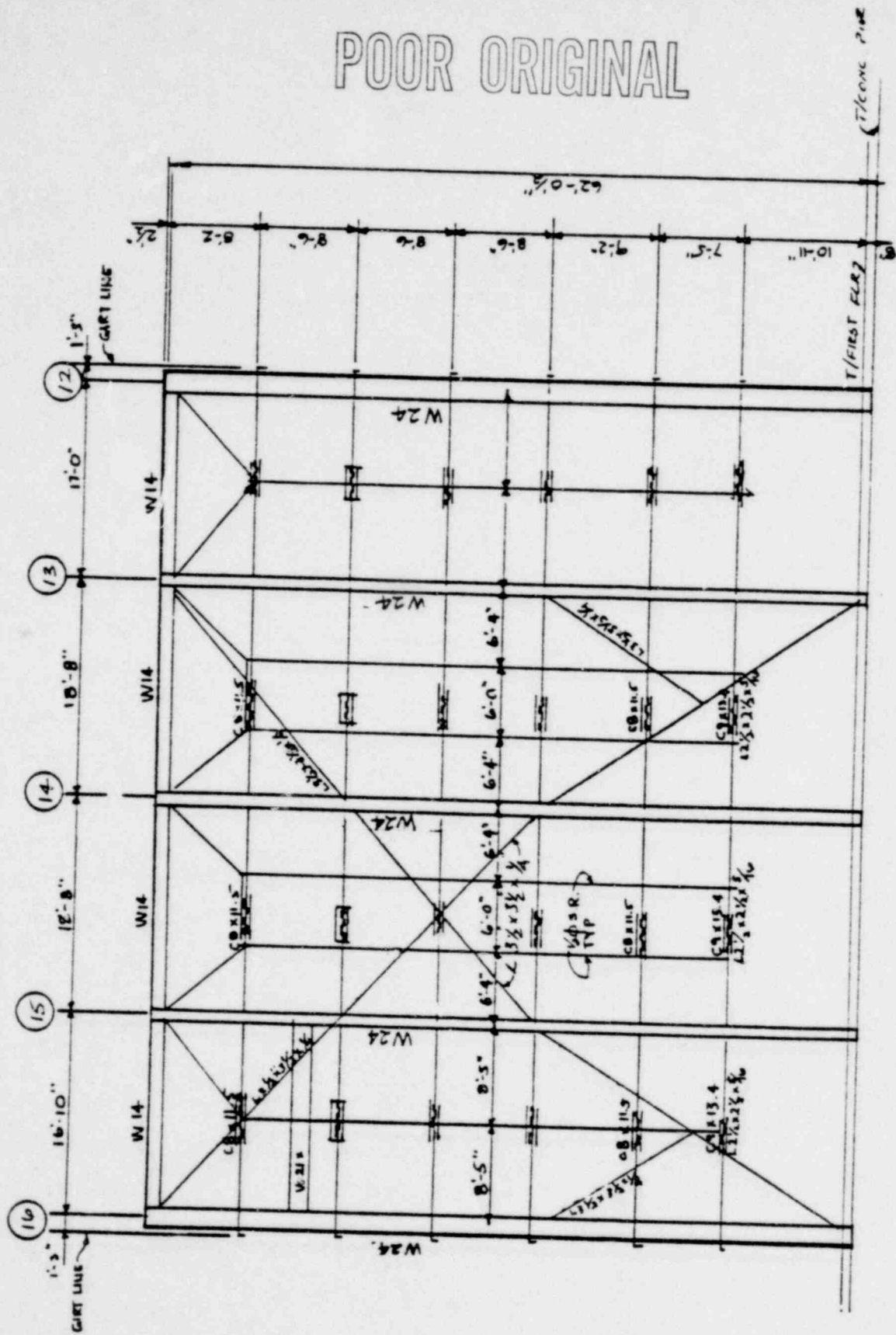


FIGURE 3-6. JN-18 WEST WALL BRACED FRAME

3-51

1363 071

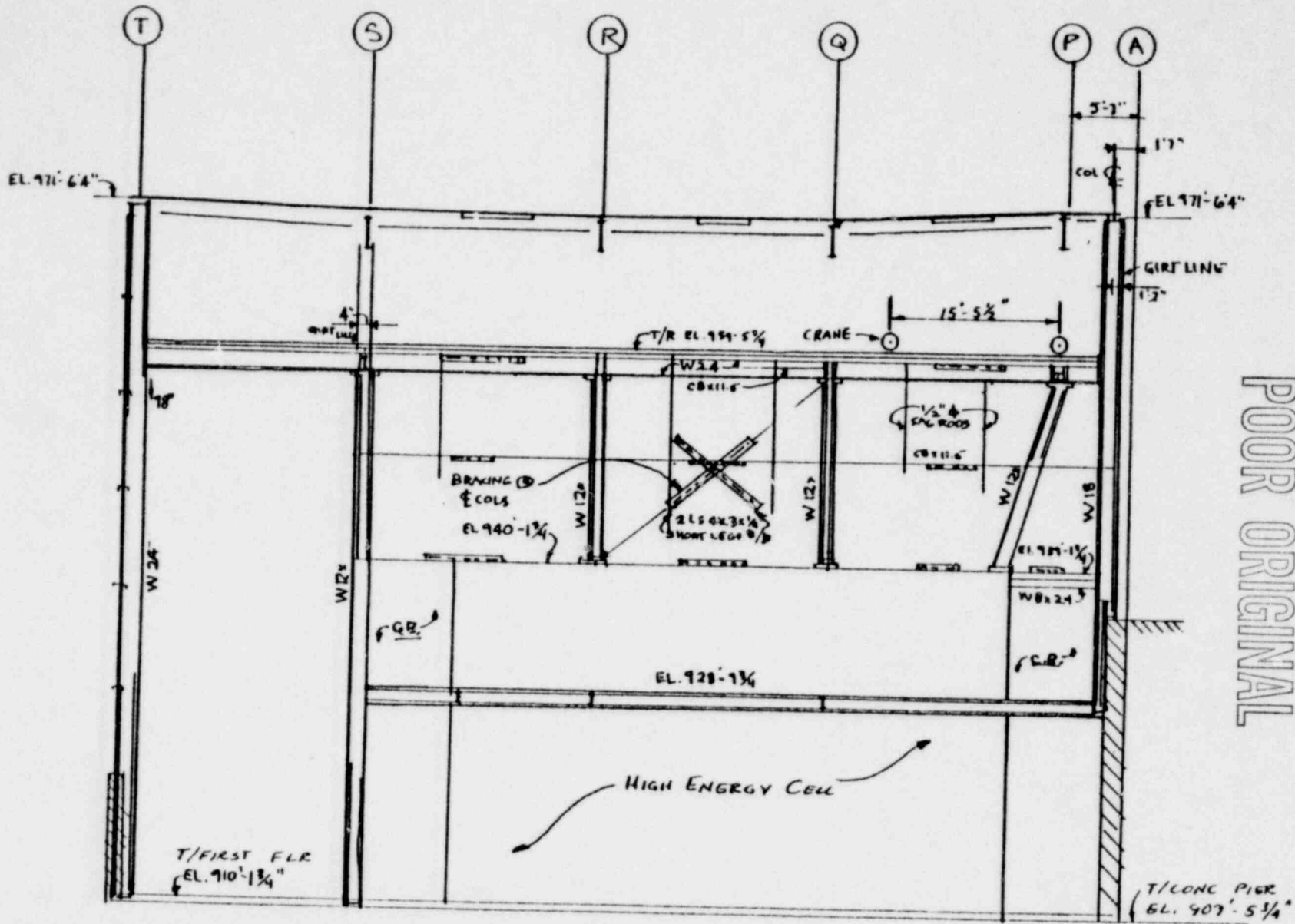


FIGURE 3-7. JN-1B CROSS BRACING FOR CRANE FRAMING AT LINE 13

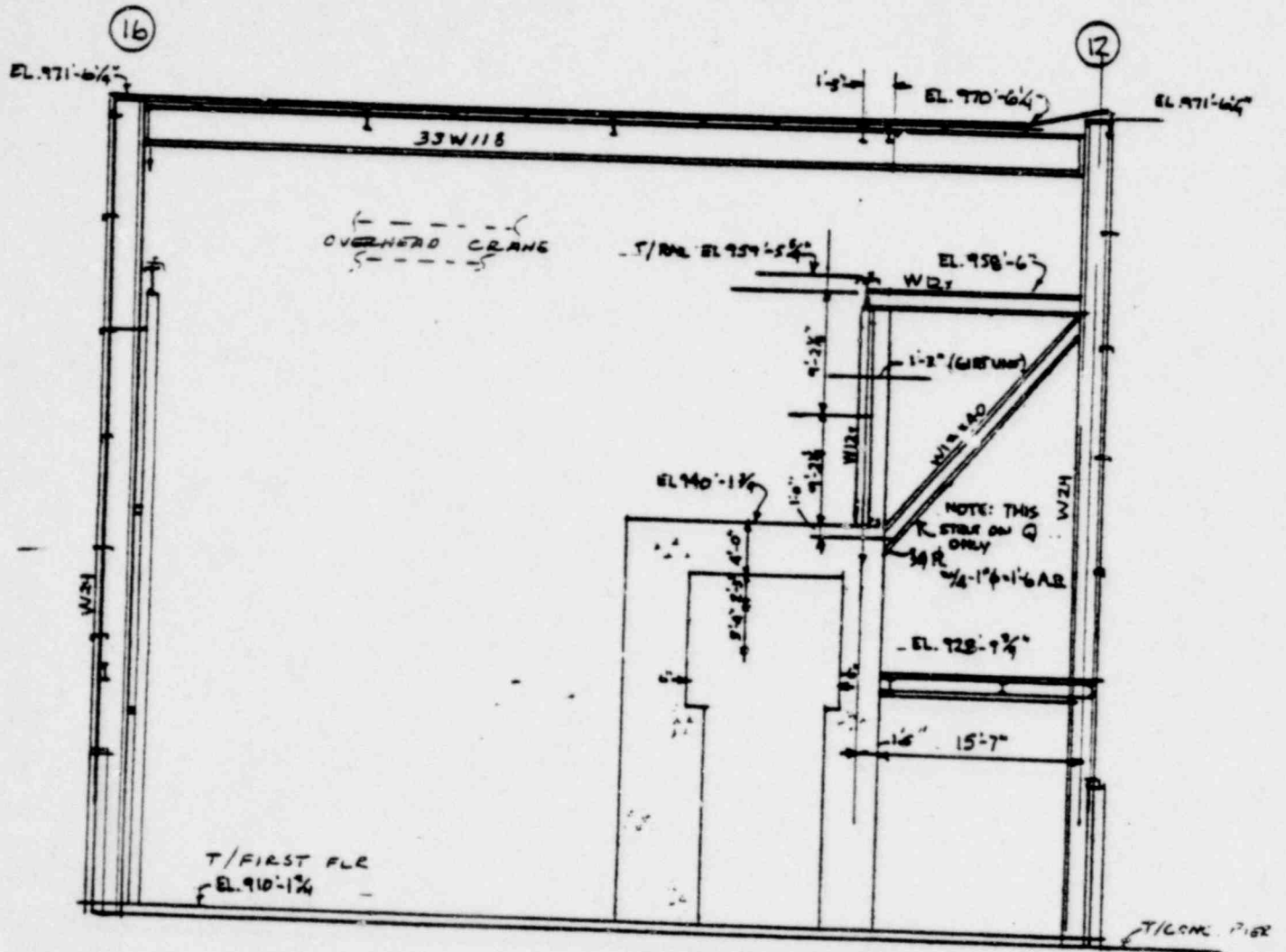
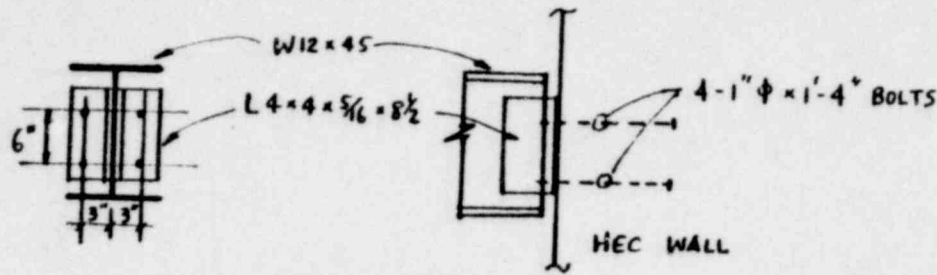


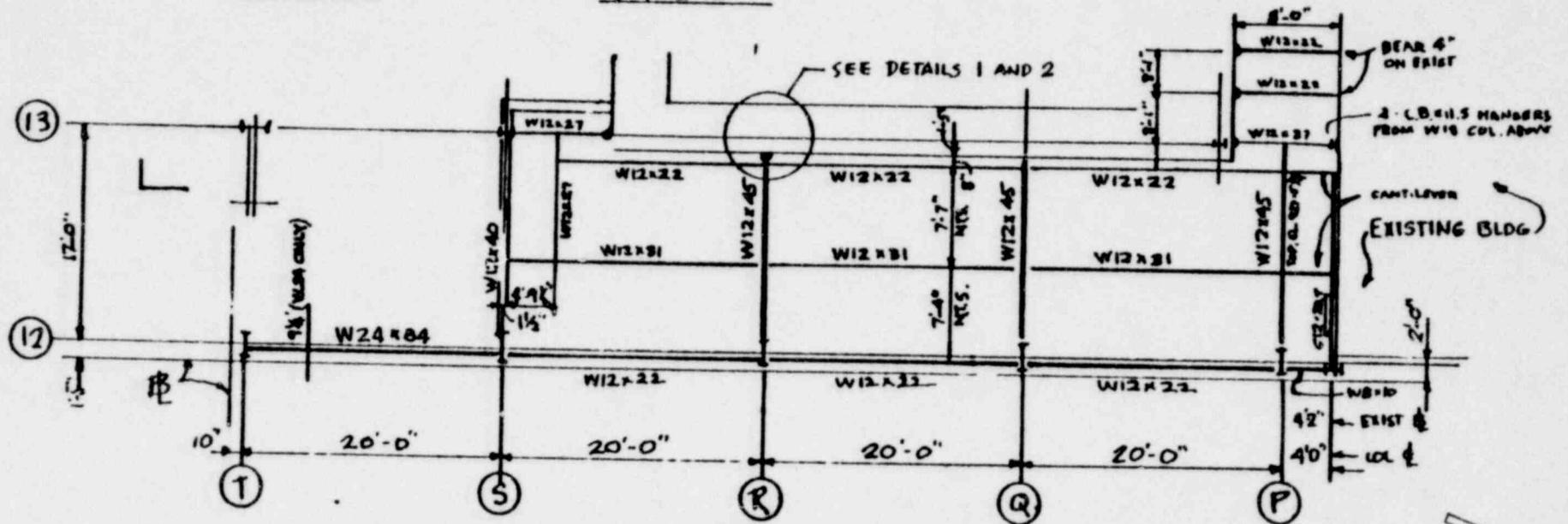
FIGURE 3-8. JN-1B DIAGONAL BRACING ALONG COLUMN LINE Q

POOR ORIGINAL



DETAIL 1

DETAIL 2



NOTE: Mezzanine slab is constructed of 4" concrete over 1-1/2" Inland-Ryerson 20 gage Type 5 composite action steel deck

FIGURE 3-9. JN-1B MEZZANINE FLOOR FRAMING

3-53

1363 073

POOR ORIGINAL

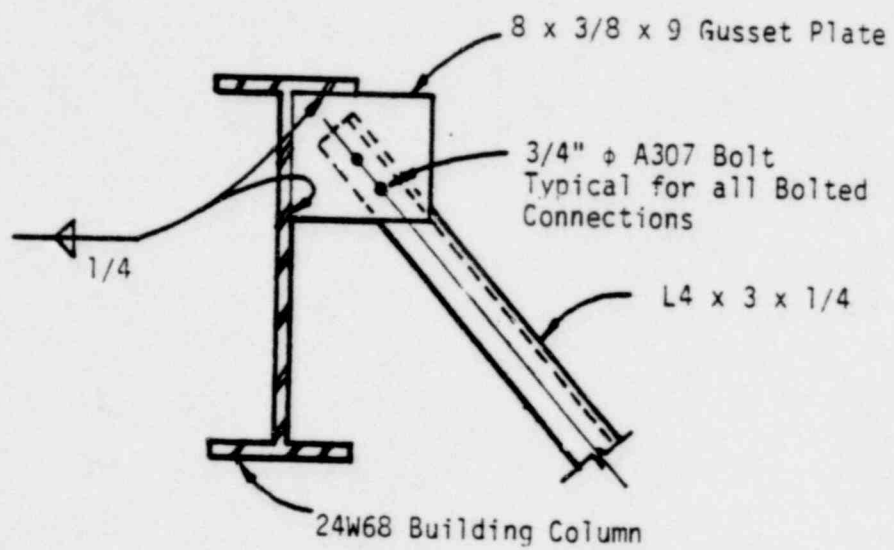


FIGURE 3-10. TYPICAL JN-1B BOLTED CONNECTION OF THE ROOF TRUSS

POOR ORIGINAL

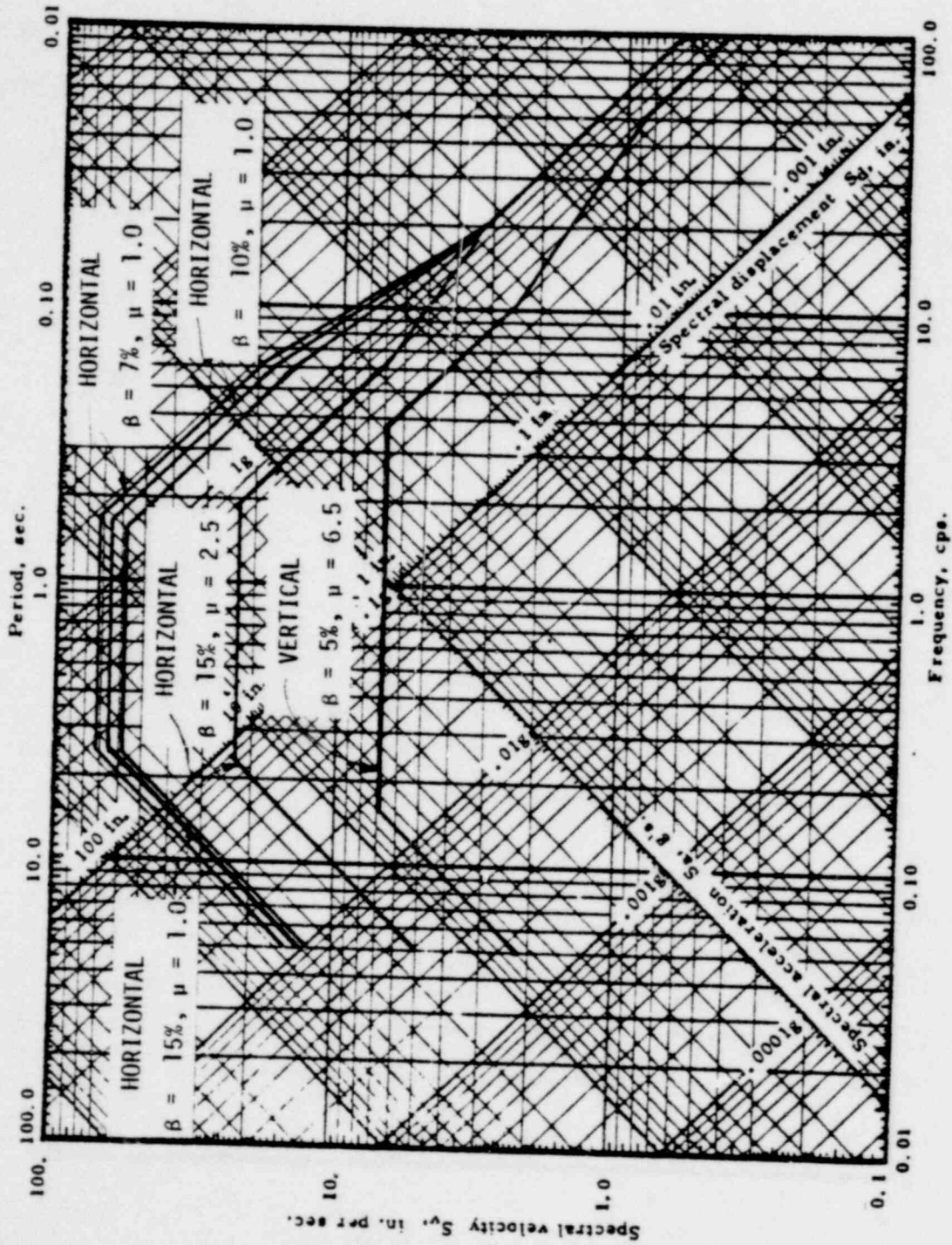


FIGURE 3-11. MEDIAN ALLUVIUM SITE RESPONSE SPECTRA (REFERENCE 7)

1363 075

Node Mass Property

Node No.	1	2	3	4	5
Mass (lb-sec ² /in)	2514	2073	2073	1595	1416

Beam Properties

Beam No.	Area (in ²)	Shear Area (in ²)	Moment of Inertia (in ⁴)
All Beams	76570	25170	4.9 x 10 ⁸

Boundary Element Properties

Element No.	1 (lb/in)	2 (in-lb)/rad
Stiffness	1.1 x 10 ⁷	1.7 x 10 ¹¹

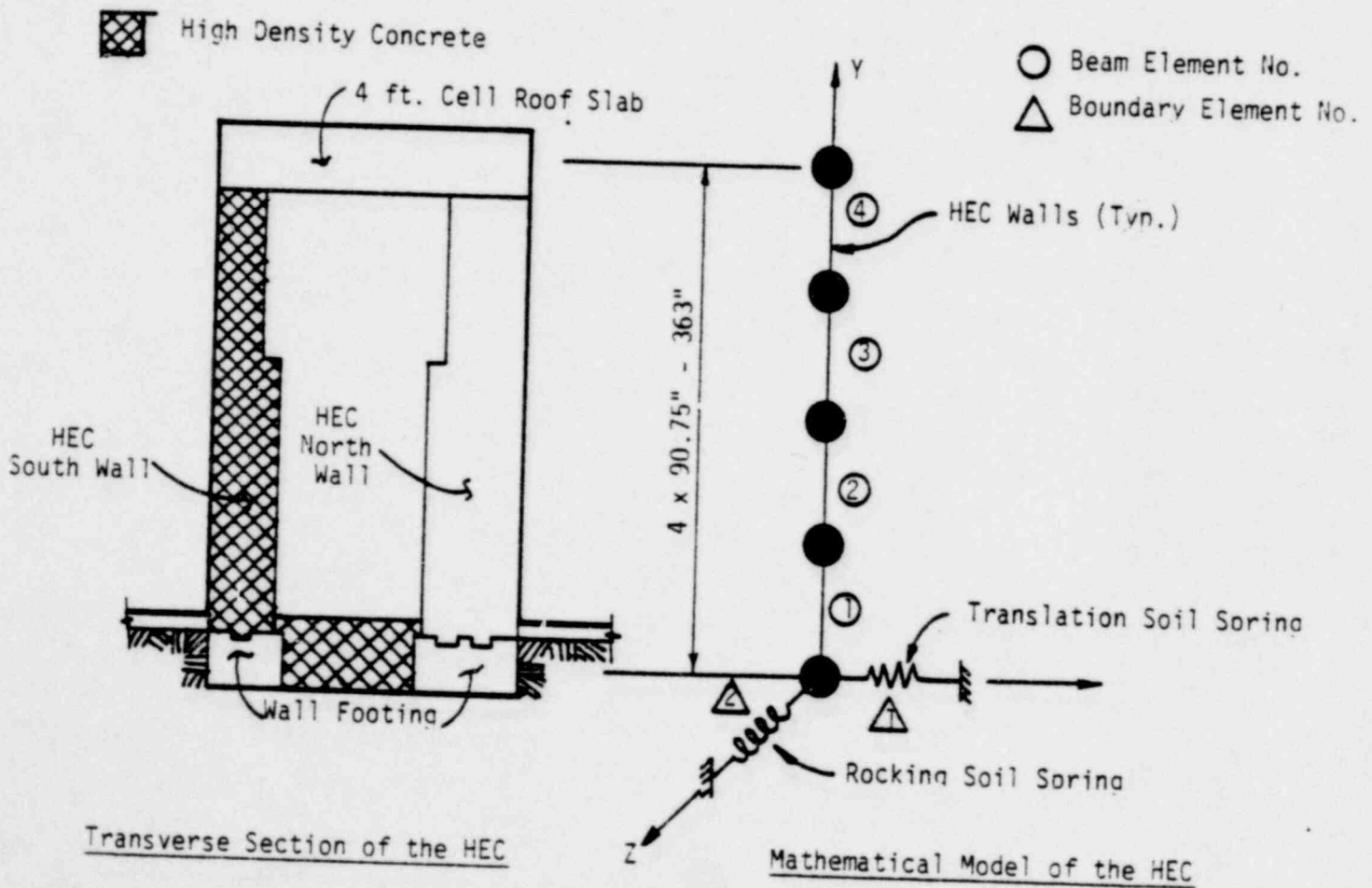


FIGURE 3-12. FINITE ELEMENT MODEL OF THE HIGH ENERGY CELL

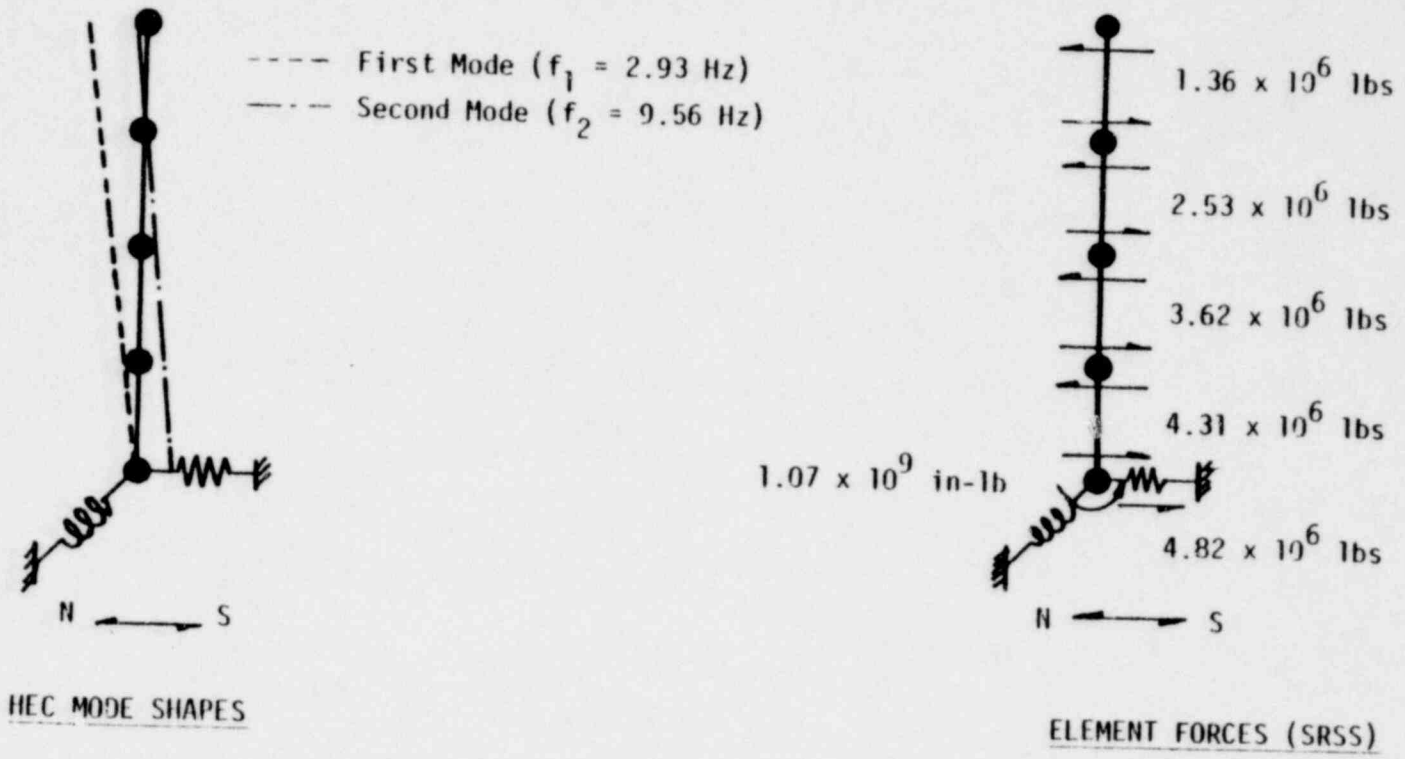


FIGURE 3-13. DYNAMIC RESPONSE ANALYSIS RESULTS OF THE HEC

1363 077

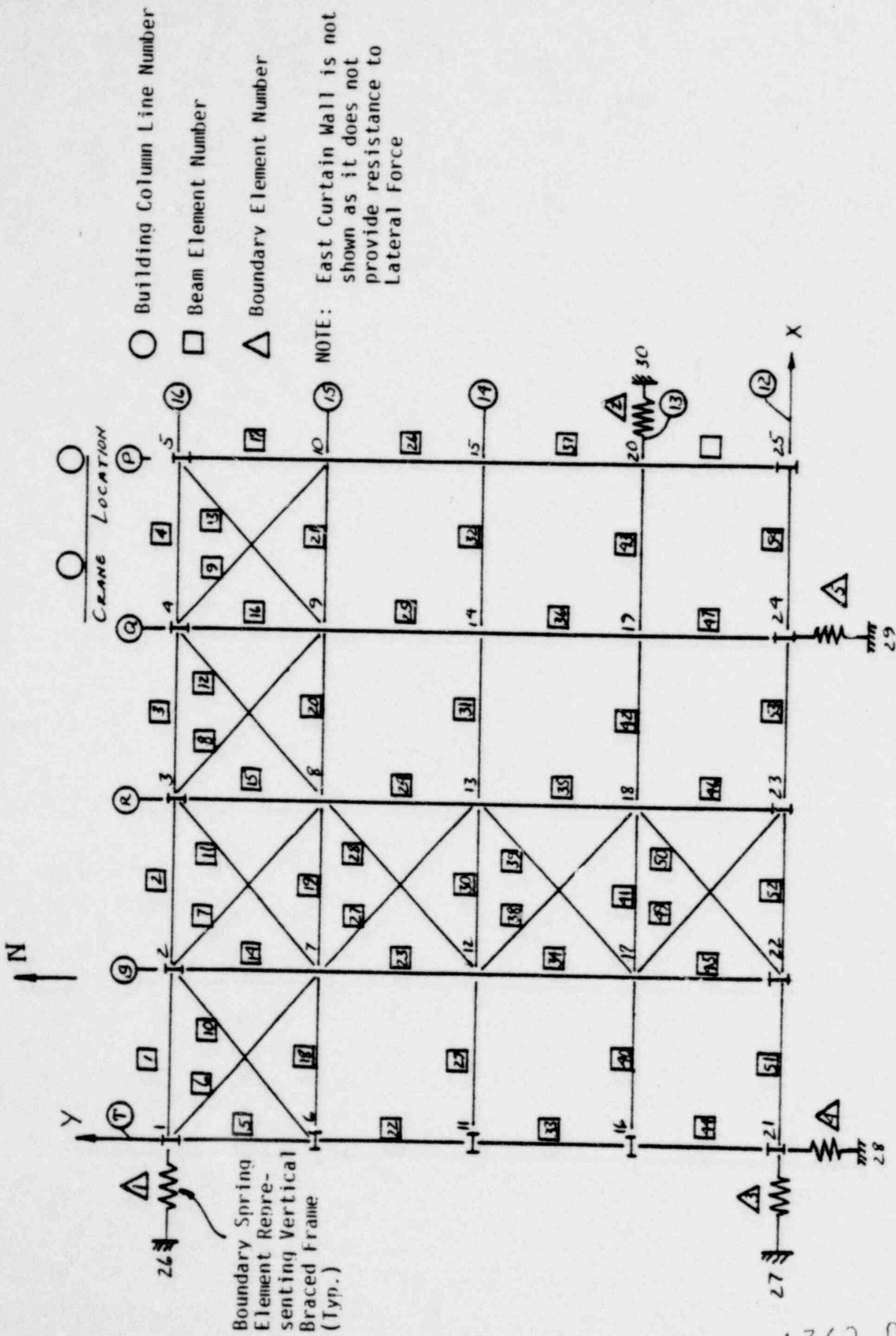


FIGURE 3-14. MATHEMATICAL MODEL OF JN-1B ROOF TRUSS

1363 078

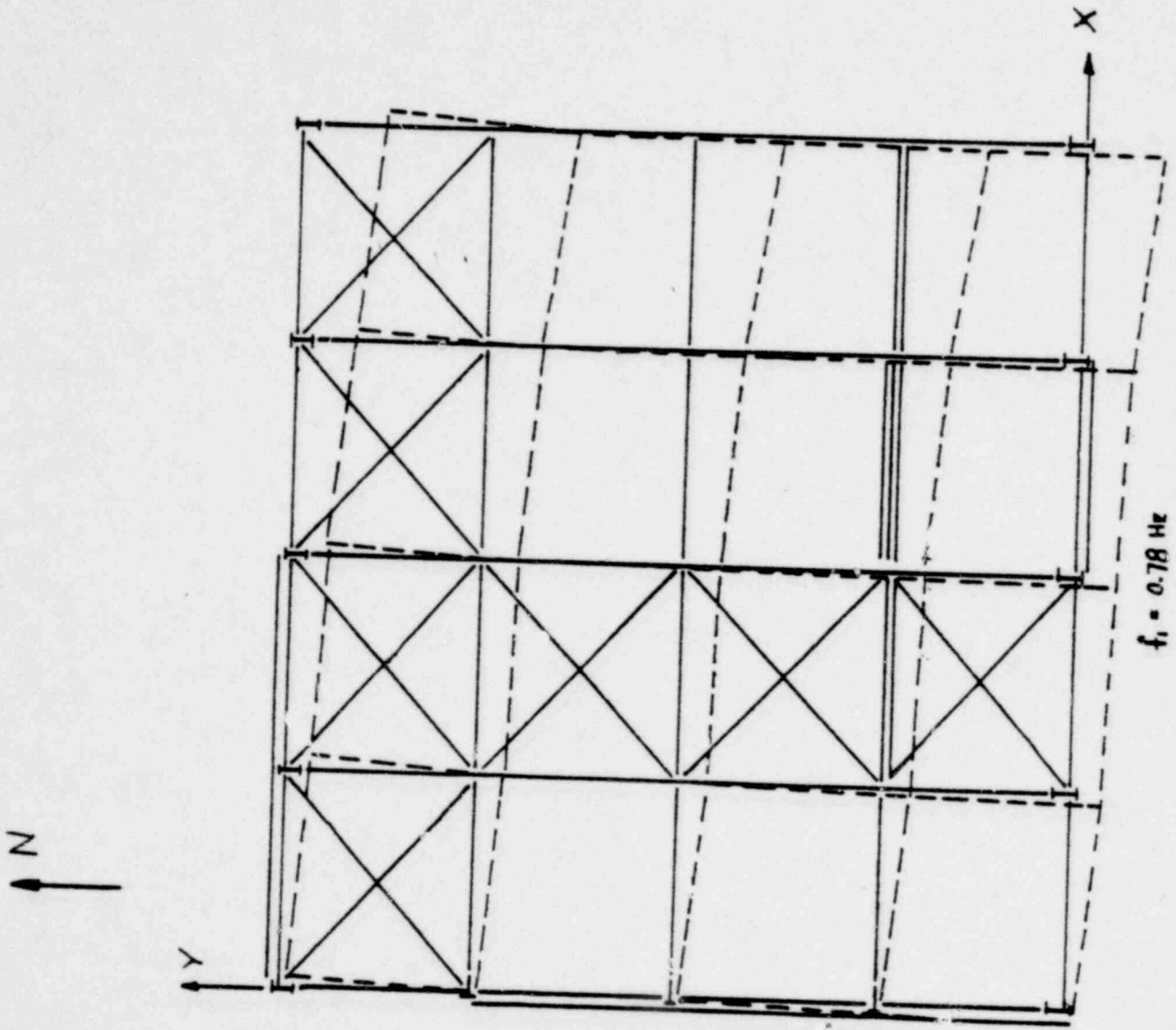


FIGURE 3-15. FIRST MODE OF THE JM-1B STRUCTURE (PLAN)

1363 079

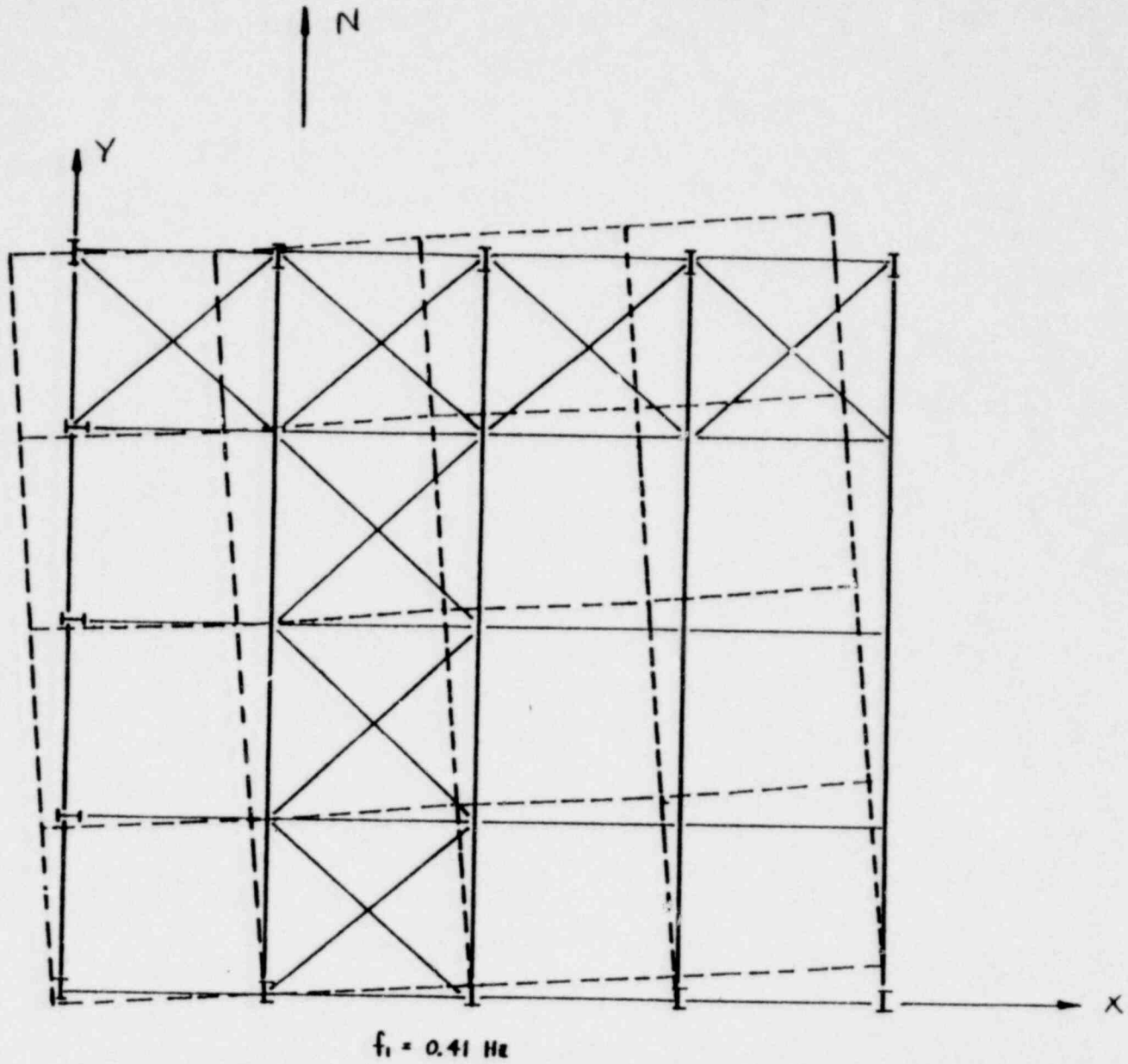


FIGURE 3-15a. FIRST MODE OF THE JN-1B STRUCTURE WITH BUCKLED NORTH FRAME CROSS BRACE (PLAN)

3-60

1363 080

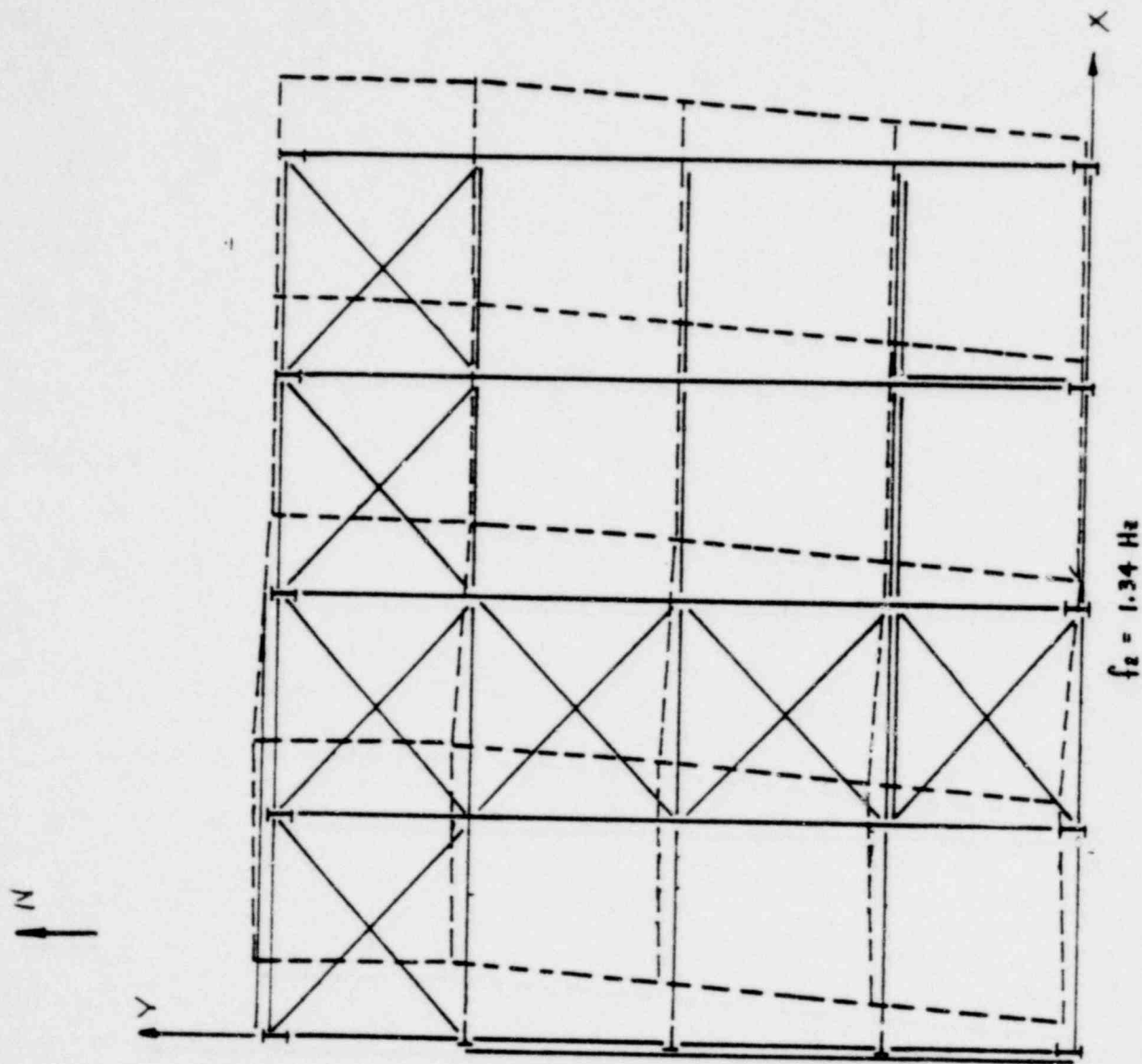


FIGURE 3-16. SECOND MODE OF THE JN-1B STRUCTURE (PLAN)

1363 081

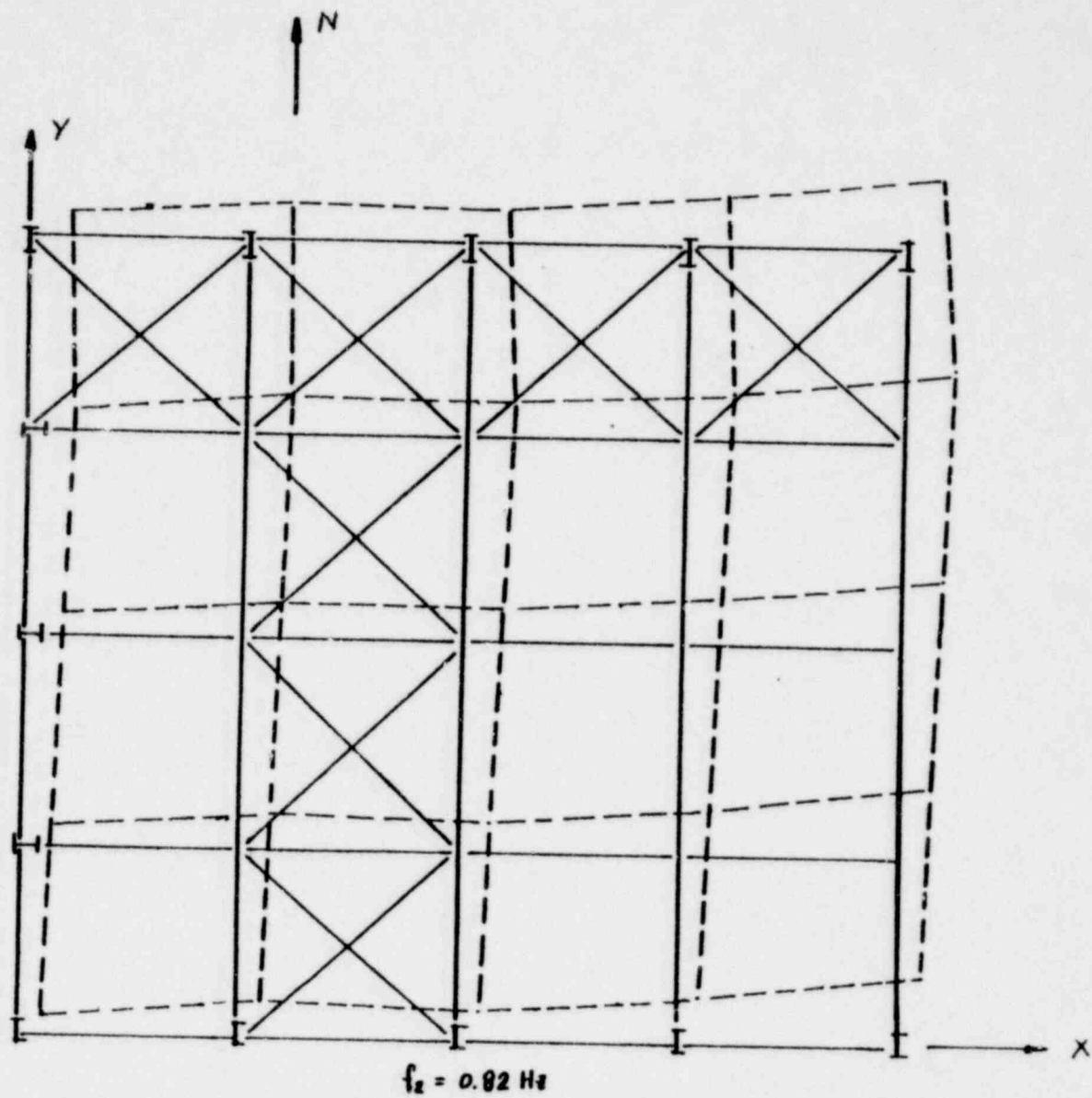


FIGURE 3-16a. SECOND MODE OF THE JN-1B STRUCTURE WITH BUCKLED NORTH FRAME CROSS BRACE (PLAN)

3-62

1363 082

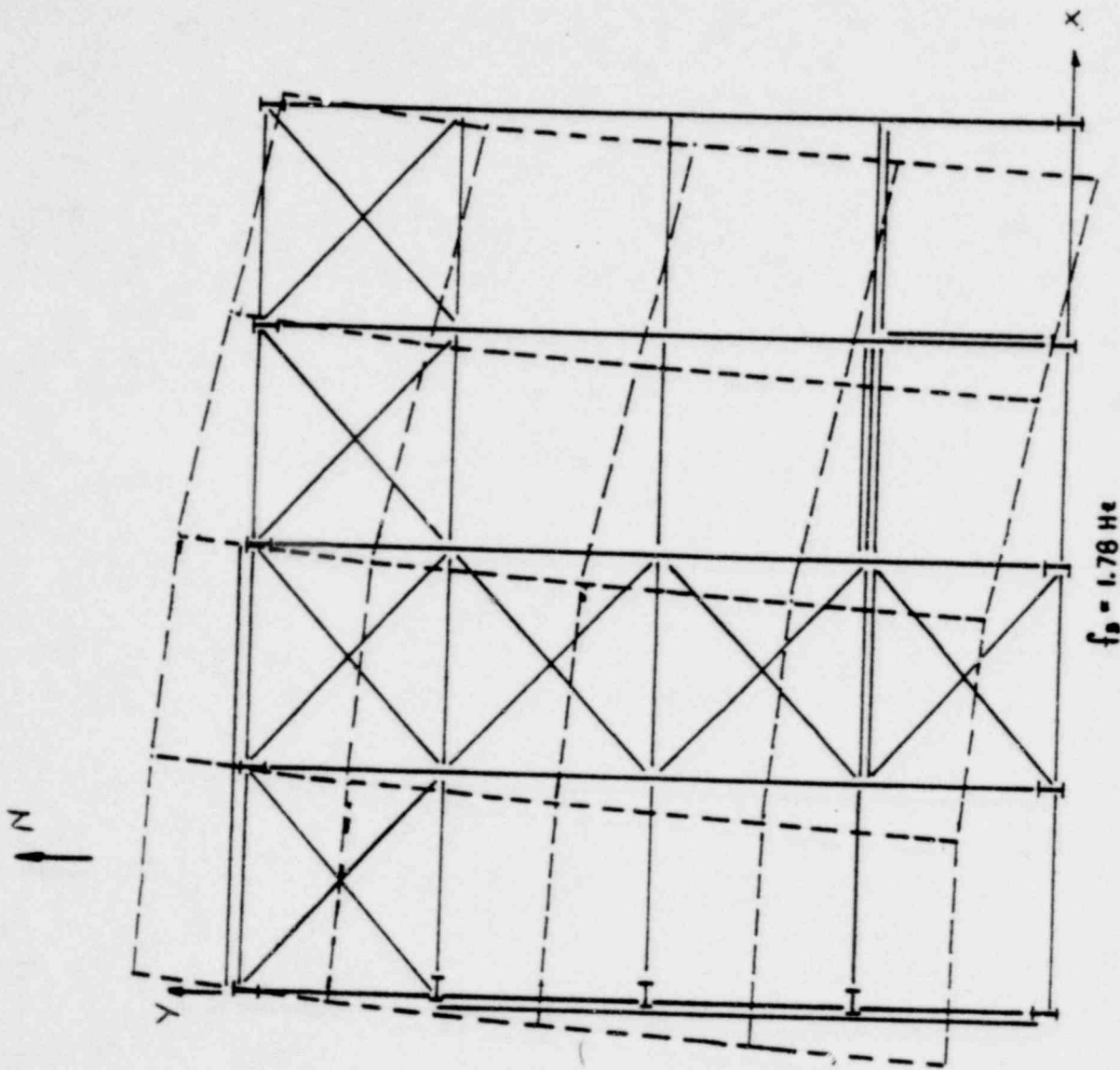


FIGURE 3-17. THIRD MODE OF THE JN-1B STRUCTURE (PLAN)

1363 083

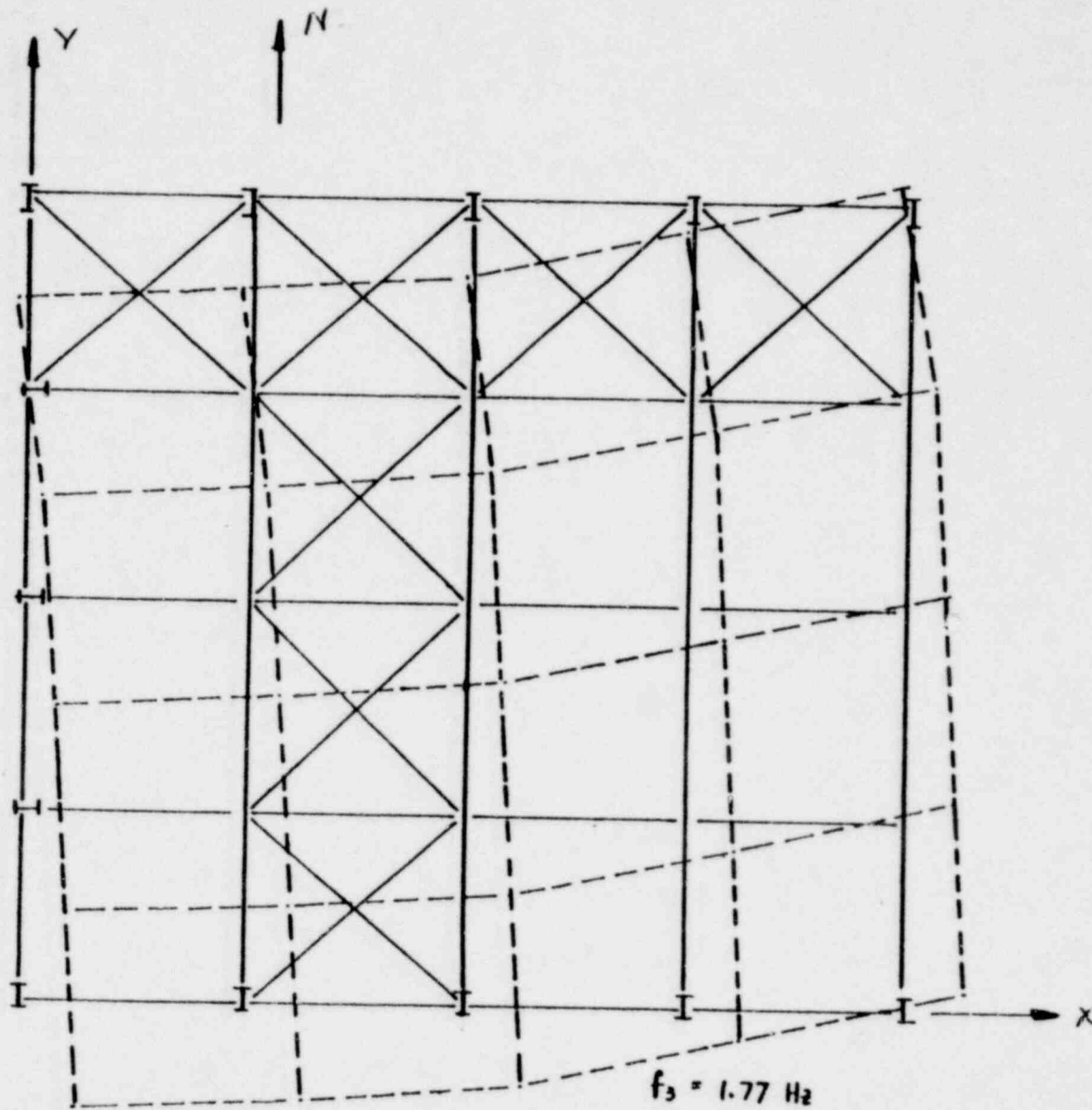


FIGURE 3-17a. THIRD MODE OF THE JN-1B STRUCTURE WITH BUCKLED NORTH FRAME CROSS BRACE (PLAN)

3-64

1363 084

3-55

1363 085

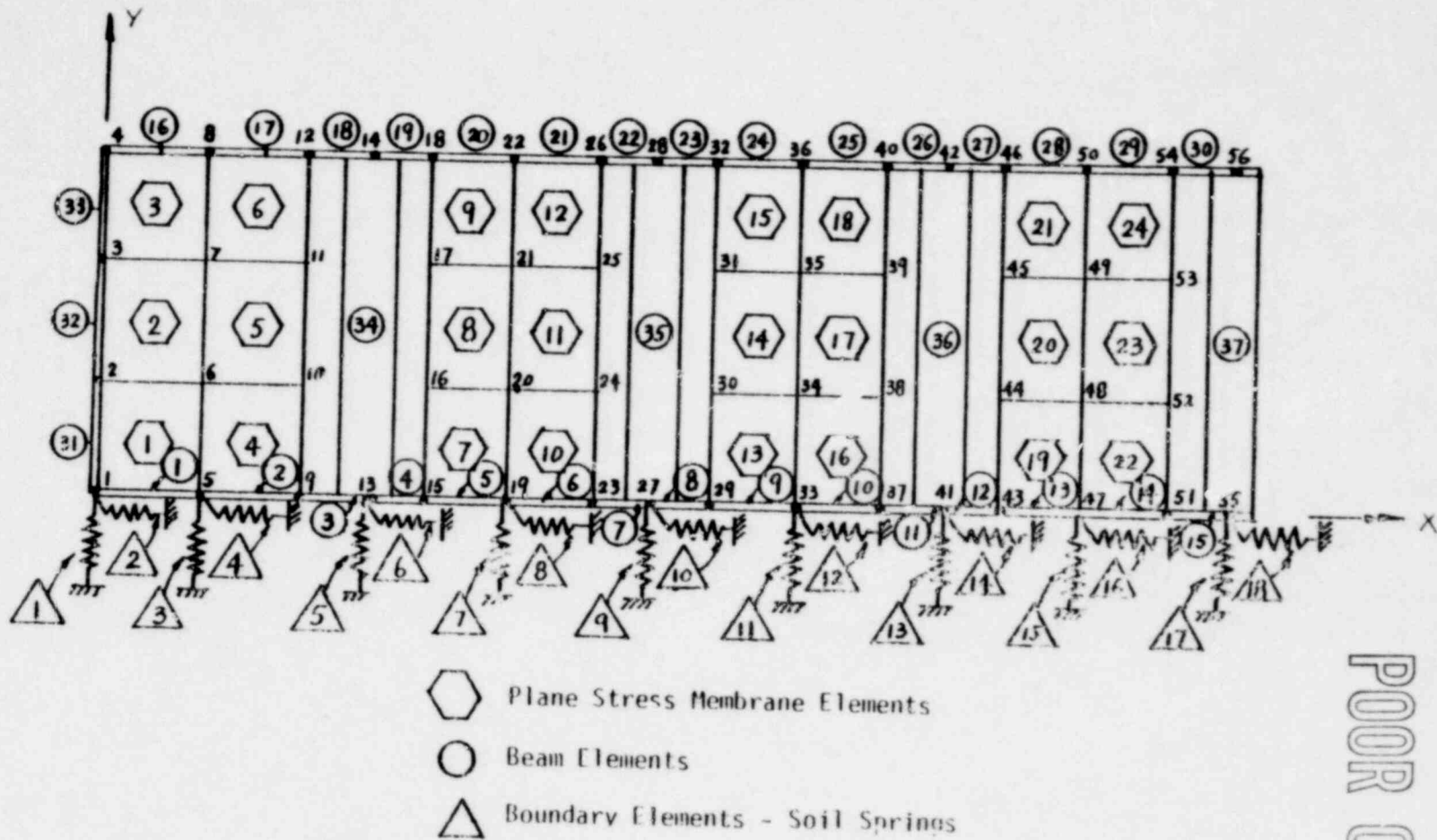
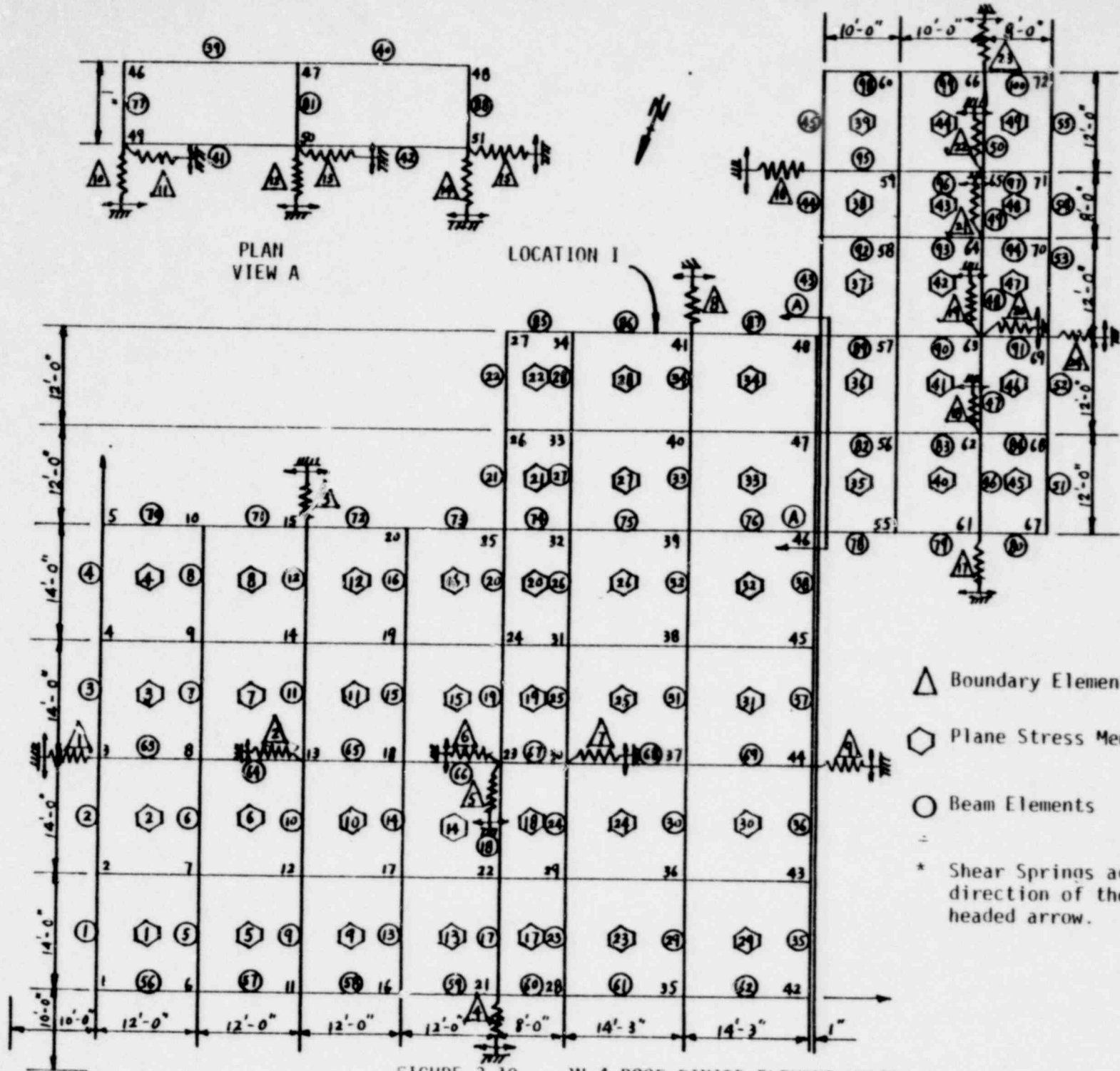


FIGURE 3-18. JN-4 SOUTH EXTERIOR MASONRY WALL - FINITE ELEMENT MODEL

POOR ORIGINAL

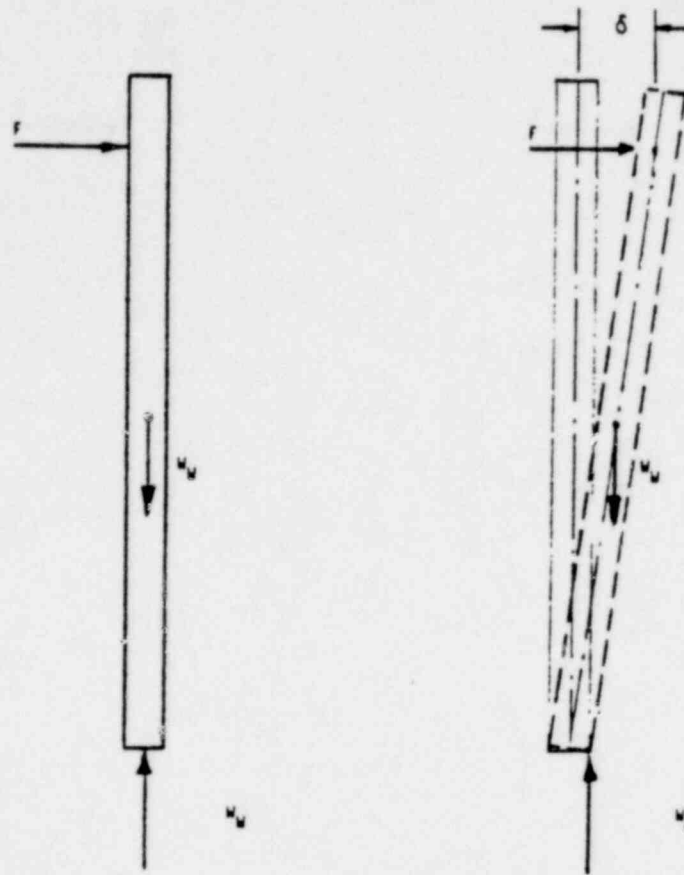
3-66

1363 086



POOR ORIGINAL

FIGURE 3-19. JH-4 ROOF FINITE ELEMENT MODEL



F - LATERAL FORCE AT ROOF LINE
 W_w - WEIGHT OF THE WALL
 δ - DEFLECTION AT ROOF LINE
 δ_{RB} - DEFLECTION δ AT START OF INSTABILITY

POOR ORIGINAL

FIGURE 3-20. TYPICAL RIGID BODY WALL SYSTEM

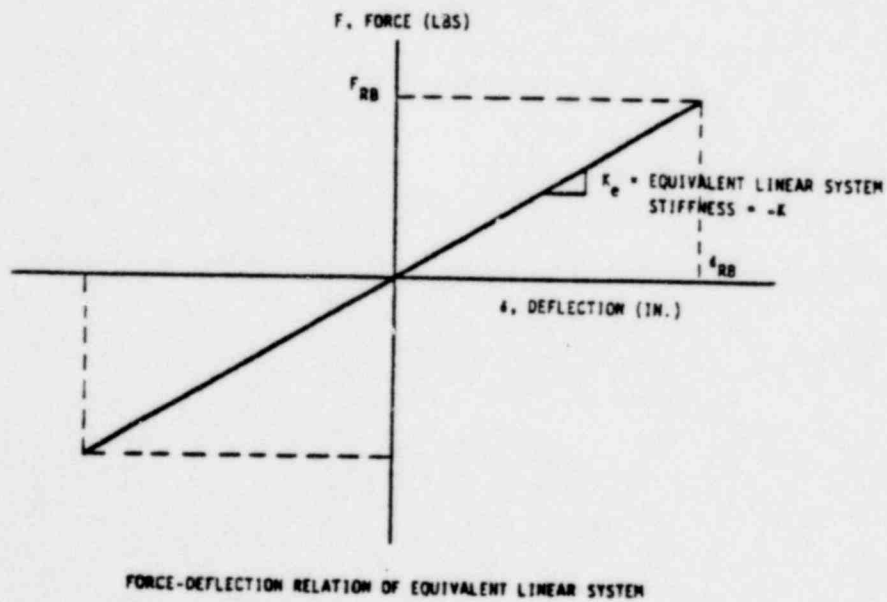
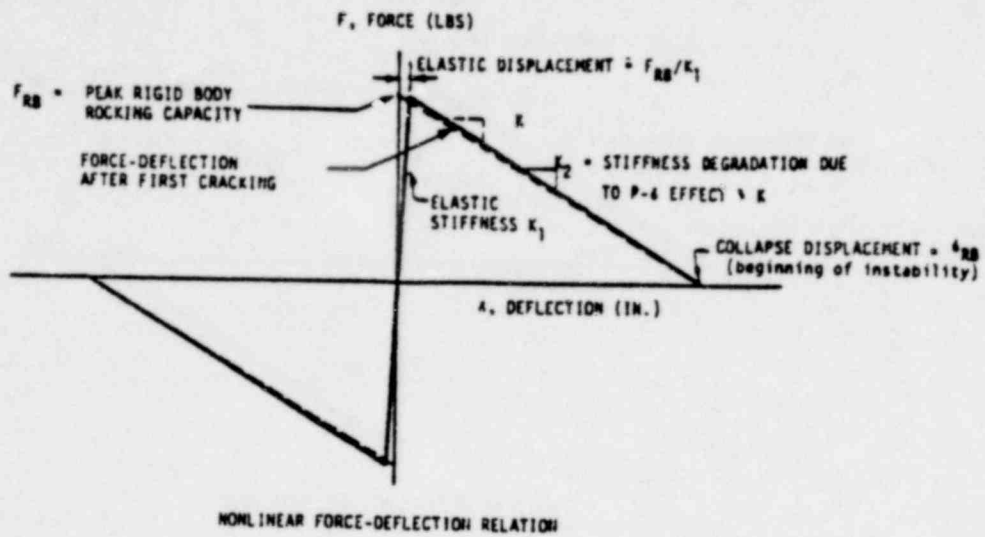


FIGURE 3-21. FORCE-DEFLECTION RELATIONS FOR TYPICAL RIGID BODY SYSTEM

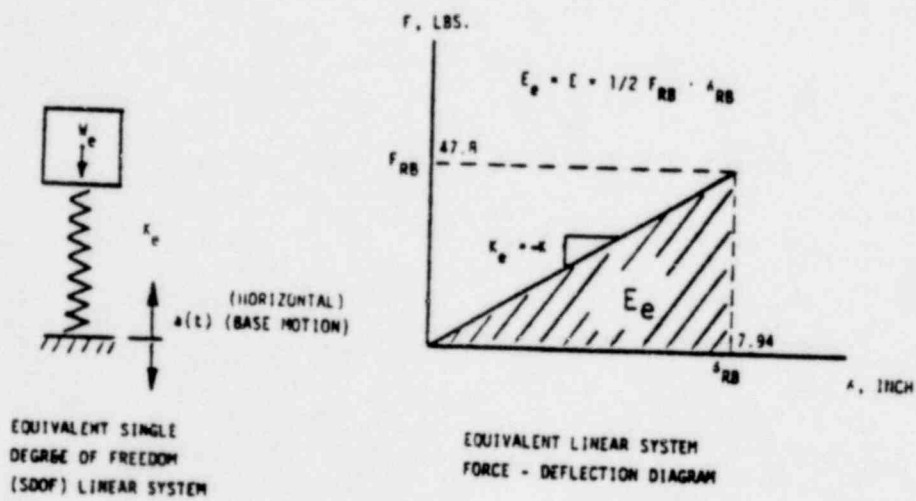
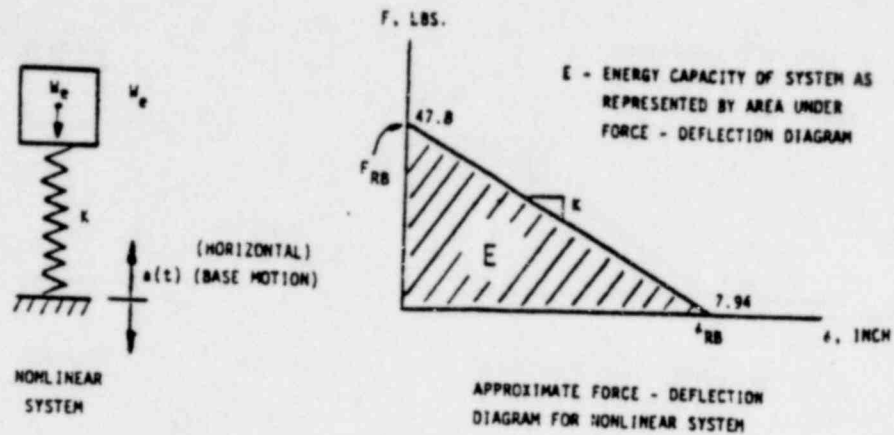


FIGURE 3-22. WALL/ROOF SYSTEM MODELS

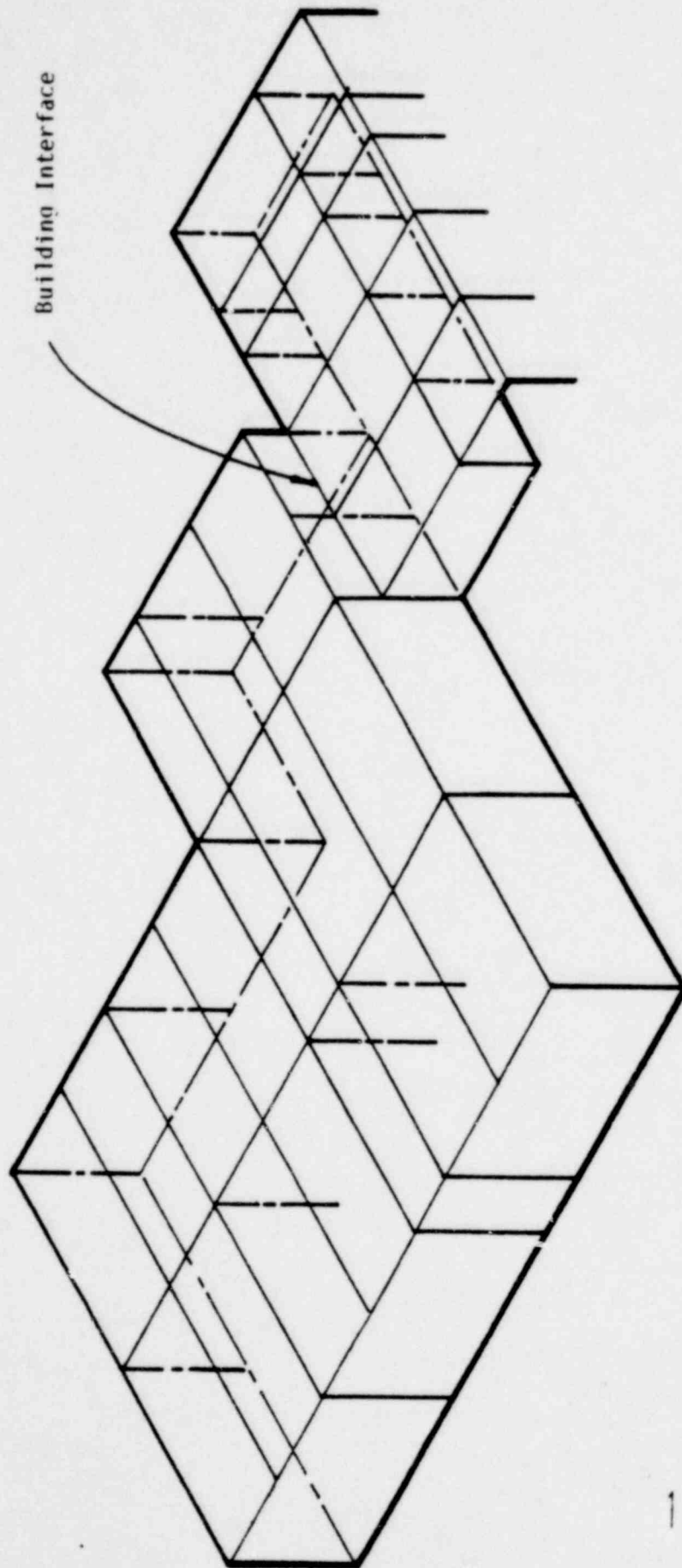


FIGURE 3-23. STRUCTURAL STEEL FRAMING FOR THE JN-4 FACILITY

1363 090

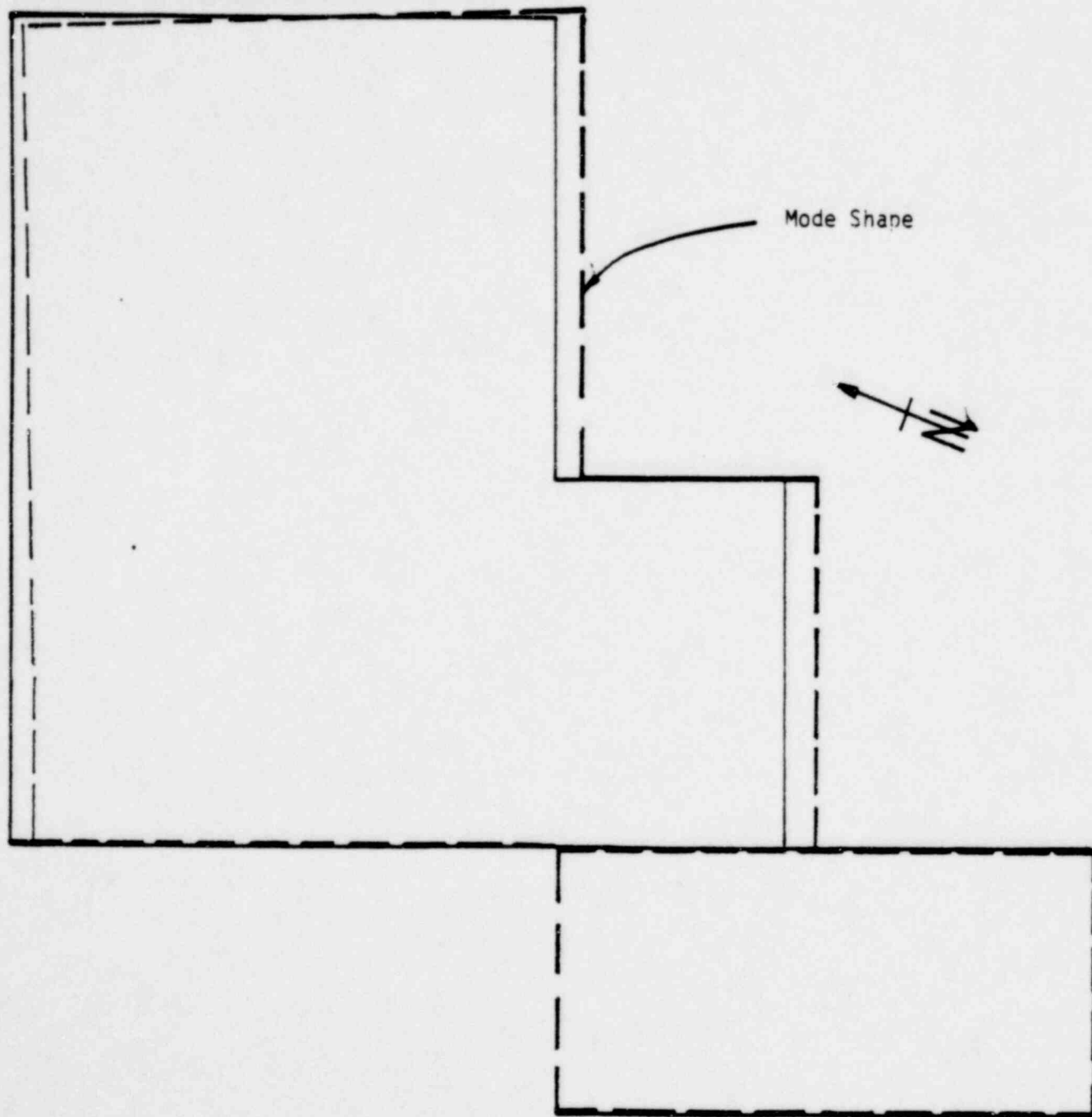


FIGURE 3-24. FUNDAMENTAL MODE OF THE JN-4 FACILITY

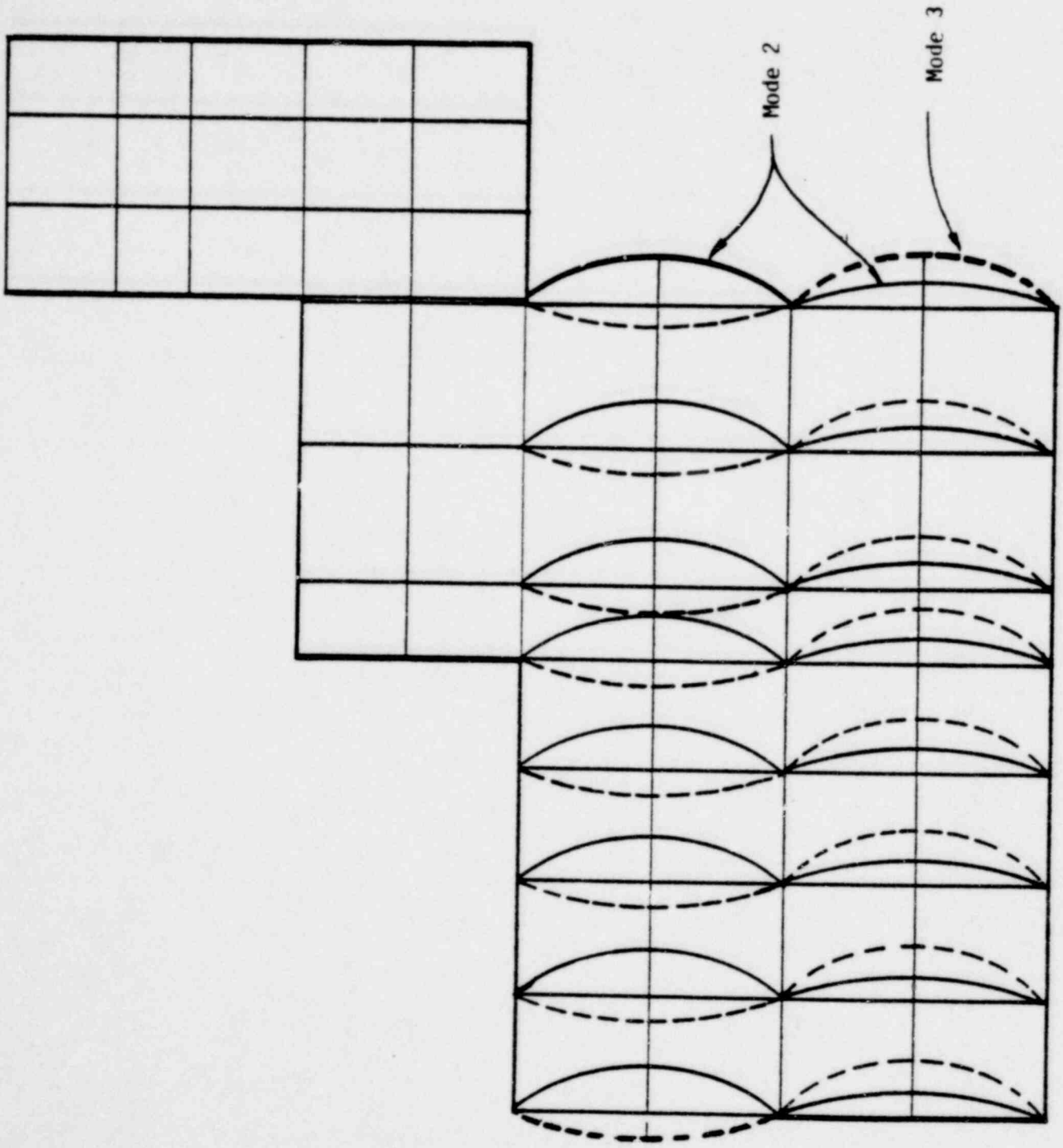


FIGURE 3-25. MODIFIED ELASTIC MODEL MODE SHAPES

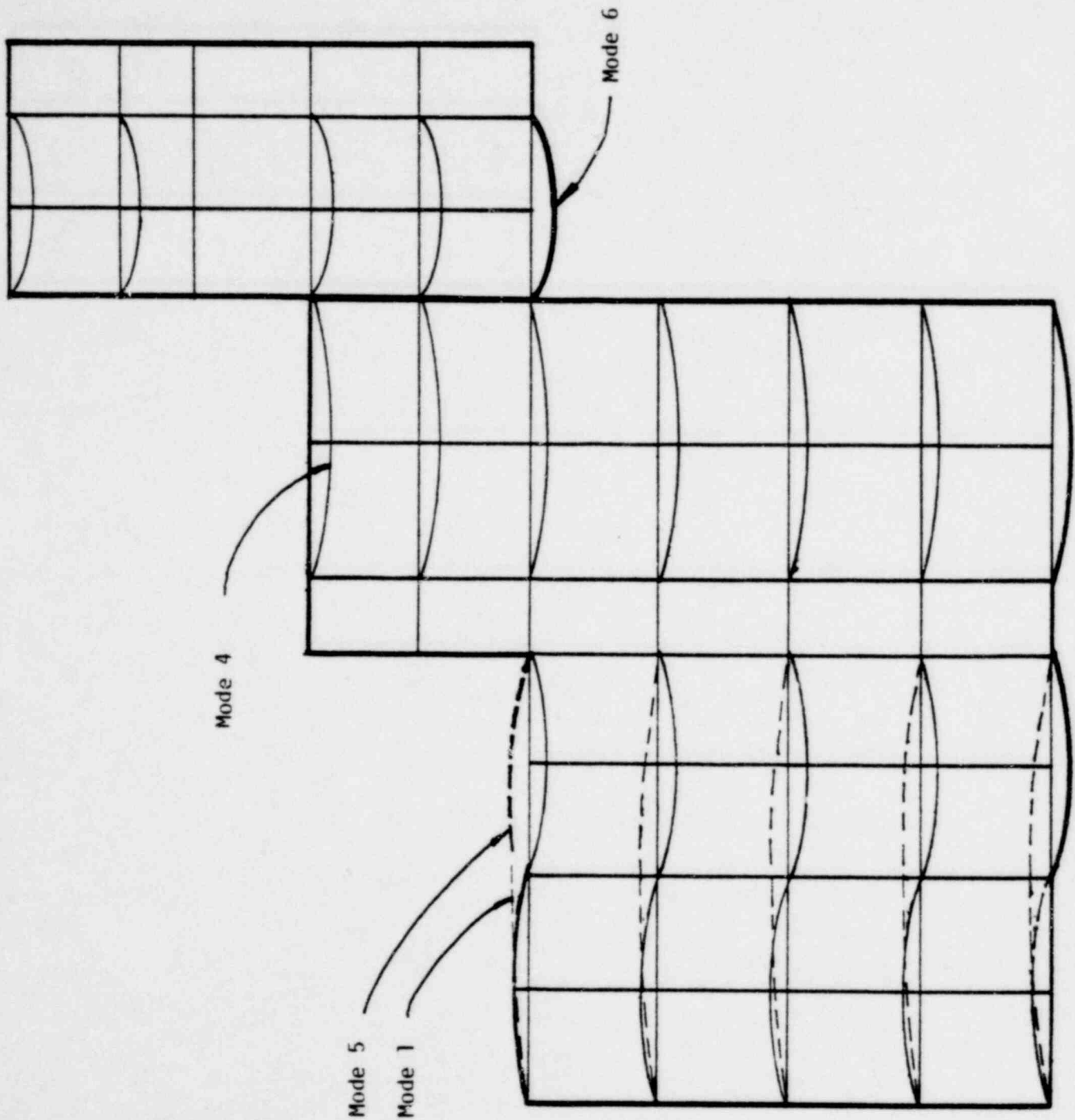


FIGURE 3-26. MODIFIED ELASTIC MODEL-MODE SHAPES

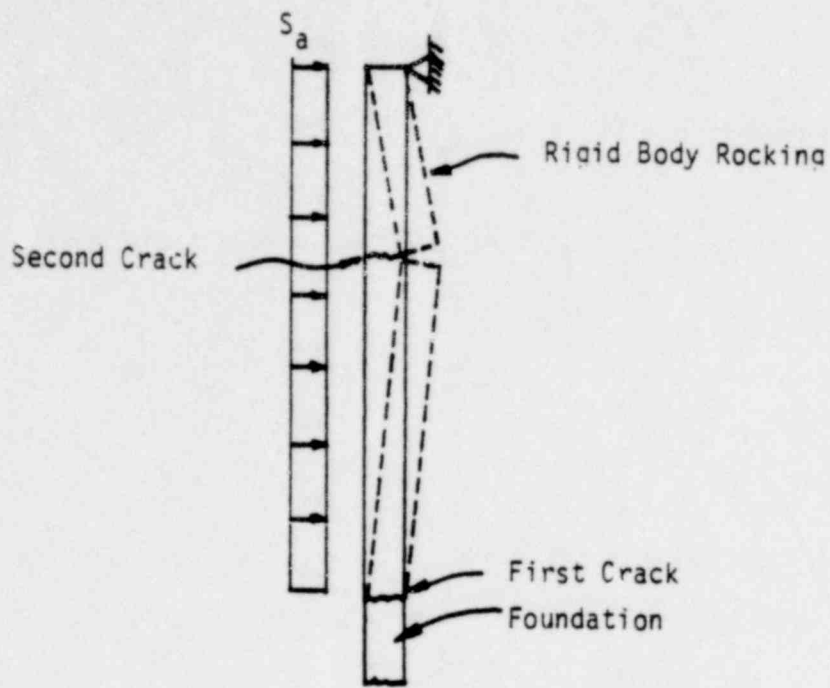


FIGURE 3-27. RIGID BODY WALL ROCKING FAILURE MODE ASSUMING RIGID ROOF FRAMING

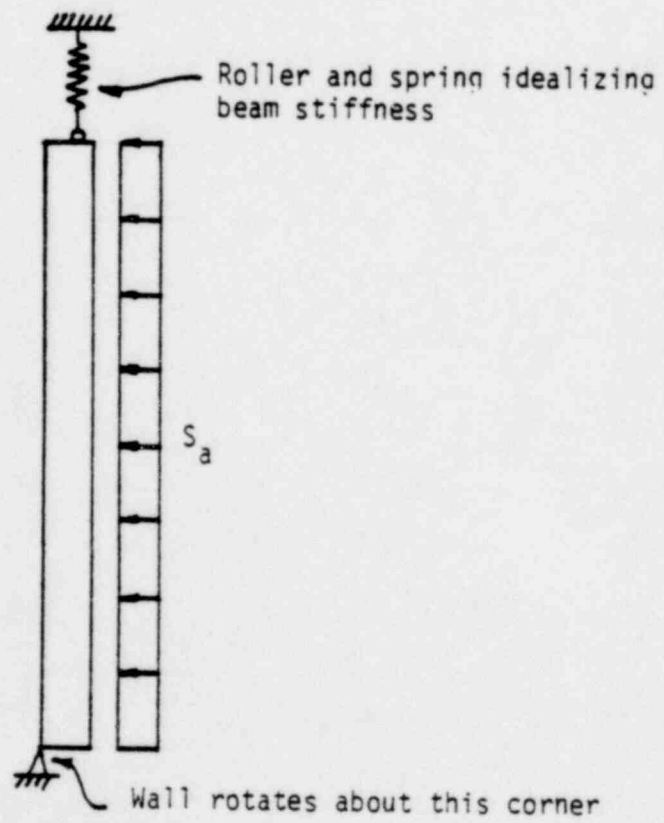


FIGURE 3-28. RIGID BODY WALL ROCKING WITH FLEXIBLE ROOF BEAM INTERFERENCE CONSIDERED

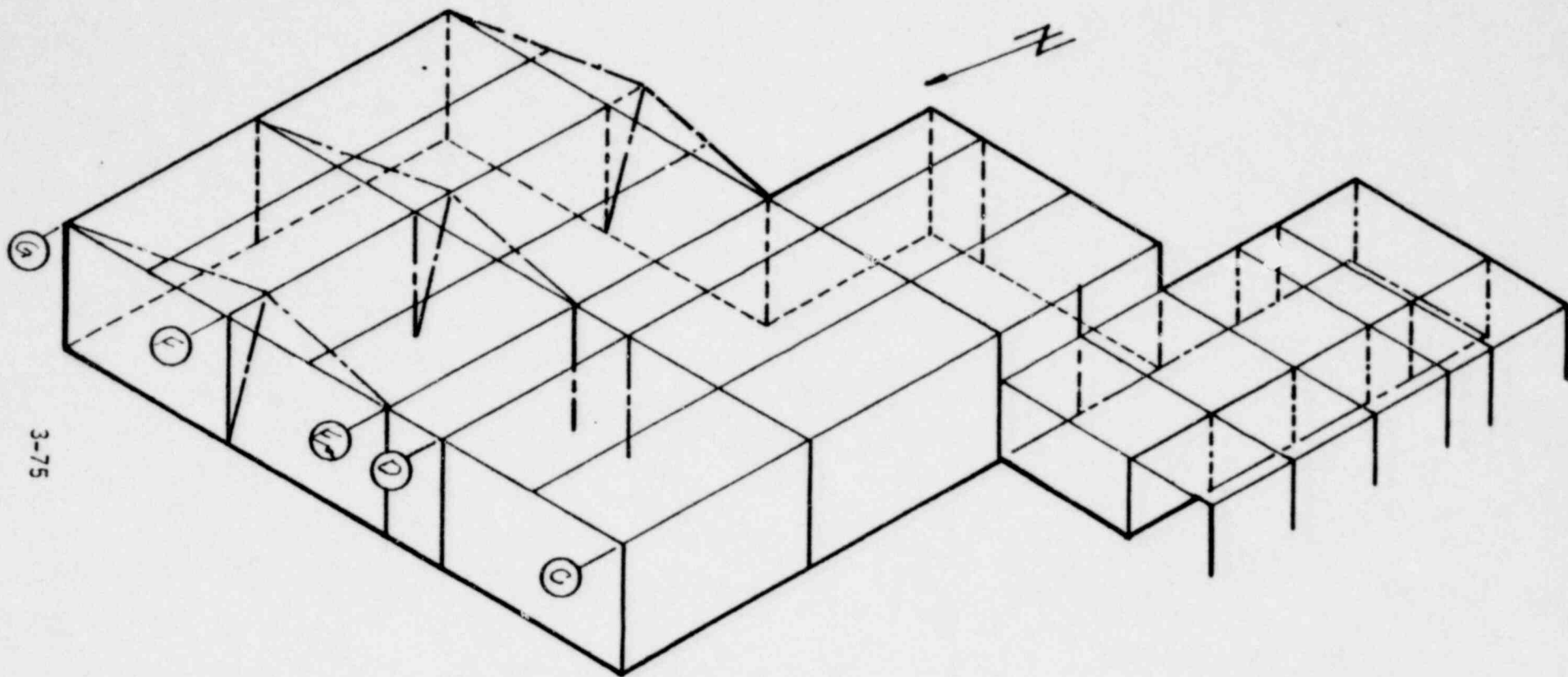


FIGURE 3-29. RIGID BODY ROCKING OF THE JN-4 FACILITY FOR N-S EXCITATION

1363 095

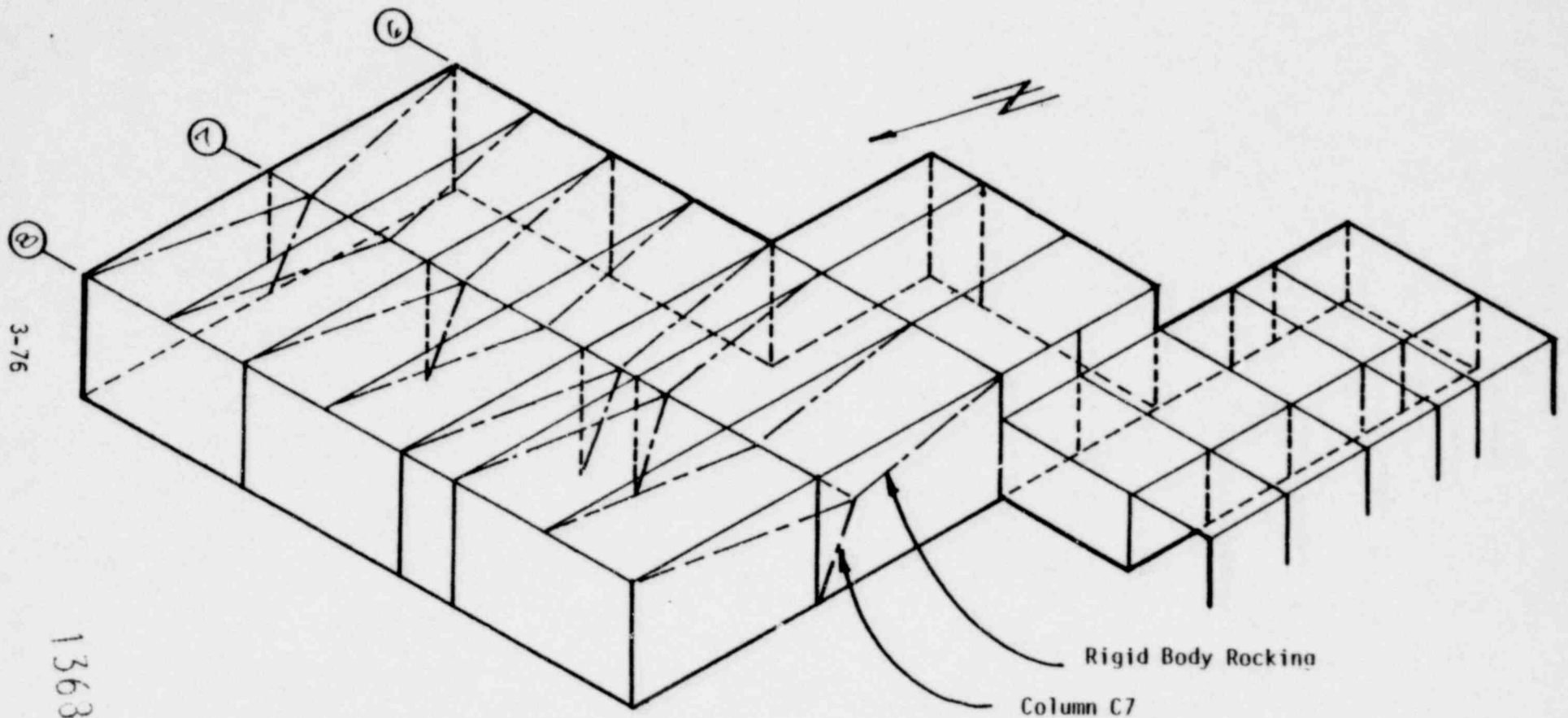


FIGURE 3-39. RIGID BODY ROCKING OF THE JN-4 FACILITY FOR E-W EXCITATION

POOR ORIGINAL

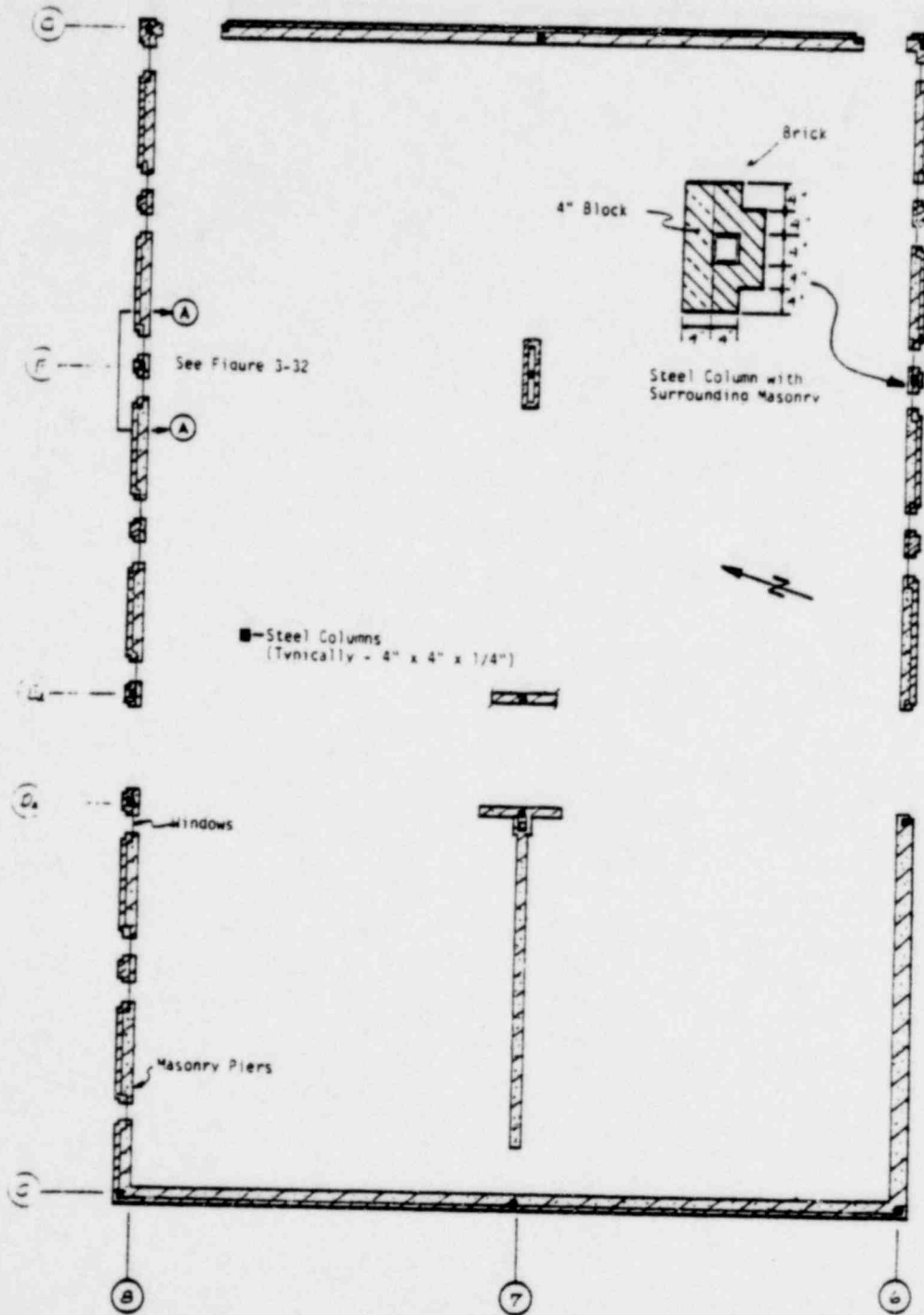


FIGURE 3-31. PLAN OF JN-4 MAIN LABORATORY

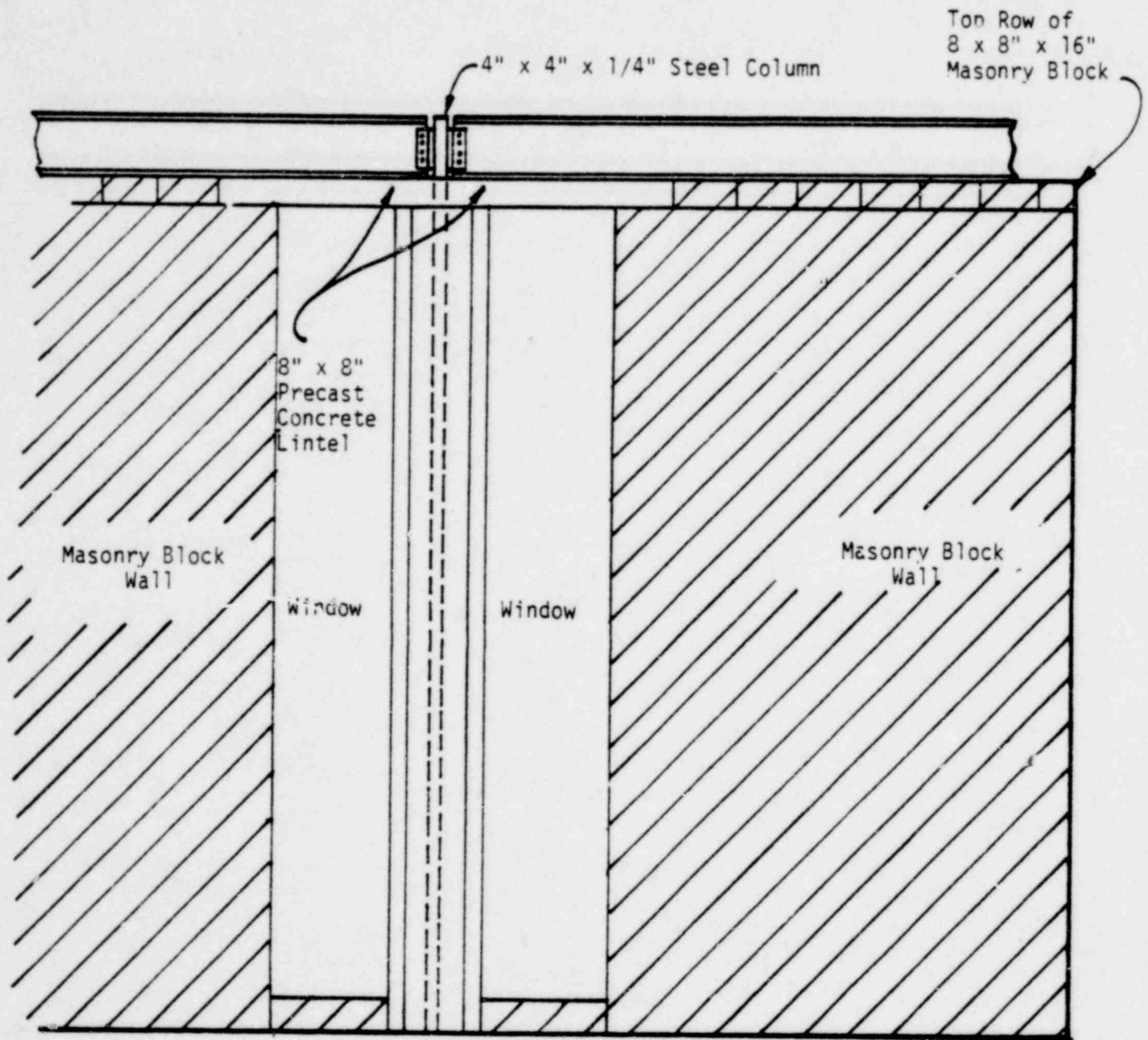


FIGURE 3-32. ELEVATION OF A TYPICAL EXTERIOR COLUMN, LINTEL, AND WALL PIER SYSTEM

1363 098

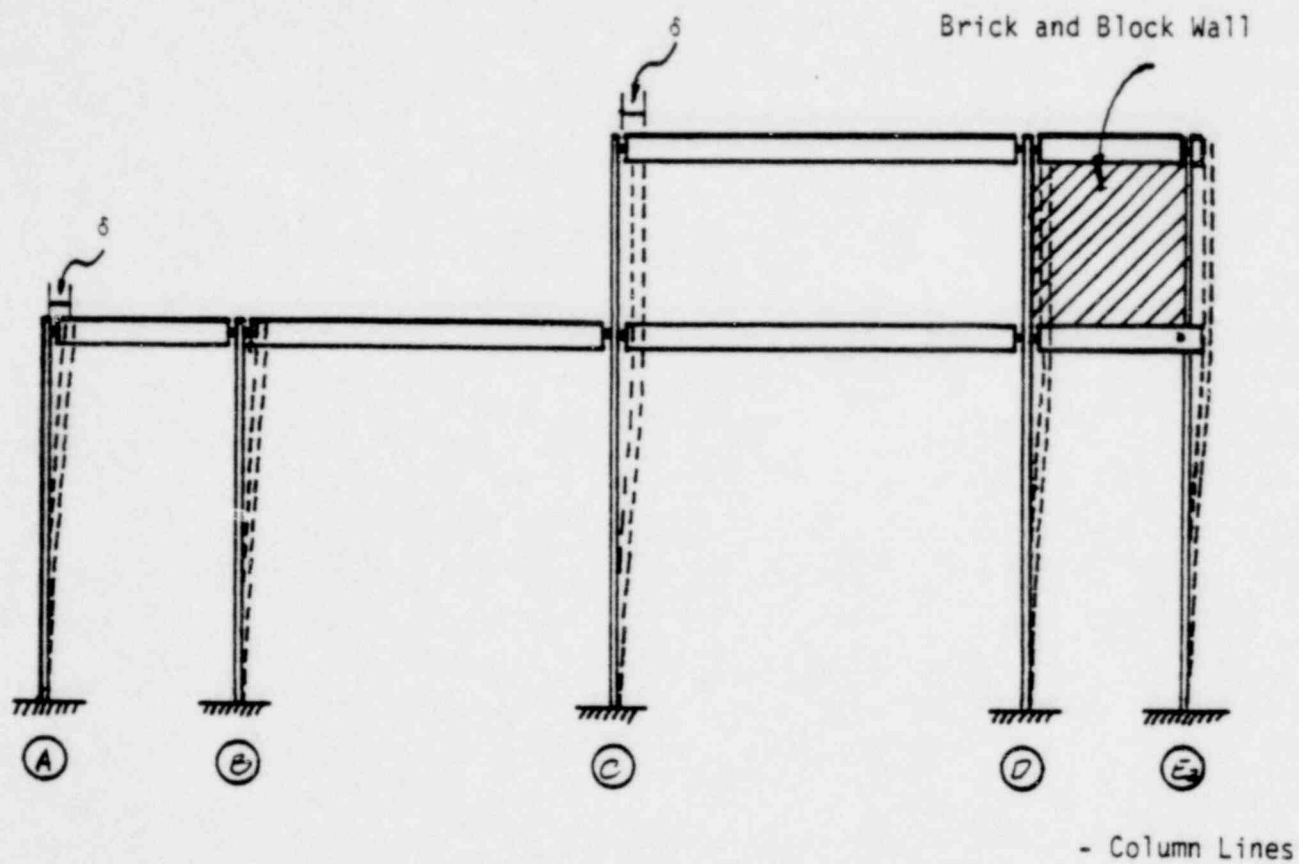


FIGURE 3-35. RIGID BODY ROCKING MODEL AT CLERESTORY DROP ALONG COLUMN LINE 4

4. EVALUATION OF CRITICAL EQUIPMENT

This section of the report presents a discussion of the analysis of the critical equipment items including analysis procedures used in the evaluation and the results. The Task I Report (Reference 4) provides additional background information concerning a number of construction details of the equipment. However, for convenient reference, selected data and equipment details which are most pertinent to the critical equipment are abstracted from the Task I Report and presented both in this section and in Appendix C. In addition, several minor details are included which were not available at the time of the Task I release.

The material in this section is organized into equipment considered in the analysis of the JN-1B Hot Cell Laboratory and the JN-4 Plutonium Laboratory. Methods of analysis are briefly described and the results of the analysis are presented. The procedure used to determine the uncertainty bounds is presented in Appendix A.

4.1 JN-1B CRITICAL EQUIPMENT CONSIDERED

Within the JN-1B facility, the primary area of concern is the High Energy Cell (HEC). This was discussed in the preceding section. However, the capacity of the cell exhaust system is also of some concern since the cell is not airtight and the exhaust system is required to maintain a net pressure difference across the cell boundary with corresponding in-leakage.

1363 100

Two air conditioning units located on the east end of the mezzanine supply air throughout the operating area. These units and their associated ducting are not critical since there is no direct connection with any areas containing hazardous chemicals and since this equipment provides no contribution to the confinement boundaries. Conditioned air enters the HEC through two 32-1/4 x 40-1/4 inch openings located 3 feet above the mezzanine floor on the east wall of the cell. Aeromold filters are mounted flush with the outside cell wall. The air is exhausted through the primary 24 by 48 inch aeromold filters embedded in the north cell wall to the final absolute filters located external to the cell above the mezzanine as shown in Figure 2-3. The filtered air is then exhausted through the roof by means of three motor driven fans. These fans maintain a pressure difference of 0.5 inch of water across the cell. Loss of these fans will eliminate the pressure differential across the HEC and thus conceivably allow some escape of unfiltered air from the cell by means of the small openings around the cell door, shield plugs, drop-in and drop-out tubes, etc. The total leakage area available under this condition with all the plugs in place, doors closed, etc., is approximately 560 square inches of unfiltered area. In addition, the inlet filters comprise a single-pass filtered area with a total of 2600 square inches. At very high seismic response levels, some additional unfiltered area may become exposed due to shaking out of some plugs as discussed in a subsequent section.

In addition to the primary filters embedded in the cell wall, the exhaust air passes through a final filter external to the cell through a 12-inch diameter duct to the exhaust fans, and

1363 101

finally through a 24-inch diameter duct to atmosphere through the roof. The final 24-inch duct was not considered critical in this evaluation. The fans and motor assemblies are mounted to the mezzanine floor by means of vibration isolators and connected at the inlet and outlet ducts with flexible connections. Other flexible connections are attached between the filter assemblies and the 12-inch diameter ducts.

4.2 JN-1B EQUIPMENT ANALYSIS PROCEDURES

The seismic capacities of the HEC exhaust system components were evaluated in order to determine the ground motion capacity at which loss of the pressure differential across the cell wall was likely to occur. In addition, components subject to potential damage from falling objects were evaluated with regard to the size of missile and free-fall distance they could withstand. Shield plugs within the cell walls were investigated to determine the ground motion levels at which they could be shaken from their locations. These capacities can then be compared with the primary capacity of concern, namely the overturning of the HEC, as well as the collapse capacity of the steel frame structure.

4.2.1 JN-1B Equipment Response

The response of the critical items of the HEC exhaust system was evaluated by means of lumped mass models simulating the dynamic characteristics of the individual components. The final filter system was modeled as a rigid planar body supported by equivalent springs representing the 8-inch diameter pipes from the HEC. Although some panel modes and small gages and their associated piping may be expected to exhibit some amplification, the primary pressure boundary is expected to behave such that the simplified models provide an adequate representation. All fundamental response

1363 102

frequencies were found to be above 20 hertz and hence in the rigid portion of the response spectrum. Since no amplification results for these high frequency modes, no consideration of damping or ductility modified response spectra was required, and the response was obtained directly from the response of the HEC at the elevation of the 8-inch diameter exhaust pipes. The response of the 12-inch diameter ducting from the final filters to the exhaust fans was also evaluated by means of planar models. Since the ducting is separated by flexible connections from both the final filters and the fans, no consideration of the interaction of the ducting with the other system components was required. The fan and motor assemblies are also separated from the exhaust ducts by flexible connections. The fan/motor assembly was treated as a rigid body supported on the flexible vibration isolation mounts. In this case, however, due to the geometry of the system and the relatively soft equivalent spring rates of the isolation mounts, the analysis was conducted on the basis of a coupled 6-degree-of-freedom system. The response was obtained assuming the mezzanine was rigidly coupled to the HEC so the input motion into the fans was controlled by the response of the HEC rather than the remainder of the steel building framing.

4.2.2 JN-1B EQUIPMENT OBJECT IMPACT

In the JN-1B facility, breach of confinement is not of primary importance for the HEC exhaust system components considered. This results from the fact that even if the confinement boundary is breached, the primary filters embedded in the cell wall will remain intact. If breach of confinement occurs downstream of the final filters, then both sets of filters would be effective in preventing release of any hazardous chemicals. Evaluation of impact damage, then is of relatively minor importance with the exception of potential loss of the fans. The most vulnerable portion of the fan

system to damage is the electrical system although buckling of a fan plenum and subsequent cessation of fan rotation is also possible for missiles originating from elevations near the roof (approximately 42 feet free-fall height). Although the fans and ducting are exposed on the mezzanine, they are shielded from falling missiles to some extent by the 12WF27 crane framing at column lines P, Q, R, and S. Also, since there are three fans a significant mechanical redundancy exists although all three fans share a common electrical system.

4.3 JN-1B EQUIPMENT ANALYSIS RESULTS

The final filters are supported by short lengths of 8-inch diameter pipe directly from the HEC. The fundamental frequencies in the three principal directions are all calculated to be greater than 20 hertz and the filter assemblies will therefore respond as rigid bodies attached to the HEC. The minimum response levels are greater than 5g in all three principal directions. Although some light tubing and gauges (Figure 4-1) are attached and may be expected to exhibit resonance at frequencies below 20 hertz and possibly failure levels below 5g, these were not considered vital to the function of the filters and were not evaluated. The final filter assemblies may therefore be considered to remain intact until collapse of the steel building structure.

The 12-inch diameter ducts are separated from both the final filter assemblies and the motor driven fans by means of flexible, multi-ply expansion joints. The ducts are supported in gusseted steel plate saddles approximately 10 inches above the mezzanine floor. The lowest calculated fundamental frequency was above 18 hertz in the axial direction. Very little dynamic amplification results and the response capacity of the ducts is also

greater than 5g based on anchor bolt pullout from the mezzanine floor. Although buckling of the ducts can result from missile impact, the ducts can be considered to remain effective until collapse of the building.

The HEC exhaust fans are Buffalo Forge Model 30AW with 7-1/2 horsepower, 240V, 3 phase motors. The catalog weight of the fan in the Arrangement No. 9 configuration is 405 lb. and a 275 lb. motor weight was used in the evaluation. The fan-motor assemblies are supported on vibration isolation mounts and are connected to both the inlet and exhaust ducts by means of flexible connections. The units were analyzed as rigid bodies with 6 degrees-of-freedom. The frequencies of the coupled rotational-translational modes range from approximately 5.2 to 29 hertz. Therefore, some dynamic amplification of the ground motion will result, both at the resonant frequencies of the unit and due to the rocking (N-S) of the HEC at 2.9 hertz. Based on the rubber adhesion and shear stresses resulting in the isolators, a median ground motion for failure of the fan-motor mounts of 0.7g was calculated. Again the collapse of the steel building frame system will control the ground motion level at which operation of the fans and hence the HEC exhaust system is expected to remain functional.

Several items were investigated with regard to exposure of unfiltered access to the HEC. As previously discussed, a total "leak path" area of approximately 560 square inches exists assuming all access doors are closed, and shield plugs, etc., are in place. The shield doors for the drop-in and drop-out tubes are exposed to falling objects on the outside of the HEC walls. These shield doors are 9 x 14 x 18 inch lead filled with 3/8-inch steel shells. Failure of a hinge with resulting exposure of the 6-inch sch. 80 pipe (Area = 26 sq. in) could be expected if impacted at the outer edge by a 6 to 15 pound object falling from the roof elevation.

The vision inserts and shield plugs are flush mounted or recessed and, hence, damage from falling objects is extremely remote. The vision inserts are tapered and retained on the cell hot side by means of welded bars. The inertia loads required to fail these bars is greater than that resulting at HEC overturning. Therefore the vision inserts are expected to remain in place. The shield plugs, on the other hand, are not restrained except by friction. Using a range of coefficient of friction of mild steel on steel from 0.4 to 0.8 and assuming a component of ground acceleration equal to 0.4 times the horizontal input simultaneously in the vertical (upward) direction, ground acceleration levels at which sliding occurs of from 0.21 to 0.39g result. However, in order to shake a plug completely out of the cell wall, a number of cycles are required. Typically, some sliding motion would be in the direction back into the wall. In order to evaluate this completely, a series of time history analyses would be required. In view of the relative lack of severity associated with increasing the leak area, however, time history analyses were not considered necessary. The number of cycles was estimated assuming the outward motion was approximately twice that of the inward motion for a given number of cycles. On this basis and assuming 3 to 4 cycles of strong motion excitation for a typical eastern U.S. earthquake, median ground acceleration levels of 0.3 to 0.4g would be required to dislodge the plugs. For 0.55g or higher, the plugs could be dislodged in a single cycle. A maximum of approximately 8380 square inches of unfiltered area could exist assuming all plugs without positive retention are shaken loose and the drop-in and drop-out shield doors are sheared off.

1363 106

4.4 JN-4 CRITICAL EQUIPMENT CONSIDERED

The primary areas of concern within the JN-4 Plutonium Laboratory are glove boxes 20 and 37. In addition, the integrity of the filters for these glove boxes is also of concern which required an evaluation of the JN-4 exhaust system. To evaluate the extent that dispersion of hazardous chemicals due to fire resulting from an earthquake could occur, the natural gas line to the service room and a hydraulic reservoir located near glove box 20 were also considered.

Glove box 20 is actually composed of two boxes of similar construction connected by means of 20-1/2 inch diameter by 4-inch long by 3/8-inch wall stainless steel tubing as shown in Figure 4-2. The larger of the boxes is shown in Figure 4-3 in more detail. Both boxes are similar in construction and configuration with the exception that one is somewhat smaller and has only one inclined face. The boxes are fabricated of 1/4 inch thick type 304 stainless steel of all welded construction. A 12 x 24 inch rectangular view panel is provided on the inclined faces of the boxes and two 12-inch diameter view ports are located on each top surface. One-inch-thick glass plates supported in neoprene gaskets provide visual access to the box at all viewpoint locations. The boxes are welded to stands fabricated from 2-inch schedule 40 pipe sections with adjustable feet and 2 x 2 x 1/4 inch angle sections. The glove boxes are attached to the floor by means of brackets as shown in Figure 4-4. Glove box 37 is of similar construction and configuration with the exception of lack of the inclined sides.

Both glove boxes 20 and 37 are inerted with nitrogen gas. Exhaust is by means of a 2-inch diameter copper tube through a HEPA filter enclosed in an 8-inch diameter canister and through another

1363 107

2-inch copper tube into the 9-inch diameter exhaust piping as shown in Figure 4-5. The filter is attached to the tubing by clamps and the tubing provides the only support for the filter. The 9-inch diameter piping leads from the floor mounted filters, through collection pipe and headers to the final filters which are suspended from the precast concrete roof channels. The 9-inch exhaust ducts are supported by rod hangers. The final filters, in turn, exhaust through fans mounted on the roof. As in the JN-1B facility, the fans are mounted on vibration isolators to 6-inch-thick concrete slabs and are separated from both the inlet and exhaust pipes by flexible connections. The absolute filters for both the floor and ceiling mounted units are enclosed in frames fabricated from 2 x 2 x 1/4 inch angle sections held together by 3/8-inch diameter 304 stainless steel turnbuckles. Figure 4-6 shows the configuration of the floor mounted filters and Figure 4-7 shows the mounting of the final filters between the roof and ceiling. Figure 4-8 shows an overall view of the exhaust duct system in the Main Laboratory part of the facility.

A 2-1/2 inch diameter black steel natural gas pipe runs along the block wall between service room and the office area and to the boiler. The line is supported by rod hangers which are spaced at 2 to 3 foot intervals. Also, there are hydraulic fluid reservoirs located at several glove boxes. One of possible interest is located at the end of glove box 38. This reservoir is 12 x 12 x 18 inches and is housed in 3/16 inch stainless steel sheet together with the pump and electrical conduits. The housing is free-standing on the floor with the reservoir connected to the glove box through high pressure tubing. Both the gas line and hydraulic reservoir contribute to the release of hazardous chemicals from seismic events only in the case of fire with resulting damage to a confinement barrier such as the gloves of a glove box.

4.5 JN-4 EQUIPMENT ANALYSIS PROCEDURES

The seismic response capacity of the critical glove boxes and their associated exhaust filter systems was evaluated in terms of ground motion levels where overturning of the gloveboxes would be expected. In addition, the effects of relative end motion between the glove box mounted filters and the roof-hung piping were evaluated. The glove boxes and particularly their glass view ports were investigated with regard to falling objects assuming all missiles originated at the roof level.

4.5.1 JN-4 EQUIPMENT RESPONSE

The response of the glove boxes was determined by means of planar lumped mass models simulating the response in the principal directions. The response was determined from the ground response spectra using the WASH 1255 (Reference 7) median alluvial spectra with 5% critical damping. The legs were modeled as pin-ended at the floor level in order to simulate the single anchor bolt and were modeled as built-in at the bottom of the box to reflect the 1/4-inch-thick gusset plates.

The 8-inch diameter filter housings are attached by means of 2-inch diameter copper tubing to both the glove box and the 9-inch diameter ceiling exhaust duct as shown in Figure 4-5. The response of the system to inertia loading as well as relative end point motion was evaluated.

With the exception of the floor mounted filters, the majority of the JN-4 filter system is suspended in the four foot space between the roof and the ceiling. This is a complex system

POOR ORIGINAL

with a large number of resonant frequencies resulting in the individual duct elements, major equipment masses, and the overall system modes. The response frequencies of the overall system suspended below the roof result from both pendulum effects of the hangars as well as the stiffening resulting from the floor mounted filters which are anchored to the floor. A rigorous analysis of this system was not conducted. Rather, the frequencies of the system evaluated as a planar body at the elevation between the roof and ceiling were estimated neglecting the flexibility of the 16-inch diameter horizontal ducting elements in order to determine the inertia loads. The ductility requirements to ensure that the system will remain intact until building collapse were then determined.

The integrity of the roof mounted motor-driven fans was not investigated since they are downstream of the final filters and their failure will not affect any confinement barriers.

4.5.2 JN-4 EQUIPMENT OBJECT IMPACT

In the JN-4 facility, breach of confinement resulting from missile impact is of primary concern for the critical glove boxes. Of particular concern are the glass view ports. Although buckling of the glove box shell and legs was also evaluated, these aspects are somewhat less important. Buckling of a box can occur, for instance, without rupture of confinement, while buckling of the box support stand would result in rupture of the 2-inch copper filter tube which could occur either upstream or downstream of the filter with approximately equal probability.

1363 110

POOR ORIGINAL

4.6 JN-4 EQUIPMENT ANALYSIS RESULTS

The response of the glove boxes was determined from the lumped-mass planar models previously described. The fundamental frequencies computed are all in the range of 7 to 8 hertz. Since there is little rocking of the boxes on the unbraced stands, the frequencies in the two horizontal principal axes are virtually identical. Some torsion results in glove box 20 due to the stiff coupling of the smaller and larger boxes (7.5 and 7 hertz uncoupled fundamental frequencies respectively). For all boxes, the failure was found to be governed by the pullout capacity of the 1/2-inch diameter anchor bolts. For 5% critical damping and simultaneous components of ground acceleration equal to 0.4 times the principal horizontal input in the other orthogonal directions, the boxes are capable of withstanding over 3g median ground accelerations in both the strong and weak horizontal axis directions.

The response of the 8-inch diameter filters mounted above the glove boxes was evaluated by means of simple beam models with distributed mass for the tube and a lumped-mass simulating the filter. Dynamic input for the system was determined after accounting for both the glove box and roof mounted piping dynamic amplification. The simple copper tubing/filter system investigated has a inertia capability corresponding to over 3g ground motion for these conditions. In addition, the system can accommodate relative horizontal end point motions of over 10 inches. An axial deformation in the copper tube of approximately 0.47 inches results with corresponding axial strain in the tubing of .0078 inches/inch. However, the filter is attached to the tubing by clamps. If these clamps should allow slippage under the axial loads, tube buckling can result as a result of roof drift reversal. This will not cause a breach of confinement, however.

POOR ORIGINAL

At low response levels, the exhaust duct system suspended between the ceiling and roof will exhibit frequencies significantly below those of the building structure. At these ground motion levels (less than 0.08g), the building is quite stiff and the duct system will behave essentially as though ground mounted with predominant resonant frequencies in the range of 1 to 3 hertz. For 5 percent critical damping, duct response will remain elastic with relative deformations less than one inch throughout the system. As ground response levels increase, the building structure experiences nonlinear behavior with subsequent increase of the building response periods. At increased ground acceleration levels, the building response frequencies will correspond with the resonant frequencies of the ducting and significant amplification will occur. Concurrently, the damping of the ducting may be expected to increase and gaps such as the one between the roof slabs and dampers will open and close and yielding at several locations will occur resulting in nonlinear response of the ducting as well as the building. Although resonance of the ducting with the building fundamentals will occur at certain frequencies and acceleration levels, the inertia loads within the ducting are less important than the ultimate roof story drift relative deformations when considering the collapse of the ducting. At near building collapse, ductility requirements of approximately 4.9 are required for N-S response and approximately 4.8 for E-W response. Although these are attainable for welded steel ducting, it is likely that just prior to building collapse significant damage in terms of failed hangars, buckling of sheet metal and possibly weld failures are expected. This corresponds to median ground acceleration levels of 0.23g in the N-S direction and 0.17g in the E-W direction; both of which have return periods well beyond 2,000 years.

1363 112

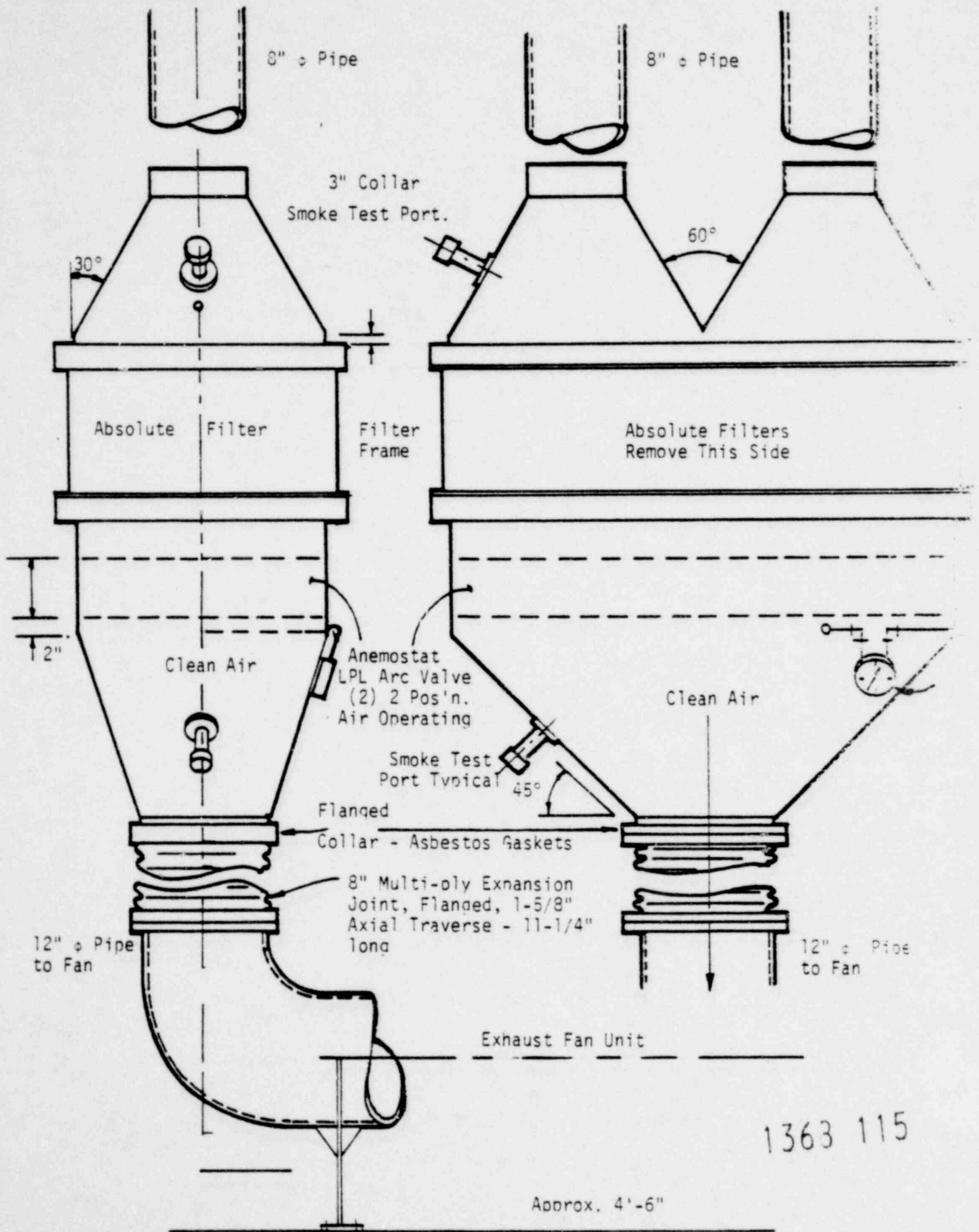
Failure of a glove box can result from crushing or fracture of the viewports from free-falling objects originating at the ceiling or roof. The free-fall height for these cases is six to ten feet to the top of the glove box. The most critical items from falling object damage are the 12-inch diameter horizontal plate glass viewports. The weight of missile these viewports can withstand depends to some extent on the missile hardness as reflected in the rise time of the impact pulse. For "hard" objects with pulse durations of the order of 0.001 seconds, objects of approximately 8 pounds originating at the roof can be expected to cause fracture of the glass. For "soft" objects with a pulse duration of approximately 0.005 seconds, the flexibility of the neoprene gasket becomes effective and missile weights in the range of 27 pounds are required for fracture. The 12 x 24 inch rectangular viewports on the inclined faces were calculated to withstand falling objects with weights of from 24 to 44 pounds for pulse durations of from 0.001 to 0.003 seconds.

Buckling of the glove box structure was calculated to occur from impact of objects in the range of 80 to 150 pounds and leg buckling from objects of approximately 120 to 460 pounds for one to four legs, again assuming a 0.005 second pulse. Breach of confinement due to box buckling will not necessarily result unless a viewport is fractured or a glove is torn. However, deformations in the region of the 8-inch diameter HEPA filter in excess of approximately one inch will likely cause the filter clamps to be pulled loose and thus expose a 2-inch diameter path to the atmosphere. The weight of one concrete channel roof slab is approximately 500 pounds.

1363 113

The natural gas line to the boiler in the JN-4 service room is suspended on hangars at intervals of 2 to 3 feet. The line passes through the Old Lab portion of the building which was not evaluated. Fire resulting from collapse of the structure and resulting rupture of the natural gas line could occur at ground acceleration levels in the range of 0.26g for E-W direction excitation. Another possibility for fire exists at the hydraulic reservoir. Sliding of the reservoir on the floor is not calculated to occur at levels below the roof collapse. Thus, even if fire should result, it would not be expected to occur until collapse of the glove boxes from building collapse occurs.

1363 114



1363 115

FIGURE 4-1. JN-1B FINAL FILTER UNIT ASSEMBLY

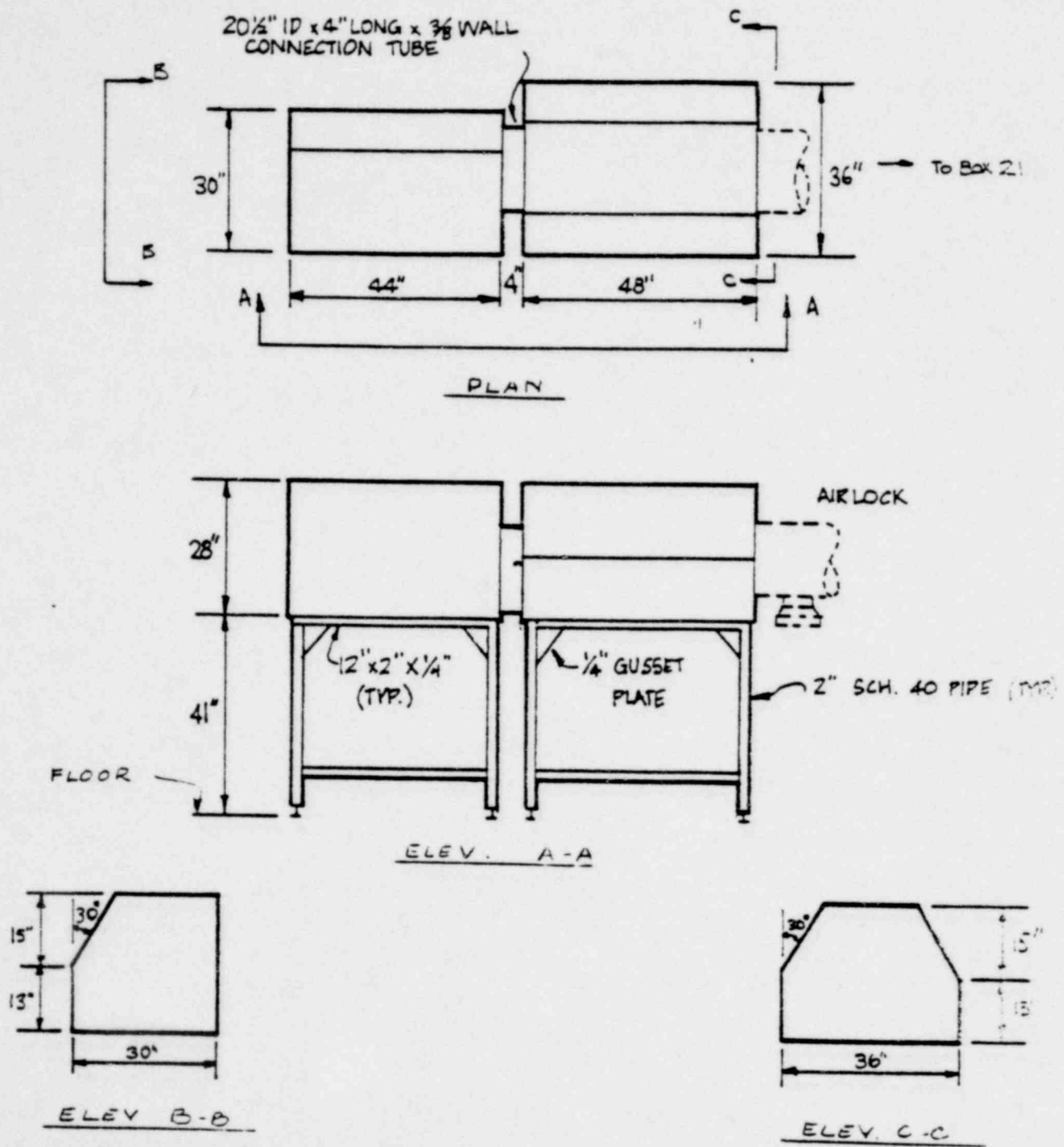


FIGURE 4-2. GLOVE BOX 20 CONFIGURATION

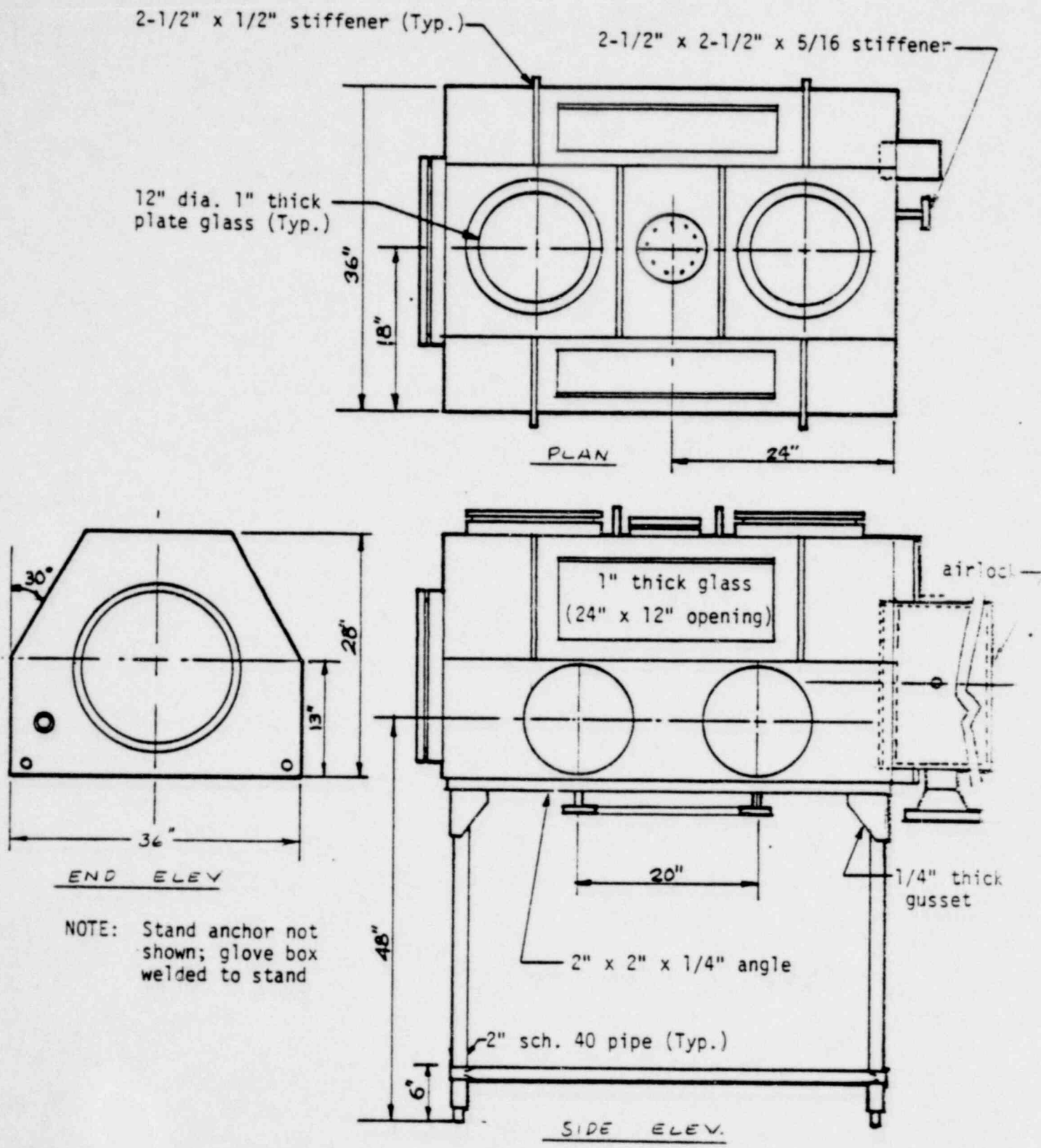


FIGURE 4-3. GLOVE BOX 20 (LARGER)

1363 117

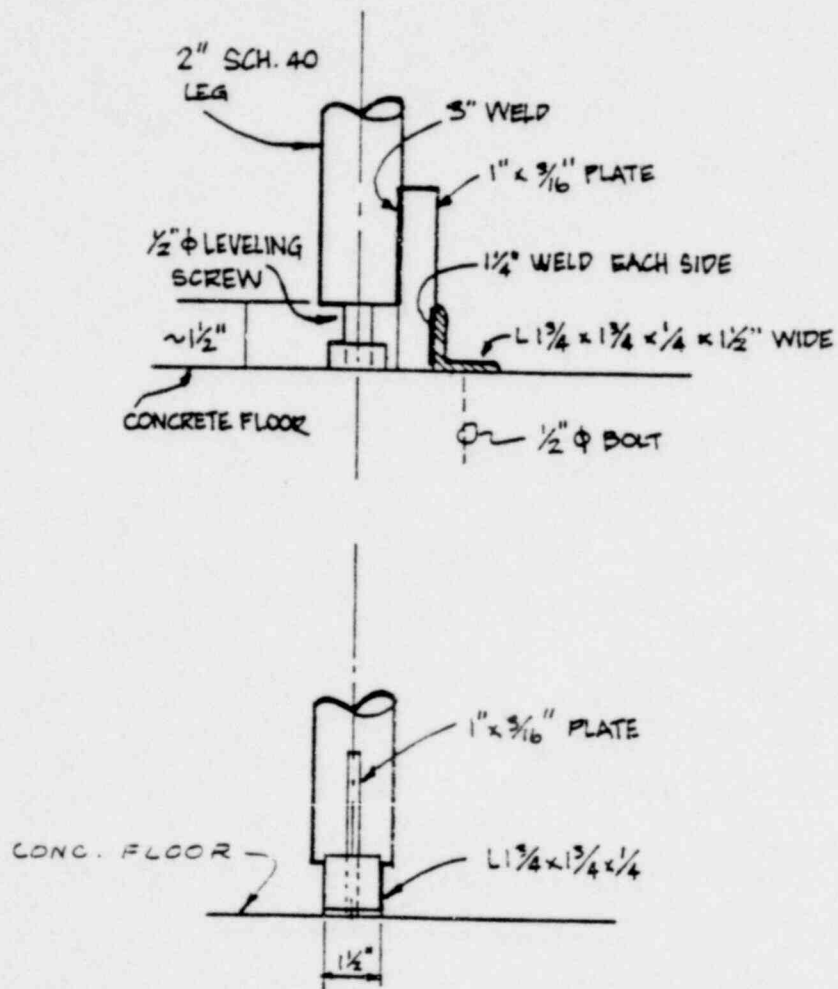


FIGURE 4-4. GLOVE BOX STAND ANCHOR BRACKET

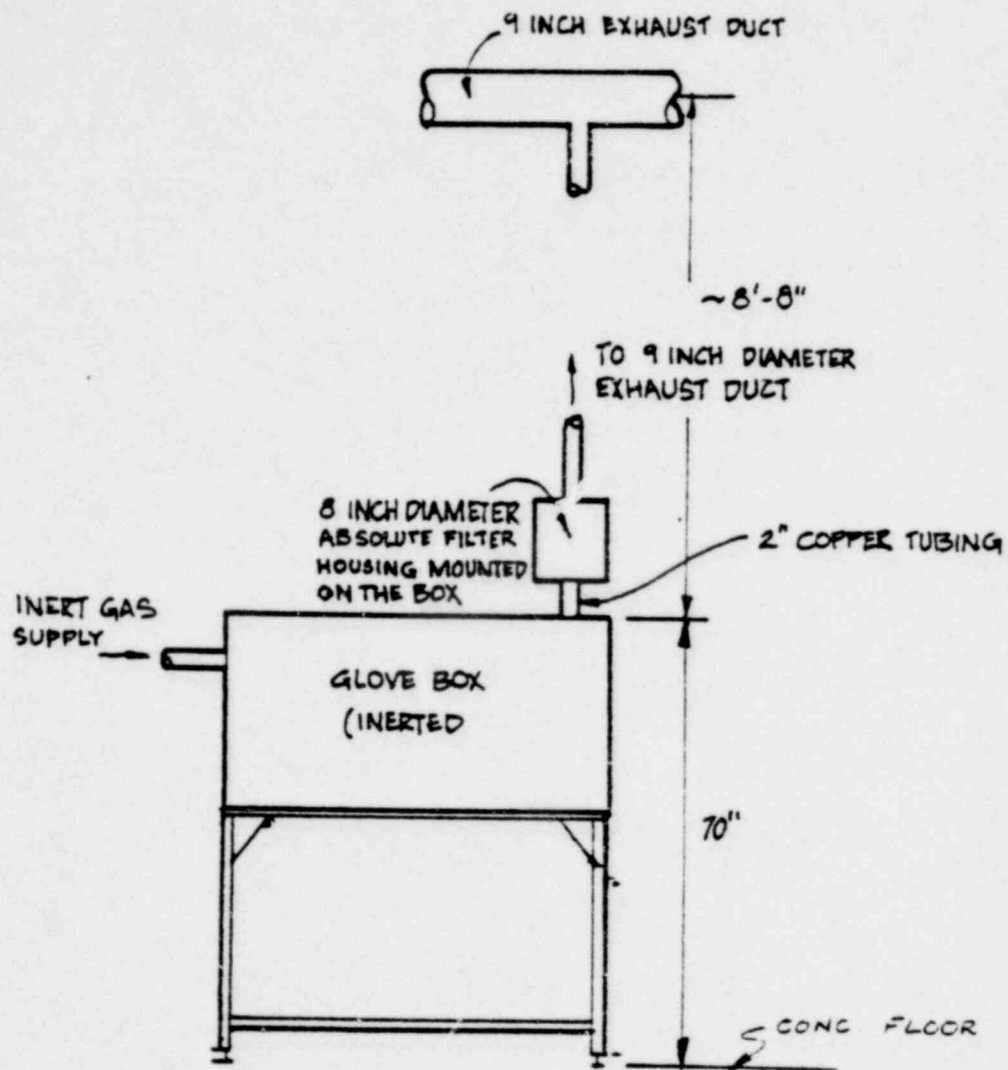


FIGURE 4-5. TYPICAL BOX-MOUNTED EXHAUST FILTER

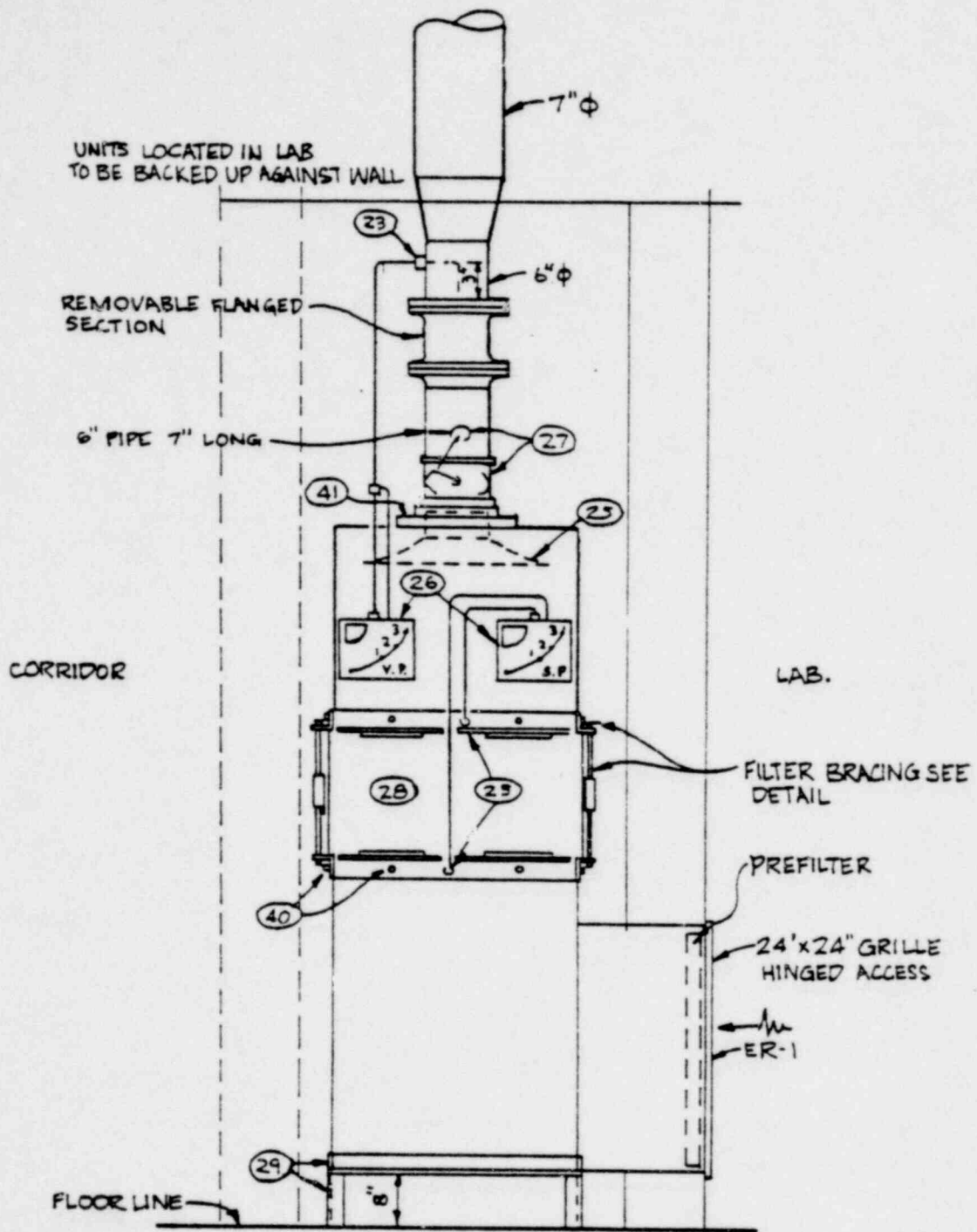


FIGURE 4-6. JN-4 FILTER AT FLOOR

1363 120

4-22
1363 121

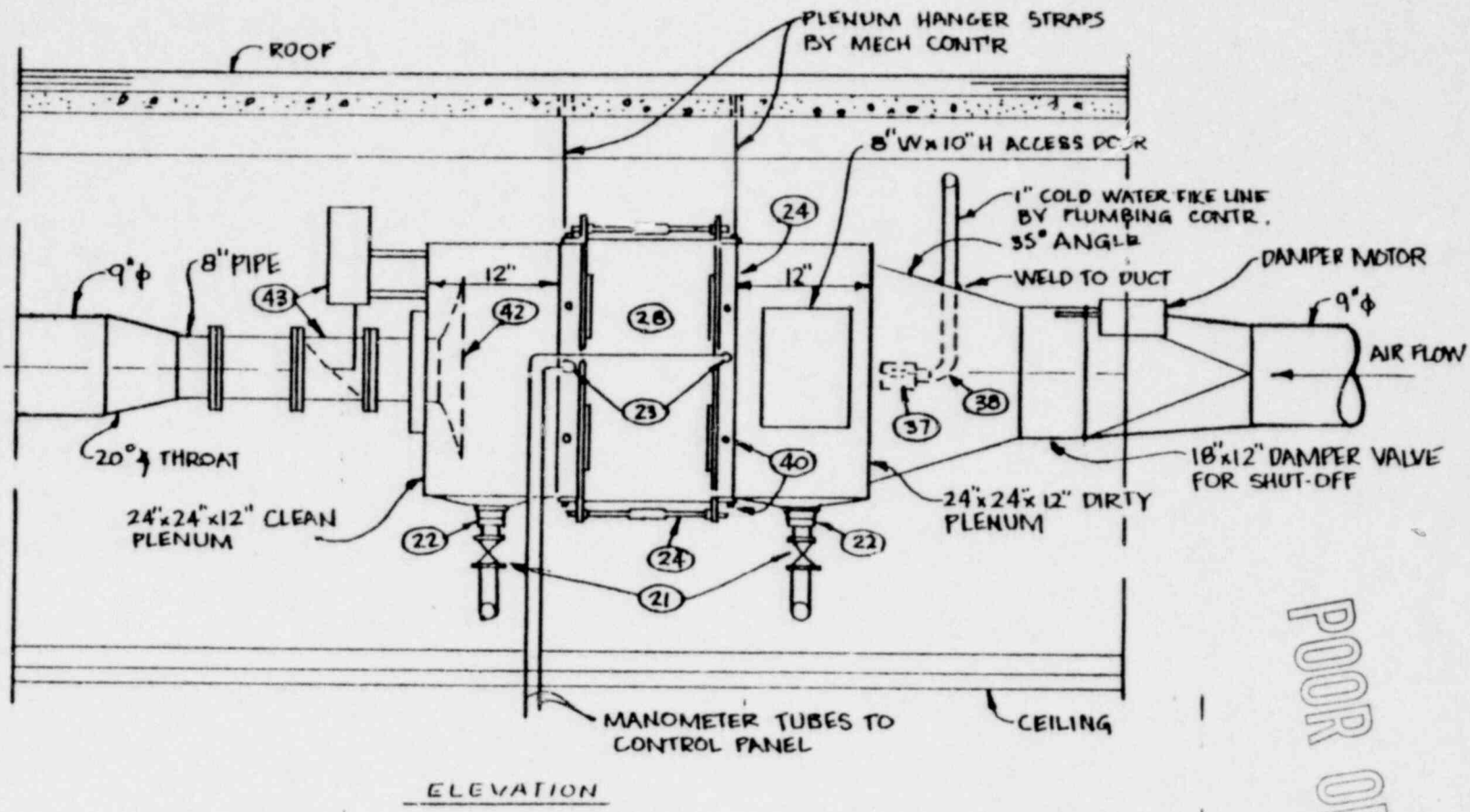


FIGURE 4-7. JH-4 FILTER ABOVE CEILING

POOR ORIGINAL

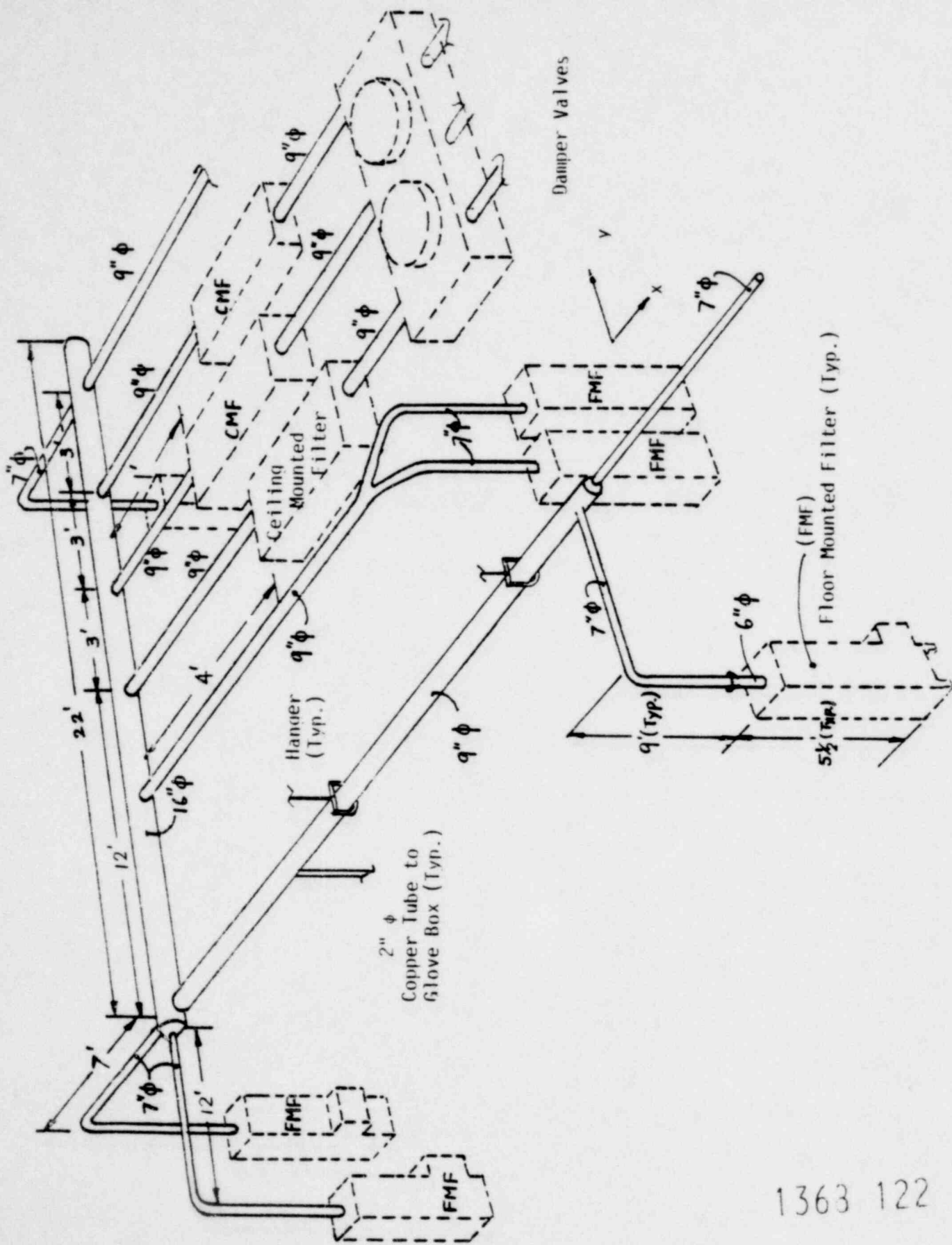


FIGURE 4-3. EXHAUST SYSTEM - GLOVE BOX 20 (HW) 37 AREA

1363 122

5. SUMMARY OF RESULTS AND STRUCTURAL DAMAGE SCENARIO

This section presents a summary tabulation of the results of the analyses previously described and presents the interpretation of these results in terms of a structural damage scenario which describes the progression of expected damage to the BMI facility with increasing intensity of earthquake ground motion.

Table 5-1 presents a tabulation of the critical seismic capacities of the structural and equipment systems evaluated during the Task II effort. These capacities are associated with probable structural collapse and as such establish the ground motion acceleration levels associated with probable release of hazardous material. The High Energy Cell in the JN-1B facility has a substantially greater seismic capacity than the steel frame structure which encloses it. Furthermore, collapse of the steel structure is unlikely to significantly damage the cell. The equipment associated with the HEC exhaust system was also shown to have a higher seismic capacity than the building structure. Therefore, the seismic ground motion which causes collapse of the JN-1B building will result in an unfiltered leak path to the cell only. Evaluation of the glove boxes and exhaust piping/ductwork in the JN-4 Plutonium Laboratory indicates that these equipment systems also have ground acceleration capacities in excess of the building structural collapse capacities. However, the equipment systems cannot withstand the impact of the falling weight of the collapsing structure. Thus, for the JN-4 facility, these ground motion acceleration capacities represent the level of seismic motion which causes virtually complete loss of confinement for hazardous materials.

The analyses of structural capacity were conducted using median material strength properties and median estimates of dynamic response to ground shaking. Based upon the assumption that the important contributing variables are approximately lognormally distributed, the calculated upper and lower bound capacity values represent and estimated one standard deviation variation. The median capacity values represent the evaluation of the various systems as they currently exist in the BMI facility.

For breach of primary confinement boundaries to occur in any BMI facility or component, median ground motion acceleration levels in excess of 0.17g must occur. This level is above that upon which sufficient data are available to base reliable return periods (Reference 5). Thus, accurate estimates of the return periods for loss of confinement of the various critical systems, and for all ground motion acceleration levels above 0.14g ($T \approx 2,000$ years) return periods are quoted as "greater than 2,000 years". The following scenarios present a general description of behavior of the structures and equipment resulting from increasing ground motion acceleration. The scenarios are based upon the median predicted capacities of the BMI structural systems.

GROUND SHAKING OF 0.03 to 0.09g ($T = 70$ to 700 years)

At ground acceleration levels below 0.03g all structures and equipment will behave elastically and there will be no significant effects resulting from an earthquake. At 0.03g in the E-W direction, the diaphragm action in the JN-4 roof will begin to be lost and slipping of the concrete channels will occur. At 0.04g N-S excitation, plastic hinges will begin to form at the base of the

columns along column line F, and the diaphragm action in the roof will be lost at 0.076g for N-S excitation. Plastic hinges will begin to form along column line 7 for E-W excitation at approximately 0.09g. Both horizontal and vertical cracking of the masonry will occur with some vertical cracks remaining open after the disturbance. Breaking of windows will occur in the JN-4 building but no significant damage will result in the critical equipment.

In the JN-1B facility, cracking at the base of the exterior walls will occur at about 0.08g. At this same ground level for N-S excitation, yielding of bolts will occur in some of the diagonal member connections of the roof truss. At 0.08g E-W excitation, yielding of the bolts in the diagonal member of the north wall braced frame will occur. Again no damage of any structure or equipment which could lead to release of hazardous chemicals will result in the JN-1B facility for ground motion levels in this range.

GROUND SHAKING OF 0.11 to 0.23g (T = 1100 to Greater than 2,000 Years)

At 0.11g ground excitation in the E-W direction, buckling of the diagonal member occurs in the north wall braced frame of the JN-1B building and the lateral forces must be resisted by the remaining south and west walls and crane framing. At 0.23g rigid body rocking of the HEC reaches the point at which uplift of the footing begins. The structural integrity of the cell will remain intact, however, and no structural failure of the cell's filter and exhaust system is expected at these ground motion levels.

1363 125

POOR ORIGINAL

At 0.17g median ground acceleration in the E-W direction, collapse of the JN-4 Main Laboratory steel framing and roof system occurs due to excessive wall displacement. Loss of the buildings filter and exhaust system will occur and crushing and rupture of the majority of the glove boxes will result from impact by the falling concrete roof slabs. Similar damage results at 0.23g due to excitation in the N-S direction. The mode of failure for either direction is rigid body out-of-plane rocking of the walls with maximum displacements occurring in the middle of the bay away from the shear walls. At least some parts of the shear walls may remain standing as well as the service room and initial office room portions of the structure.

GROUND SHAKING GREATER THAN .25g (T > 2,000 Years)

At approximately 0.26g excitation in the E-W direction, collapse of the remaining building structure of the JN-4 facility is expected to occur.

At median ground acceleration levels of approximately 0.27g, collapse of the 10-foot-high nonload bearing masonry walls of the JN-1B facility are expected to collapse. At 0.3g, shear failure of the bolts in the diagonal members of the JN-1B roof truss occur. Loss of the diaphragm action in the truss will result in collapse of the steel frame structure and loss of the HEC exhaust system. As discussed above, this will result in an unfiltered leak path to the HEC but not failure of the concrete structure. Overturning of the HEC is not expected to occur until ground motions in excess of 3g occur, although some shield plugs may be shaken out of the cell walls at 0.3 to 0.4g and thus increase the unfiltered leak path area.

TABLE 5-1

SUMMARY OF CRITICAL SEISMIC CAPACITIES

Structural and Equipment Damage	Ground Acceleration Capacity (g)		
	Lower	Median	Upper
Buckling of the Diagonal Member in the JN-1B North Wall for E-W Excitation	0.08	0.11	0.15
Collapse of the Steel Framing and Roof of the JN-4 Main Lab for E-W Excitation	0.11	0.17	0.26
Initiation of Uplift of the HEC	0.18	0.23	0.31
Collapse of the Steel Framing and Roof of the JN-4 Main Lab for N-S Excitation	0.17	0.26	0.38
Loss of Roof Truss and Collapse of JN-1B Frame	0.17	0.3	0.54
Shaking Loose of HEC Shield Plugs	0.21	0.35	0.55
Overturning of the HEC	—	> 3	—

1363 127

REFERENCES

1. Ayer, J. A., and W. Burkhardt, "Analysis of the Effects of Abnormal Natural Phenomena on Existing Plutonium Fabrication Plants", United States Nuclear Regulatory Commission, Washington, D.C., 1976.
2. Letter, J. E. Ayer to J. Mishima, dated November 16, 1978 Docket No. 70-8, Project M-3.
3. Mishima, J., "Identification of Features within Plutonium Fabrication Facilities Whose Failure May Have a Significant Effect on the Source Terms", Working Paper on Increment of Analysis for Battelle Columbus Laboratories, West Jefferson Site, Part of USNRC Study of Analysis of the Effect of Natural Phenomena Upon Existing Plutonium Fabrication Facilities, Battelle, Pacific Northwest Laboratory, Richland, Washington, March, 1977.
4. Engineering Decision Analysis Company, Inc. (EDAC), "Structural Condition Documentation and Structural Capacity Evaluation of the Battelle Memorial Institute Columbus Laboratories West Jefferson Site for Earthquake and Flood, Task I -- Structural Condition" for Lawrence Livermore Laboratory, Livermore, California, November, 1978.
5. TERA Corporation, "Seismic Risk Analysis for Battelle Memorial Institute Nuclear Research Facility, West Jefferson, Ohio", Berkeley, California, December, 1978.
6. G. K. Jewell and Associates, "Soils Investigation, Proposed Hot Cell Pool, Nuclear Research Facility, West Jefferson, Ohio", Columbus, Ohio", March, 1971.
7. Nathan M. Newmark Consulting Engineering Services, "A Study of Vertical and Horizontal Earthquake Spectra, WASH-1255, April, 1973.
8. Inryco, Inc., "Lateral Diaphragm Data Manual, No. 20-2", Milwaukee, Wisconsin, 1975.
9. Richart, F. E., J. R. Hall, and R. D. Woods, Vibration of Soils and Foundations, Prentice-Hall, Inc., New Jersey, 1970.

1363 128

10. Novak, M., "Vibrations of Embedded Footings and Structures", Meeting Preprint 2029, presented at the ASCE National Structural Engineering Meeting, April 9-13, 1973, San Francisco, California.
11. Beredugo, Y. O., and M. Novak, "Coupled Horizontal and Rocking Vibration of Embedded Footings", Canadian Geotechnical Journal, Vol. 9, 1972, pp. 477-497.
12. Blume, J. A., N. M. Newmark, and L. H. Corning, Design of Multi-story Reinforced concrete Buildings for Earthquake Motion, Portland Cement Association, 1961.
13. Newmark, N. M., and E. Rosenblueth, Fundamentals of Earthquake Engineering, Prentice-Hall, Inc., 1971, Chapter 11.
14. Newmark, N. M., "Earthquake Response Analysis of Reactor Structures", Nuclear Engineering and Design, Volume 20, 1972, pp. 303-322.
15. Newmark, N. M., and W. J. Hall, "Procedures and Criteria for Earthquake Resistant Design", Building Practices for Disaster Mitigation, National Bureau of Standards (Washington, D.C.) Building Science Series 46, Vol. 1, February 1973, pp. 209-236.
16. Applied Technology Council, An Evaluation of a Response Spectrum Approach to Seismic Design of Buildings, ATC-2, U.S. Department of Commerce, National Bureau of Standards, 1974.
17. Newmark, N. M., "A Response Spectrum Approach for Inelastic Seismic Design of Nuclear Reactor Facilities", Transactions Third International Conference on Structural Mechanics in Reactor Technology (London), Paper K5/1, Vol. 4, Part K, 1975.
18. Applied Technology Council, Tentative Provisions for the Development of Seismic Regulations for Buildings, ATC-3, National Science Foundation, National Bureau of Standards, 1978.
19. Newmark, N. M., "Inelastic Design of Nuclear Reactor Structures and Its Implication of Design of Critical Equipment", Transactions Fourth International Conference on Structural Mechanics in Reactor Technology (San Francisco), Paper K4/1, Vol. K(a), 1977.
20. Manual of Steel Construction, Seventh Edition, American Institute of Steel Construction, 1970.
21. Bresler, B., T. Y. Lin, and J. B. Scalzi, Design of Steel Structures, John Wiley and Sons, New York, 1968.

1363 129

22. PCI Design Handbook, Prestressed Concrete Institute, 1971.
23. Ollgaard, J. G., Slutter, R. G., and J. W. Fisher, "Shear Strength of Stud Connectors in Lightweight and Normal-Weight Concrete" AISC Engineering Journal, April, 1971, pp. 55-64.
24. McMackin, P. J., Slutter, R. G., and J. W. Fisher, "Headed Steel Anchors under Combined Loading", AISC Engineering Journal, Second Quarter, 1973, pp. 43-52.
25. Becker, J. M. and C. Llorente, "Seismic Design of Precast Concrete Panel Buildings", presented at the NSF Workshop on Earthquake Resistant Concrete Building Construction, University of California, Berkeley, July 11-16, 1977.
26. Hawkins, N. M., "Analytical and Experimental Studies of Prestressed and Precast Concrete Elements", presented at the NSF Workshop on Earthquake Resistant Concrete Building Construction, University of California, Berkeley, July 11-16, 1977.
27. Perry, E. S. and J. Nabil, "Pullout Bond Stress Distribution Under Static and Dynamic Repeated Loadings", ACI Journal, May, 1969, pp. 377-380.
28. Bathe, K. J., Wilson, E. L., and F. E. Peterson, "SAP IV - A Structural Analysis Program for Static and Dynamic Response of Linear Systems", Report No. EERC 73-11, University of California, Berkeley, June, 1973.
29. Engineering Decision Analysis Company, Inc., "Structural Condition Documentation and Structural Capacity Evaluation of the Babcock & Wilcox Facility at Leechburg, Pennsylvania for Earthquake and Flood, Task II -- Structural Capacity Evaluation, Vol. I - Seismic Evaluation", EDAC 175-030.02R, Irvine California, May, 1978, Revision.
30. Hall, W. J., B. Mohraz, and N. M. Newmark, "Statistical Analysis of Earthquake Response Spectra", Transactions Third International Conference on Structural Mechanics in Reactor Technology, (London), Paper KI/6, 1975.
31. Freudenthal, A. M., Garrelts, J. M., and Shinozuka, M., "The Analysis of Structural Safety", Journal of the Structural Division, ASCE, ST1, February, 1966, pp. 267-325.

32. Kennedy, R. P., "A Statistical Analysis of the Shear Strength of Reinforced Concrete Beams", Technical Report No. 78, Department of Civil Engineering, Stanford University, Stanford, California, April, 1967.
33. Kennedy, R. P., and C. V. Chelapati, "Conditional Probability of a Local Flexural Wall Failure for a Reactor Building as a Result of Aircraft Impact", Holmes & Narver, Inc. for General Electric Company, San Jose, California, June 1970.
34. Benjamin, J. R., and C. A. Cornell, Probability, Statistics and Decision for Civil Engineers, McGraw-Hill Book Company, New York, N.Y., 1970.
35. Housner, G. W., "The Behavior of Inverted Pendulum Structures During Earthquakes", Bulletin of the Seismological Society of America, Vol. 53, No. 2, pp. 403-417, February, 1963.
36. Steinbrugge, K. V., "Earthquake Damage and Structural Performance in the United States", Earthquake Engineering, R. L. Wiegel, coordinating editor, Prentice-Hall, 1970, Chapter 9.
37. Murtel, R. W., "Earthquake Damage to Type III Buildings in Long Beach, 1933", Earthquake Investigation in the Western United States 1931-1964, D. S. Carder, Editor, U.S. Department of Commerce, Publication 41-2, U.S. Government Printing Office, Washington D.C., 1964.
38. Housner, G. W. and P. C. Jennings "Earthquake Design Criteria for Structures", California Institute of Technology, EERL 77-06, Pasadena, 1977.
39. C. F. Richter, Elementary Seismology, W. H. Freeman and Company, San Francisco, 1958.
40. Lomenick, T. F., and NSIC Staff, "Earthquakes and Nuclear Power Plant Design", ORNL-NSIC-28, Oak Ridge National Laboratory, Oak Ridge, Tennessee, 1970.
41. Nigam, N. C. and P. C. Jennings, "Calculation of Response Spectra from Strong-motion Earthquake Records", Bulletin of the Seismological Society of America, Vol. 59, No. 2, pp. 909-922, April, 1969.

1363 131

APPENDIX A

UNCERTAINTY BOUND ANALYSIS PROCEDURE

1363 132

APPENDIX A

Uncertainty Bound Analysis Procedure

The procedure used in the probabilistic seismic capacity study was based upon the general properties of a lognormal distribution. The procedure involved the identification of each major random variable which can be considered as a potential source of substantial variability affecting component and structural resistance and response values. For each variable, median and standard deviation estimates are made.

Lognormal distributions were selected for use since the statistical variation of many material properties and seismic response variables may reasonably be represented by this distribution so long as one is not primarily concerned with the extreme tails of the distribution. Use of this distribution for estimating conditional probabilities of failure on the order of one percent or greater is considered to be quite reasonable. Lower conditional probability estimates which are associated with the extreme tails of the distribution must be considered more suspect. However, use of the lognormal distribution for estimating very low conditional probabilities of component or structural failure associated with the tails of the distribution is considered to be conservative since the low probability tails of the lognormal distribution generally extend further from the median than actual structural resistance or response data might extend since such data generally shows cut-off limits beyond which there is essentially zero probability of occurrence.

It is generally acknowledged (Reference 31, 32) that the mechanical strength properties (e.g., yield and tensile strength) of structural materials may be reasonably represented by a lognormal distribution. In addition, studies (Reference 30) have indicated that the statistical variation of response to seismic ground motion, as characterized by response spectra (Reference 7), may be represented by a lognormal distribution. Thus, while a lognormal distribution may not provide a perfect fit of the distribution for structural element

1363 133

capacities or element forces due to dynamic response, it provides a sufficient approximation. Furthermore, it is computationally convenient since the assumption of a lognormal distribution leads to a simplified combination of product and quotient random variables which are used in this study to determine structural capacities and dynamic responses considering several contributing variables. In addition, the central limit theorem states that a distribution, D , consisting of products and quotients of distributions of several variables tends to be lognormal even if the individual variable distributions are not lognormal.

A.1 BASIC RELATIONS

Some general relationships for lognormally distribution variables are presented which are used more specifically in development of median values and logarithmic standard deviations. Background and further information on these relationships are given in References 33 and 34.

A random variable x is said to be lognormally distributed if its natural logarithm \bar{x} given by

$$\bar{x} = \ln(x) \tag{A-1}$$

is normally distributed with the mean of \bar{x} equal to $\ln \check{x}$ where \check{x} is the median of x , and with the standard deviation of \bar{x} equal to β which will be defined herein as the logarithmic standard deviation of x . Then, the coefficient of variation, COV, is given by the relationship:

$$\text{COV} = \sqrt{\exp(\beta^2) - 1} \tag{A-2}$$

For β values less than about 0.5, this equation becomes approximately:

$$\text{COV} \approx \beta \tag{A-3}$$

and COV and β are often used interchangeably.

For a lognormal distribution the median value is used as the characteristic parameter of central tendency (50% of the values are above the median value and 50% are below the median value). The logarithmic standard deviation, β , or the coefficient of variation, COV, are used as a measure of the dispersion of the distribution.

The relationship between the median value, \check{x} , logarithmic standard deviation, β , and any value x of the random variable can be expressed as:

$$x = \check{x} \cdot \exp (f \cdot \beta) \quad (A-4)$$

where f is the standardized Gaussian random variable (mean zero, standard deviation one). Therefore, the probability that x is less than any value x' equals the probability that f is less than f' where:

$$f' = \frac{\ln (x' / \check{x})}{\beta} \quad (A-5)$$

Because f is a standardized Gaussian random variable one can simply enter standardized Gaussian tables to find the probability that f is less than f' which equals the probability that x is less than x' .

Using cumulative distribution tables for the standardized Gaussian random variable, it can be shown that $\check{x} \cdot \exp (+ \beta)$ of a lognormal distribution corresponds to the 84 percentile value, i.e., 84 percent of the data fall below the $+ \beta$ value. The $\check{x} \cdot \exp (- \beta)$ value corresponds to the value for which 16 percent of the data fall below.

One implication of the usage of the lognormal distribution is that if a , b , and c are independent lognormally distributed random variables, and if

$$d = \frac{a^r \cdot b^s}{c^t} \quad (A-6)$$

where r , s and t are given exponents, then d is also a lognormally distributed random variable. Further, the median value of d , denoted by \check{d} , and the logarithmic variance β_d^2 , which is the square of the logarithmic standard deviation, β_d , of d , are given by:

$$\check{d} = \frac{\check{a}^r \cdot \check{b}^s}{\check{c}^t} \quad (A-7)$$

and

$$\beta_d^2 = r^2 \beta_a^2 + s^2 \beta_b^2 + t^2 \beta_c^2 \quad (A-8)$$

where \check{a} , \check{b} , and \check{c} are the median values, and β_a , β_b , and β_c are the logarithmic standard deviations a, b, and c, respectively. The logarithmic standard deviation for each independent variable may be estimated as shown below for the variable a, from the estimated lower bound, median, and upper bound values given by a_l , a_m , and a_u respectively.

$$\beta_a \cong \frac{1}{2} \left[\ln \left(\frac{a_m}{a_l} \right) + \ln \left(\frac{a_u}{a_m} \right) \right] \quad (\text{A-9})$$

Note that if a is exactly lognormal,

$$\beta_a = \ln \left(\frac{a_m}{a_l} \right) = \ln \left(\frac{a_u}{a_m} \right) \quad (\text{A-10})$$

Given the estimated logarithmic standard deviation for each variable, it follows that the estimated one standard deviation upper and lower bound values of d, given by d_u and d_l , may be computed as

$$d_u = \check{d} \exp(\beta_d) \quad (\text{A-11})$$

$$d_l = \check{d} \exp(-\beta_d) \quad (\text{A-12})$$

The coefficient of variation of d is given by Eq. A-2 as

$$\text{COV}_d = \sqrt{\exp(\beta_d^2) - 1} \quad (\text{A-13})$$

1363 136

A.2 APPLICATION TO CAPACITY EVALUATION

The application of the statistical procedure described above to the evaluation of the structural system is demonstrated in the following discussion. From Equation 3-2, the median ground acceleration capacity, $(A_g)_m$, of a structural element may be computed as follows:

$$(A_g)_m = F_C / F_{SRSS,1g} \quad (A-14)$$

where

F_C = Median element force capacity

$F_{SRSS,1g}$ = Median element force response determined by square-root-sum-of-square (SRSS) combination of modal response components obtained from a modal spectral analysis of building models using median 1.0 g ground acceleration non-linear (reduced) response spectrum with median damping, β , and median ductility factor, μ .

The estimate of median element force response, may be expressed (Equation 3-1) as

$$F_{SRSS,1g} = \sqrt{\sum_n (F_{n,1g})^2} \quad (A-15)$$

1363 137

where $F_{n,1g}$ represent the modal components of element force response. Given that the modal component corresponding to the fundamental frequency (or period) of the structural system is 2 or 3 times the other modal response components, the fundamental component ($n = 1$) will account for 85-95% of the SRSS estimate given by Equation A-14. Thus, due to the dominance of the first mode, the median element force response may be considered to be approximately proportional to the spectral acceleration, SA_{1g} , given by the ordinate of the median response spectrum (normalized to 1.0g) associated with the fundamental frequency of the structural system. It should be noted that this approximation is also valid for element response governed by a mode other than the fundamental as long as the dominant modal component exceeds the remaining modal components by a factor of 2 or greater.

The variation in element force capacity, F_C , is considered to be independently a function of the variation in material strength and construction quality. The variation in element force response, F_{SRSS} , is considered to be independently a function of the structural idealization represented by the dynamic model and the spectral acceleration associated with the dominant modal frequency. The variability associated with the capability of the dynamic model to duplicate actual structural response due to earthquake ground motion is assessed by a subjective judgement factor. For simplicity, the variability of the spectral acceleration is considered to be independently a function of the variation in the spectral response ordinate, SA , due to the variation of input ground motion, the variation in system damping, β , and the variation in the value of spectral acceleration reduction factor, R , as influenced by the variation in system ductility factor, μ . The factor R is taken as unity for the ground acceleration portion of the response spectrum, $1/\sqrt{2\mu - 1}$ for the amplified acceleration spectral region and $1/\mu$ for the spectral velocity and spectral displacement regions. Thus, the ground acceleration capacity may be expressed as a function of the following variables centered on median values:

1363 138

$$A_g = \left(A_g \right)_m E_c W_c J / S_a C_B D_u \quad (A-16)$$

where

- E_c = Factor expressing the variation of element capacity as a function of the ratio of material strength to the median material strength governing the element failure mode (median value for $E_c = 1.0$).
- W_c = Subjective factor expressing the variation of element capacity as a function of construction quality and workmanship (median value for $W_c = 1.0$).
- S_a = Factor expressing the variation of spectral acceleration response due to the variance in ground motion input (given median system damping β , and median system ductility, μ) as a function of the ratio of response spectrum ordinate to the median response spectrum ordinate at the system frequency at the dominant mode. (Median value for $S_a = 1.0$).
- C_B = Factor expressing the variation of spectral acceleration response due to the variance in system damping (given median response spectra and median system ductility) as a function of the ratio of response spectrum ordinate to the median response spectrum ordinate at the dominant system frequency. (Median value for $C_B = 1.0$).

- D_{μ} = Factor expressing the variation of spectral acceleration response due to the variance in system ductility, characterized by the spectral reduction factor, as a function of the ratio of response spectrum ordinate to the median response spectrum ordinate at the dominant system frequency.
(Median value for $D_{\mu} = 1.0$).
- J = Subjective judgement factor expressing the variation of ground acceleration capacity as a function of the overall assessment of the procedure accuracy, element force capacity conservatism, and capability of the building dynamic model to duplicate actual structural response due to earthquake ground motion.
(Median value for $J = 1.0$).

The logarithmic variance in ground acceleration capacity may then be defined in terms of the logarithmic variance of each of the independent contributing random variables

$$\beta_{A_g}^2 = \beta_{T_c}^2 + \beta_{W_c}^2 + \beta_{S_a}^2 + \beta_{C_B}^2 + \beta_{D_{\mu}}^2 + \beta_J^2 \quad (A-17)$$

Thus, the upper and lower bound values for the seismic acceleration capacity may be computed as

$$\begin{aligned} (A_g)_u &= (A_g)_m \exp(\beta_{A_g}) \\ (A_g)_l &= (A_g)_m \exp(-\beta_{A_g}) \end{aligned} \quad (A-18)$$

A.3

UNCERTAINTY BOUND CONTRIBUTING FACTORS

This section provides the values assigned to the various factors utilized in the uncertainty bound analysis. The uncertainty bound analysis was performed utilizing the relations developed above with the values for the factors as given herein. The results are given in Section 3 of this report for the controlling elements/systems.

For each type of system analyzed with similar capacity analysis procedures, generally only one analysis for uncertainty bounds is required for systems with natural frequencies in the same region of the response spectra. These frequency regions are constant displacement ($f \leq 0.25$ Hz), constant velocity ($0.25 \leq f \leq 2.0$ Hz) amplified acceleration ($2.0 \leq f \leq 6.0$ Hz), transition region ($6.0 \leq f \leq 20.0$ Hz) and high frequency region ($f \geq 20.0$ Hz). For the transition region, the bounds are linearly interpolated between those calculated for the amplified acceleration region and those for the high frequency region. The effect of the variation in ground motion (variable S_a) and the effect of the variation in system damping (variable C_g) were assessed from the criteria spectra data presented in WASH 1255 (Reference 7). Table A-1, which was abstracted from Reference 7, presents the median (50 percentile) and the one standard deviation (84.1 percentile values of spectral amplification for various levels of damping and for the three major spectral frequency regions. The results of the determination of the variation in spectral acceleration response due to the independent variation input motion, damping, and ductility are tabulated in Table A-2(a) for the dynamic response of JN-1B steel frame ($f = 0.78$ Hz to 1.78 Hz) with the median values normalized to 1.0. Tables A-2(b), (c), and (d) give the results for the JN-4 facility at three different frequency regions.

1363 141

The variation of material strengths for each element failure mode which governs each major capacity estimate for the BMI facility is tabulated in Table A-3. It should be noted that for rigid body analyses, the capacity is not significantly affected by variations in strength. In the cracking analysis the variation of the modulus of rupture (MOR) is of small significance as the pre-compression due to dead load is the largest factor contributing to cracking capacity. In this case the small effect of variation in MOR is included in the overall analysis variation factor J for convenience. This is reflected in the element capacity factor presented in Table A-4(b). The resulting normalized contributing factors, as defined for Equation A-11, are tabulated in Tables A-4(a) and (b) for JN-1B and JN-4 facilities respectively.

Some further explanation is required for the values presented in Table A-4(b). For the rigid body capacity analyses, the reserve energy method was judged to give slightly unconservative results (Reference 29). This is because of the small differences between the theoretical model and the actual physical system. For example, vertical accelerations of the ground are not considered and the walls are generally not constructed perfectly plumb. (J)m, the analysis judgement factor, is thus taken as 0.95. All of the median value rigid body results summarized in Section 3 have been adjusted accordingly.

A.3.1 Example Calculation: JN-1B Roof Truss Capacity

The failure of the roof truss (shear failure of the bolted connection of the diagonal bracings) is controlled by the second mode of response (0.82 Hz) for north-south shaking. Referring to Table A-4(a), we obtain the estimates of the logarithmic standard deviation for each contributing factor.

Roof truss response

$$\beta_{S_a} = 0.215, \quad \beta_{C_B} = 0.135, \quad \beta_{D_{\mu}} = 0.498$$

Roof truss capacity

$$\beta_{E_c} = 0.295, \quad \beta_{W_c} = 0.$$

Analysis assessment

$$\beta_J = 0.164$$

POOR ORIGINAL

Now, utilizing Equation A-17 we obtain

$$\beta_{A_g}^2 = (0.215)^2 + (0.135)^2 + (0.498)^2 + (0.295)^2 + (0.164)^2 = 0.3484$$

$$\beta_{A_g} = 0.590$$

and from Equation A-18, the ground acceleration capacity is, given
 $(A_g)_m = 0.30,$

$$A_g = 0.30 \exp(\pm 0.590)$$

$$A_{g_u} = 0.54$$

$$A_{g_l} = 0.17$$

Using Equation A-13, we obtain the coefficient of variation for the ground acceleration capacity,

$$COV_{A_g} = \sqrt{\exp(0.3484) - 1} = 0.646$$

1363 143

TABLE A-1. HORIZONTAL DESIGN SPECTRA AMPLIFICATIONS AND BOUNDS

(Reference 17)

Percentile	Damping percent	Amplification			Faring frequency hertz	Spectrum bounds (alluvium)			Spectrum bounds (rock)		
		D	V	A		D	V	A	D	V	A
						In	in/sec	g	In	in/sec	g
50	0.5	1.97	2.58	3.67	40	71	124	3.67	24	72	3.67
	2.0	1.68	2.06	2.76	30	60	99	2.76	20	58	2.76
	5.0	1.40	1.66	2.11	20	50	80	2.11	17	46	2.11
	10.0	1.15	1.34	1.65	20	41	64	1.65	14	38	1.65
75	0.5	2.66	3.41	4.65	40	96	164	4.65	32	95	4.65
	2.0	2.24	2.68	3.36	30	81	129	3.36	27	75	3.36
	5.0	1.83	2.10	2.48	20	66	101	2.48	22	59	2.48
	10.0	1.47	1.66	1.89	20	53	80	1.89	18	46	1.89
84.1 (1 σ)	0.5	2.99	3.81	5.12	40	108	183	5.12	36	107	5.12
	2.0	2.51	2.98	3.65	30	90	143	3.65	30	83	3.65
	5.0	2.04	2.32	2.67	20	73	111	2.67	25	65	2.67
	10.0	1.62	1.81	2.01	20	58	87	2.01	19	51	2.01
90	0.5	3.28	4.16	5.53	40	118	200	5.53	39	116	5.53
	2.0	2.74	3.23	3.90	30	99	155	3.90	33	90	3.90
	5.0	2.21	2.51	2.82	20	80	120	2.82	27	70	2.82
	10.0	1.75	1.94	2.11	20	63	93	2.11	21	54	2.11
95	0.5	3.65	4.60	6.05	40	131	220	6.05	44	129	6.05
	2.0	3.04	3.57	4.22	30	109	171	4.22	36	100	4.22
	5.0	2.44	2.75	3.03	20	88	132	3.03	29	77	3.03
	10.0	1.91	2.11	2.24	20	69	101	2.24	23	59	2.24
97.7 (2 σ)	0.5	4.01	5.04	6.57	40	144	242	6.57	48	141	6.57
	2.0	3.34	3.89	4.54	30	120	187	4.54	40	109	4.54
	5.0	2.67	2.98	3.23	20	96	143	3.23	32	83	3.23
	10.0	2.08	2.28	2.37	20	75	109	2.37	25	64	2.37

Ground motions	a, g	v, in/sec	d, in
alluvium	1.0	48	36
rock	1.0	28	12

TABLE A-2(a) SPECTRAL ACCELERATION RESPONSE VARIATION -
JN-1B HOT CELL FACILITY

Contributing Variable	Contributing Variable Values		
	Lower	Median	Upper
Spectral Response Input Variation ($f = 0.41 \sim 1.78$ Hz), $\beta = 15\%$, $\mu = 2.5$)	—	1.0	1.24
System Damping (β , percent of critical)	10%	15%	22%
Spectral Response Damping Variation ($f = 0.41 \sim 1.78$ Hz, Median Spectra, $\mu = 2.5$)	0.84	1.0	1.10
System Ductility (μ)	1.5	2.5	4.0
Spectral Reduction Factor ($R = 1/\mu$)	0.25	0.4	0.67
Spectral Response Ductility Variation ($f = 0.41 \sim 1.78$ Hz, Median Spectra, $\beta = 15\%$)	0.62	1.0	1.68

1363 145

TABLE A-2(b) SPECTRAL ACCELERATION RESPONSE VARIATION -
JN-4 PLUTONIUM LAB

Contributing Variable	Contributing Variable Values		
	Lower	Median	Upper
Spectral Response Input Variation ($0.25 \leq f \leq 2.0$, $\beta = 10\%$, $\mu = 1.0$)	—	1.0	1.4
System Damping (β , Percent of Critical)	7%	10%	14%
Spectral Response Damping Variation ($0.25 \leq f \leq 2.0$, Median Spectral, $\mu = 1.0$)	0.9	1.0	1.15

1363 146

TABLE A-2(c) SPECTRAL ACCELERATION RESPONSE VARIATION -
 JN-4 PLUTONIUM LAB

Contributing Variable	Contributing Variable Values		
	Lower	Median	Upper
Spectral Response Input Variation ($2.0 \leq f \leq 6.0$, $\beta = 10\%$, $\mu = 1.0$)	—	1.0	1.22
System Damping (β , Percent of Critical)	7%	10%	14%
Spectral Response Damping Variation ($2.0 \leq f \leq 6.0$, Median Spectral, $\mu = 1.0$)	0.88	1.0	1.12

1363 147

TABLE A-2(d) SPECTRAL ACCELERATION RESPONSE VARIATION -
 JN-4 PLUTONIUM LAB

Contributing Variable	Contributing Variable Values		
	Lower	Median	Upper
Spectral Response Input Variation ($f \geq 20.0$, $\beta = 10\%$, $\mu = 1.0$)	1.0	1.0	1.0
System Damping (β , Percent of Critical)	7%	10%	14%
Spectral Response Damping Variation ($f \geq 20.0$, Median Spectral, $\mu = 1.0$)	1.0	1.0	1.0

1363 148

TABLE A-3. ELEMENT MATERIAL STRENGTH VARIATION - JN-1B
HOT CELL FACILITY (REFERENCE 4)

Contributing Variable	Contributing Variable Values		
	Lower	Median	Upper
Steel Diagonal Member Buckling (A 36 Yield Strength)	40 ksi	44 ksi	48.5 ksi
Steel Member Connection Shear Capacity (A307 Ultimate Tension)	64 ksi	68 ksi	73 ksi

1363 149

TABLE A-4(a). UNCERTAINTY BOUND STATISTICAL PARAMETERS - JN-1B
HOT CELL FACILITY

Contributing Factor		Contributing Factor Values			Estimated Standard Deviation
		Lower	Median	Upper	
Spectral Response Input	S_a , $f = 0.78 \sim 1.78$ Hz	—	1.0	1.24	0.215
Spectral Response Damping	C_B , $f = 0.78 \sim 1.78$ Hz	0.84	1.0	1.10	0.135
Spectral Response Ductility	D_μ , $f = 0.78 \sim 1.78$ Hz	0.62	1.0	1.68	0.498
Element Capacity	E_C (Steel Column)	0.91	1.0	1.10	0.095
	E_C (A307 Bolts)	0.94	1.0	1.07	0.065
Construction Quality and Workmanship	W_C (Steel)	1.0	1.0	1.0	0.0
Analysis Judgement	J	0.85	1.0	1.18	0.164

A-18

1363 150

TABLE A-4(b). UNCERTAINTY BOUND STATISTICAL PARAMETERS -
JN-4 PLUTONIUM LAB

Contributing Factor			Contributing Factor Values			Estimated Standard Deviation
			Lower	Median	Upper	
Spectral Response Input	S_a	$0.25 \leq f \leq 2.0$	—	1.0	1.4	0.336
		$2.0 \leq f \leq 6.0$	—	1.0	1.22	0.199
		$f \geq 20.0$	—	1.0	1.0	0.0
Spectral Response Damping	C_B	$0.25 \leq f \leq 2.0$	0.9	1.0	1.15	0.123
		$2.0 \leq f \leq 6.0$	0.88	1.0	1.12	0.121
		$f \geq 20.0$	1.0	1.0	1.0	0.0
Element Capacity		E_c	1.0	1.0	1.0	0.0
Analysis Judgement		Rigid Body Rocking	0.80	0.95	1.15	0.181
		Elastic Cracking	0.85	1.0	1.18	0.164

A-19

1363 151

APPENDIX B

DETERMINATION OF CHANNEL SLAB SLIPPAGE
DURING JN-4 RIGID BODY ROCKING

1363 152

APPENDIX B

DETERMINATION OF CHANNEL SLAB SLIPPAGE DURING JN-4 RIGID BODY ROCKING

The slipping of the precast channel slabs relative to the steel beams is an important phenomenon when studying the rigid body rocking response and ultimate collapse capacity of the JN-4 facility. All the precast channel slabs are oriented in the same manner throughout the building (Figure B-1). Therefore, it is sufficient to examine two independent ground motions in studying the rigid body rocking response of the structure.

A. EAST-WEST GROUND MOTION

The rigid body rocking motion of the JN-4 facility for East-West (E-W) ground excitation is shown in Figure B-2. Calculations have shown that under E-W excitation the unreinforced masonry piers located along column lines 6 and 8 (Figure B-2) will interact with the steel framing. Thus the piers in effect act as shear walls and provide resistance against rigid body rocking of the Main Laboratory building.

Along column line 7 however, restraint of the steel framing is minimal. As the lateral loading at the roof level increases, the steel framing will begin to rock with maximum deflection along column line 7 (Figure B-2), and the roof beams will form plastic hinges at the connections. This rigid body rocking motion is resisted in the roof by the couples the channel slabs exert on the steel framing (Figures B-5 to B-17) and by the restoring effects developed by the vertical roof load on the steel columns. The couple action of the channel slabs on the steel

1363 153

framing was examined in some detail since the magnitudes of the forces created are not always obvious.

Figure B-3 shows a typical channel slab resting on a pair of 16W36 beams. The precast channel slabs have typical dimensions of 2-inches-thick by 2-feet-wide by 12-feet-long. A six-inch flange is located along both the 12-foot-long edges (Figure B-4). Figure B-3 idealizes the centerline of the North Bay as having no shear resistance. The ends of the steel wide flanges above unreinforced masonry walls are assumed to be pin-ended to simulate the plastic hinge.

A free-body diagram of a typical channel slab is shown in Figure B-5. If one slab on the steel framing is loaded laterally as shown in Figure B-3, a statically determinate system results. Reactions R_1 and R_3 depend on the distance L the slab is located from the shear wall.

However, if two or more channel slabs are on the steel beam and an equal inertia load is applied to all the channel slabs, a different force distribution results. Because the problem is now statically indeterminate, forces in both the beams and channel slabs depend on their relative stiffness. A finite element model was run for a series of channel slabs connected to two 16W36 beams. The beams were modeled by finite element beams and the channel slabs by plane stress membrane elements (Figure B-6). The results of the computer program showed that, as expected, all the shear loading is carried by the channel slabs. Only negligible shear stresses and bending moments occurred in the beams. In effect, all the lateral loading on an individual channel slab reacts directly along the edge of the channel slab located the closest to the shear wall. The resulting force distribution is shown in Figure B-7.

1363 154

For slip to occur along the left edge of the channel slab, assume $S_1, S_2 = 0$.

$$\sum F_y = 2\left(\frac{1}{4}\mu N\right)$$

$$14F = 2\left(\frac{1}{4}\mu N\right)$$

$$\therefore F = \frac{1}{28}\mu N$$

This slip pattern is only valid if the slab is not slipping at corner 3. A check of the maximum force shows that:

$$S_3 = 2.25 F$$

$$V_3 = \overline{S_3} + \overline{6.5 F} = \sqrt{2.25^2 + 6.5^2} F$$

$$V_3 = 6.88 F$$

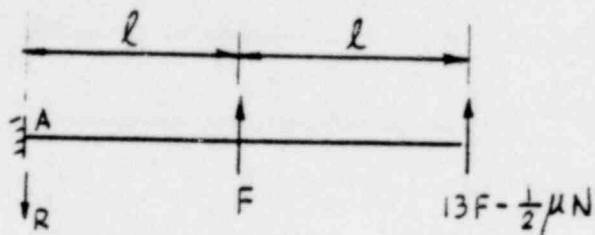
If $V_3 < 7F$ no slip occurs.

\therefore no slip occurs at corners 3 or 4 as corners 1 and 2 slip.

1363 155

Figure B-11 examines the same row of channel slabs an instant later. The forces shown on the diagram are the ones that must exist in order for both the exterior channel slab and the next slab inward to slip.

Net resultants



$$\Sigma M_A = 0$$

$$Fl + 2l(13F - \frac{1}{2}\mu N) = 0$$

$$F = \frac{1}{27}\mu N$$

$$\Sigma F_y @ A = 0$$

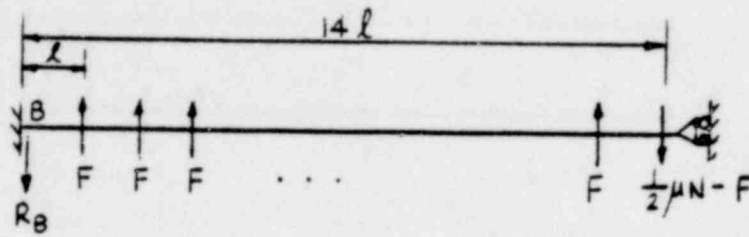
$$R = F + 13F - \frac{1}{2}\mu N$$

$$= 14(\frac{1}{27}\mu N) - \frac{1}{2}\mu N$$

$R = .0185\mu N$ — Reaction of steel beam on shear wall as first and second slabs slip.

1363 156

Figure B-12 re-examines the channel slabs at the instant when all the slabs across the bay slip. An idealization is shown below:



$$\sum M_B = 0$$

$$Fl + F \cdot 2l + \dots + F \cdot 14l - 14l \left(\frac{1}{2} \mu N \right) = 0$$

$$F \sum (1 + 2 + 3 + \dots + 14) = 7 \mu N$$

$$105 F = 7 \mu N$$

$$F = \frac{7}{105} \mu N$$

$$\sum F_y @ B = 0$$

$$14F - \frac{1}{2} \mu N - R_B = 0$$

$$R_B = 14 \left(\frac{7}{105} \right) \mu N - .5 \mu N$$

$$R_B = .433 \mu N$$

1363 157

POOR ORIGINAL

When considering the rigid body rocking model for the whole Main Laboratory an equivalent force at the bay centerline is required to account for the resistance of the channel slab-steel frame system.

$$F_T = H \cdot S \cdot F = H \cdot S \left(\frac{7}{105} \right) \mu N$$

S = number of symmetric sides of the bay = 2

F = force required to slip one row of channel slabs

μ = coefficient of friction = .6

N = total normal force for a row of channel slabs extending along the whole bay

H = one half the number of channel slabs per side = 7

$$F_T = 2 \left(\frac{7}{105} \right) (.6) (84.5) (2) (39.1) (7) = 3700 \text{ lbs.}$$

An equivalent constant force of 3700 lb. must be applied to the rigid body rocking model in the E-W direction to account for couple action of the channel slabs.

1363 158

B. NORTH-SOUTH GROUND MOTION

The critical portion of the JN-4 facility which was analyzed for N-S ground excitation is shown in Figure B-13. This particular portion of the building fails in a rigid body rocking mode because of the relatively low shear capacity of column line F as compared to much higher capacities of adjacent column lines Ea and G. Figure B-1 shows the orientation of channel slabs across the bay. Once again it is important to examine how a single channel slab slips under lateral loading in order to determine the action of the entire bay.

Figure B-14 shows a typical pair of channel slabs resting on steel beams (1/2 of the bay considered). The shear wall is again idealized as a fixed support with the centerline of the bay represented as a roller. A free-body diagram of the channel slab labeled 1 in Figure B-14 is shown in Figure B-15. In addition to the lateral inertia force in the y-direction, the only external force considered to be acting on the slab is due to the inertial load of the slabs own weight. An additional external load due to slab 2 (Figure B-14) will be considered later.

In order to correctly interpret the force distribution explained in the following paragraph, simultaneous consideration of both Figure B-14 and Figure B-15 is required. Assume an inertial load is applied to channel slab 1 in the positive y direction. The load initially attempts to distribute equally to all four corners of the channel slab. However, all of the load due to reactions R_3 and R_4 which is applied to beam B must react at shear wall I. The only possible load path for reactions R_3 and R_4 is due to the stiffness of beams A and C in out-of-plane bending. The W16 x 36 beams are very flexible when loaded out-of-plane since plastic hinges form at low response levels. This means that the total reaction, R_3 and R_4 required to deflect the beams enough so that the channel slab essentially has no restraint along its right edge, is a very small fraction of the total inertia load. The channel slabs are essentially rigid and non-deformable when compared to the beams.

1363 159

Therefore for the purposes of the following calculations, reactions R_3 and R_4 are assumed to be zero. Figure B-16 shows a new free-body diagram where a support is also assumed at point 3. This support models the condition that the channel slabs are restrained from sliding in the positive x direction because of bearing on adjacent channel slabs. Consideration of the deformation conditions which occur as rigid body rocking begins shows that the channel slab must slip at three corners simultaneously. Slip occurs at any particular corner when the vector sum of the forces at the corner equals $1/4\mu N$. Through the use of Figure B-16 and knowing corners 1, 2, and 4 slip simultaneously the following relationships can be shown.

$$\sum F_y = 0$$

$$R_1 + R_2 = F, \text{ Assume } R_1 = R_2$$

$$\therefore R_1 = \frac{F}{2}$$

$$\sum M_3 = 0$$

$$F \frac{l_2}{2} - 2R_1(l_2) + S_1 l_1 + S_2 l_1 = 0$$

$$S_1 = \frac{F l_2}{2 l_1} - S_2$$

For slip to occur at corner 4

$$S_2 = \frac{1}{4} \mu N$$

Slip at corner 1 occurs when :

$$\sqrt{S_1^2 + R_1^2} = \frac{1}{4} \mu N$$

$$\left(\frac{F l_2}{2 l_1} - \frac{1}{4} \mu N \right)^2 + \frac{F^2}{4} = \left(\frac{1}{4} \mu N \right)^2$$

$$F = .1622 \mu N$$

1363 160

The vector sum at corner 2 is the same magnitude as corner 1 but the direction it points is different.

Back substituting:

$$S_1 = \left(\frac{.1622(12)}{2(2)} - .25 \right) \mu N$$

$$S_1 = .2366 \mu N$$

The force required to cause a row of channel slabs across one-half of the bay is now easily calculated.

$$\Sigma M_A = 0$$

$$6F + 18F - 2(2S_2) - 2(2S_1) = 0$$

$$24F - 4(.2366 \mu N) - 4(.25 \mu N) = 0$$

$$F = .0811 \mu N$$

The total force required to cause all the slabs in the bay to slip is:

$$F_T = 2(.0811) \mu N (28)$$

$$= 2(28)(.6)(.0811)(2)(12)(39.1)$$

$$F_T = 2560 \text{ lbs.}$$

This force, F_T , is applied as an equivalent point load when calculating the failure of the roof using a rigid body rocking model.

C. CONSIDERATION OF SIMULTANEOUS HORIZONTAL COMPONENTS OF GROUND MOTION INPUT ON THE COUPLE ACTION OF THE ROOF CHANNEL SLABS

The effect of the simultaneous horizontal acceleration component equal to 0.4 times the principal input on the restraint capability developed by the channel roof slabs was not treated in an exact manner. The force distribution developed in the roof system is statically indeterminate. Once slipping starts, there is significant shift in the frequencies of predominant response of the structure with corresponding change in the response amplification in the principal directions. Thus, although the ground motion input components are assumed to remain at a fixed ratio of 0.4 to 1.0 with increasing levels of acceleration, the response ratios in the slab are continuously varying; not only with shift but continuously on a time history basis.

Rather than solve this highly indeterminate system on a time history basis for a number of acceleration levels with the iterations required at each level necessary to account for the amplification changes, an approximate method of accounting for the reduction in the allowable lateral load of the roof was adopted. The method adopted was to solve for the force distribution in the roof for the assumed 1.0 direction input component. The 0.4 component was then added assuming the same response ratio as the ground acceleration components.

The forces at all corners of the channel slab were then examined to see if the maximum permissible force, $1/4\mu N$, was exceeded. If this maximum force was exceeded, then a reduction factor for the slab was calculated to bring the slab back into equilibrium.

Using Figure 19 for a typical critical slab

Examine corner 2

$$(.25 + .47)\mu N > .25\mu N$$

Calculate a reduction factor

$$[.047x + .25x]\mu N = .25\mu N$$

$$x = \frac{.25}{.297} = .842$$

∴ Reduce all values by approximately 16 %.

Figure B-20 shows the corrected force distribution on the slab. Note that the vector sum for any corner is less than or equal to $1/4\mu N$. In view of the relatively small reduction in capacity based on this approximation, especially in view of other uncertainties connected with this part of the analysis such as the coefficient of friction and even the basic assumption of the 0.4 to 1.0 ratio of the input, it was considered unnecessary to refine this approach further.

1363 163

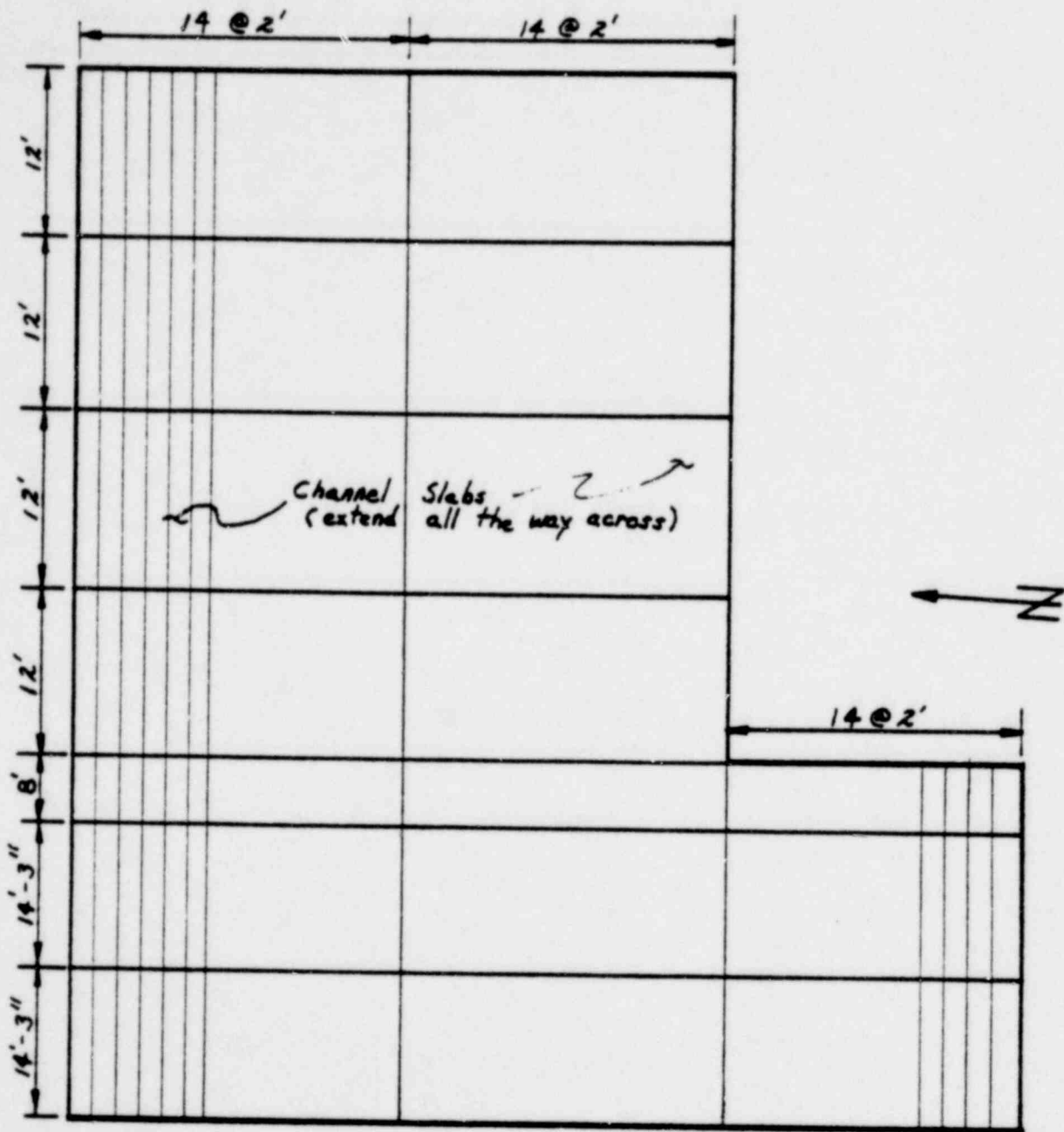


FIGURE B-1. CHANNEL SLAB ORIENTATION IN THE JN-4 BUILDING

1363 164

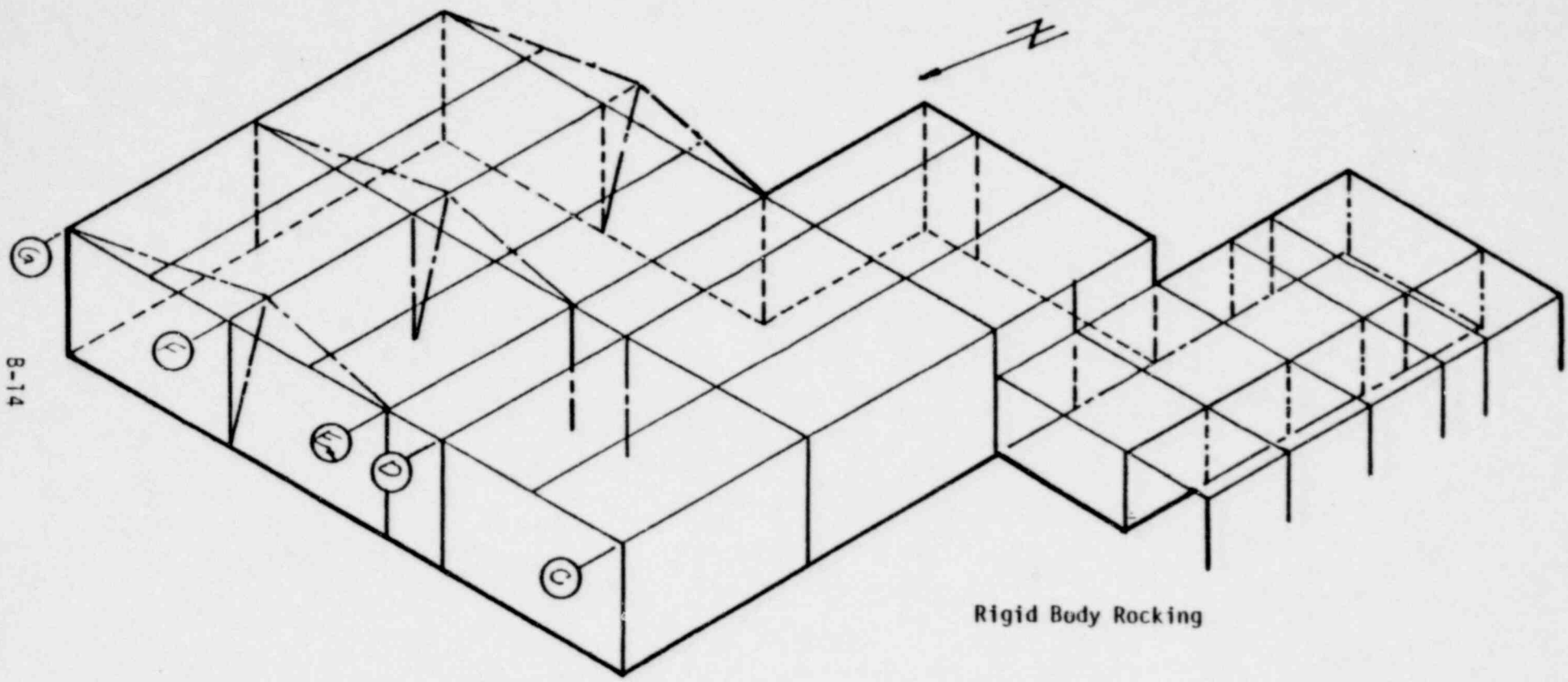


FIGURE B-2. RIGID BODY ROCKING - E-W EXCITATION

1363 165

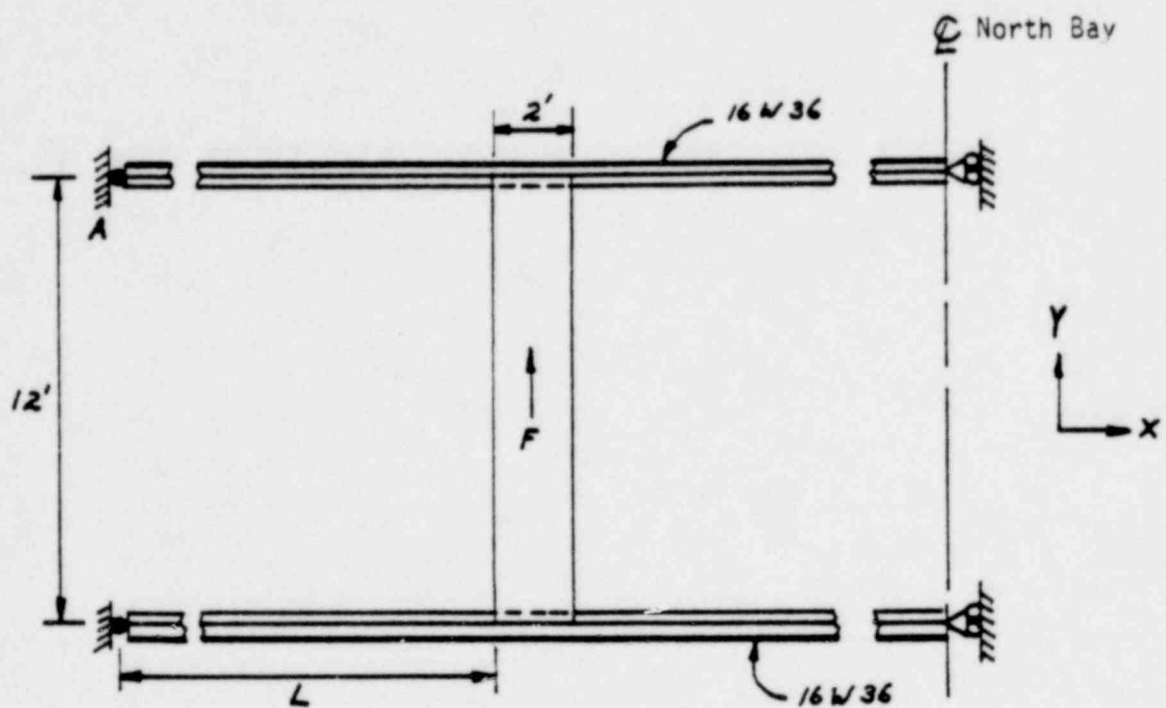


FIGURE B-3. SINGLE CHANNEL SLAB ON THE STEEL FRAMING

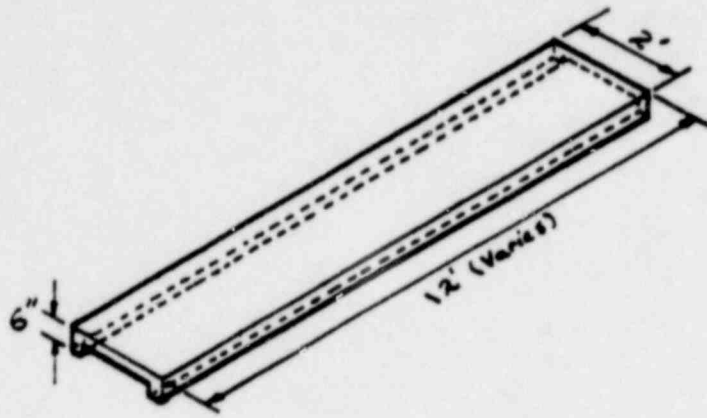


FIGURE B-4. TYPICAL CHANNEL SLAB

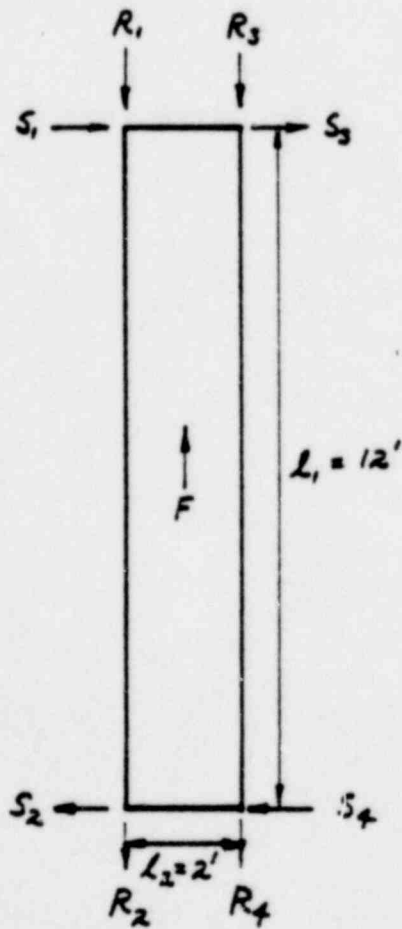


FIGURE B-5. CHANNEL SLAB FREE-BODY DIAGRAM

1363 167

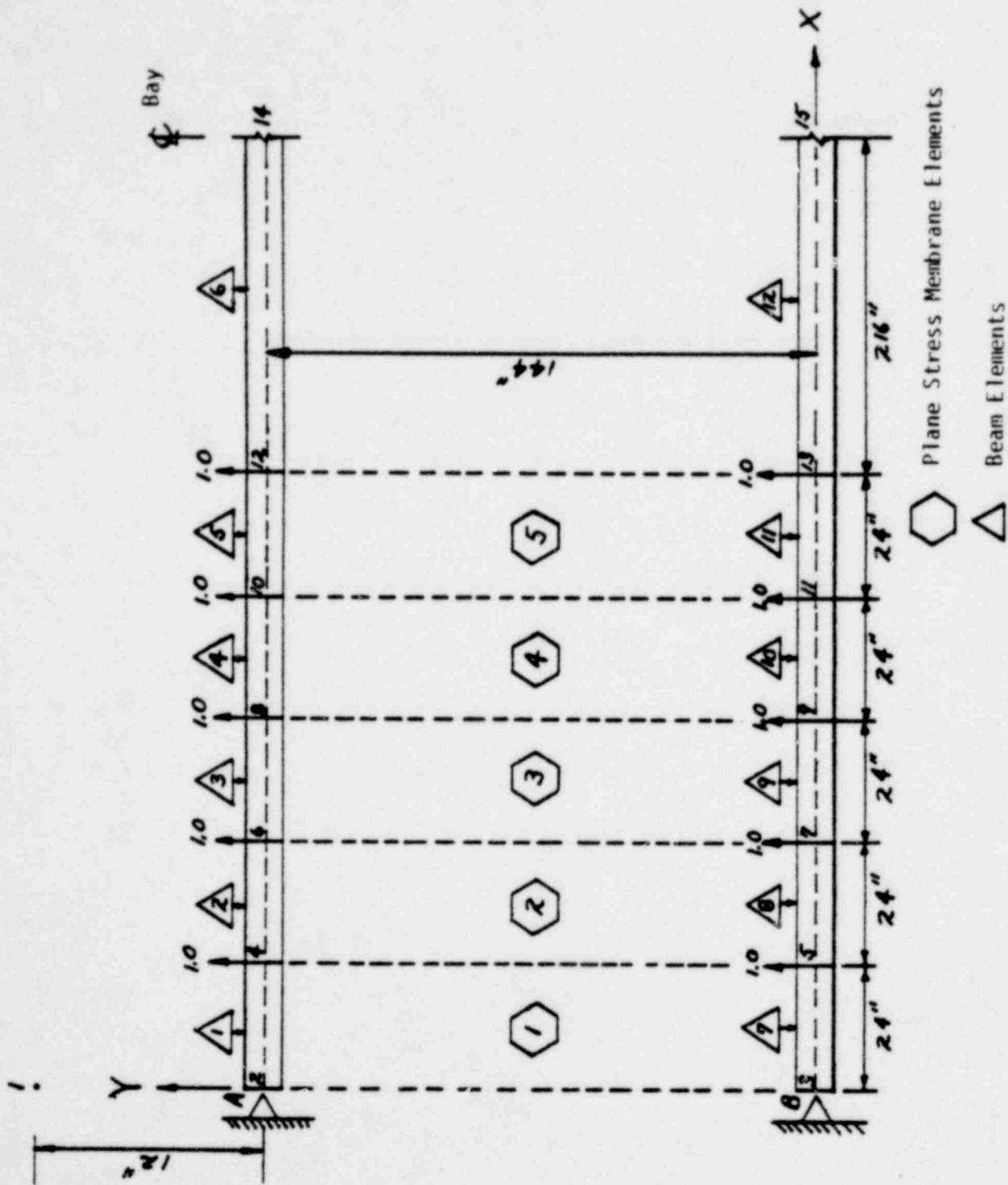


FIGURE B-6. FINITE ELEMENT MODEL OF TYPICAL ROOF SECTION

1363 168

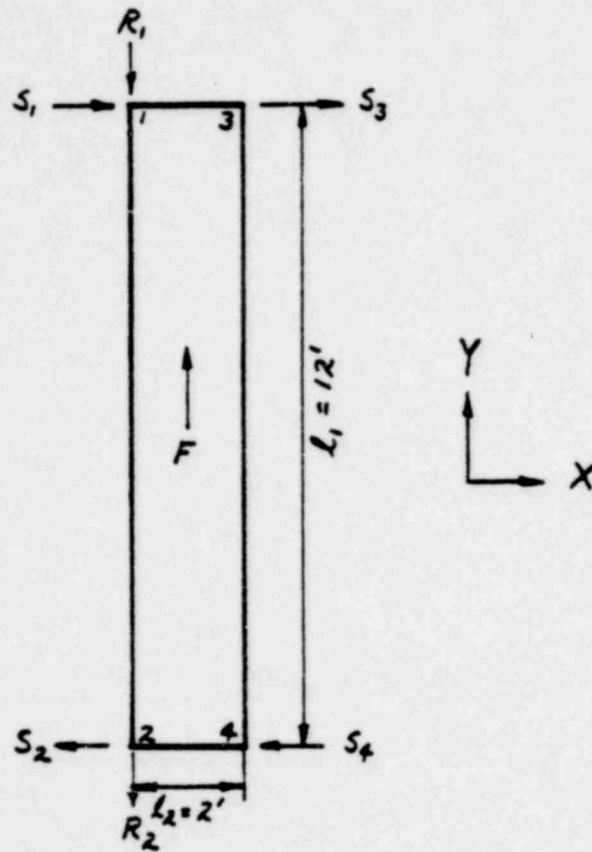


FIGURE B-7. ACTUAL FORCE DISTRIBUTION ON THE CHANNEL SLABS

1363 169

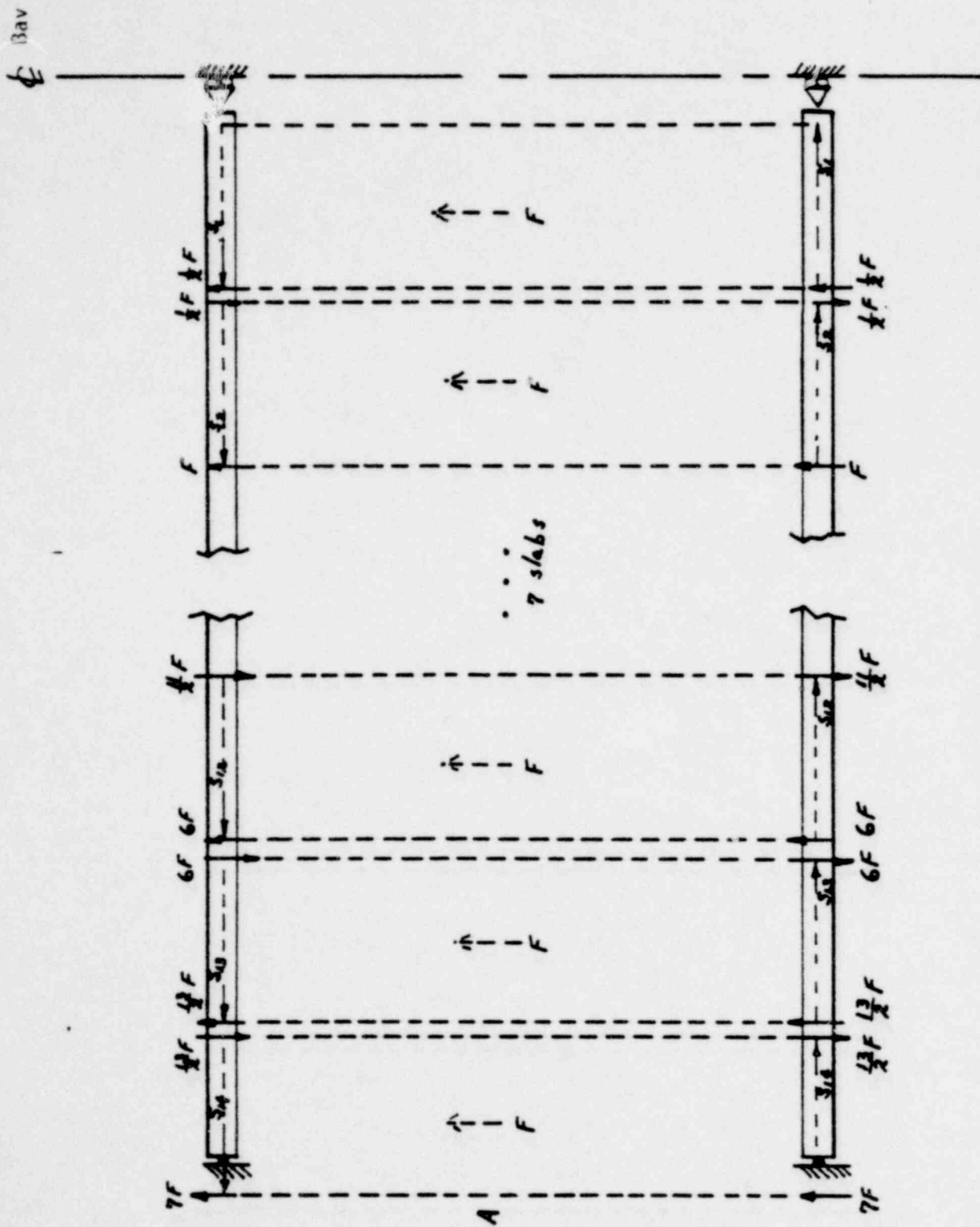


FIGURE B-8. CHANNEL SLAB FORCES ON THE BEAMS

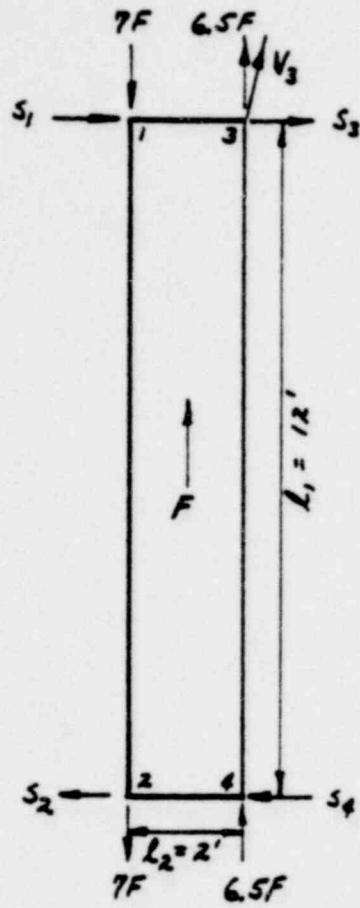


FIGURE B-9. FREE-BODY DIAGRAM OF THE EXTERIOR CHANNEL SLAB

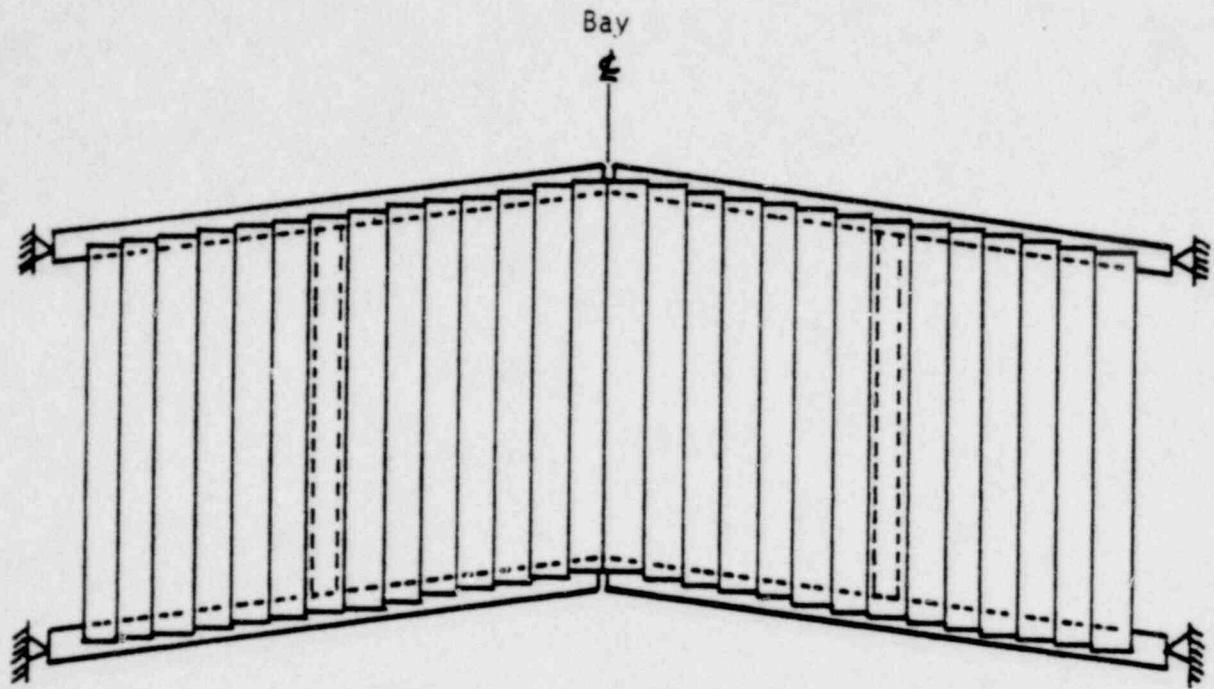


FIGURE B-10. SLIPPAGE OF ALL CHANNEL SLABS DURING RIGID BODY ROCKING OF THE STEEL FRAME

1363 172

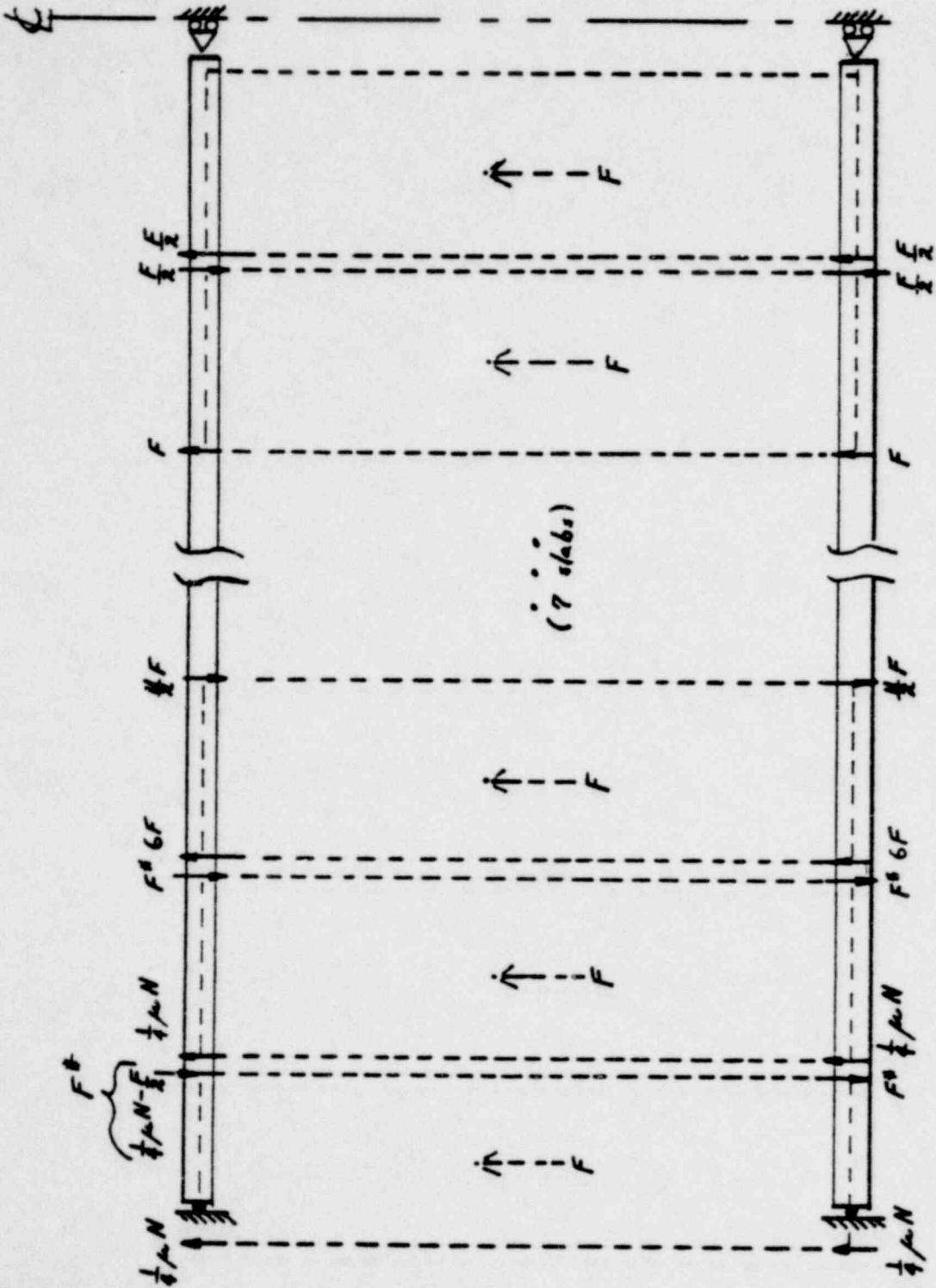


FIGURE B-11. FORCE DISTRIBUTION AS THE TWO MOST EXTERIOR CHANNEL SLABS SLIP RELATIVE TO THE STEEL FRAMING.

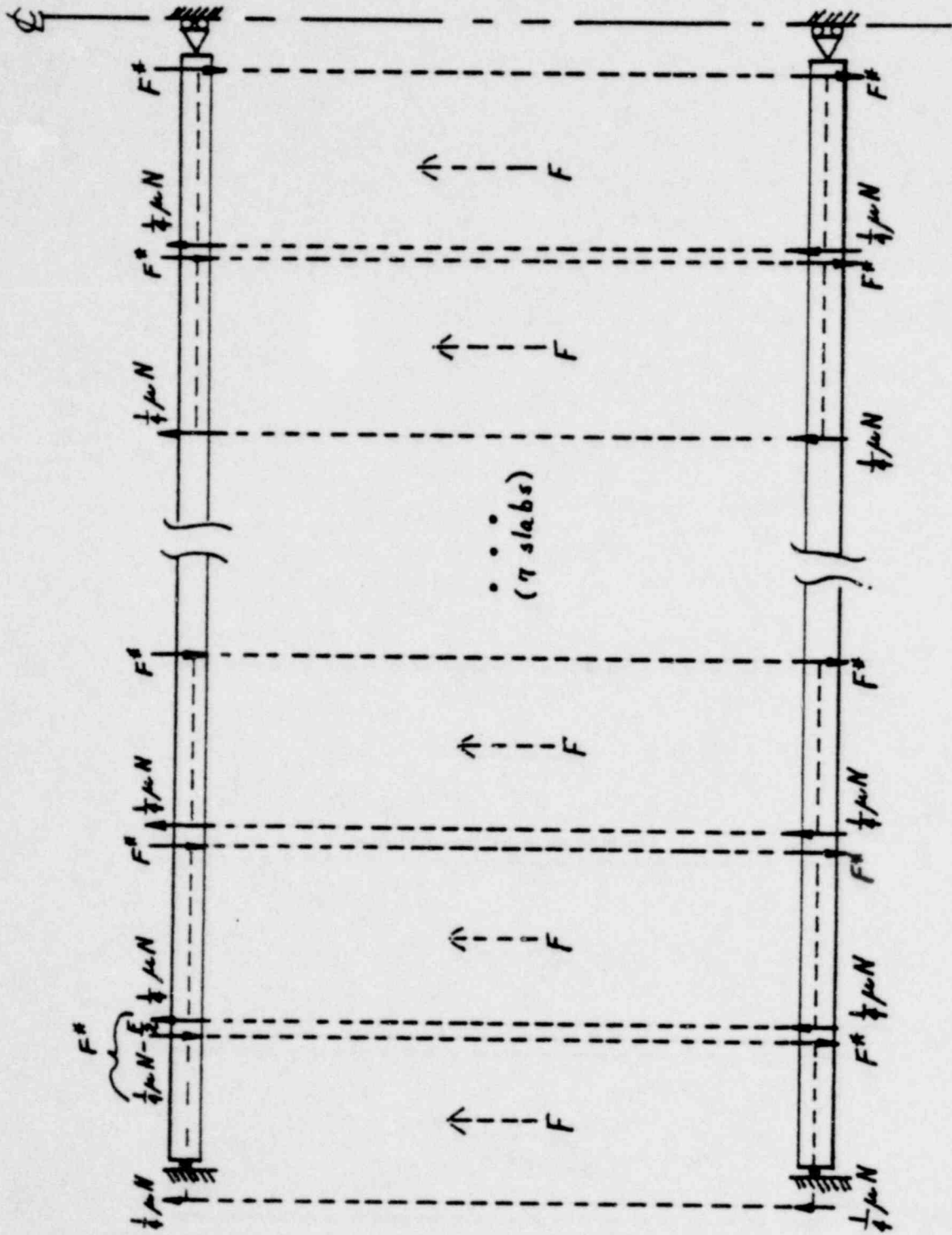
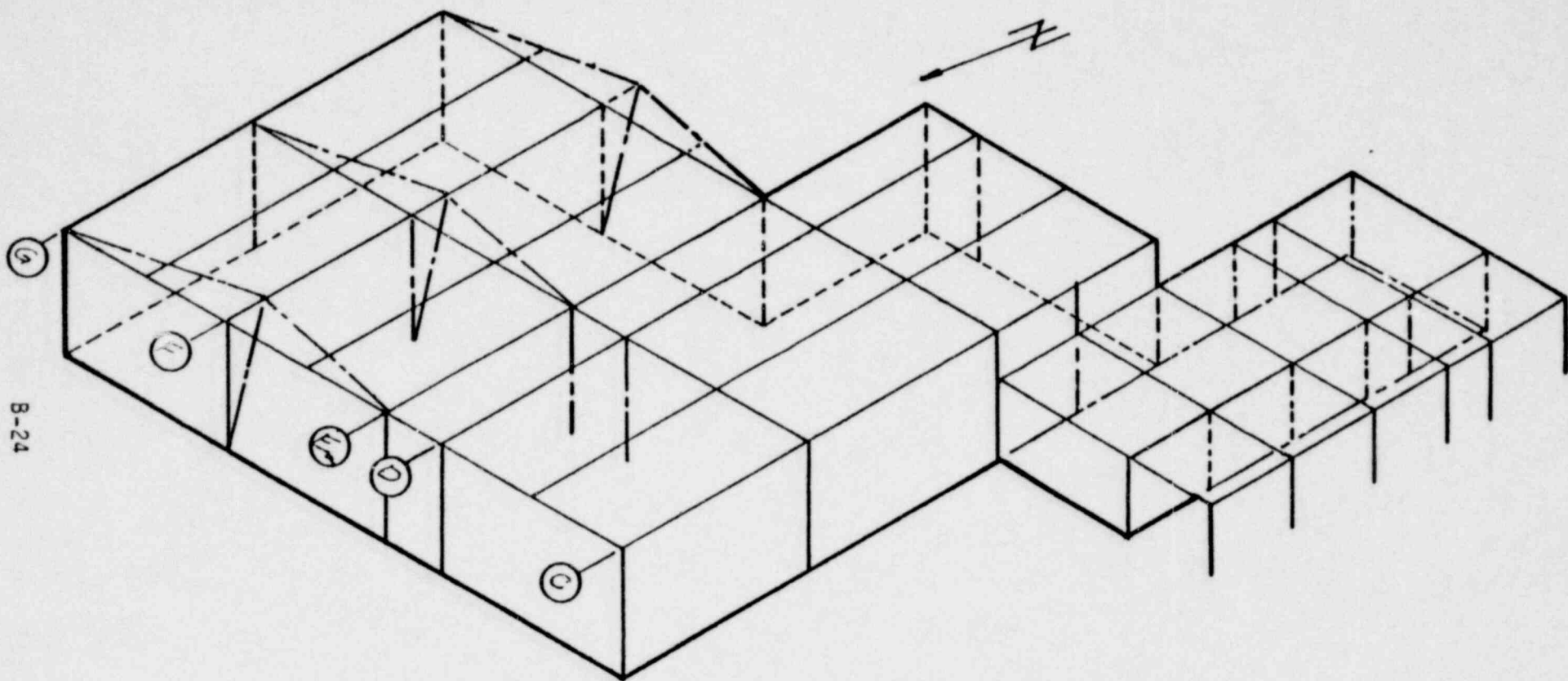


FIGURE B-12. FORCE DISTRIBUTION AS ALL CHANNEL SLABS SLIP RELATIVE TO THE STEEL FRAMING



B-24

1363 175

FIGURE B-13. RIGID BODY ROCKING OF THE JN-4 FOR N-S EXCITATION

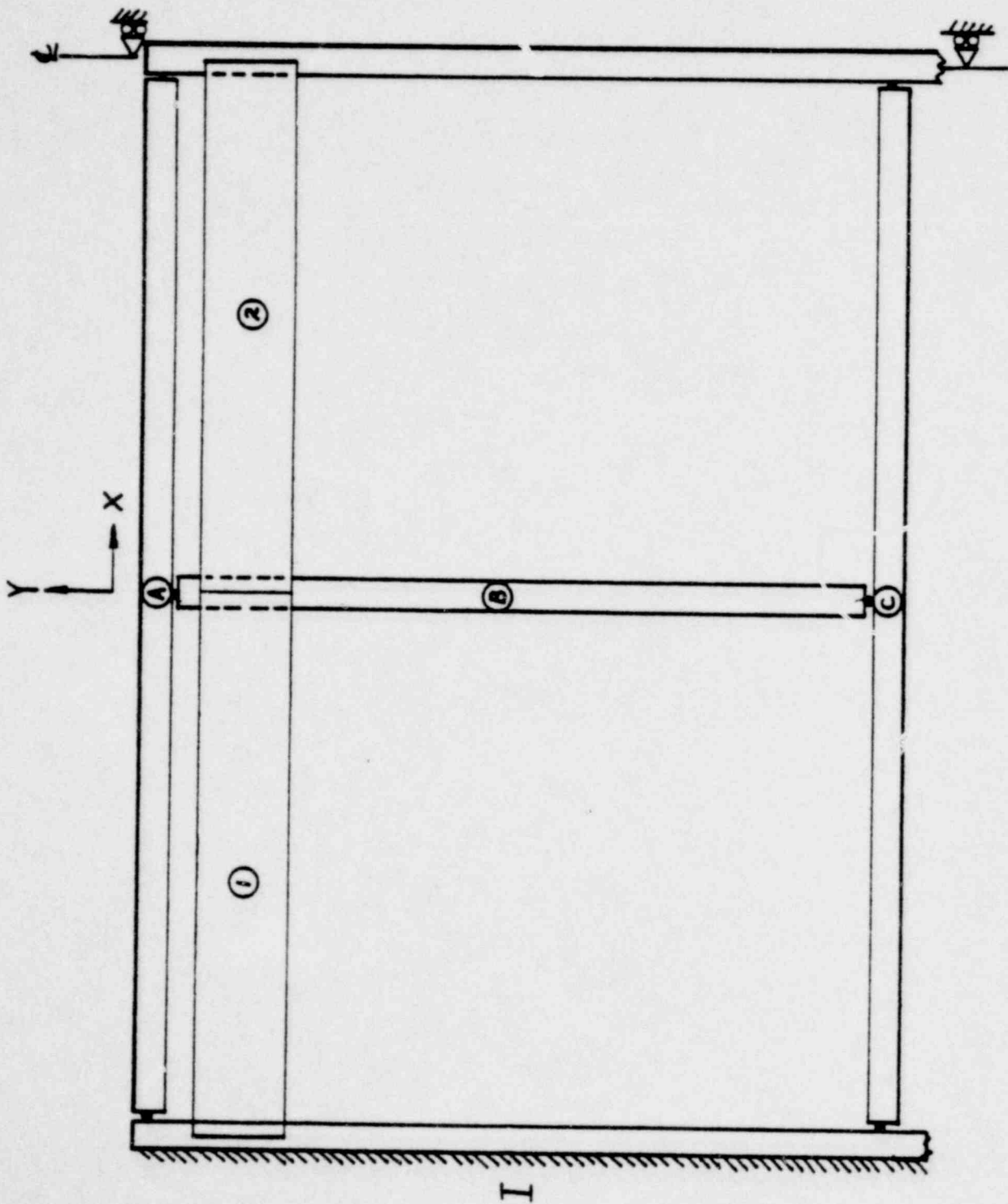


FIGURE B-14. ORIENTATION OF TWO TYPICAL CHANNEL SLABS

1363 176

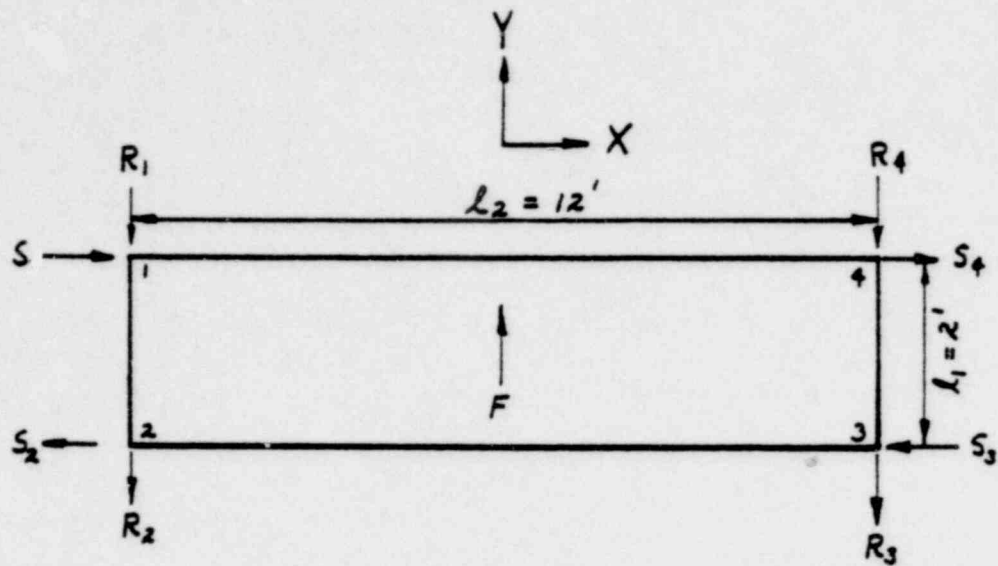


FIGURE B-15. ASSUMED FORCE DISTRIBUTION ON ROOF CHANNEL SLABS

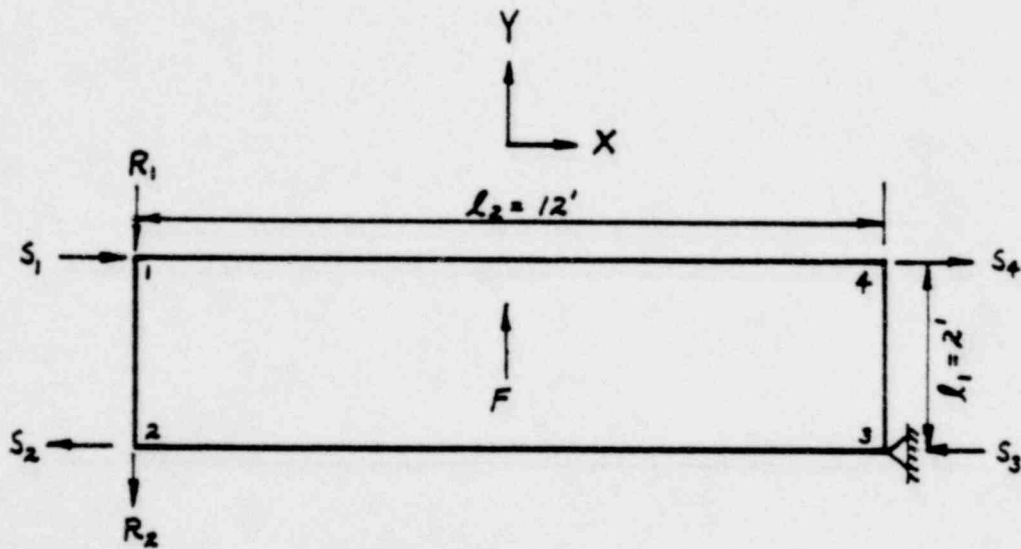


FIGURE B-16. ACTUAL FORCE DISTRIBUTION ON ROOF CHANNEL SLABS

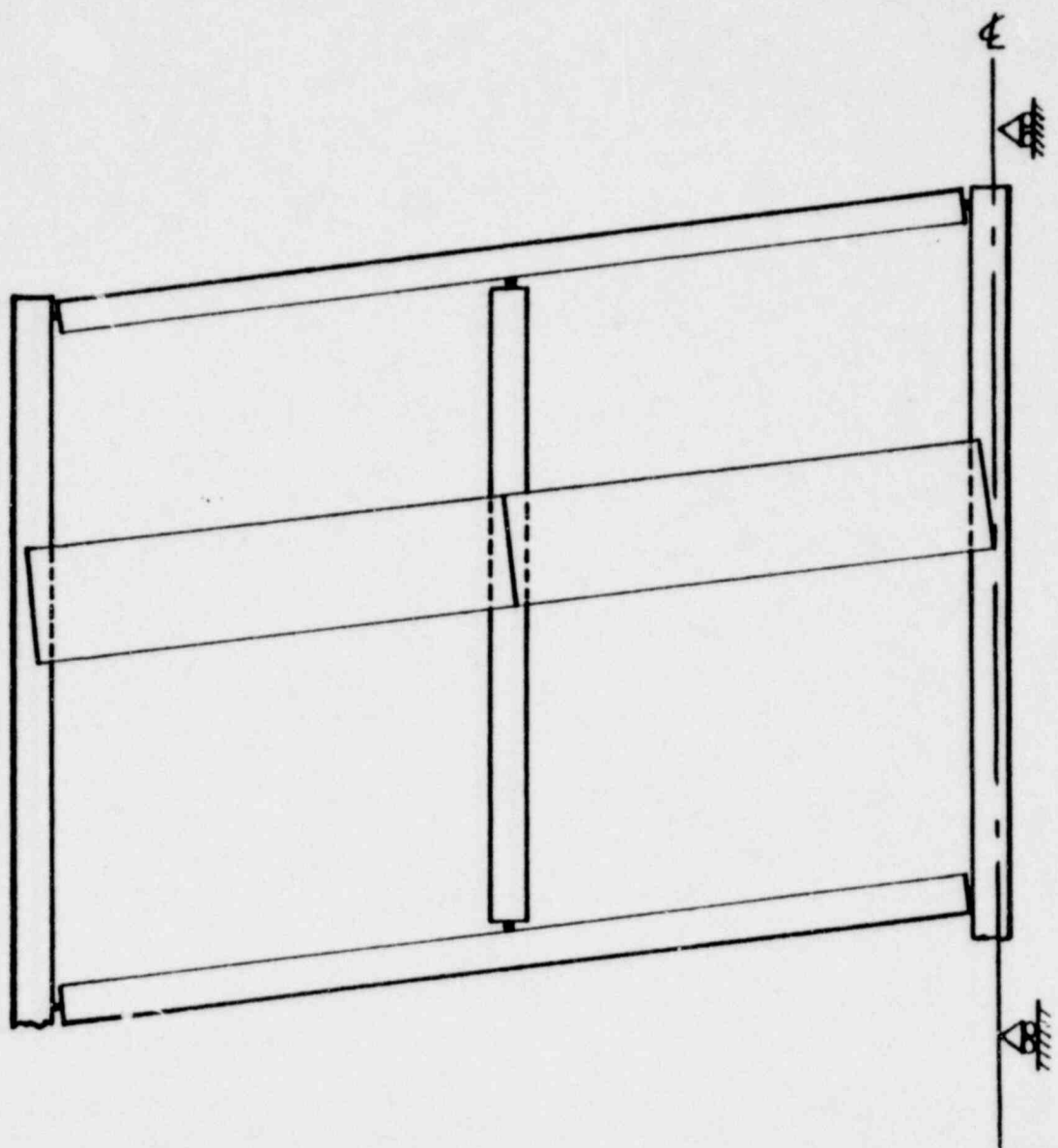


FIGURE B-17. ORIENTATION OF CHANNEL SLABS AS SLIPPAGE OCCURS RELATIVE TO THE STEEL FRAMING

B-27

1363 178

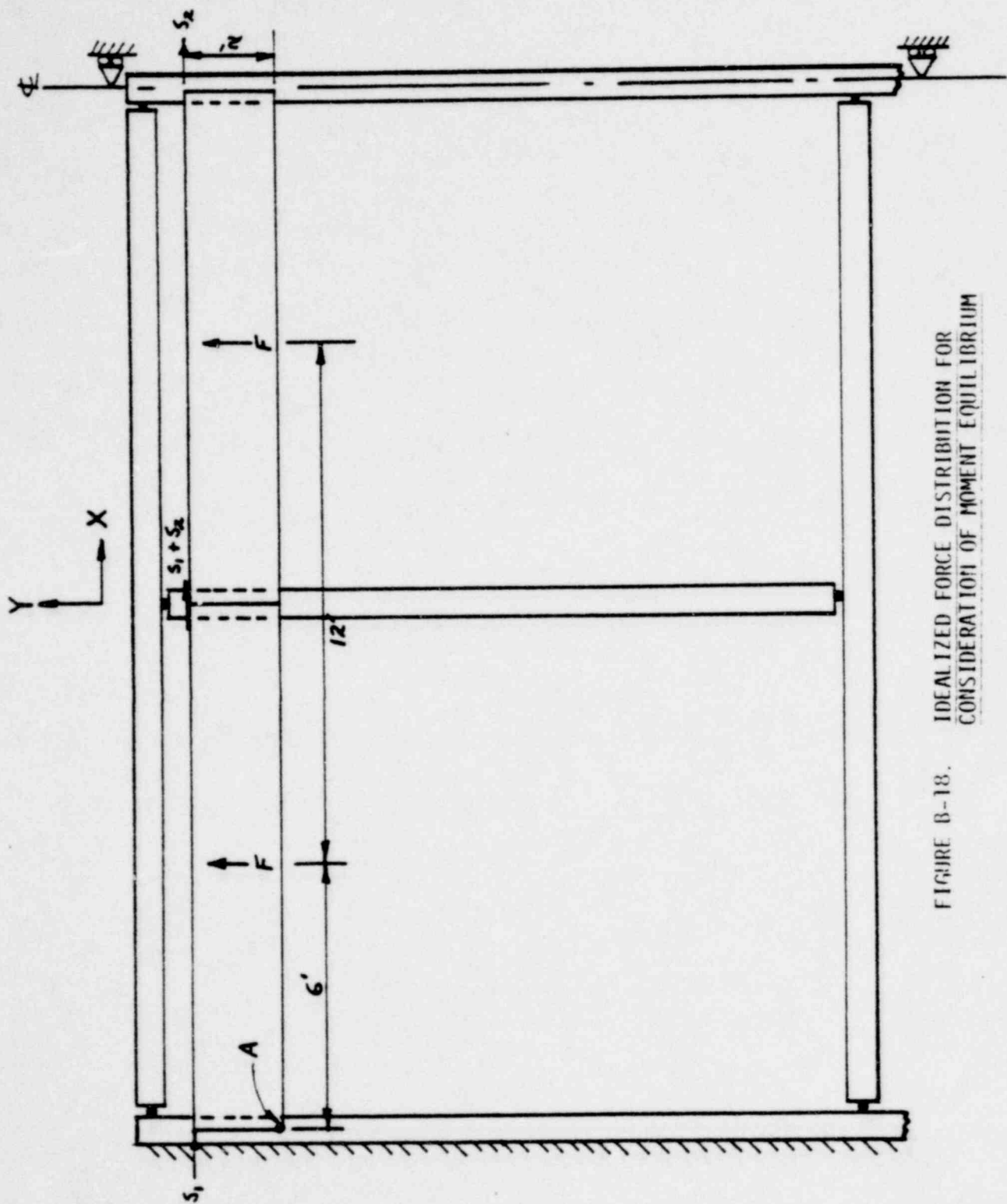


FIGURE B-18. IDEALIZED FORCE DISTRIBUTION FOR CONSIDERATION OF MOMENT EQUILIBRIUM

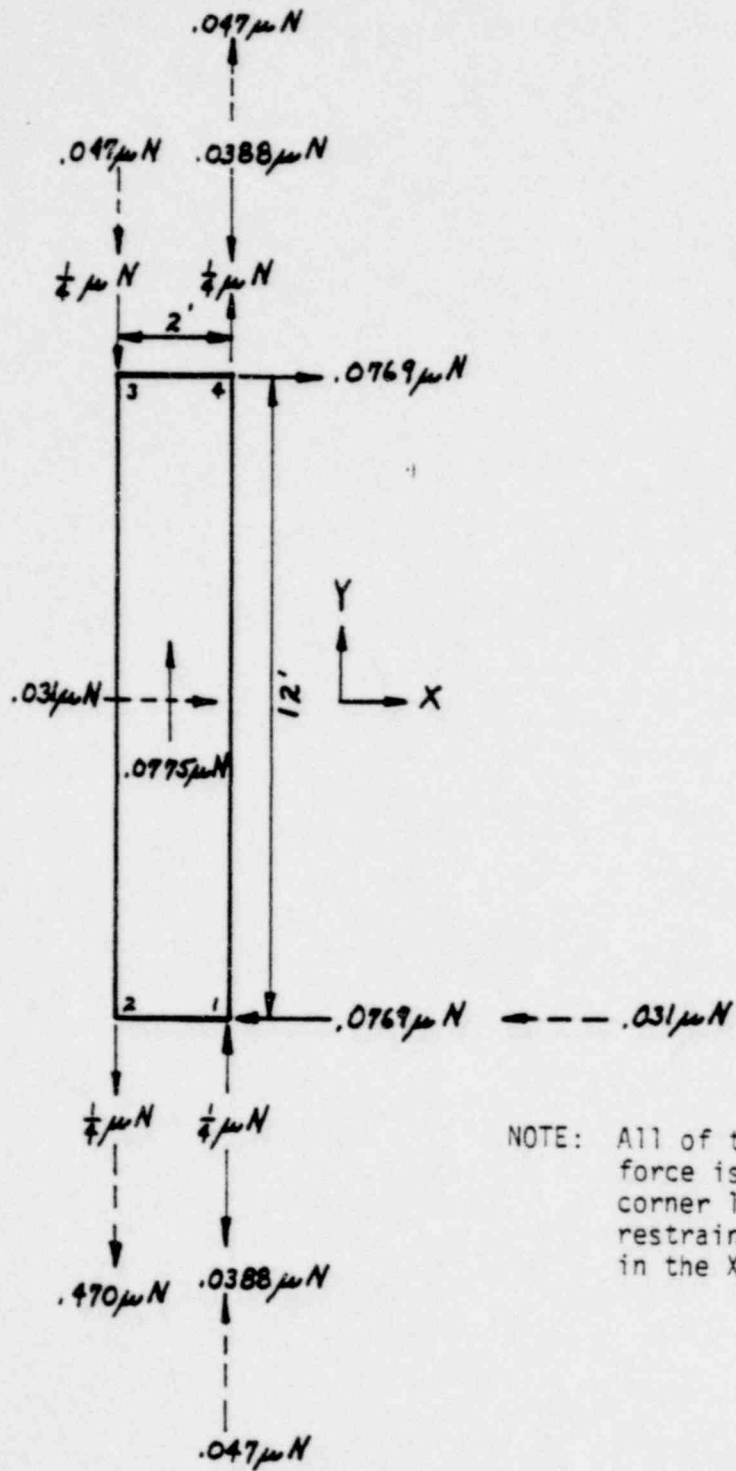


FIGURE B-19. FORCE DISTRIBUTION ON A TYPICAL CHANNEL SLAB DUE TO A 1.0 X +.4Y SPECTRAL ACCELERATION

1363 180

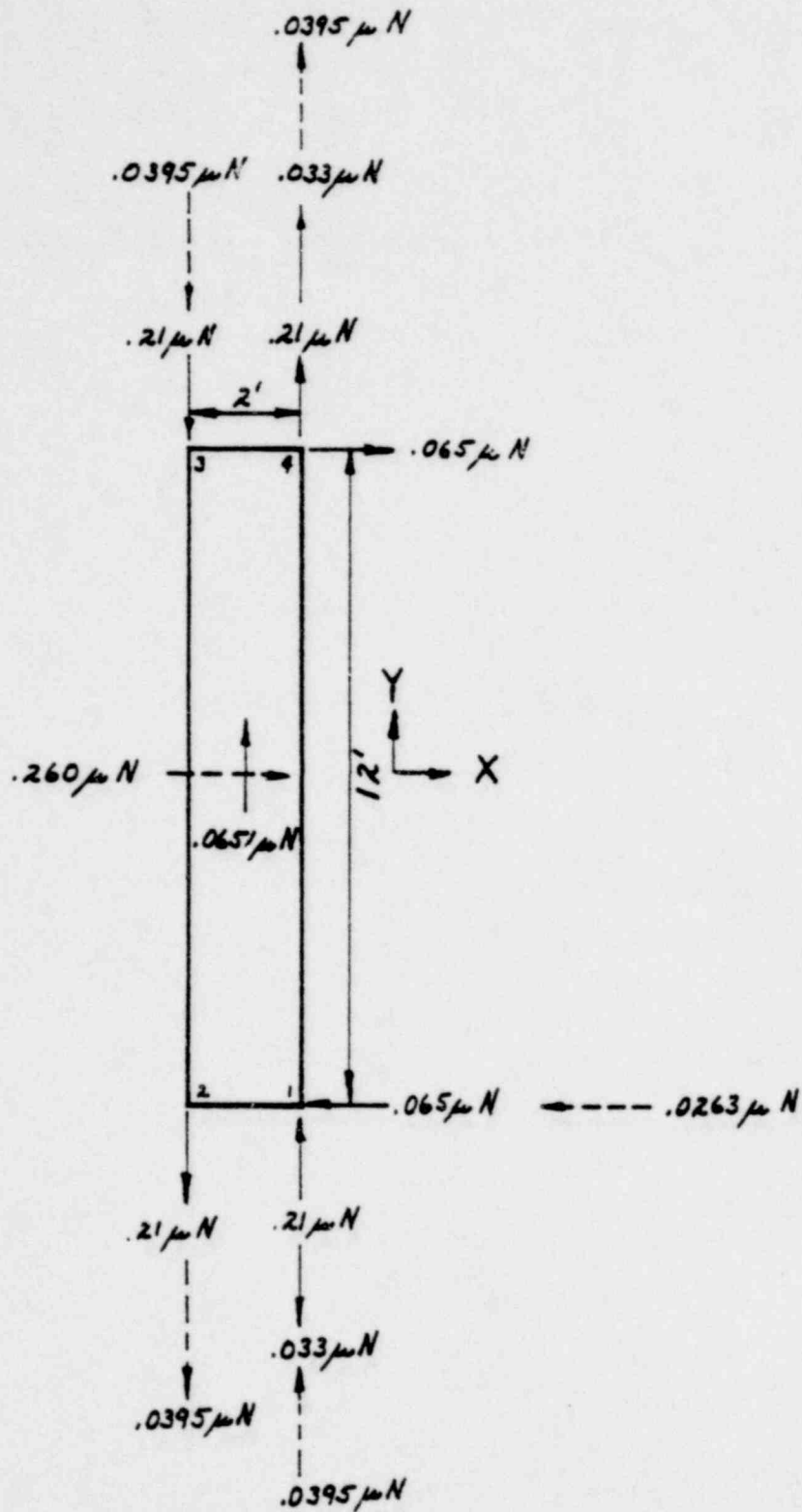


FIGURE B-20. ACTUAL FORCE DISTRIBUTION TO ACCOUNT FOR A MAXIMUM ALLOWABLE VECTOR FORCE OF $1/4 \mu N$

APPENDIX C

SELECTED DATA AND DETAILS FROM THE
TASK I REPORT

TABLE C-1. JN-1B STRUCTURAL MATERIAL PROPERTIES (TENSILE UNLESS NOTED)

Structural Element	Material Identification		Yield Strength				Ultimate Strength			
			Min. Spec. (ksi)	Lower Bound (ksi)	Median (ksi)	Upper Bound (ksi)	Min. Spec. (ksi)	Lower Bound (ksi)	Median (ksi)	Upper Bound (ksi)
Plate, Rolled Shapes and Miscellaneous Structural Steel	ASTM A36		36	40*	44*	48.5*	58	64*	68*	73*
Steel Roof Deck	ASTM A245 Grade C		—	33*	38*	45*	—	—	—	54
H Series Joists	ASTM A242		50	54*	47*	61*	70	76*	80*	85*
Reinforcing Steel (Beam Stirrups)	ASTM A615 Grade 40		40	41 ^(a)	48 ^(a)	53 ^(a)	70	76*	80*	85*
Reinforcing Steel (All Others)	ASTM A615 Grade 60		60	62 ^(b)	66 ^(b)	70.5 ^(b)	90	97*	102*	109*
Structural Bolts	ASTM A325	>1" ϕ	81	86*	89*	93*	105	110*	114*	119*
		<1" ϕ	92	97*	100*	104*	120	125*	130*	136*
Footings, Grade Beams and Pool Wall	Structural Concrete at 28 Days		—	—	—	—	4 (comp.)	4.2*	4.6*	5.0*
Other Concrete Structural Elements Not Exposed to Weather	Structural Concrete at 28 Days		—	—	—	—	3 (comp.)	3.4	4.0	4.7
Mortar	Type N ASTM C270 Vertical Bending (MOR)							.01*	.02*	.04*
	Horizontal Bending (MOR)							.02*	.04*	.08*
	Shear Strength							.02*	.04*	.08*

* Estimated Value

(a) Reference 11

(b) Reference 12

C-1

1363 183

TABLE C-2. JN-1B STEEL STRUCTURAL MEMBER PROPERTIES

Structural Component	Member Designation	Depth (in.)	Area (in. ²)	Major Axis		Minor Axis	
				I(in. ⁴)	S(in. ³)	I(in. ⁴)	S(in. ³)
Roof Framing	33W118	33	34.8	5900	359	187	32.5
	14W30	14	8.83	290	41.9	19.5	5.80
	14W22	14	6.49	198	28.9	7.0	2.80
	12W27	12	7.95	204	34.2	18.3	5.63
	8W10	8	2.96	30.8	7.8	2.08	1.06
Roof Joist	14H3	14	0.92	39.0	5.5	—	—
Roof Deck	1-1/2" - 20 Ga. Narrow Rib Galvanized Steel Deck	1.5	—	(per 12 in) 0.24	(per 12 in) 0.21	—	—
Main Column	24W68	24	20.0	1820	153	70.0	15.5
Hung Corner Column	18W40	18	11.8	612	68.4	19.1	6.3
Craneway Framing	24W84 +	24.5	34.7	3649.6	—	102.6	—
	15C33.9						
	12W40						
12W27	12	7.95	204	34.2	18.3	5.63	
Craneway Cross Bracing	JL 4 x 3 x 1/4	3	3.38	2.71	1.20	—	—

C-2

1363 184

TABLE C-2. STEEL STRUCTURAL MEMBER PROPERTIES (continued)

Structural Component	Member Designation	Depth (in.)	Area (in. ²)	Major Axis		Minor Axis	
				I (in. ⁴)	S (in. ³)	I (in. ⁴)	S (in. ³)
Mezzanine Floor Slab Support Beams	12W45	12	13.2	351	58.2	50.0	12.4
	12W40	12	11.8	310	51.9	44.1	11.0
	12W31	12	9.13	239	39.5	21.6	6.61
	12W27	12	7.95	204	34.2	18.3	5.63
	12W22	12	6.47	156	25.3	4.64	2.31
	8W10	8	2.96	30.8	7.80	2.08	1.06
Mezzanine Floor Metal Deck	Inland-Ryerson 20 ga. Type S Steel Deck	1.5	0.697 (per ft.)	0.243 (per ft.)	0.250 (per ft.)	—	—
Low Roof Support Beam	18W35	18	10.3	513	57.9	15.5	5.16
	14W30	14	8.83	290	41.9	19.5	5.80
Low Roof Joist	18H7	18	1.73	139.8	15.5	—	—
Low Roof Metal Deck	1-1/2" - 20 Ga. Narrow Rib Gal- vanized Steel Deck	1.5	—	(per 12 in) 0.24	(per 12 in) 0.21	—	—
Cross Bracing at Side Walls	L4 x 4 x 1/4	4	1.94	3.04	1.05	3.04	1.05
	L3-1/2 x 3-1/2 x 1/4	3.5	1.69	2.01	0.79	2.01	0.79
	2LS 5 x 3-1/2 x 5/16	5.0	5.12	13.20	3.87	—	—
Girt at Panel Joint	C8 x 11.5 + L2-1/2 x 2-1/2 x 1/4	—	4.57	—	—	—	—

C-3

1363 185

HIGH ROOF UNIFORM WEIGHT

	<u>lb/ft²</u>
Built-up Roofing	6
1-1/2" Rigid Insulation	2.3
1-1/2" - 20 Gage Metal Deck	2.3
Roof Framing	9.0
Ductwork and Piping	<u>1.5</u>
TOTAL	21.1

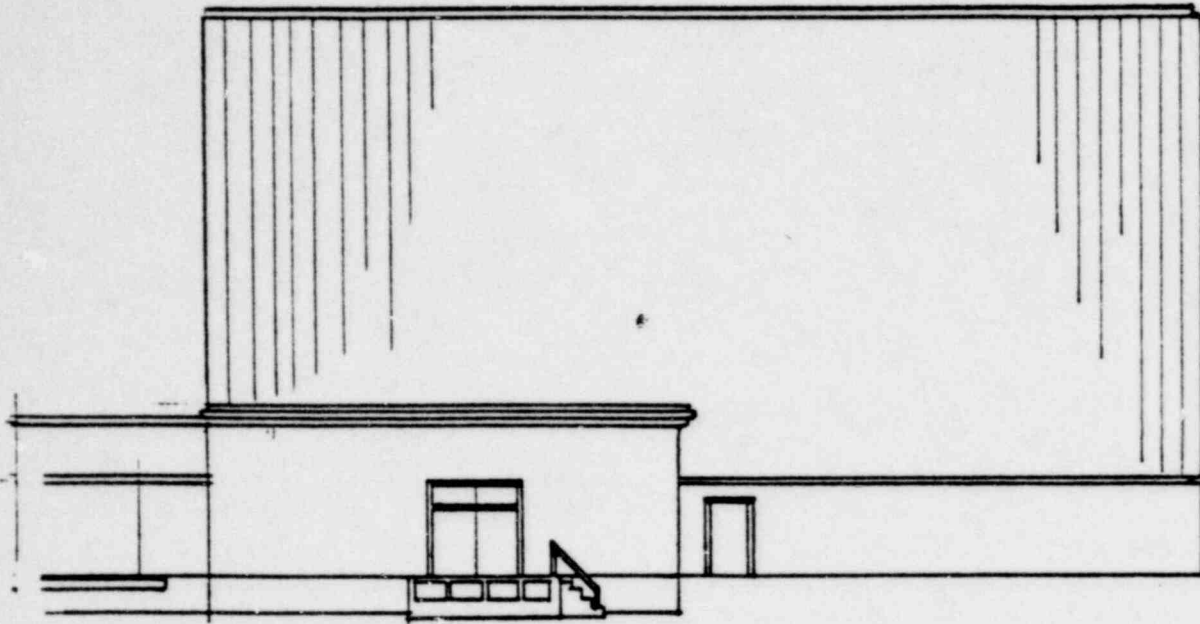
MEZZANINE UNIFORM WEIGHT

	<u>lb/ft²</u>
1-1/2" Steel Deck w/4" Concrete Fill	39
Equipment (Fans and Pumps)	15
Steel Floor Framing	8
Ductwork/Ceiling	<u>5</u>
TOTAL	67

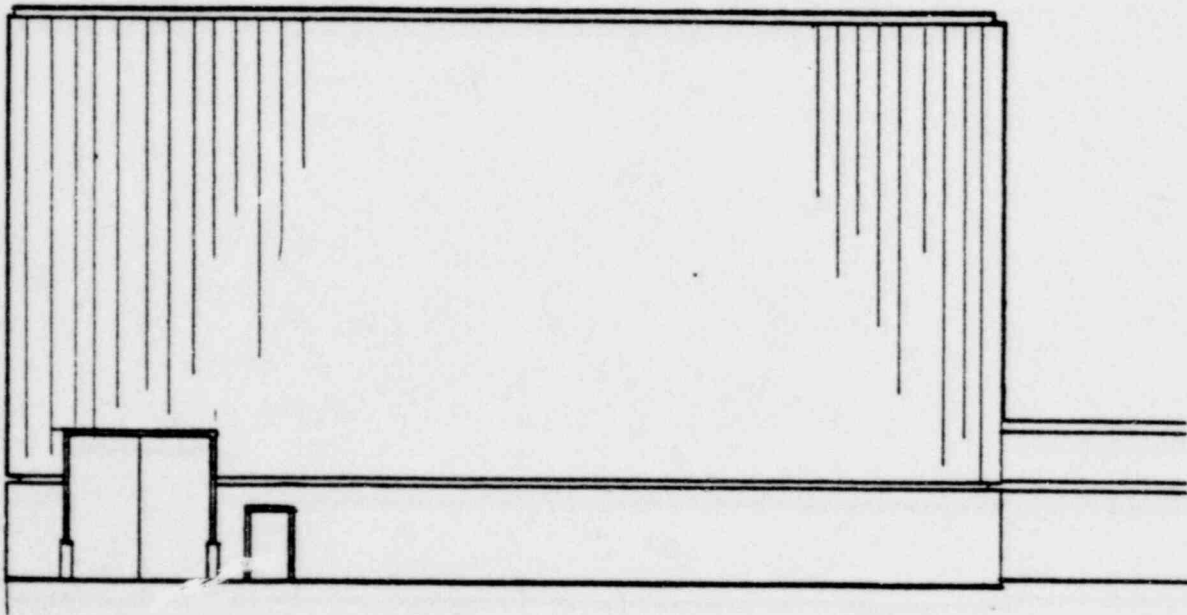
METAL WALL PANEL UNIFORM WEIGHT

	<u>lb/ft²</u>
Metal Wall Panel (2 steel sheets and insulating core)	3.0
Equivalent weight of girts and sag rods	<u>1.8</u>
TOTAL	4.8

TABLE C-3. JN-1B UNIFORM AREA WEIGHTS



JN-1B NORTH ELEVATION



JN-1B SOUTH ELEVATION

FIGURE C-1. JN-1B EXTERIOR ELEVATIONS

POOR ORIGINAL

C-7

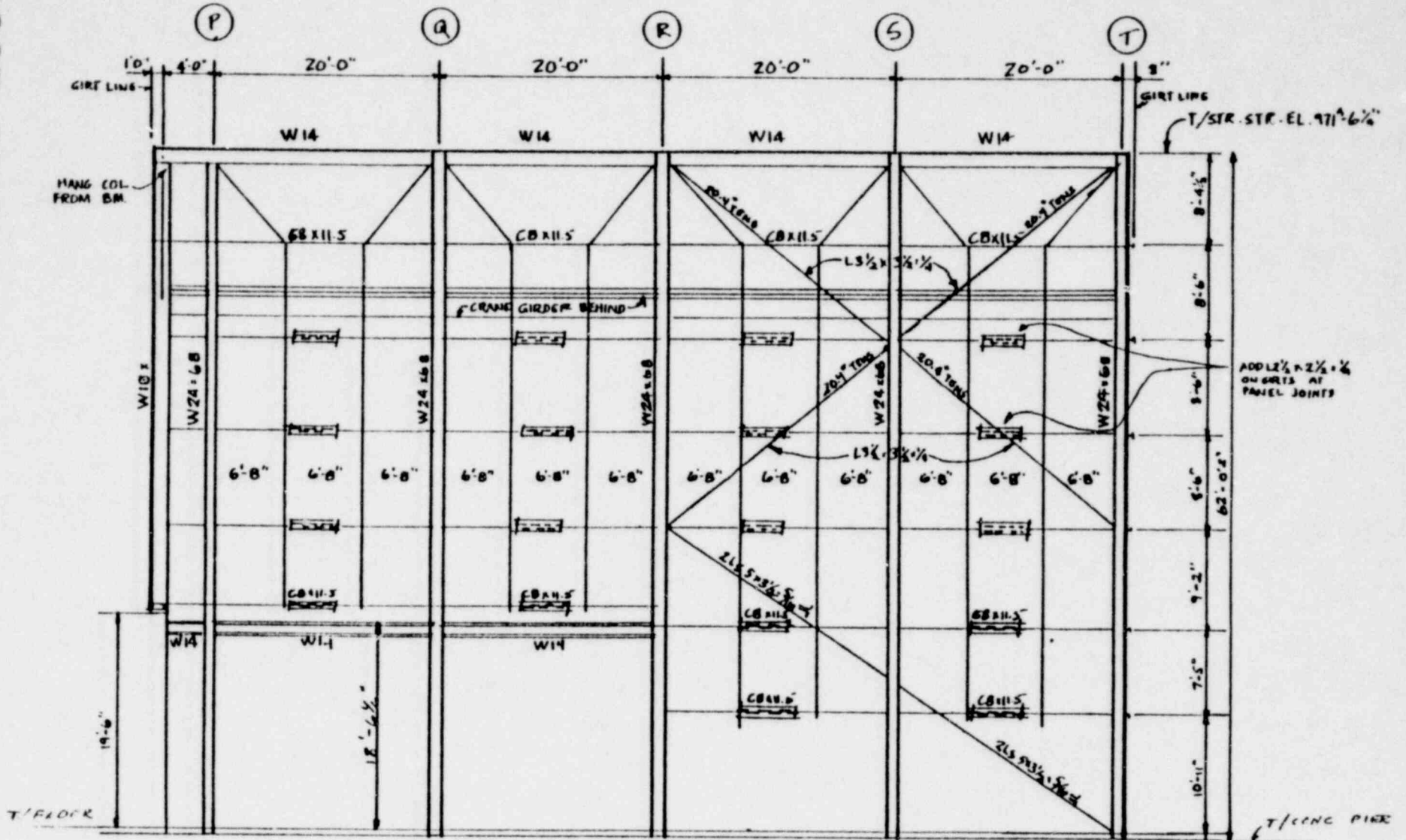


FIGURE C-3. JN-1B NORTH WALL FRAMING ELEVATION

1363 189

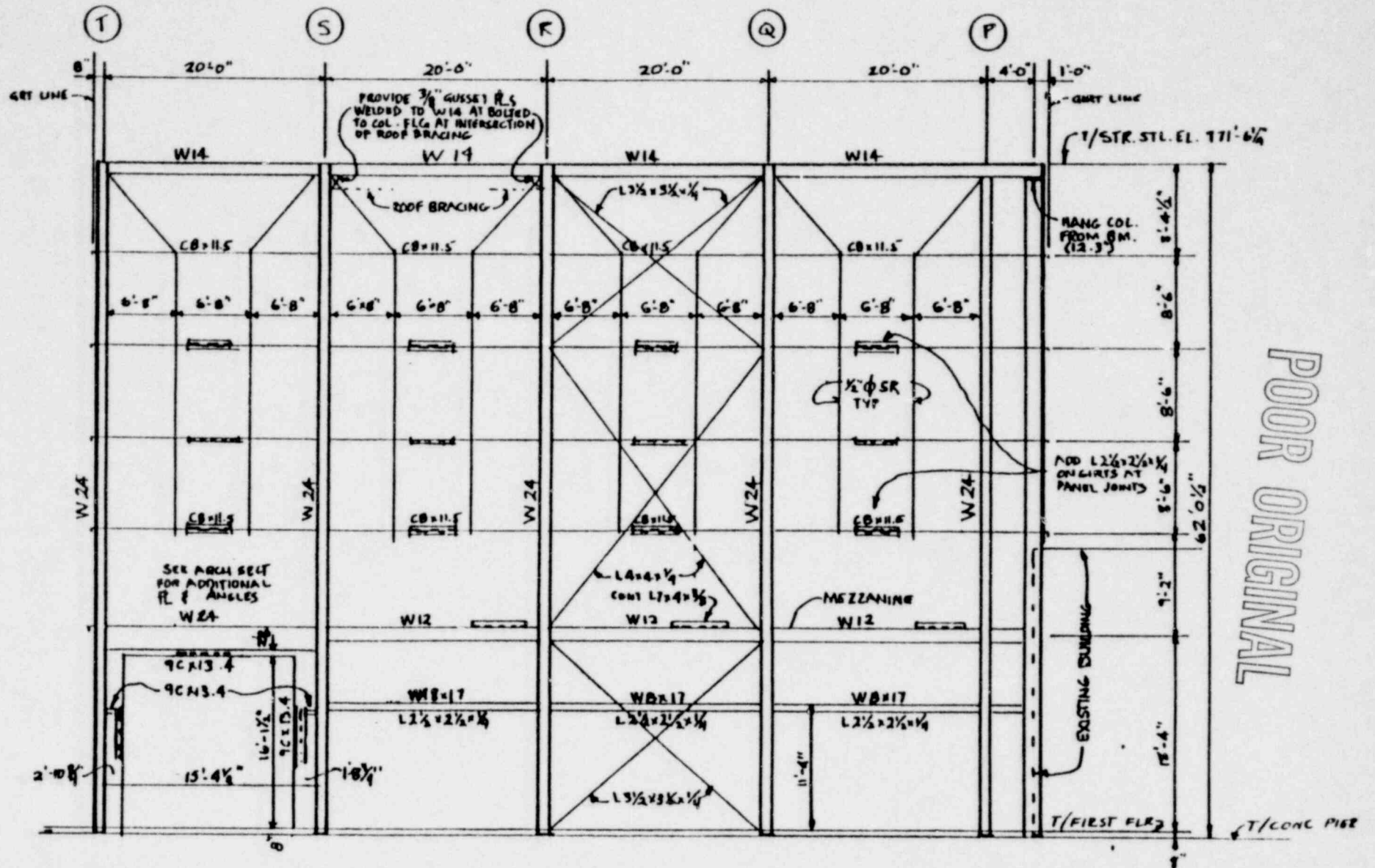


FIGURE C-4. JN-1B SOUTH WALL FRAMING ELEVATION

POOR ORIGINAL

C-8

1363 190

C-9

1363 191

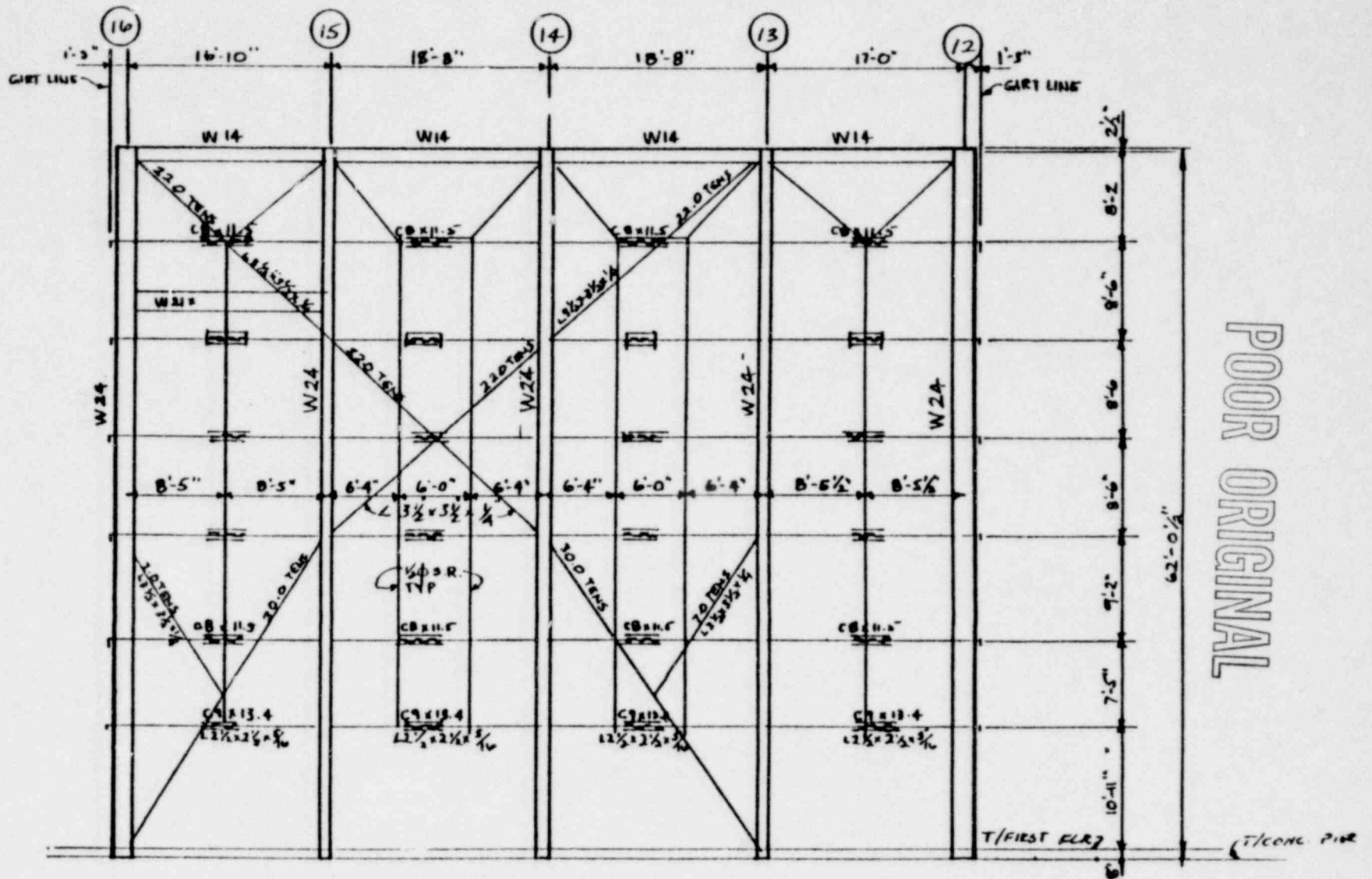


FIGURE C-5. JN-1B WEST WALL FRAMING ELEVATION

C-11

1363 192

POOR ORIGINAL

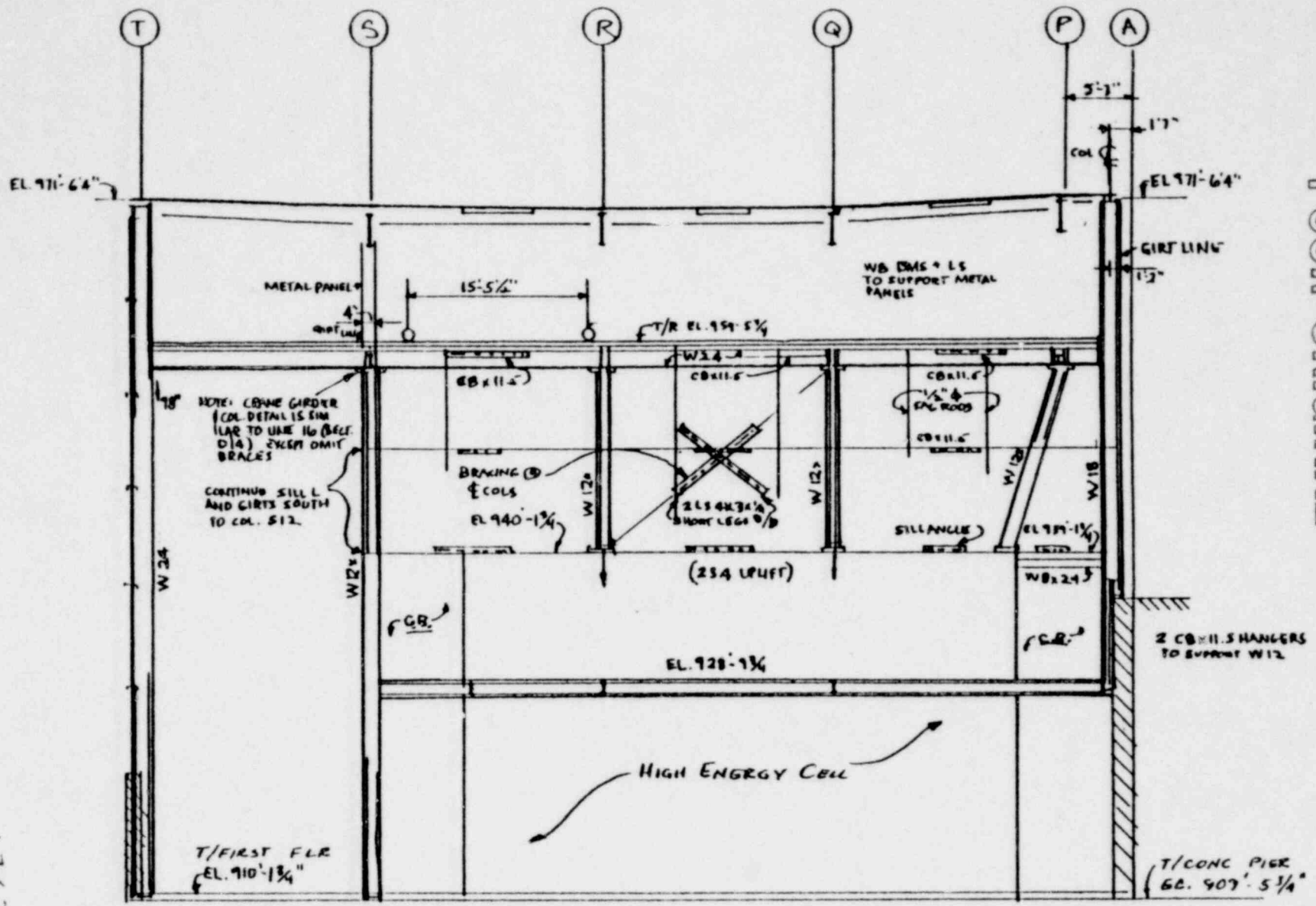


FIGURE C-7. JN-1B CROSS BRACING FOR CRANE FRAMING AT LINE 13

POOR ORIGINAL

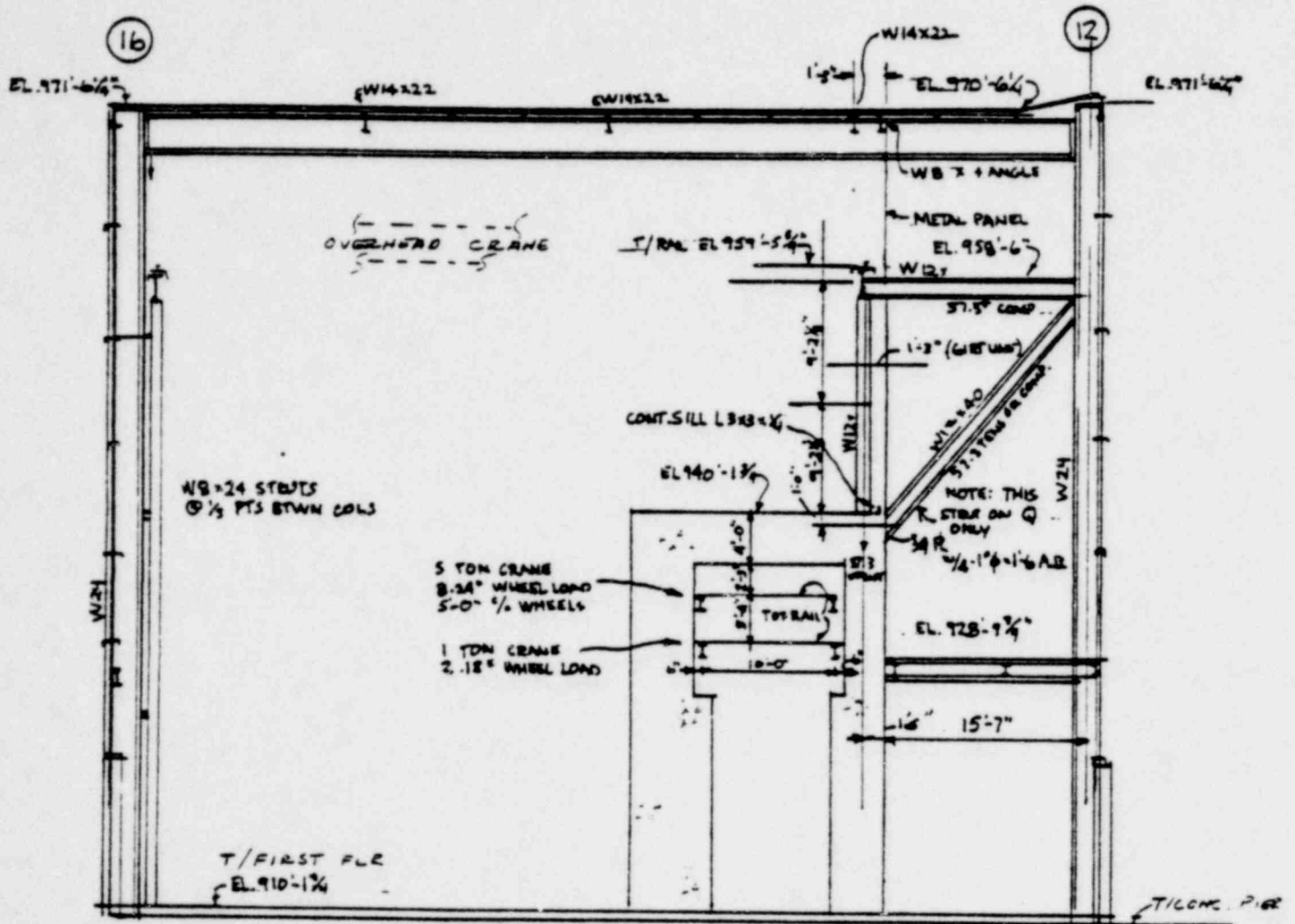
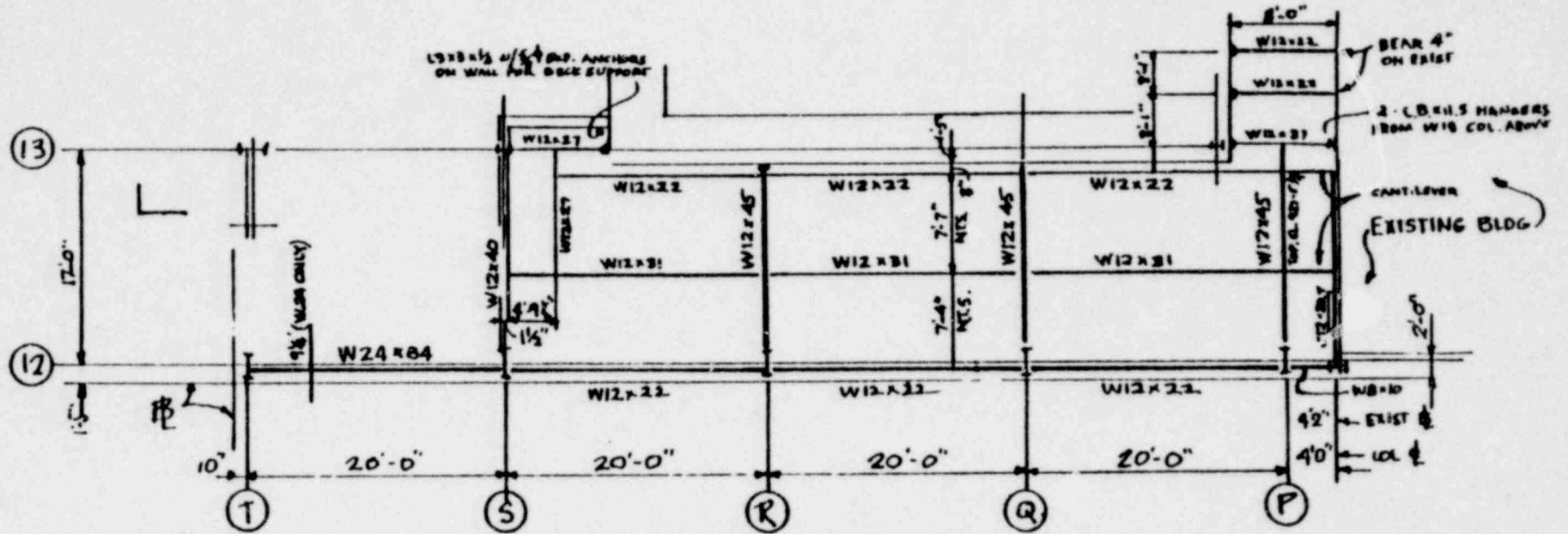


FIGURE C-8. JN-1B DIAGONAL BRACING ALONG COLUMN LINE Q

C-14



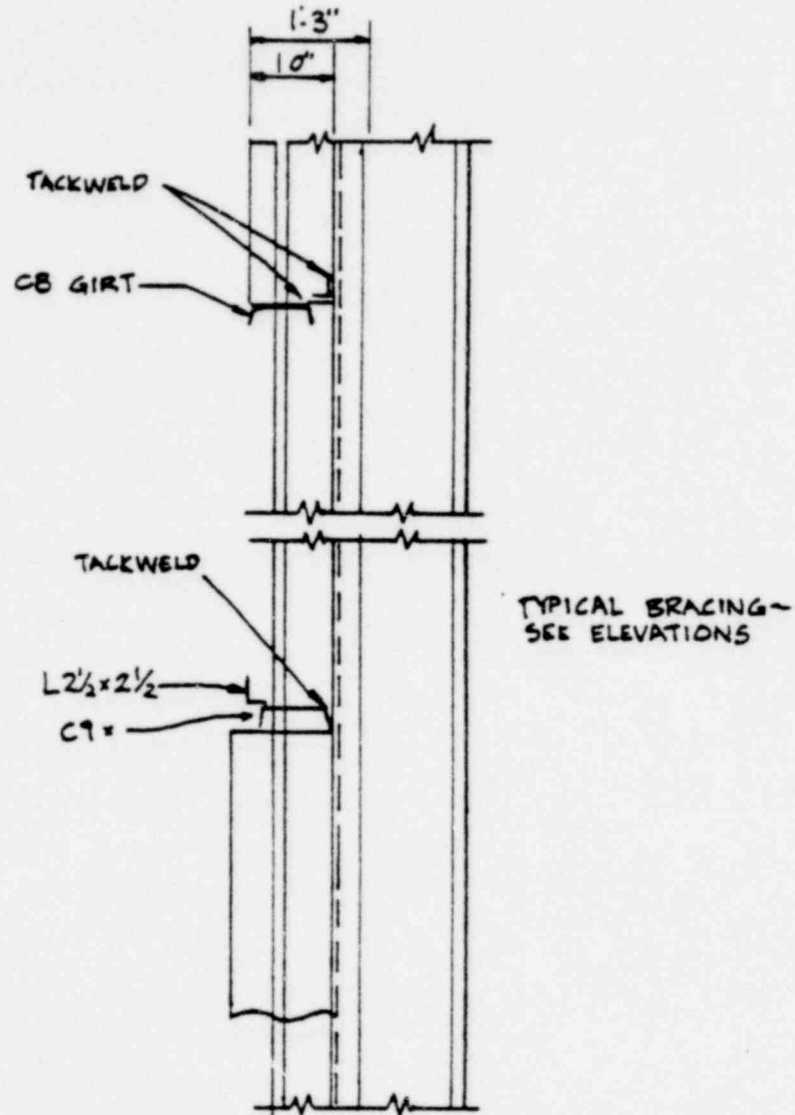
NOTE: Mezzanine slab is constructed of 4" concrete over 1-1/2" Inland-Ryerson 20 gage Type S composite action steel deck

FIGURE C-10. JN-1B MEZZANINE FLOOR PLAN

1363 195

POOR ORIGINAL

COLUMN FOOTING SCHEDULE						
Mark	Size	Depth	Reinforcing			Remarks
			Ea. Way	L.W.	S.W.	
(A)	6'-6"x6'-6"	1'-10"	9#5			
(B)	6'-0"x6'-0"	1'- 8"	8#5			
(C)	4'-0"x4'-0"	1'- 0"	4#5			
(D)	8'-8"x6'-1"	2'- 6"		12#7x8'-2"	17#7x5'-7"	#6@12"EW -.Top & Bot.
(E)	4'-6"x4'-6"	1'-0"	6#5			



1363 196

FIGURE C-11. JN-1B COLUMN FOOTING SCHEDULE AND WALL BRACING DETAIL

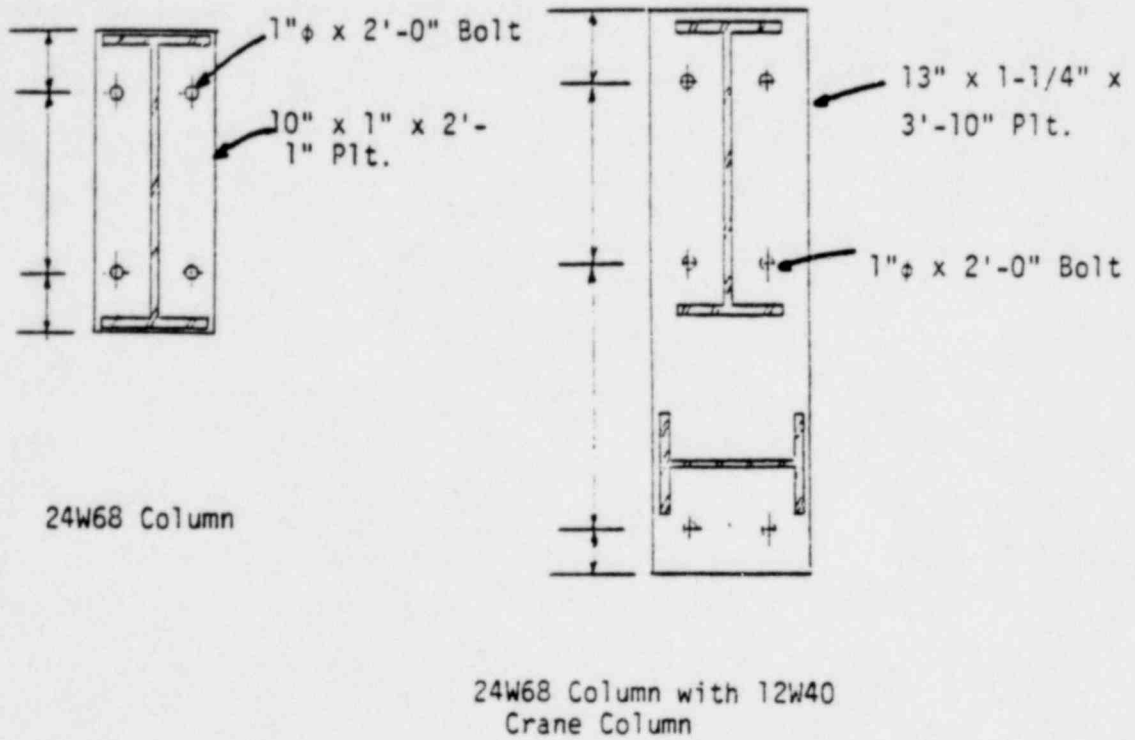
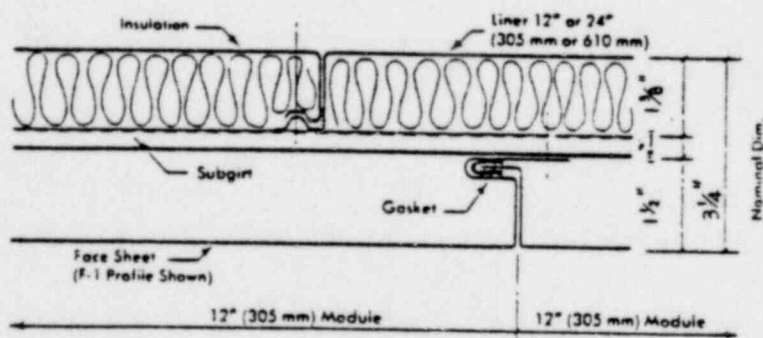
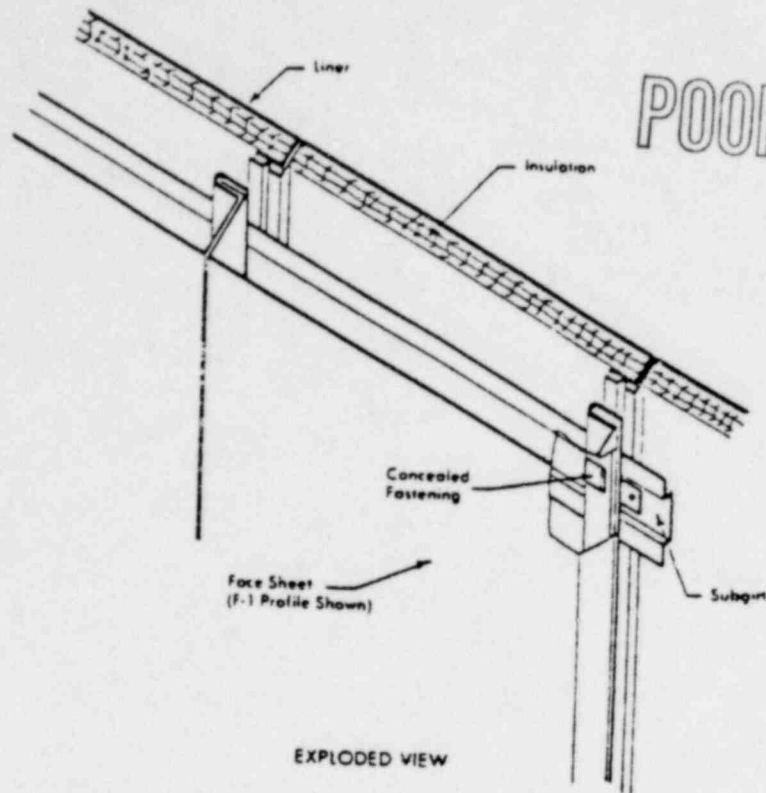


FIGURE C-12. JN-1B COLUMN BEARING PLATE AND ANCHOR BOLT DETAILS

1363 197



CONCEALED FASTENING SYSTEM

FIGURE C-13. JN-1B DETAIL OF METAL WALL PANEL

1363 198

TABLE C-4. JN-4 STEEL STRUCTURAL MEMBER PROPERTIES

Structural Component	Designation	Depth (in.) (Approx)	Area (in ²)	Major Axis		Minor Axis	
				I (in ⁴)	S (in ³)	I (in ⁴)	S (in ³)
Roof Framing	21WF62	21	18.2	1327	126.4	53.1	12.9
	18WF50	18	14.7	800.6	89.0	37.2	9.9
	16WF45	16	13.2	583.3	72.4	30.5	8.7
	16WF40	16	11.8	515.5	64.4	26.5	7.6
	16WF36	16	10.6	446.3	56.3	22.1	6.3
	16B31	16	9.12	372.5	47.0	11.57	4.19
	16B26	16	7.65	298.1	38.1	8.71	3.17
	12WF27	12	7.97	204.1	34.1	16.6	5.1
	12B14	12	4.14	88.2	14.8	2.25	1.13
	8WF17	8	5.00	56.4	14.1	6.72	2.6
	8B13	8	3.83	39.5	9.88	2.62	1.31
	8B10	8	2.95	30.8	7.79	1.99	1.01
Columns	6 x 4 x 5/16	—	5.52	25.4	8.46	13.5	6.74
	5 x 5 x 1/4	—	4.54	16.60	6.638	16.60	6.638
	4 x 4 x 3/8	—	4.95	10.15	5.076	10.15	5.076
	4 x 4 x 5/16	—	4.24	9.203	4.602	9.203	4.602
	4 x 4 x 1/4	—	3.54	7.988	3.994	7.988	3.994

1363 199

Wall Thickness	Masonry Unit Size	Bearing Area (1) (in ²)	Moment of Inertia (1) (in ⁴)	Moment of Inertia (2) (in ⁴)	Remarks
8 in.	8 x 8 x 16	46.2	4.25	445	
12 in.	12 x 8 x 16	59.6	1311	1420	

(1) Based on approx. 80% of Net Block Section (100% Flange Area and 40% of Web Area)

(2) Based on Net Block Section (ASTM C90 Hollow Block)

FIGURE C-14. GEOMETRIC PROPERTIES OF CONCRETE BLOCK

C-19

1363 200

TABLE C-5. JN-4 STRUCTURAL MATERIAL PROPERTIES (TENSILE UNLESS NOTED)

Structural Element	Material Identification	Yield Strength				Ultimate Strength				Modulus of Elasticity	Comments
		Min. Spec. (ksi)	Lower Bound (ksi)	Median (ksi)	Upper Bound (ksi)	Min. Spec. (ksi)	Lower Bound (ksi)	Median (ksi)	Upper Bound (ksi)	Median (psi)	
Plate, Rolled Shapes and Miscellaneous Structural Steel	ASTM A36	36	40*	44*	48.5*	58	64*	68*	73*	29.0 · 10 ⁶	
Reinforcing Steel	ASTM A61 Grade 40	40	44(a)	48(a)	53(a)	70	76*	80*	85*	29.0 · 10 ⁶	
Miscellaneous Bolting and Connections	ASTM A307 3/4 In. ⌀	36*	40*	44*	49*	60	64* (42)*	68* (48)*	73* (56)*	29.0 · 10 ⁶	1. Tension (shear) 2. Note: Assumed Type of Material
Footings, Grade Beams and Floor	Structural Concrete at 28 Days	—	—	—	—	3.20 (Comp.)	3.4	4.0	4.7	3.2 · 10 ⁶	
Roof Slabs	6" "Rackie" Slab						4.2* (Comp.)	5.0* (Comp.)	6.0* (Comp.)		
Masonry	ASTM C90 Grade N	—	—	—	—	1.00 (Comp.)	—	—	—	1.5 · 10 ⁶	Assumed Masonry Grade
Mortar	Type N ASTM C270										
	Vertical Bending (MOR)						.01*	.02*	.04*		
	Horizontal Bending (MOR)						.02*	.04*	.08*		
	Shear Strength						.02*	.04*	.08*		

* Estimated Value (a) Reference 11

C-20

1363 201

TABLE C-6. JN-4 UNIFORM AREA WEIGHTS

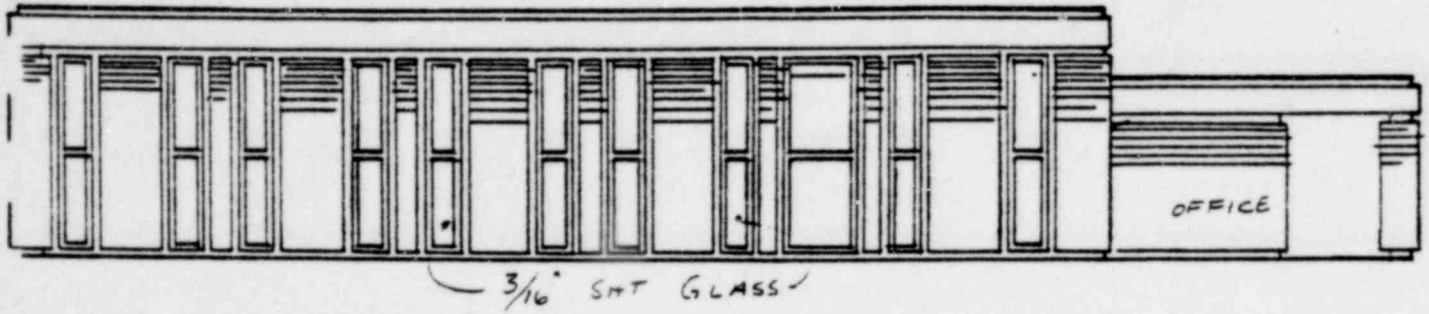
Roof System Uniform Weight	<u>lb/ft²</u>
Built-up Top and Gravel Roof	6
Insulation (1.4" thick)	2.1
Precast Channel Slabs	21
Piping and Equipment*	8
	<hr/>
TOTAL	39.1**
	 <u>lb/ft²</u>
Wall Uniform Weight	
Exterior 12 in. (4 in. brick and 8 in. block)	95
Interior 8 in.	55
	 <u>lb/ft</u>
Porcelain Facia*	10

* Estimate

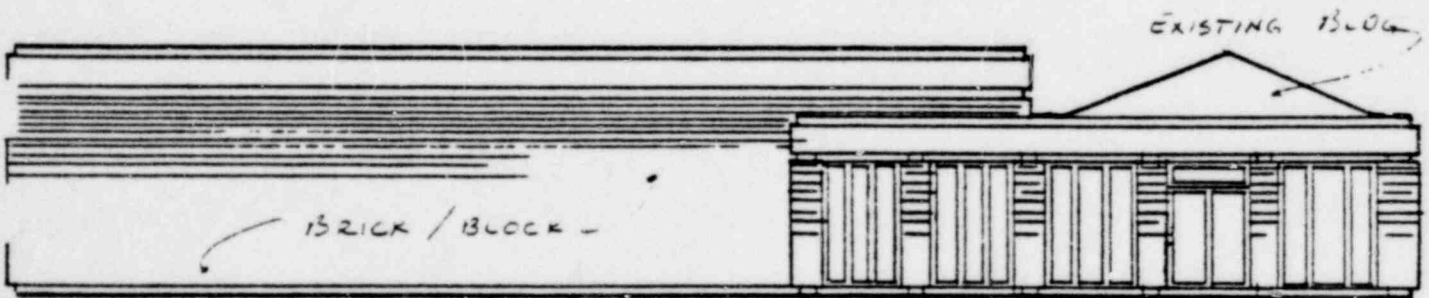
** Does not account for beam weights - see structural framing plans.

1363 202

POOR ORIGINAL



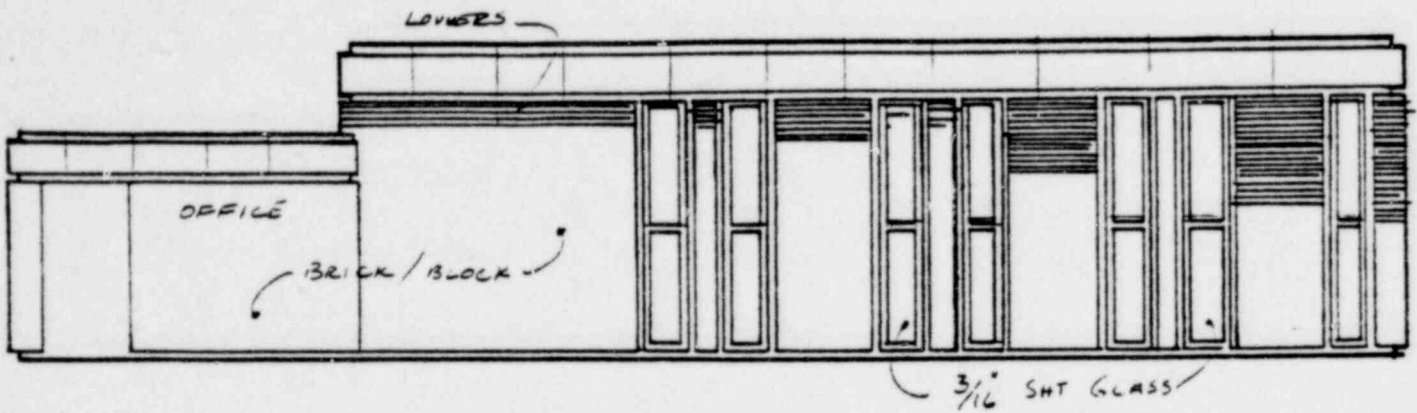
NORTH ELEVATION



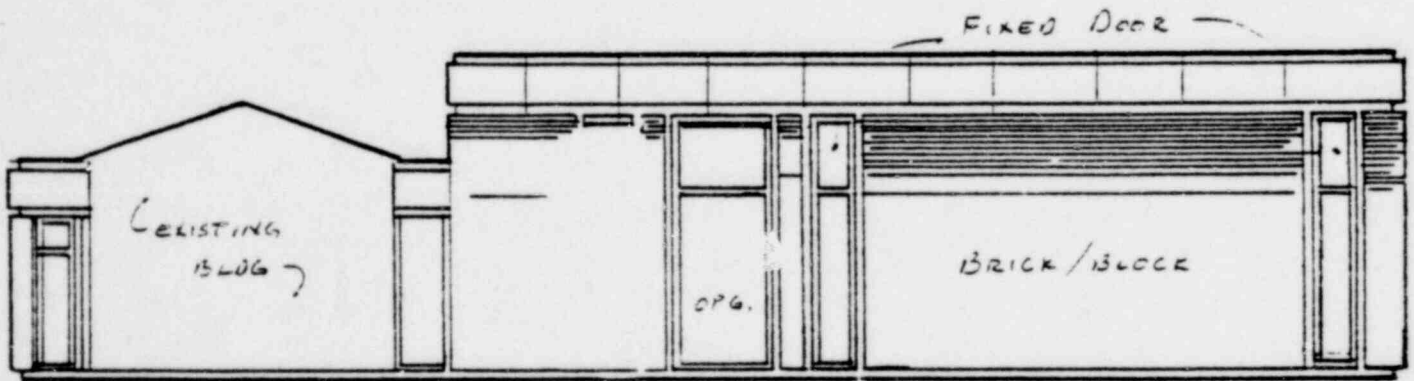
WEST ELEVATION

FIGURE C-15. JN-4 NORTH AND WEST ELEVATIONS

POOR ORIGINAL



SOUTH ELEVATION



EAST ELEVATION

FIGURE C-16. JN-4 SOUTH AND EAST ELEVATIONS

POOR ORIGINAL

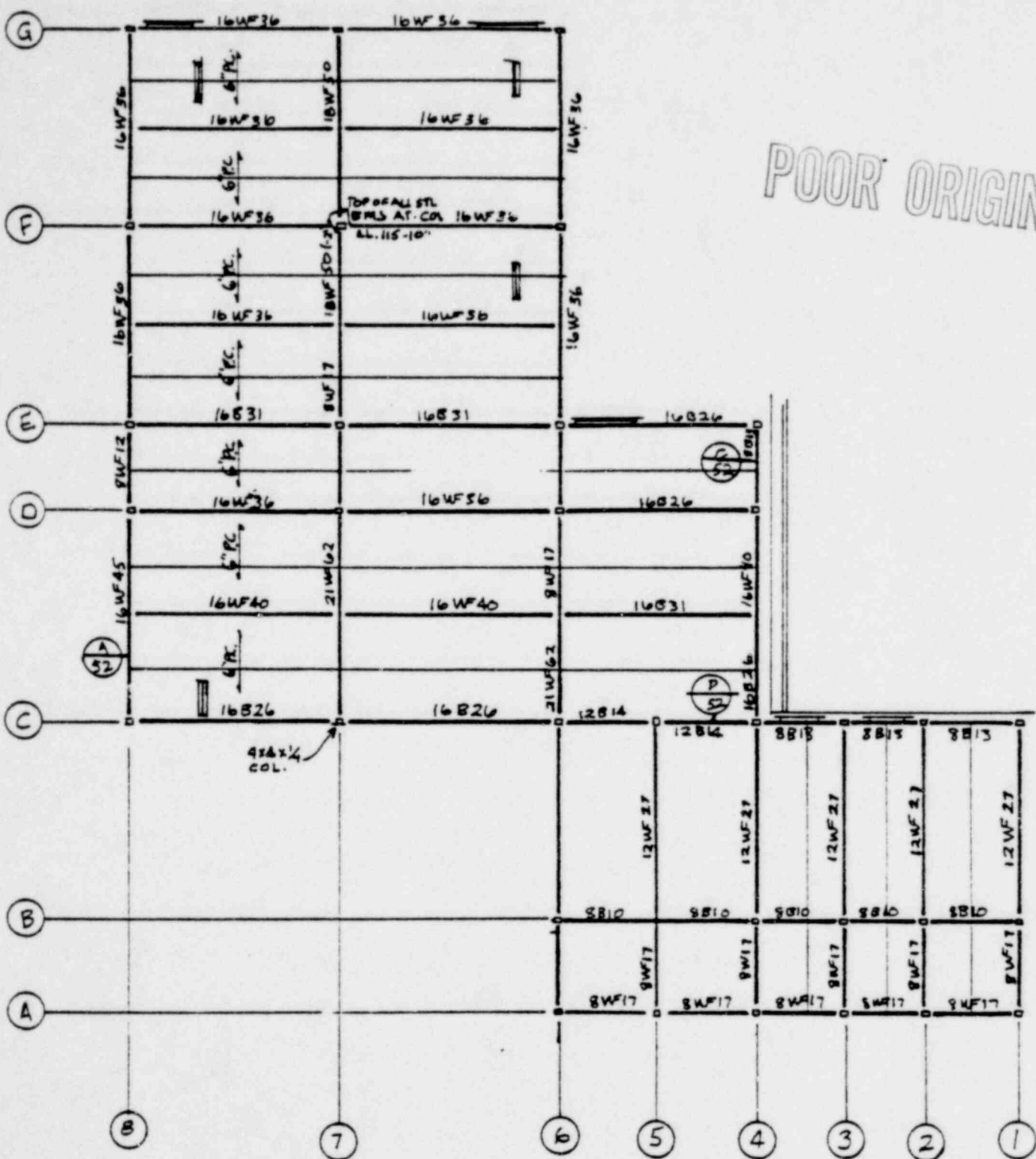


FIGURE C-17. JN-4 ROOF FRAMING PLAN

POOR ORIGINAL

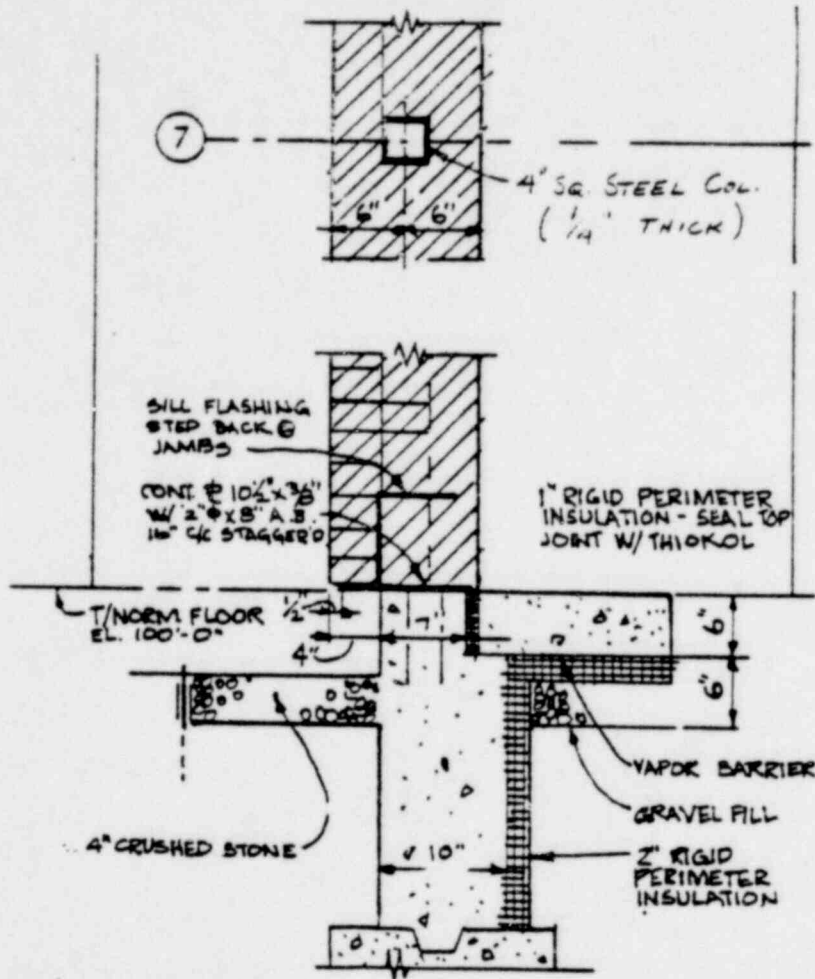


FIGURE C-18. JN-4 TYPICAL EXTERIOR WALL SECTION

1363 206

POOR ORIGINAL

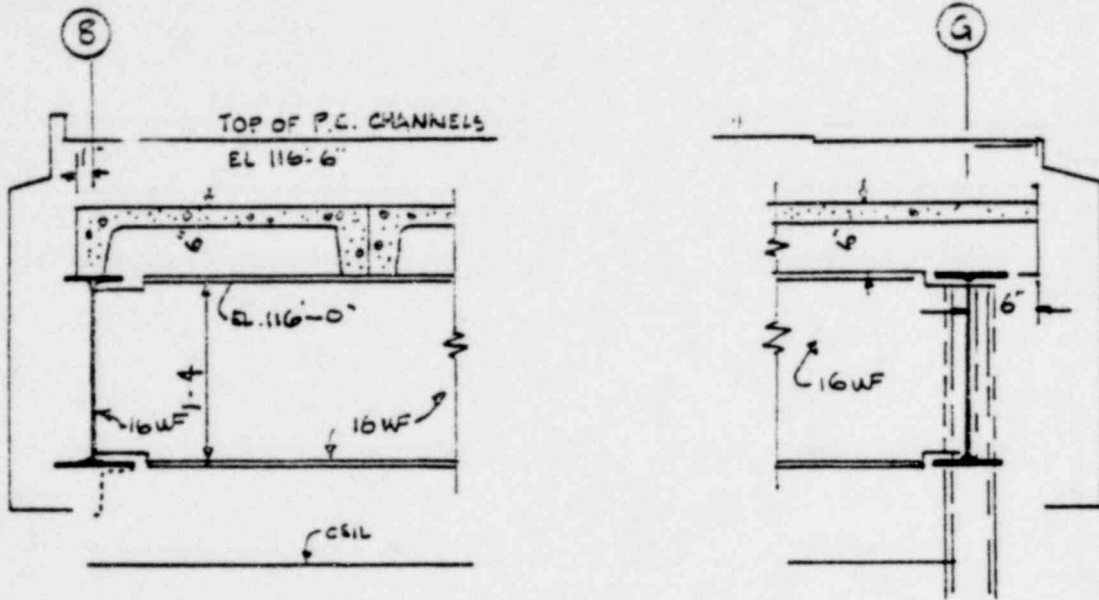
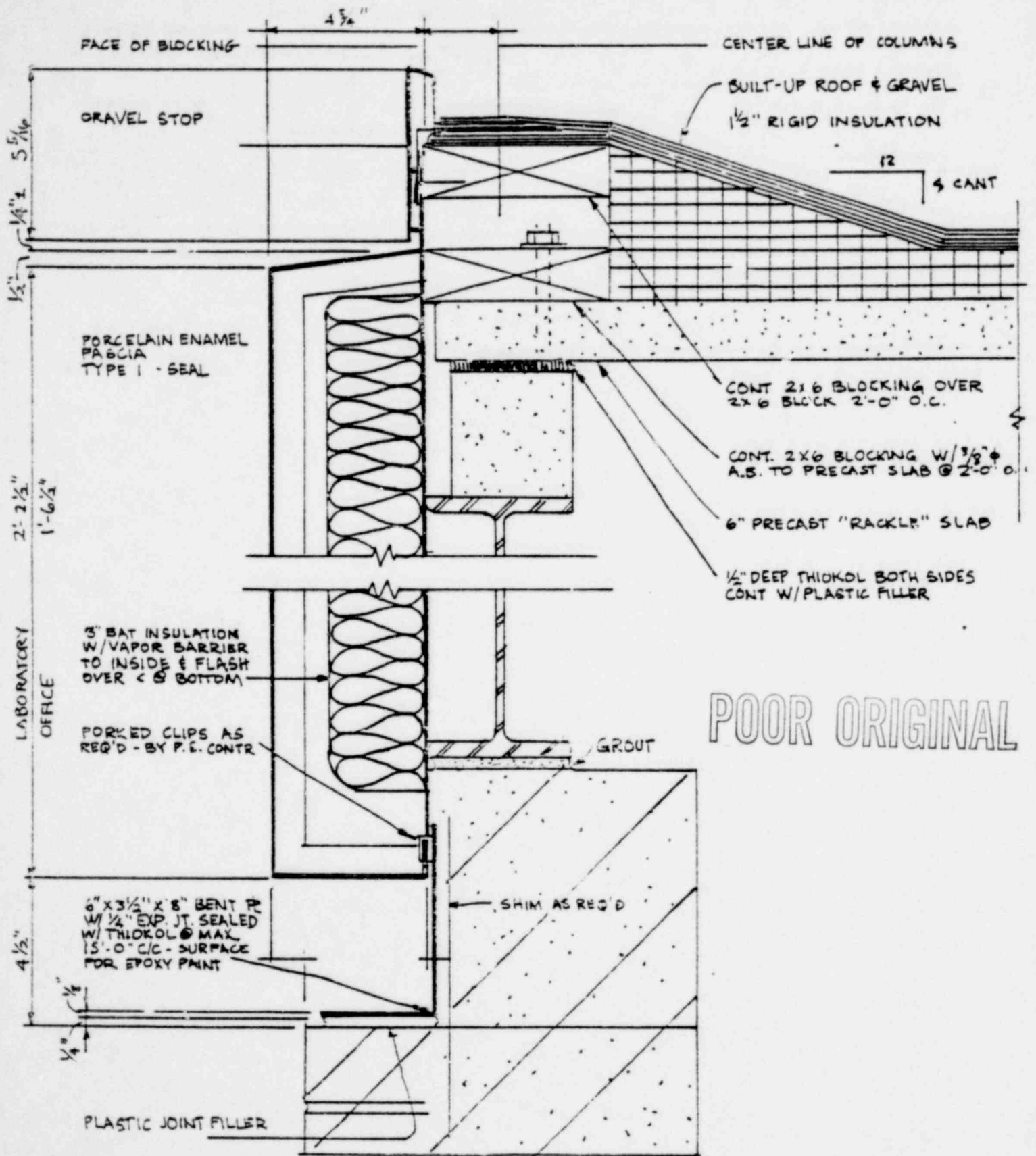


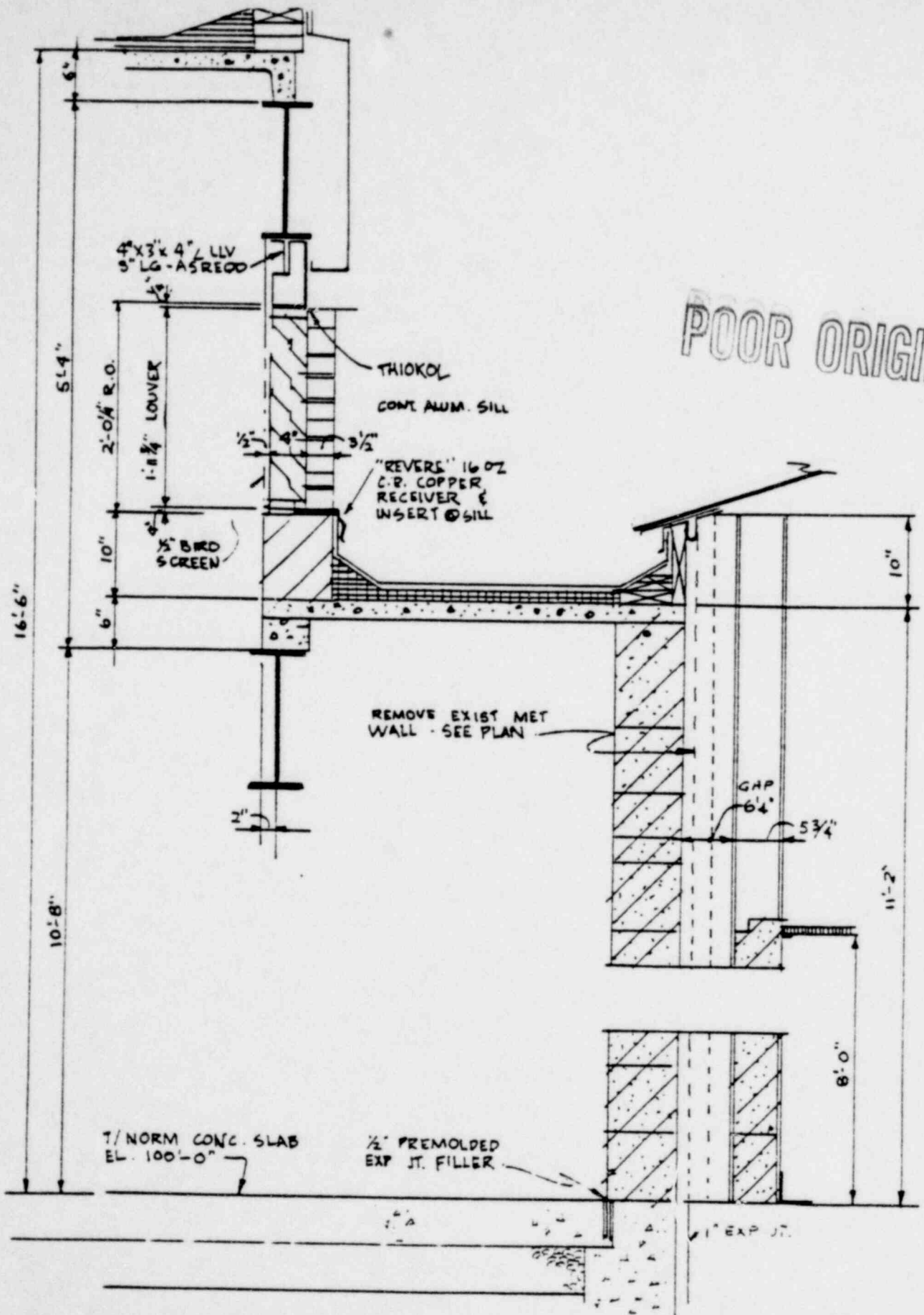
FIGURE C-19. JN-4 CONCRETE CHANNEL ROOF PLACEMENT



POOR ORIGINAL

FIGURE C-20. EXTERIOR WALL TO ROOF SECTION

1363 208



POOR ORIGINAL

FIGURE C-21. SECTION AT SERVICE ROOM - OLD LAB CORRIDOR OF JN-4 FACILITY

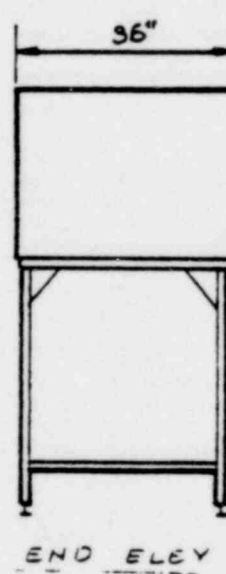
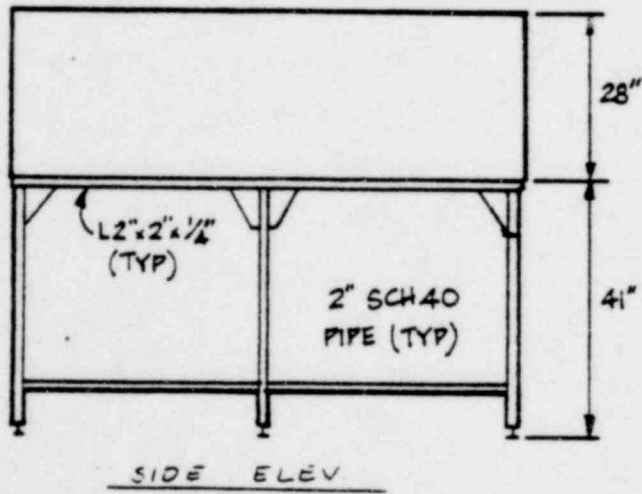
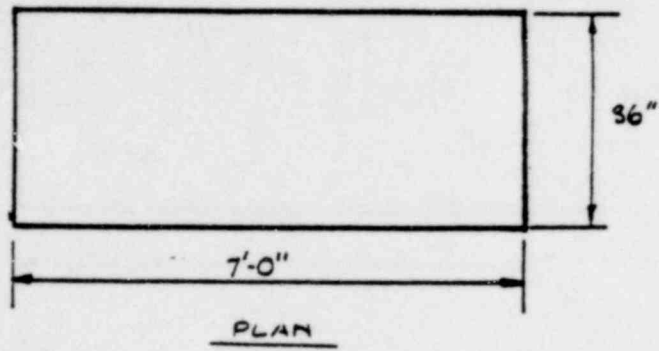
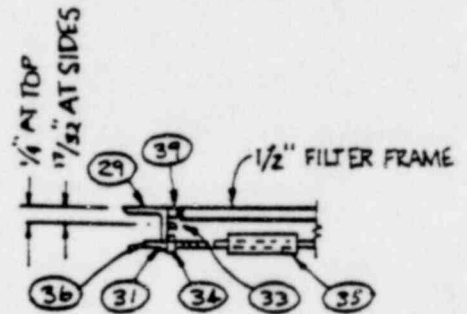
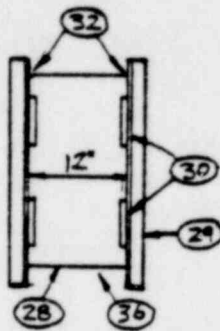
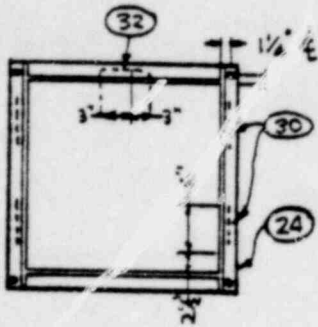


FIGURE C-22. GLOVE BOX 37 CONFIGURATION

POOR ORIGINAL



- ②⑧ 24"x24"x12" Absolute Filter
- ②⑨ 2"x2"x1/4" @ 3.19 St. Angles
- ③⑩ Guide Bars
- ③① 1/2" Drill Hole in Angle
- ③② Top Stop
- ③③ Weld 1/2"x1/4"x6" Steel Guides and Stop Bar to L
- ③④ Weld 3/8"-16 R.H. & L.H. Type 304 Hex Heavy Full Nut to Angle Iron Frame
- ③⑤ 3/4" Cold Roll Steel Hex Bar with 3/8" Hole and Weld to Stainless Steel Rod (3" Hex Length)
- ③⑥ 3/8" 16 R.H. & L.H. Type 304 Stainless Steel Rod x 2" Thd. Length - 14" Rod Length

FIGURE C-23. ABSOLUTE FILTER AND FRAME ASSEMBLY

APPENDIX D

VERIFICATION OF APPROXIMATE ANALYSIS
METHOD FOR WALL/ROOF SYSTEMS

As a part of the analysis of another facility, a verification of the Reserve Energy Method of analysis by means of the time history method (Reference 29) was conducted. The type of wall construction was essentially the same as for the BMI facility so that the verification was not duplicated. The results of the comparisons developed in Reference 29 are included here for easy reference however.

1363 212

APPENDIX D

VERIFICATION OF APPROXIMATE ANALYSIS METHOD FOR WALL/ROOF SYSTEMS

The use of the RE method was validated as an estimator of collapse capacity for the roof/wall transverse systems in two basic ways. First, the results for the B&W analyses as reported in Section 3 correlate reasonably with observations and experience from actual earthquakes. Second, a series of nonlinear time history dynamic analyses were performed using a typical B&W wall system model. Results of the approximate RE analyses compare very closely with results of the time history analyses. An additional confirmation is provided by consideration of the stability criteria developed by Housner (Reference 35) for inverted pendulum structures subjected to earthquake ground motion.

COMPARISON OF RESULTS WITH EARTHQUAKE EXPERIENCE

General observations as to behavior of masonry buildings in earthquakes was provided in the Task I Report (Reference 4). Further discussions as related to mechanics of collapse and the method of analysis are provided in Reference 29. The discussion herein is intended to show that collapse levels observed from past earthquake experience correlate reasonably with the capacities predicted by the approximate analyses used for this study.

Unreinforced masonry is one of the types of construction most vulnerable to earthquake damage and relative to other construction assemblies has a high incidence of failure for major seismic events. Despite this fact, major collapse and total failures observed in moderate to major earthquakes for unreinforced masonry construction are statistically low for construction

such as found in North America. Table D-1 indicates the percentage of unreinforced buildings collapsed or subsequently torn down because of major damage from some past California earthquakes. These data were based on information gathered by Steinbrugge (Reference 36) and Martel (Reference 37). The Table also provides the Modified Mercalli Intensities for ground shaking levels for these events at the sites of interest.

The percentages shown in Table D-1 are approximate values based on interpretation of the data tabulated in the References. For example, the basic data for the Long Beach Earthquake are in categories which indicate percent of damage. The 53 percent figure given in Table D-1 is for commercial buildings which were demolished. An additional 41 percent of buildings had damage estimated at between 25 and 75 percent. It is judged that none of the buildings in this damage range suffered major collapse. However, the damage in Compton, was relatively high, was based on a relatively few buildings, and was for an area which evidently had a relatively high intensity of shaking. The incidence of major damage and partial collapse in Long Beach was considerably lower, based on Reference 37.

The data was more easily interpreted for the Santa Barbara Earthquake in which of 340 buildings, mainly of unreinforced brick construction with lime mortar, 38 were demolished. The next category of damage "seriously damaged" included major cracking but evidently no major collapse of walls and roof.

The data on the Kern County Earthquake were not as clear. Sixteen percent of unreinforced brick buildings were torn down and this is the number reported. An additional 20% of such buildings were in question as to demolition, and another 42% of buildings were repaired with 22% undamaged.

The above data indicates that for severe earthquake ground shaking in the range of peak accelerations from about 0.15g to 0.5g (which is a rough estimate of the range of peak accelerations which occurred for the three earthquakes and the sites considered) the probability of major collapse is relatively low, within the range of 10 to 40 percent.

A similar inference may be drawn on the basis of experience from the San Fernando Earthquake (1971). Housner and Jennings (Reference 38) indicate that, for the type of buildings considered, major damage and partial collapse can be expected at peak ground acceleration levels of between 0.2g and 0.4g. Housner and Jennings values as reported are based on estimated capacities of various types of construction under ground shaking and conditions of the 1971 San Fernando Earthquake.

The specific past earthquake history and other data cited above indicates no collapse or a very low probability of collapse at ground levels of below .15g. Also, based on the above data a rather qualitative estimate of median collapse levels for unreinforced masonry buildings is in the range of 0.15g to 0.4g.

A more quantitative correlation may be obtained by observing the approximate relation between intensity and ground acceleration as coordinated with performance of unreinforced masonry construction. Such a correlation based on past earthquake experience is given by the Modified Mercalli Intensity (MM) scale with approximate intensity and acceleration levels, Figure D-1. These data are based on work by Richter (Reference 39) and as discussed in Reference 40.

Utilizing this information and considering ordinary workmanship and unreinforced masonry, the construction of interest is "Masonry C". In Figure D-1 under MM VIII, correlation is provided indicating damage and partial collapse of "Masonry C" at peak ground accelerations of

between 0.15g and 0.3g. This is a good correlation with the range of collapse prediction for rigid body systems (without roof diaphragms) as calculated for the structures considered in Reference 29. Reference 29 also shows a range (from lower to upper bound predictions) of collapse for controlling structural wall-roof systems of 0.14g to 0.33g. Also, a collapse capacity for all cantilevered rigid body wall/roof systems is shown to range from 0.14g to 0.41g in the same reference.

Figure D-1 shows that for MM IX and ground acceleration levels of 0.3g to 0.7g, "Masonry C" is indicated to be heavily damaged and sometimes totally collapsed.

In summary the comparisons indicated between observed damage from past earthquakes and the capacities analytically predicted in this study compare quite favorably.

COMPARISON OF RESULTS BY ANALYSIS

A second confirmation of the approximate analysis procedures used in this study was provided by a series of nonlinear time history verification analyses. In order to demonstrate that the RE method of analyses provides a good estimate of wall/roof system capacities considering rigid body response modes, verification analyses were made for a simple but representative wall/roof system. The RE analysis method was verified by showing that the capacity of a representative system obtained using the RE method of analysis compares well with the capacity of the system as determined independently using nonlinear time history analysis. The effect of concurrent vertical motion was also investigated using two uncorrelated time history input motions.

The representative simplified system selected is a single wall supporting a uniform roof load, modeled after the east wall of FAB 6. The 12 inch hollow block wall with corresponding wall and roof weights is

shown in Figure D-2. This system is the same as that used to illustrate application of the Reserve Energy (RE) approximate analysis method in Reference 29. As reported in Reference 29, the actual seismic capacity in transverse shaking of FAB 6 was determined utilizing a more complex model involving an entire structural system comprised of east and west walls and the roof structure.

GROUND MOTION CRITERIA

The peak ground acceleration capacity, as determined to demonstrate verification of the RE method, was based on a seismic input definition different than the criteria input. The reason for selection of the particular input for verification analysis was that artificial time history acceleration records corresponding to given response spectra were readily available; but of even more importance, the time history records utilized have a number of near peak amplitudes corresponding to a number of frequencies distributed over a broad frequency band. These broad band earthquake records are thus representative of strong earthquake ground shaking for a wide variety of earthquakes which may occur at the site.

The horizontal and vertical time histories and corresponding response spectra (10% damping) are shown in Figures D-3 and D-4, normalized to an arbitrarily chosen value of peak ground acceleration (0.3g). The corresponding WASH-1255 spectra (median) are also indicated to provide a basis of comparison. The artificial time histories were originally generated to produce spectral shapes which envelop the Regulatory Guide 1.60 design spectra. It should be noted that the horizontal and vertical time histories are essentially uncorrelated.

Comparison of results from the nonlinear analysis using the selected input time histories and the spectra analysis using the corresponding spectrum and the equivalent structural system, should provide verification of the RE method. Nominal results obtained from

both analyses are expected to be conservative estimates of collapse and would correspond closer to an upper bound or design envelope prediction than to a median value, because the response spectra utilized are higher than the WASH-1255 criteria spectra (Reference 7).

RESERVE ENERGY CAPACITY ANALYSIS

The nonlinear force-deflection characteristic for the example wall, under lateral force F at the roof line, is shown in Figure D-5 together with the equivalent linear diagram. It should be noted that the force-deflection relationship differs from the example wall considered in Appendix A of Reference 29 since the eccentricity of the roof load is not included. The effect of eccentricity, while destabilizing for a single wall, is a stabilizing factor when a structural system is considered, such as the example given subsequently. Thus the effects of eccentricity are not included in the simplified wall system considered for the verification analysis.

The nonlinear single-degree-of-freedom (SDOF) wall model is compared with the equivalent linear model developed for use in the RE method in Figure D-6, indicating the energy equivalence of the two models. The RE analysis for the system is shown in Figure D-7. The RE analysis procedure is described in additional detail in Reference 29. Results of the RE method indicate collapse at .09g peak ground acceleration. The equivalent rigid body system has a maximum force F_{RB} capacity of 47.8 lbs/in and a peak top displacement, δ_{RB} (at the point of instability) of 7.94 inches.

NONLINEAR CAPACITY ANALYSIS

A preliminary study of a simple nonlinear spring-mass system was conducted utilizing the force-deflection characteristic indicated by the solid line in the upper diagram of Figure D-5. A nonlinear EDAC computer program (TDYNE) which is intended for nonlinear time history analysis of spring-mass structural systems was used to compute the

POOR ORIGINAL

response to the horizontal ground motion (scaled) shown in Figure D-3. The results of this analysis indicated that stable oscillations occurred for ground motion scaled to 0.09g peak acceleration and below, and unstable behavior for ground motion scaled to 0.095g peak acceleration. Stability was regained for 0.10g motion, with unstable behavior for ground motion scaled to 0.11g and higher.

To further investigate this apparent behavior and to include the effects of concurrent vertical ground motion, a more precise model of the rocking wall system was developed which would correctly account for rigid body kinematics. The governing equation of motion for a rigid block is presented in Figure D-8. Restriction of the block proportions to a very slender object and the rotation to small angles allows the governing equation to be linearized as indicated. The redefinition of terms allows the governing equation to be expressed in the form of a SDOF nonlinear spring-mass system. The governing equation as presented is for rigid body about point O. For a rocking block, the equations may be cast as shown in Figure D-9. This representation allows both rotation about points O and O' as well as an elastic transition region representative of the cantilever response of the wall. By suitable grouping of terms, the governing equation for a rocking slender wall, may be modeled as an inverted pendulum with an elasto-plastic base spring (no hysteresis). By expressing the equation as a damped linear oscillator, with a forcing function consisting of the horizontal acceleration time history, stiffness degradation effect (including vertical ground motion), and a correction moment term, the equation may be integrated using the algorithm, indicated in Figure D-9. The solution technique utilized was based on the method presented in Reference 28 with the correction moment and stiffness degrading terms assumed constant during the time step interval. The response of the example wall to a half-sine acceleration pulse was solved initially as a sample problem to verify solution accuracy for various time step increments. The sample problem response checked within 2% of the manually computed

response for the time step utilized in the verification analysis.

For the verification problem, the effective base spring stiffness, K_r , was selected to approximate the elastic cantilever response of the example wall within the rocking transition region denoted in Figure D-9 by $-\theta^* < \theta < \theta^*$. The critical damping parameter, β , was given a value $\beta = 0.10$ for the verification analysis. The actual damping mechanism of the rocking wall is uncertain, but is assumed to be related to the crushing of mortar within a joint during the transition to rigid body behavior. Consideration of the flexural mechanics of a fully cracked section indicated that an actual transition would be complete by at least six times the idealized transition angle, θ^* . Thus, to prevent damping of the rigid body behavior, the damping factor, β , was set to zero for angles of rotation in excess of six times the transition angle, θ^* .

The solutions obtained for horizontal ground motion are shown in Figure D-10. Stable response was obtained for input scaled to 0.09g or less peak acceleration. Unstable response was obtained for 0.095 - 0.110g motion with a stable response occurring for 0.115g scaling. Unstable response was obtained for 0.120g or greater peak acceleration. Thus, the 0.09g capacity estimate provided by the RE method is verified by the time history analysis. For ground motions exceeding 0.09g the peak displacement was found to increase very rapidly and the response was found to be highly sensitive to exact phasing of the pulses of the applied time history.

The effects of concurrent vertical ground motion on the stable 0.09g peak horizontal response case are shown in Figures D-11 and D-12 for $\pm 0.06g$ and $\pm 0.14g$ peak vertical ground motion. While the general character of the response is somewhat changed by the concurrent vertical motion, the stability of the rigid system is not affected.

In conclusion, the displacements from nonlinear analyses for the scaled ground motion as predicted from the RE method (0.09g) are below collapse values and the wall is stable. However, with a very small increase in ground acceleration (less than 5 percent increase) beyond the capacity predicted by the RE method, the displacements increase radically and response, in general, is a function of ground motion phasing as the system nears instability. Thus for this simple system the RE method is shown to predict a collapse capacity very close to the capacity predicted by time history analysis. Though the RE method is based on systems being dynamically equivalent when the energies available are equal in the inelastic and equivalent elastic systems, there is no assurance that this equivalence holds for all types of inelastic systems. However, the verification analysis results as discussed above, provides a strong indication that the equivalence does hold for the linear degrading models which represent the rigid body systems considered herein.

The actual capacity analyses using the RE method are generally applied to more complex and detailed models for B&W rigid body wall/roof systems. These models and analyses results are discussed in Reference 29. A subsequent section provides one of the actual analyses by the RE method as applied to a complete and detailed model of a B&W wall/roof system (FAB 6) for easterly motion. This calculation is typical of the details considered in evaluating all rigid body systems.

HOUSNER STABILITY CRITERIA

In Reference 35, Housner considered the earthquake response of inverted pendulum structures. The following stability criteria is developed:

$$S_v = S_{ac}/2\pi f_e = \alpha \frac{I_0 g}{M R}$$

where S_v is the spectral velocity. For the example wall system considered herein, $S_{ac} = 0.0448g$. Given $AF = .49$ (Figure D-3, $T = 4$ secs), then the capacity given by the above criteria is $S_a = 0.091g$, thus providing additional verification of the RE method.

TYPICAL DETAILED ANALYSIS OF WALL/ROOF SYSTEM

This section illustrates the capacity evaluation of an actual wall/roof system of the B&W Facility utilizing the RE method. This is a representative analysis for all complex structural systems in the facility, and the details of the model and analysis are given. The system selected for this analysis is the FAB 6 wall/roof system undergoing easterly motion. This is the controlling (lowest collapse capacity) system of FAB 6 as indicated in Reference 29. The median capacity calculated by rigid body analyses using the RE method is adjusted by a factor of .95 as explained in the uncertainty bound analyses, Appendix A. Thus there is a difference in the capacity indicated in the analysis herein (.23g) and the median tabulated capacity in Reference 29 (.22g).

The detailed model for rigid body response undergoing easterly motion is shown in Figure D-13. The detail considered is typical of the detail in other rigid body analyses. This includes the eccentricity of the roof weight as applied through roof joist bearing points on the wall. As shown in the details of Figure D-13 rigid body rocking induces essentially point bearings which is also the approximation considered for the base pivot point.

Statically determinant structural models result when wall sections are considered cracked through at the base and moving together in a rigid body rotational mode. As indicated in the analysis procedures (I) shown in Figure D-14 equations of statics are developed for each wall which provide the relation between weights, reactions, and equivalent lateral force F applied at the top of the walls at the roof line. On the basis of these equations and the physical properties (weights and dimensions) a final equation is developed relating lateral Force F and top displacement δ .

1368 222

In Part II of Figure D-14 the RE analysis is shown to reduce to the same procedure as that for the simple system described in a previous section of this Appendix. Again F_{RB} , the maximum rigid body force at a top displacement of 0 is found from Equation (D-1) by setting $\delta = 0$. Similarly $\delta_{RB} = (\delta_{max})$ is found by setting $F = 0$ in Equation (D-1). The remainder of the calculations shown are self-explanatory considering the modal response of the SDOF elastic system with equivalent energy, stiffness, and maximum displacement as that of the nonlinear system. Note that the spectral acceleration capacity is just the maximum rigid body lateral force capacity divided by the equivalent weight contributing to inertial forces at the roof line, W_e , or the lateral force that would occur for a top of wall spectral acceleration of 1g.

The final result of 0.23g shown was modified by a factor to obtain a median value of 0.22g as explained in Appendix A. Because we are developing an equivalent single degree-of-freedom system from a partially distributed mass system, the equivalent inertial force, W_e , at 1g acceleration, as applied at the roof line, is not exactly $g \times M_e$ for the system. However, for the systems considered the use of $W_e/g = M_e$ is a reasonable approximation.

1363 223

TABLE D-1

PERCENT OF COLLAPSE OF UNREINFORCED MASONRY BUILDINGS

Earthquake	Modified Mercalli Intensity	Per cent of Collapsed Building
Santa Barbara 1925	VIII to IX	11
Long Beach (*)1933	IX	53
Kern County 1952	VIII to IX	16

(*) Based only on buildings in Compton.

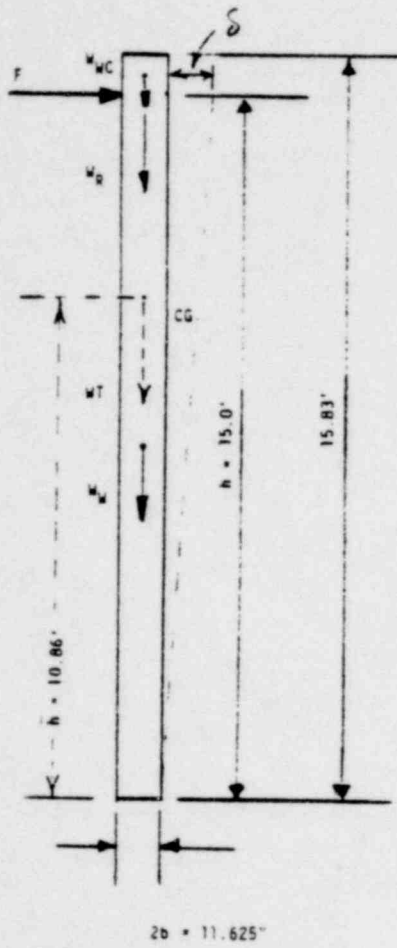
1363 224

POOR ORIGINAL

Modified Mercalli Intensity Scale	Description of Effects (Masonry A, B, C, and D Are Defined Below* From Ref. 37)	Maximum Acceleration (g)	Richter Magnitude	Energy Release (ergs)
I	Not felt, marginal and long-period effects of large earthquakes evident		M2	10^{14}
II	Felt by persons at rest, on upper floors, or favorably placed		M3	10^{15}
III	Felt indoors; hanging objects swing; vibration like passing of light trucks occurs; duration estimated; might not be recognized as an earthquake	0.003 to 0.007	M4	10^{16}
IV	Hanging objects swing; vibration occurs that is like passing of heavy trucks, or there is a sensation of a jolt like a heavy ball striking the walls; standing motor cars rock; windows, dishes, and doors rattle; glasses clink; crockery clashes; in the upper range of IV, wooden walls and frame creak	0.007 to 0.015	M4	10^{17}
V	Felt outdoors; duration estimated; sleepers waken; liquids become disturbed, some spill; small unstable objects are displaced or upset; doors swing, close, and open; shutters and pictures move; pendulum clocks stop, start, and change rate	0.015 to 0.03	M5	10^{18}
VI	Felt by all; many are frightened and run outdoors; persons walk unsteadily; windows, dishes, glassware break; knickknacks, books, etc., fall off shelves; pictures fall off walls; furniture moves or overturns; weak plaster and masonry D cracks; small bells ring (church, school); trees, bushes shake	0.03 to 0.09	M5	10^{19}
VII	Difficult to stand; noticed by drivers of motor cars; hanging objects quiver; furniture breaks; damage occurs to masonry D, including cracks; weak chimneys break at roof line; plaster, loose bricks, stones, tiles, cornices fall; some cracks appear in masonry C; waves appear on ponds; water turbid with mud; small slides and cavins occur along sand or gravel banks; large bells ring	0.07 to 0.22	M6	10^{20}
VIII	Steering of motor cars affected; damage occurs to masonry C, with partial collapse; some damage occurs to masonry B, but none to masonry A; stucco and some masonry walls fall; twisting, fall of chimneys, factory stacks, monuments, towers, and elevated tanks occur; frame houses move on foundations if not bolted down; loose panel walls are thrown out; changes occur in flow or temperature of springs and wells; cracks appear in wet ground and on steep slopes	0.15 to 0.3	M6	10^{21}
IX	General panic; masonry D is destroyed; masonry C is heavily damaged, sometimes with complete collapse; masonry B is seriously damaged; general damage occurs to foundations; frame structures shift off foundations, if not bolted; frames crack; serious damage occurs to reservoirs; underground pipes break; conspicuous cracks appear in ground; sand and mud ejected in alluvial areas; earthquake fountains and sand craters occur	0.3 to 0.7	M7	10^{22}
X	Most masonry and frame structures are destroyed, with their foundations; some well-built wooden structures and bridges are destroyed; serious damage occurs to dams, dikes, and embankments; large landslides occur; water is thrown on banks of canals, rivers, lakes, etc.; sand and mud shift horizontally on beaches and flat land; rails are bent slightly	0.45 to 1.1	M8	10^{23}
XI	Rails are bent greatly; underground pipelines are completely out of service	0.5 to 3	M8	10^{24}
XII	Damage nearly total; large rock masses are displaced; lines of sight and level are distorted; objects are thrown into air	0.5 to 7	M9	10^{25}

*Masonry A. Good workmanship, mortar, and design; reinforced, especially laterally, and bound together by using steel, concrete, etc., designed to resist lateral forces.
 Masonry B. Good workmanship and mortar; reinforced, but not designed in detail to resist lateral forces.
 Masonry C. Ordinary workmanship and mortar; no extreme weaknesses like failing to tie in at corners, but neither reinforced nor designed against horizontal forces.
 Masonry D. Weak materials, such as adobe; poor mortar; low standards of workmanship; weak horizontally.

FIGURE D-1. APPROXIMATE RELATIONSHIPS BETWEEN INTENSITY, ACCELERATION, MAGNITUDE, AND ENERGY RELEASE (REFS. 39 and 40)

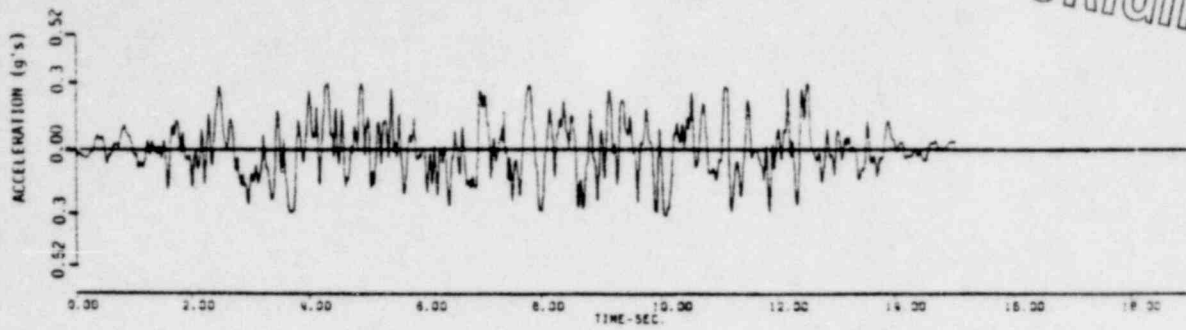


- F - LATERAL FORCE APPLIED AT ROOF LINE
- W_{WC} - WEIGHT OF THE WALL ABOVE ROOF LINE
 $= 0.83' \times 55 \text{ #/1}' = 46\#$
- W_W - WEIGHT OF THE WALL BELOW THE ROOF LINE
 $= 15' \times 55 \text{ #/1}' = 825\#$
- W_R - TRIBUTARY ROOF WEIGHT
 $= 43.2 \text{ #/1}' \times 29'/2 = 626\#$
- $W_T = W_{WC} + W_W + W_R = 1497\#$
- W_I - WEIGHT CONTRIBUTING TO INERTIA FORCES
 $= 1497 \times 10.86/15 = 1084\#$
 (SEE FIGURE B-7)

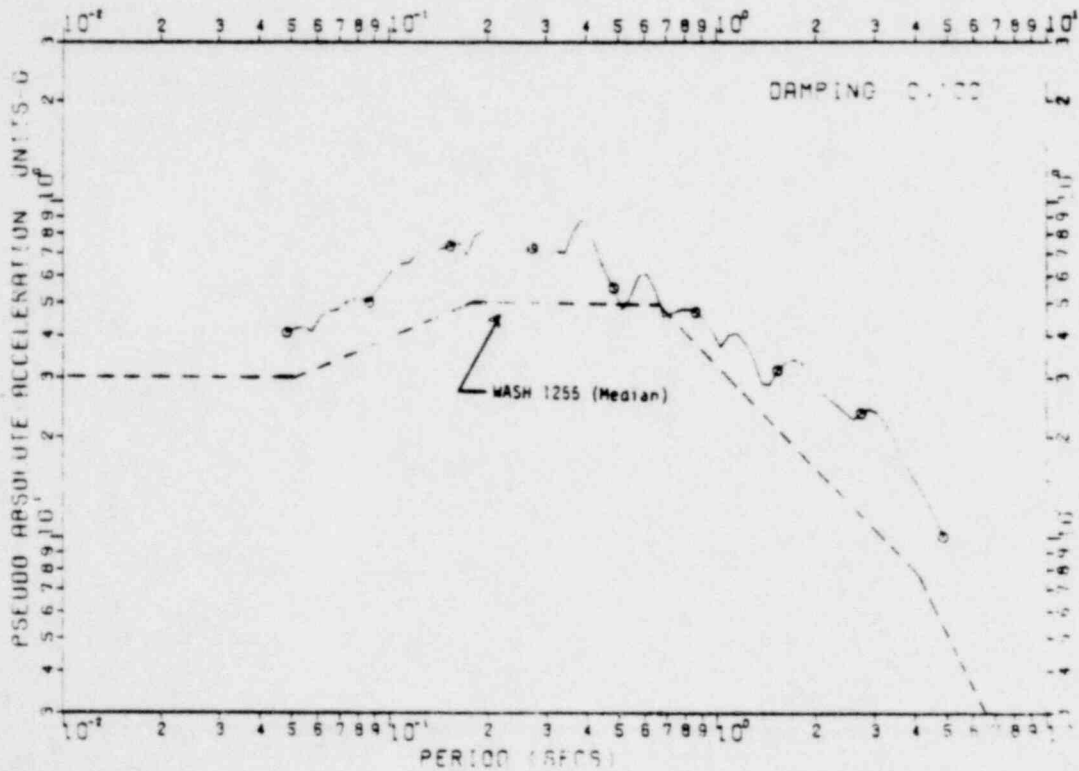
POOR ORIGINAL

FIGURE D-2 REPRESENTATIVE RIGID BODY SYSTEM FOR VERIFICATION ANALYSES

POOR ORIGINAL

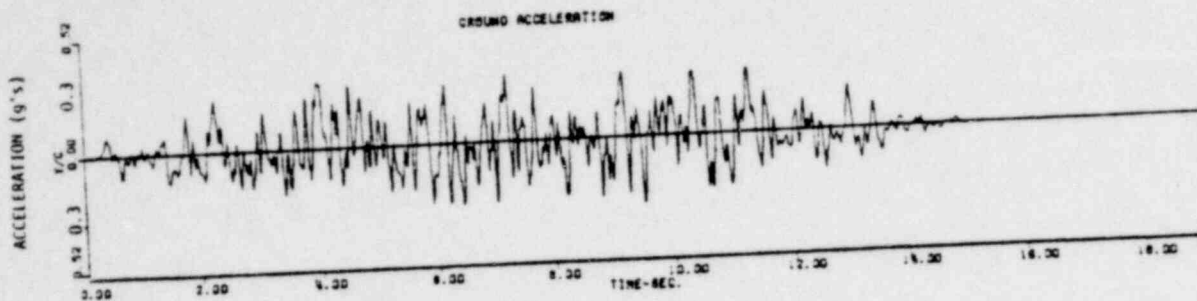


ARTIFICIAL EARTHQUAKE HORIZONTAL ACCELERATION TIME HISTORY
(NORMALIZED TO .3g PEAK ACCELERATION)



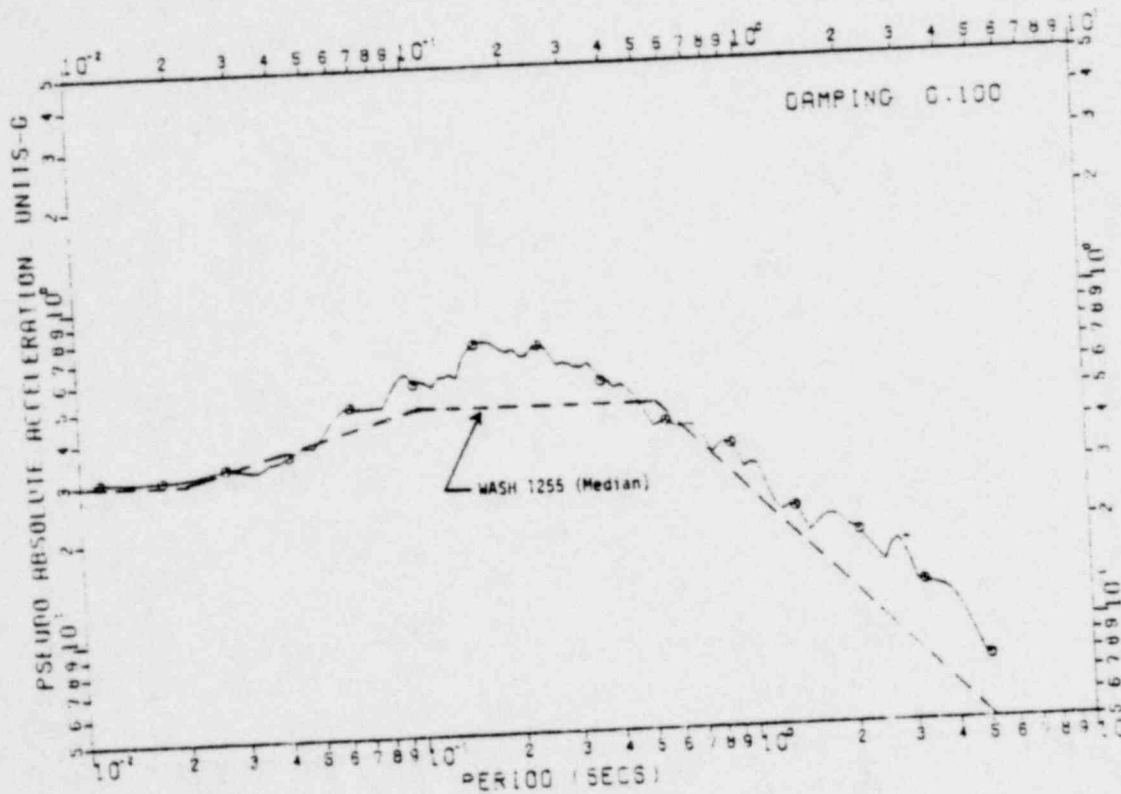
RESPONSE SPECTRUM OF HORIZONTAL .3G PEAK GROUND MOTION

FIGURE D-3. HORIZONTAL RESPONSE SPECTRUM AND TIME HISTORY FOR VERIFICATION ANALYSES



ARTIFICIAL EARTHQUAKE VERTICAL ACCELERATION TIME HISTORY
(NORMALIZED TO .3g PEAK ACCELERATION)

POOR ORIGINAL



RESPONSE SPECTRUM OF VERTICAL 0.36 PEAK GROUND MOTION

FIGURE D-4. VERTICAL RESPONSE SPECTRUM AND TIME HISTORY FOR VERIFICATION ANALYSIS

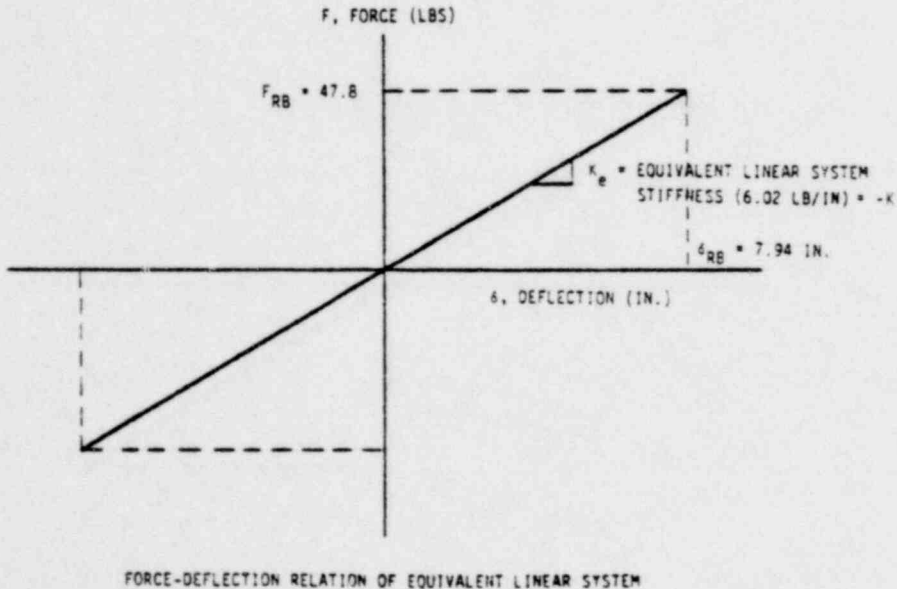
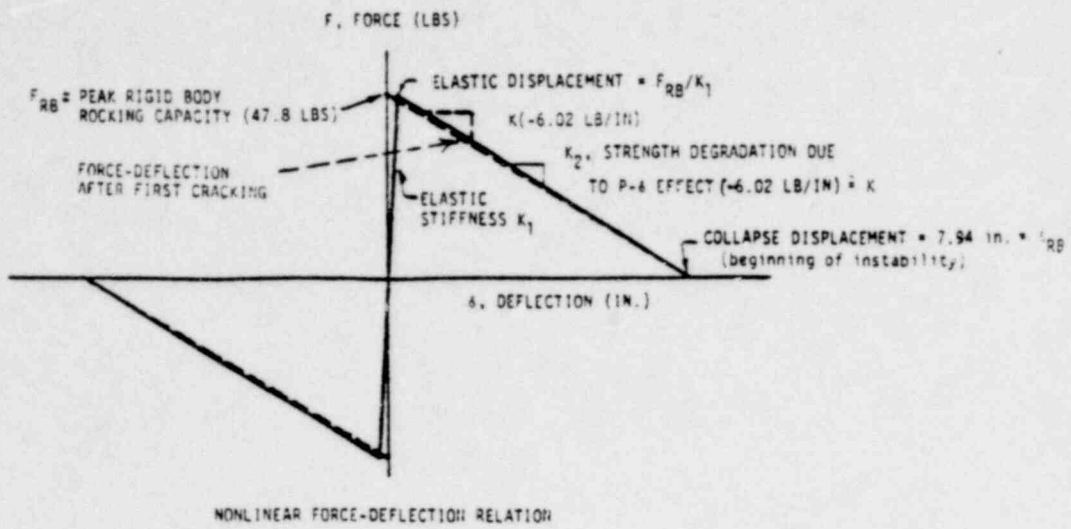


FIGURE D-5. FORCE-DEFLECTION RELATIONS FOR TYPICAL RIGID BODY SYSTEM

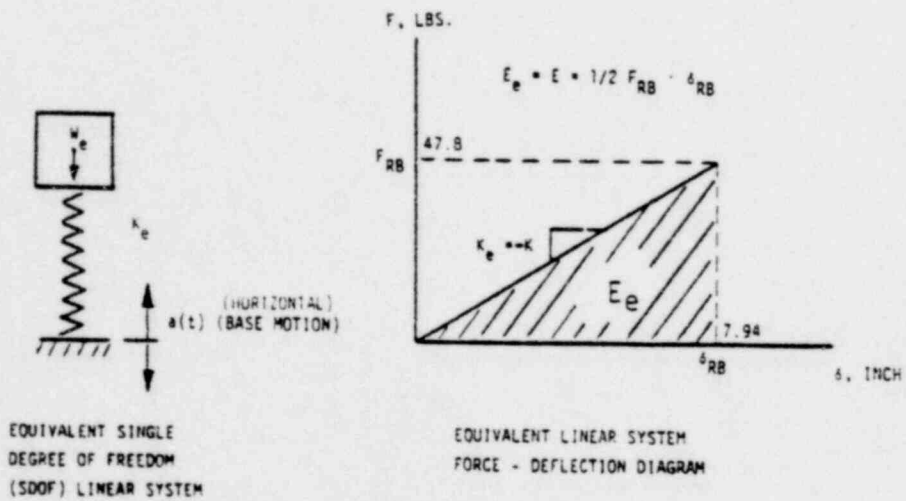
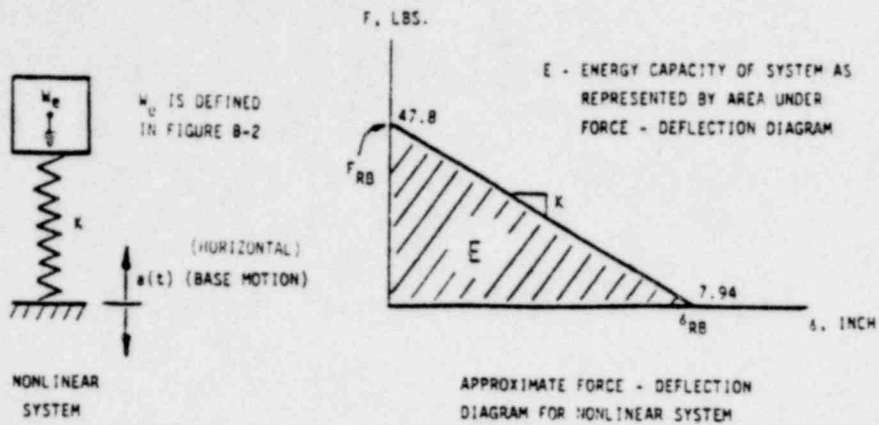


FIGURE B-6. WALL/ROOF SYSTEM MODELS

1363 230

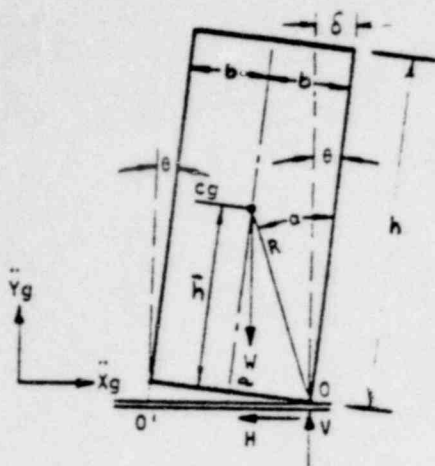
TYPICAL CAPACITY
CALCULATION FOR
SIMPLE SYSTEM

$$\begin{aligned}
 (1) \quad f_e &= \frac{1}{2\pi} \sqrt{\frac{K_e}{M_e}} = 0.25 \text{ CPS} \\
 (2) \quad S_{ac} &= \frac{F_{RB}}{W_e} = 0.044 \text{ g} \\
 (3) \quad AF & \text{ (From Figure B-3 Spectrum)} = 0.49 \\
 (4) \quad a_{gc} &= \frac{S_{ac}}{AF} = 0.09 \text{ g} \\
 & \text{(capacity)}
 \end{aligned}$$

DEFINITIONS:

- W_e = Weight contributing to inertia forces of simple system under base motion (1084 lbs, Figure D-2)
- M_e = Mass of equivalent SDOF system (2.45 lb-sec²/in)
- F_{RB} = Maximum rigid body force capacity of wall system at roof line (47.8 lbs)
- δ_{RB} = Maximum rigid body deflection of wall system at roof line (7.94 in, at point of incipient collapse)
- K = Approximate stiffness of nonlinear system ($F_{RB}/\delta_{RB} = 6.02 \text{ lb/in}$)
- K_e = Stiffness of simple equivalent linear system ($= F_{RB}/\delta_{RB}$)
- f_e = Natural frequency of equivalent system
- $a(t)$ = Base motion defined by response spectra (Figure D-3)
- AF = Spectral Acceleration (Amplification/Deamplification) Factor at calculated frequency of system ($= S_a/a_g$) for given response spectrum (10% damping)
- S_a = Spectral acceleration at a particular frequency corresponding to a given level of ground shaking
- a_g = Peak ground acceleration associated with the level of ground shaking for S_a
- S_{ac} = Maximum spectral acceleration capacity of equivalent system. See Equation (2)
- a_{gc} = Maximum base ground acceleration capacity of equivalent system

FIGURE D-7. CALCULATION OF SEISMIC CAPACITY OF SIMPLE SYSTEM



$$\begin{aligned}
 I_c &= \text{Mass Moment of Inertia about cg} \\
 I_o &= I_c + \bar{M} R^2 \equiv \text{Mass Moment of Inertia about } O \text{ or } O' \\
 \bar{M} &= \text{Mass} \\
 W &= \bar{M} g \\
 R^2 &= \bar{h}^2 + b^2 \\
 \alpha &= \tan^{-1} b/\bar{h}
 \end{aligned}$$

GOVERNING EQUATION

$$I_o \ddot{\theta} = -\bar{M} R \ddot{x}_g \cos(\alpha - \theta) - \bar{M} R (\ddot{y}_g + g) \sin(\alpha - \theta)$$

LINEARIZATION

$$\begin{aligned}
 \alpha, \theta < 10^\circ; \quad b/\bar{h} < 0.18 \\
 \cos(\alpha - \theta) \approx 1; \quad \sin(\alpha - \theta) \approx \alpha - \theta
 \end{aligned}$$

thus governing equation is approximated by

$$\ddot{\theta} - p^2 (1 + \ddot{y}_g/g) \theta = -p^2 \ddot{x}_g/g - p^2 (1 + \ddot{y}_g/g) \alpha$$

$$\text{where } p^2 = WR/I_o$$

$$\text{If } M_{R0} = WR (1 + \ddot{y}_g/g) \alpha \approx Wb (1 + \ddot{y}_g/g)$$

$$\text{then } I_o \ddot{\theta} + M_R = -WR \ddot{x}_g/g$$

$$\begin{aligned}
 \text{where } k &= WR (1 + \ddot{y}_g/g) \\
 M_R &= M_{R0} - k\theta \quad \text{or}
 \end{aligned}$$

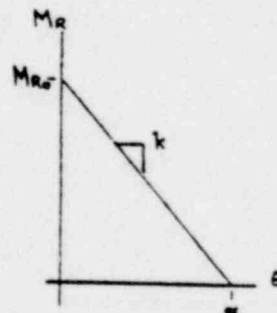
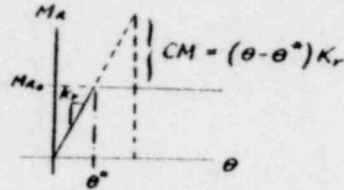


FIGURE D-8. GOVERNING EQUATION OF MOTION FOR A ROTATING RIGID BLOCK

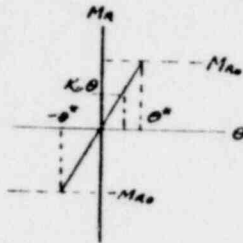
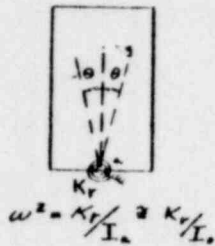
$$\ddot{\theta} + 2\omega\beta\dot{\theta} + \omega^2\theta = -P^2\ddot{y}_g/g + P^2(1 + \ddot{y}_g/g)\theta + \frac{CM}{I_0}$$



ELASTIC TRANSITION REGION

$$\ddot{\theta} + 2\omega\beta\dot{\theta} + \omega^2\theta = -P^2\ddot{y}_g/g + P^2(1 + \ddot{y}_g/g)\theta$$

$-\theta^* < \theta < \theta^*$

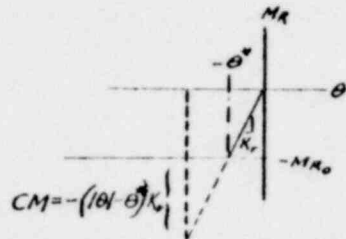


D-21

$$\omega^2 = K_r/I_0 = K_r/I_0$$

RIGID BODY ROTATION ABOUT POINT O

$$\ddot{\theta} + 2\omega\beta\dot{\theta} + \omega^2\theta = -P^2\ddot{y}_g/g + P^2(1 + \ddot{y}_g/g)\theta + \frac{CM}{I_0}$$



SOLUTION TECHNIQUE (Reference 41)

$$\ddot{\theta} + 2\omega\beta\dot{\theta} + \omega^2\theta = -[A_{t_i} + \frac{\Delta A_{t_i}}{\Delta t}(t-t_i) + A_c]$$

$$A_{t_i} = P^2\ddot{y}_g^i, \quad \Delta A_{t_i} = P^2(\ddot{y}_g^{i+1} - \ddot{y}_g^i)$$

$$A_c = -P^2(1 + \ddot{y}_g/g)\bar{\theta} - \frac{CM}{I_0}$$

$$\bar{\theta} = 1.5\theta_i - 0.5\theta_{i-1}$$

$$\ddot{y}_g = \frac{1}{2}(\ddot{y}_g^i + \ddot{y}_g^{i+1})$$

$$\theta^* = M_{A0}/K_r = \frac{wb}{K_r}(1 + \ddot{y}_g/g)$$

$$|\bar{\theta}| \leq \theta^*, \quad CM = 0$$

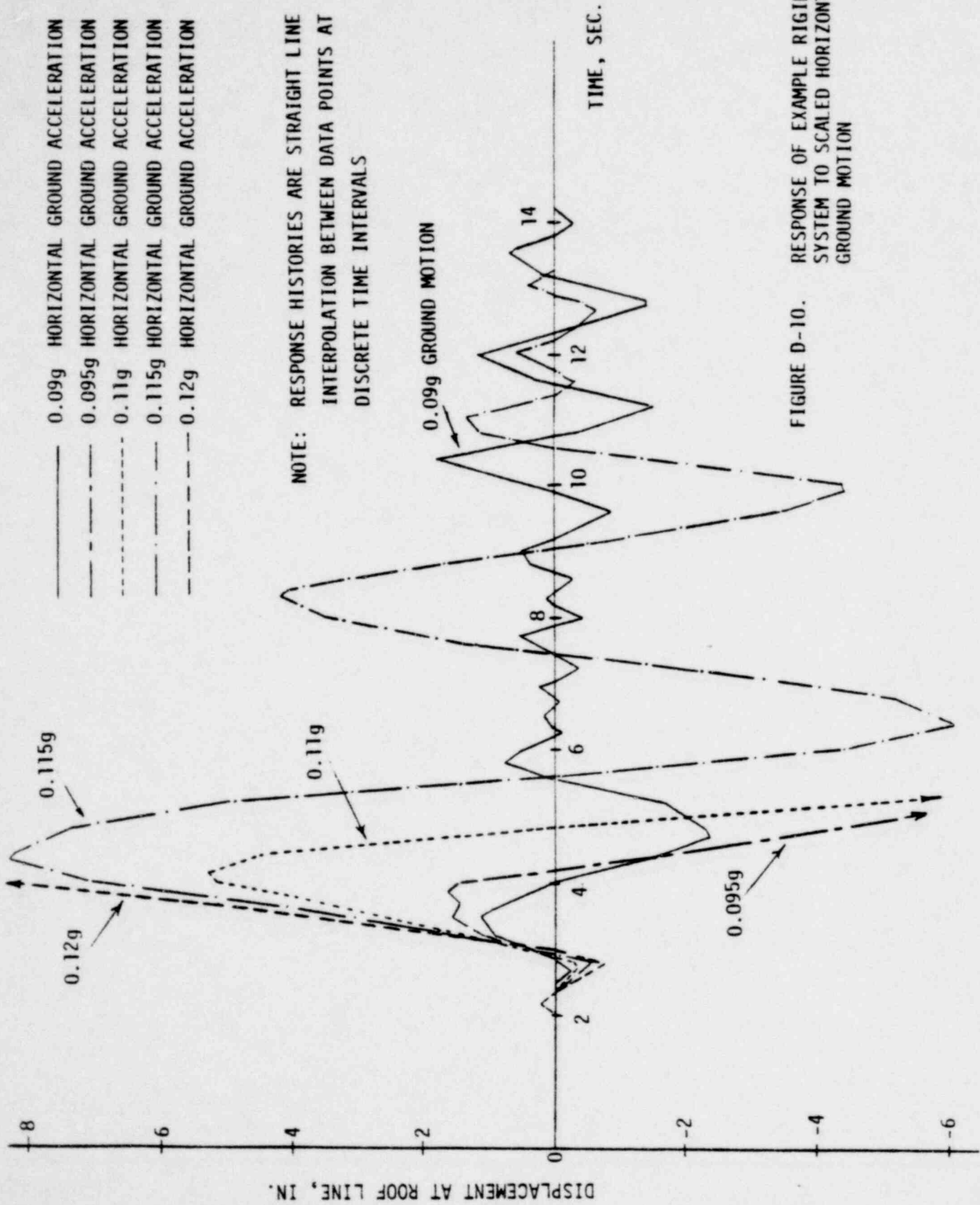
$$|\bar{\theta}| > \theta^*, \quad CM = |\bar{\theta}|/\theta^*(|\bar{\theta}| - \theta^*)K_r$$

$$|\bar{\theta}| \leq n\theta^*, \quad \beta = \bar{\beta} \quad (n=6, \bar{\beta}=0.10)$$

$$|\bar{\theta}| > n\theta^*, \quad \beta = 0$$

FIGURE D-9. ROCKING BLOCK MODEL AND SOLUTION ALGORITHM

1363 233



- 0.09g HORIZONTAL GROUND ACCELERATION
- - - 0.095g HORIZONTAL GROUND ACCELERATION
- · - · 0.11g HORIZONTAL GROUND ACCELERATION
- · - · 0.115g HORIZONTAL GROUND ACCELERATION
- - - 0.12g HORIZONTAL GROUND ACCELERATION

FIGURE D-10. RESPONSE OF EXAMPLE RIGID BODY SYSTEM TO SCALED HORIZONTAL GROUND MOTION

- 0.09g HORIZONTAL GROUND ACCELERATION
- - - - 0.09g HORIZONTAL & (+) 0.06g VERTICAL GROUND ACCELERATION
- . - . 0.09g HORIZONTAL & (-) 0.06g VERTICAL GROUND ACCELERATION

NOTE: RESPONSE HISTORIES ARE STRAIGHT LINE
 INTERPOLATION BETWEEN DATA POINTS
 SAMPLED AT DISCRETE TIME INTERVALS

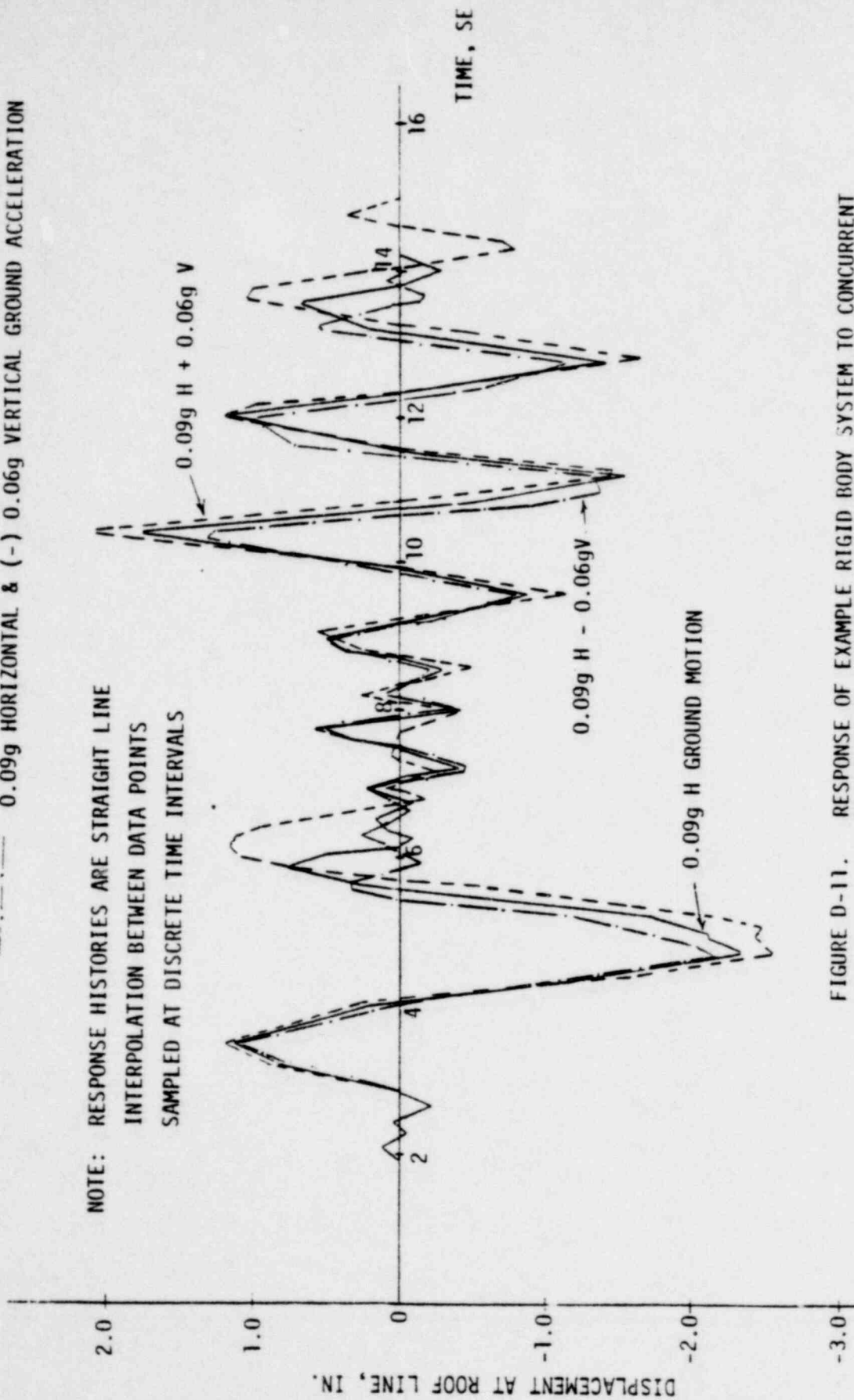


FIGURE D-11. RESPONSE OF EXAMPLE RIGID BODY SYSTEM TO CONCURRENT HORIZONTAL AND VERTICAL GROUND MOTION

0.09g HORIZONTAL ACCELERATION

0.09g HORIZONTAL & (+) 0.14g VERTICAL GROUND ACCELERATION

0.09g HORIZONTAL & (-) 0.14g VERTICAL GROUND ACCELERATION

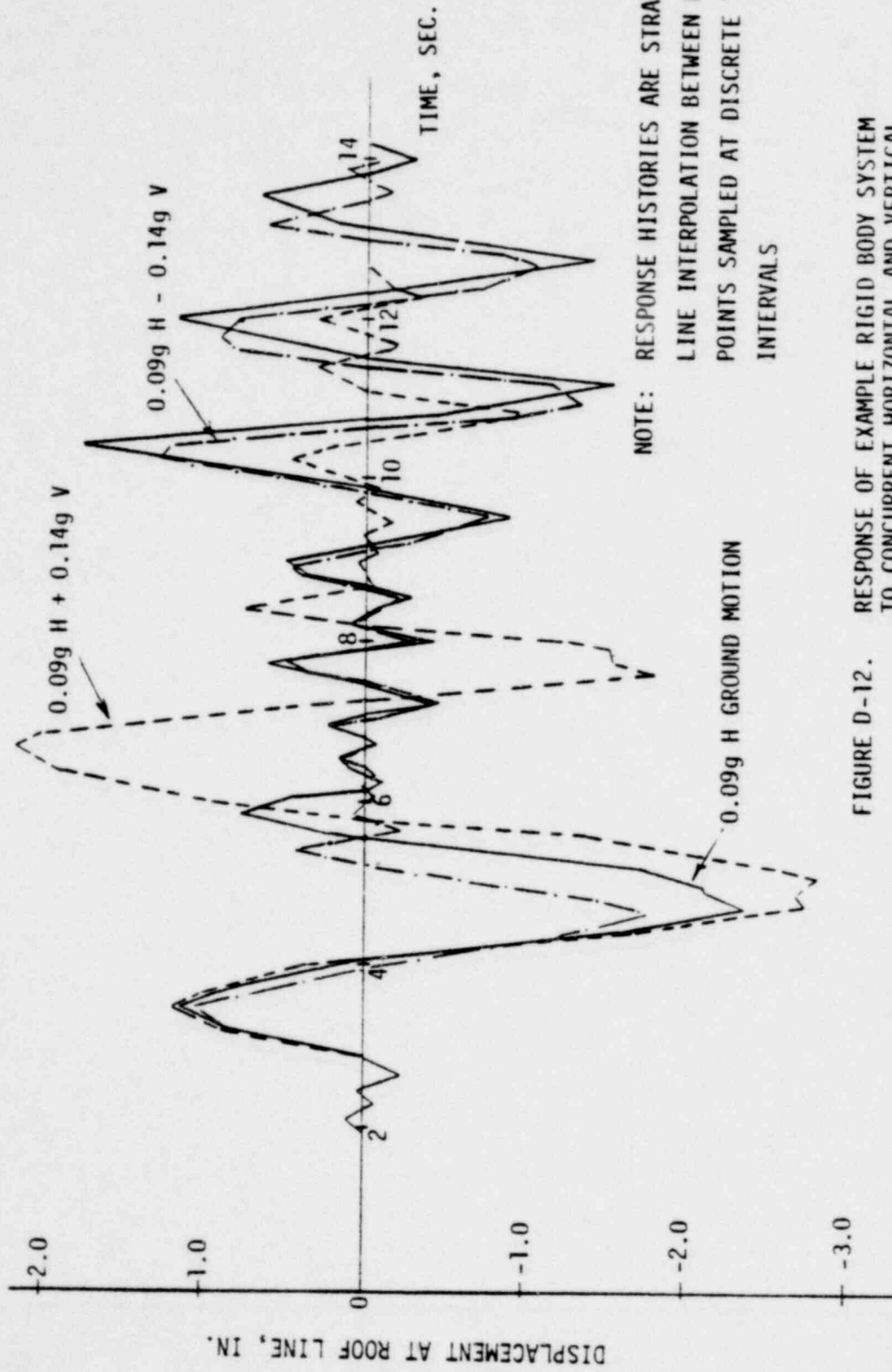
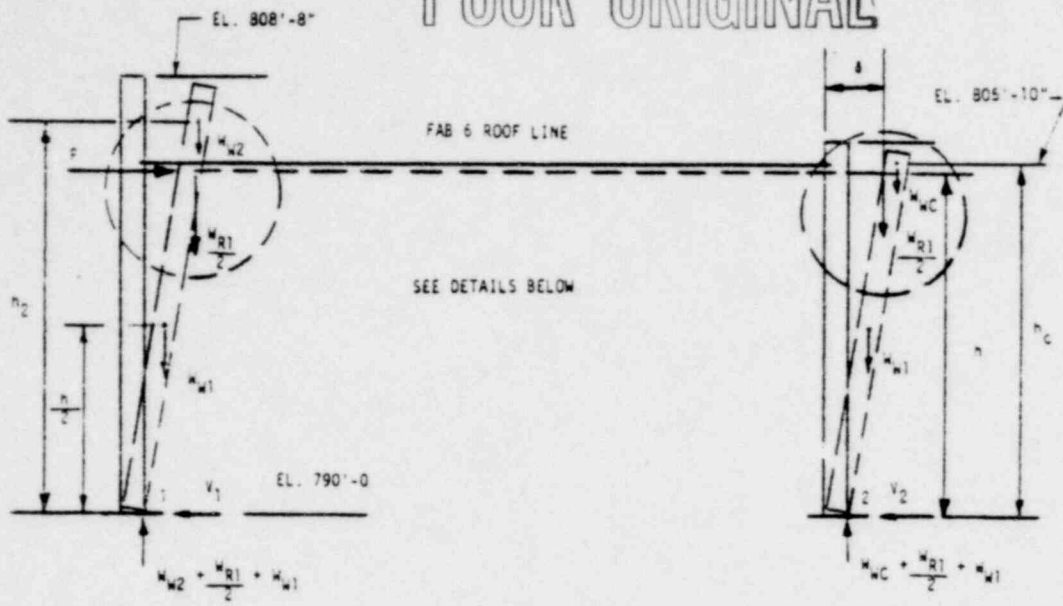
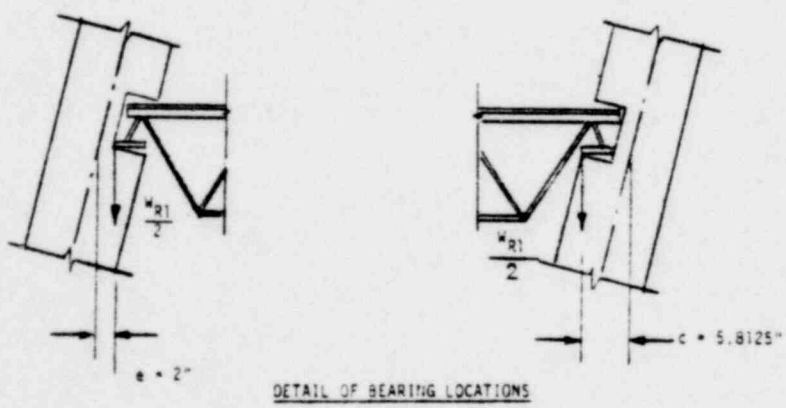


FIGURE D-12. RESPONSE OF EXAMPLE RIGID BODY SYSTEM TO CONCURRENT HORIZONTAL AND VERTICAL GROUND MOTION

POOR ORIGINAL



FAB 6 TRANSVERSE SYSTEM



DETAIL OF BEARING LOCATIONS

- WHERE:
- $M_{w1} = 825.0^{\#}$
 - $M_{w2} = 202.0^{\#}$
 - $M_{wC} = 45.7^{\#}$
 - $\frac{M_{R1}}{2} = 626.0^{\#}$
 - $h = 180.0"$
 - $h_2 = 202.0"$
 - $h_c = 185.0"$

FIGURE D-13. DETAILED MODEL FOR FAB 6 RIGID BODY CAPACITY ANALYSIS EAST WEST SHAKING